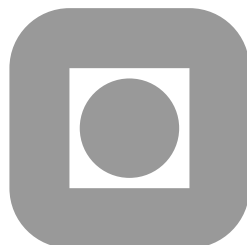


On process model representation and AlF_3 dynamics of aluminum electrolysis cells

Dr. ing. thesis

Tormod Drengstig



Department of Engineering Cybernetics
Norwegian University of Science and Technology
N-7034 Trondheim, Norway
August 1997

Report 97-54-W

Preface

This thesis is submitted in partial fulfillment of the requirements for the degree of *doktor ingeniør* at the Norwegian University of Science and Technology (NTNU). The work has been carried out at the Department of Engineering Cybernetics, NTNU, from February 1994 to August 1997. It has been financed by the Research Council of Norway through the Expomat and Prosmat research programs, Hydro Aluminium a.s. and PROST¹.

I am indebted to my supervisor, Professor Bjarne A. Foss, at the Department of Engineering Cybernetics, NTNU, for our many fruitful and encouraging discussions. His enthusiasm and genuine interest in my work has been a source of inspiration.

I would like to thank Dr. Dag Ljungquist for cooperation and invaluable support in the development and verification of the aluminum electrolysis cell model. Further, I would like to thank Dr. Stein O. Wasbø for our fruitful discussions on work regarding the modeling methodology.

I want to also acknowledge Professor Wolfgang Marquardt from RWTH Aachen, Germany, and his group of Ph.D. students for the stimulating discussions during my research visit from September 1995 to February 1996.

Special acknowledgment is due to Johannes Aalbu and the management at Hydro Aluminium a.s. in Årdal, Norway, for initiating the project.

I would also like to thank my fellow students and colleagues at the Department of Engineering Cybernetics, NTNU, in particular Erling Aarsand Johannessen for sharing an office with me, for his advice with \LaTeX and for what may turn out to be some very profitable discussions. Petter Lågstad is acknowledged for his help on Unix, Xfig and \LaTeX issues, and Stewart Clark at the Administration, NTNU, for editing the English in this thesis.

Finally, I would like to express my gratitude to my family for all the encouragement and support.

Tormod Drenngstig
Trondheim, August 1997

¹Strong Point Center in Process Systems Engineering, Trondheim, Norway.

Summary

This thesis has developed a formal graphical based process representation scheme intended for modeling complex, non-standard unit processes. The scheme is based on topological and phenomenological decompositions. The topological decomposition is the modularization of processes into modules representing volumes and boundaries, whereas the phenomenological decomposition focuses on physical phenomena and characteristics inside these topological modules. The representation is an attempt to define legal and illegal connections between components at all levels. This formalization facilitates a full implementation of the methodology into a computer aided modeling tool that is able to interpret graphical symbols and guide modelers towards a consistent mathematical model of the process. The modeling methodology is implemented in Simulink.

Furthermore, this thesis presents new results on the excess AlF_3 and bath temperature dynamics of an aluminum electrolysis cell. A dynamic model of an aluminum electrolysis cell is developed and validated against known behavior and real process data. The model validation indicates that there are dynamics that the model does not capture. For this reason, real data of excess AlF_3 and bath temperature are used to estimate equivalent AlF_3 and energy disturbances, respectively. The estimation results show that the energy disturbance is the dominating disturbance. Moreover, assuming that the excess AlF_3 and bath temperature measurements are suitable to calculate the current efficiency *a posteriori*, a possible explanation of the estimated energy disturbance is variations in the current efficiency. On the other hand, due to the inherent *positive* feedback from the back reaction to bath temperature, it is hypothesized here that long-term *prediction* of bath temperature and excess AlF_3 is impossible with a current efficiency model considering only bath composition and temperature.

A control strategy for excess AlF_3 and bath temperature is proposed, based on an almost constant AlF_3 input close to average consumption and energy manipulations to compensate for the disturbances. This requires the possibility that the reference resistance can be reduced without decreasing

the current efficiency. Compared to present control strategies, this introduces an additional degree of freedom in the controller. An alternative cell operation directly affecting the energy balance is careful monitoring and maintenance of the crust thickness. The proposed control strategy is likely to have a significant economic potential since it may result in increased and stabilized current efficiency, reduced and stabilized energy consumption, reduced consumption of expensive additives and prolongation of cell life.

Contents

Preface	i
Summary	iii
Contents	v
List of figures	xi
List of tables	xvii
Nomenclature	xix
1 Introduction	1
1.1 Motivation and background	1
1.1.1 Modeling of chemical processes	1
1.1.2 AlF_3 and bath temperature dynamics	4
1.2 Previous work	5
1.2.1 Unit process modeling and representation	5
1.2.2 AlF_3 and bath temperature control	7
1.3 Contributions of the thesis	9
1.4 Outline of the thesis	10

I	Modeling methodology	13
2	A formal graphical based process representation	15
2.1	Introduction	15
2.2	Topological process abstraction	16
2.2.1	Definitions	16
2.2.2	Topological sets	16
2.2.3	Topological component symbols	18
2.2.4	Aggregation vs. decomposition	19
2.2.5	Modeling rules	20
2.3	Phenomenological process abstraction	22
2.3.1	Definitions	23
2.3.2	Phenomenological sets	23
2.3.3	Phenomenological component symbols	25
2.4	Separated mass and energy representation	30
2.4.1	Refinement of sets	30
2.4.2	Modeling rules	31
2.5	Conceptual interpretation of symbols	34
2.6	Relation between symbols and equations	35
2.6.1	Relation to conservation equations	36
2.6.2	Relation to rate equations	39
2.6.3	Relation to constitutive equations	40
2.7	Discussion	41
3	Model assumptions and the modeling process	43
3.1	Model assumptions	43
3.1.1	A priori assumptions	44
3.1.2	A posteriori assumptions	45
3.1.3	Symbols	46
3.1.4	Classification of model assumptions	50
3.1.5	Procedure for consistent process model generation	51
3.1.6	Examples	52
3.2	The modeling process	58
3.2.1	Modeling the PTD	58
3.2.2	Modeling the TRAV	61
3.2.3	Initialization of elements of the set A	63
3.2.4	Specification of elements of the set T	64
3.2.5	Specification of elements of the set RG	65
3.3	Discussion	66

4	Implementation of the modeling methodology	67
4.1	Introduction	67
4.2	About Simulink	68
4.2.1	General	68
4.2.2	S-Functions and S-functions	69
4.2.3	S-function behavior	70
4.2.4	Masking	72
4.2.5	Multiplexing	72
4.3	Topological and phenomenological symbols	73
4.4	Transformation of the modeling methodology	74
4.4.1	Topological modeling	74
4.4.2	Phenomenological modeling	76
4.4.3	Rearranging the symbols	77
4.4.4	Resolving the consistency	78
4.5	Model initialization and specification	78
4.5.1	Initialization of elements of the set A	78
4.5.2	Specification of elements of the set T	81
4.5.3	Specification of elements of the set RG	83
4.5.4	Specification of constitutive equations	83
4.6	Discussion	84
II	Application	85
5	Process description	87
5.1	Introduction	87
5.1.1	History	87
5.1.2	Performance measures	89
5.1.3	Electric input	90
5.2	Raw materials	92
5.2.1	Aluminum oxide	93
5.2.2	Cryolite	94

5.2.3	Aluminum fluoride	95
5.2.4	Carbon	95
5.3	Fundamentals of the Hall-Héroult process	96
5.3.1	Bath properties	96
5.3.2	Sludge formation and sodium swelling	98
5.3.3	Side ledge properties	100
5.3.4	Fluoride vaporization	102
5.4	Cell control	103
5.4.1	Alumina control	103
5.4.2	Fluoride and temperature control	105
5.5	Electrochemical thermodynamics	107
5.5.1	Galvanic and electrolytic cells	107
5.5.2	Reaction rates	107
5.5.3	Standard potential of cell reactions	108
5.5.4	Cell potential at reversible, non-standard condition	110
5.5.5	Overall cell voltage	111
5.5.6	Energy consumption	112
6	Model development	115
6.1	Introduction	115
6.2	Mass based model development	118
6.2.1	Elementary devices, ED_{mass}	118
6.2.2	Elementary connections, EC_{mass}	124
6.2.3	Mass based representation	138
6.3	Energy based model development	139
6.3.1	Elementary devices, ED_{energy}	139
6.3.2	Elementary connections, EC_{energy}	142
6.3.3	Energy based representation	145
6.4	Additional model assumptions	146
6.5	Simplified model representation	147
6.6	Discussion	149

7	Model validation	151
7.1	Validation against known behavior	151
7.2	Validation against measurements using real input data . . .	155
8	Estimation of equivalent AlF_3 and energy disturbances	159
8.1	Estimating equivalent AlF_3 disturbance	159
8.2	Estimating equivalent energy disturbance	163
8.3	Discussion of estimation results	166
8.4	The impact of current efficiency	167
8.5	Discussion and concluding remarks	170
9	A novel control strategy	171
9.1	Possible explanations of the observed cell behavior	171
9.2	Brief description of the proposed control strategy	172
9.3	Possible consequences of the proposed control strategy . . .	173
9.4	Superheat as a parameter for control	174
10	Conclusions and suggestions for future work	177
10.1	Conclusions	177
10.1.1	Modeling methodology	177
10.1.2	AlF_3 and bath temperature dynamics	177
10.2	Suggestions for future work	178
10.2.1	Implementation of the modeling methodology	178
10.2.2	Decision support system	178
	References	181
	Appendices	189
A	System classification	191
A.1	Process classification	191
A.1.1	Thermodynamic classification	191
A.1.2	Fundamental transport processes	192
A.1.3	Classification of reactions and generation	192
A.1.4	Classification based on chemical phase	193
A.2	Model classification	193
A.2.1	Knowledge classification	193
A.2.2	Model representations	194
A.2.3	Mathematical classification	194

B	Symbol notation	197
B.1	Topological symbols	197
B.2	Phenomenological symbols	198
B.3	Model assumption symbols	199
C	Model files	201
C.1	Accumulation S-function file	201
C.2	Model behavior file	207
D	Thermodynamic data	211
D.1	General introduction to notation	211
D.1.1	Process in thermodynamics	211
D.1.2	Standard state	211
D.1.3	Standard thermodynamic quantities	212
D.1.4	Reference state	212
D.1.5	Chosen standard state	212
D.2	Enthalpy of reaction and formation, and heat capacity . . .	213
D.3	Tabulated values	215
D.3.1	How to use the tables	215
D.3.2	Approximated thermodynamic data	215
D.4	Enthalpy of mixing, solution and vaporization	219
D.5	Summary of values	220
D.5.1	Examples	221
D.6	The energy and enthalpy balances	223
E	Model simulation	225
E.1	Constant heat loss	225
E.2	Temperature dependent heat loss	226
E.3	Analytical determination of the time constant	227

List of figures

1.1	Sketch of a simple CSTR with one reaction.	3
1.2	Illustration of an aluminum electrolysis cell.	3
1.3	Visualization of the highly multivariable aluminum electro- lysis cell.	4
2.1	PTD of the CSTR example.	21
2.2	Use of composite components in the CSTR example.	22
2.3	PTD of the reactor part.	22
2.4	Elementary topology components related to phenomena sets.	25
2.5	PTD and TRAV of the CSTR example.	29
2.6	Elementary topology components related to phenomena sets.	30
2.7	Mass based PTD and TRAV of the CSTR example.	33
2.8	Reduced energy based PTD and TRAV of the CSTR example.	34
2.9	Relation between species accumulation symbols and mass balance equation structure.	37
2.10	Relation between energy accumulation symbols and energy balance equation structure.	38
2.11	Relation between transport symbols and rate equations.	39
2.12	Relation between topological symbols and constitutive equa- tions.	40
3.1	Possible classification of model assumptions.	51
3.2	Possible structuring of the overall model generation.	52
3.3	Reaction equilibrium modeling.	53
3.4	A precipitation process with several equilibrium reactions.	54

3.5	PTD and TRAV of a vaporizer with assumed chemical equilibrium.	56
3.6	A gas reactor with assumed constant volume and pressure.	57
3.7	Alternative representations of mass based PTD and TRAV of constant amount of species B	57
3.8	Alternative PTD representation of the CSTR.	59
3.9	A topological network applied to the CSTR example.	60
3.10	PTD structure of the CSTR applied in a network.	60
3.11	A possible user interface for the <code>pipe_in</code> connection.	62
3.12	A possible user interface for specification of T_S elements.	64
3.13	A possible user interface for specification of R''' elements.	66
4.1	The embedding of S-functions into S-Function blocks.	69
4.2	The relation between S-function model file, instantiations and S-Function blocks.	70
4.3	The relation between the two S-function files, the instantiations and the additional model files.	71
4.4	A masked S-Function block and its mask menu.	72
4.5	Some useful accessories.	72
4.6	Elementary device symbols	73
4.7	Elementary connection symbols	73
4.8	Relating element symbols	73
4.9	Mass and energy accumulation symbols	73
4.10	Reaction and generation symbols	73
4.11	Transport symbols	73
4.12	The transformation between graphical representation and implementation for topological components.	74
4.13	The implementation of the reactor part of the CSTR.	75
4.14	Visualization of the block diagram concept in Simulink.	75
4.15	Visualization of mapping.	76
4.16	The information flow between phenomenological components.	76
4.17	The implementation of Fig. 4.16.	76
4.18	Rearranging the layout from Fig. 4.17.	77

4.19	Block diagram including the energy balance and dependent state variables.	77
4.20	The inverter and To Workspace block.	78
4.21	The mask menu for specifying the mass balance.	79
4.22	The mask menu for source input.	80
4.23	The mask menu for specifying the energy balance.	80
4.24	The mask menu for flow of species.	81
4.25	The mask menu for heat flow.	82
4.26	The mask menu for volume reaction.	83
4.27	The mask menu for the dependent variables.	83
5.1	Illustration of a prebaked anode cell.	88
5.2	Decomposition of the voltage drop through a cell	91
5.3	Raw material, products and byproducts of aluminum production.	92
5.4	Schematic sketch of sludge.	99
5.5	AlF ₃ additions as a function of days.	99
5.6	Sketch of a phase diagram of the system NaF – AlF ₃	100
5.7	Side ledge profile and self-feeding.	101
5.8	Temperature profile from bath to side ledge.	101
5.9	Illustration of gaseous and particulate fluoride vaporization.	102
5.10	Typical measured resistance vs. alumina concentration.	104
5.11	The derivative of the resistance curve.	104
5.12	The multivariable nature of an aluminum cell.	105
5.13	A typical relation between bath temperature and excess AlF ₃	106
6.1	A topological network applied to the aluminum cell.	117
6.2	Preliminary mass based PTD of the aluminum cell.	118
6.3	Complete mass based PTD of the aluminum electrolysis cell	125
6.4	Visualization of a melting situation.	126
6.5	User interface for Na ₃ AlF ₆ in bath/ledge connection.	128
6.6	PTD and TRAV of AlF ₃ and Al ₂ O ₃ additions.	129

6.7	User interface for Al_2O_3 in feed/bath::sludge connection. . .	130
6.8	Fig. 6.6 revisited, including freezing of Na_3AlF_6	131
6.9	User interface for Na_3AlF_6 in the feed/bath::sludge connection.	132
6.10	PTD and TRAV of primary and back reaction.	135
6.11	User interface of the primary reaction.	136
6.12	User interface of the back reaction.	137
6.13	PTD and TRAV of the aluminum electrolysis cell, mass aspect.	138
6.14	Preliminary energy based PTD of the aluminum cell.	140
6.15	Reduced preliminary energy based PTD of the aluminum cell.	141
6.16	Complete energy based PTD of the aluminum electrolysis cell.	143
6.17	PTD and TRAV of the aluminum electrolysis cell, energy aspect.	145
6.18	Simplified PTD and TRAV of the aluminum electrolysis cell, mass aspect.	148
6.19	Simplified PTD and TRAV of the aluminum electrolysis cell, energy aspect.	148
7.1	A negative step in reference resistance.	152
7.2	A pulse in AlF_3 input.	152
7.3	Bath temperature response.	153
7.4	Excess AlF_3 response.	153
7.5	Side ledge thickness response.	153
7.6	Superheat response.	154
7.7	Convective heat loss from bath to surroundings upwards. . .	154
7.8	Registered AlF_3 input.	155
7.9	Calculated energy input to bath.	156
7.10	Excess AlF_3 response, Case 1	157
7.11	Bath temperature response, Case 1	157
7.12	Heat loss from bath to surroundings upwards, Case 1	157
8.1	Illustration of the equivalent AlF_3 disturbance estimation. .	160
8.2	Estimated equivalent AlF_3 disturbance, Case 2	160
8.3	Bath temperature response, Case 2	161

8.4	Heat loss from bath to surroundings upwards, Case 2	161
8.5	Number of moles of AlF_3 , Case 2	162
8.6	Calculated superheat, Case 2	162
8.7	Side ledge thickness, Case 2	162
8.8	Mass fraction of CaF_2 , Case 2	163
8.9	Illustration of equivalent energy disturbance estimation. . .	163
8.10	Estimated equivalent energy disturbance, Case 3	164
8.11	Excess AlF_3 response, Case 3	164
8.12	Number of moles of AlF_3 , Case 3	165
8.13	Calculated superheat, Case 3	165
8.14	Side ledge thickness, Case 3	165
8.15	Mass fraction of CaF_2 , Case 3	166
8.16	Calculated current efficiency.	168
8.17	Excess AlF_3 response.	169
8.18	Bath temperature response.	169
9.1	The multivariable nature of an aluminum cell, revisited. . .	172
9.2	Al_2O_3 addition during normal operation.	174
9.3	Superheat during normal operation.	175
9.4	Heat loss from bath to surroundings upwards	175
9.5	Registered Al_2O_3 addition.	176
9.6	Superheat based on bath temperature measurement and li- quidus temperature calculation.	176
D.1	The discontinuity in $\Delta_f H_{\text{Al}_2\text{O}_3}^\circ$ as a function of temperature. .	214
D.2	Visualization of discontinuities in $(H_T^\circ - H_{298}^\circ)$	214
D.3	Visualization of the approximation of c_p	216
E.1	Bath temperature response.	225
E.2	Excess AlF_3 response.	225
E.3	Side ledge thickness response.	226
E.4	Superheat response.	226
E.5	Bath temperature response.	226
E.6	Excess AlF_3 response.	226
E.7	Side ledge thickness response.	227
E.8	Superheat response.	227
E.9	Convective heat loss from bath to surroundings upwards. . .	227

List of tables

2.1	Symbols for the elements of the ED set.	18
2.2	Symbols for the elements of the EC set.	18
2.3	Symbols for the elements of the CTC set.	18
2.4	Symbols for the elements of the CE set.	19
2.5	Symbols for the elements of the accumulation set A	26
2.6	Symbols for the elements of the reaction/generation set RG	26
2.7	Symbols for the elements of the transport set T	26
2.8	Set of arrows.	27
3.1	Arrows for equilibrium modeling.	47
3.2	Main symbols for specified (constrained) and forced quantities.	48
3.3	Symbols of constrained phenomenological components.	49
3.4	Symbols of forced phenomenological components of balanced quantities.	49
3.5	Symbols of forced phenomenological components of flows.	49
3.6	Symbols of constrained topological components.	50
5.1	Inputs required to produce 1000 kg aluminum in prebaked cells.	92
5.2	Relation between \mathcal{CE} , $\Delta_r G_{1250}^\circ$ and E°	110
D.1	Approximated thermodynamic data of Al.	217
D.2	Approximated thermodynamic data of AlF_3	217
D.3	Approximated thermodynamic data of Na_3AlF_6	218
D.4	Approximated thermodynamic data of Al_2O_3	218
D.5	Approximated thermodynamic data of CaF_2	219
D.6	Thermodynamic data of species related to aluminum production.	220

Nomenclature

The notation here tries to follow the recommendations given by the International Union of Pure and Applied Chemistry (IUPAC), (Parsons 1974, Whiffen 1979, Cox 1982). The nomenclature list is not complete and the omitted symbols will be explained when first introduced.

The list of thermodynamic data used in this thesis is given in Table D.6.

General notation

Variable	Description	Unit
t	time	s
θ	temperature	°C
T	absolute temperature	K
A	area	m ²
V	volume	m ³
p	pressure	Pa
p_B	partial pressure of B	Pa
M	molar weight	kg mol ⁻¹
R	universal gas constant, $R = 8.314$	J mol ⁻¹ K ⁻¹
Q_a	reaction quotient	
a	activity	
ν	stoichiometric coefficient	
n	amount of substance	mol
j	molar flow	mol s ⁻¹
r	reaction rate	mol s ⁻¹

continued on next page

General notation continued

Variable	Description	Unit
x	molar fraction	-
w	mass fraction	-
c	molar density (concentration)	mol m^{-3}
ρ	mass density	kg m^{-3}
E	total energy	J
E_K	kinetic energy	J
E_P	potential energy	J
ϵ	rate of energy flow	J s^{-1}
U	inner energy	J
H	enthalpy	J
\tilde{H}	molar specific enthalpy	J mol^{-1}
$\tilde{\tilde{H}}$	approximate value of \tilde{H}	J mol^{-1}
\tilde{H}_T	molar specific enthalpy at temperature T	J mol^{-1}
W_s	shaft work	J s^{-1}
Q	heat flow	J s^{-1}
P	electrical power	J s^{-1}
q	area specific heat flow (heat flux)	$\text{J s}^{-1}\text{m}^{-2}$
C_p	heat capacity at constant pressure	J K^{-1}
c_p	specific heat capacity at constant pressure	$\text{J mol}^{-1}\text{K}^{-1}$
\tilde{c}_p	approximate value of c_p	$\text{J mol}^{-1}\text{K}^{-1}$
$\Delta_{\text{fus}}H^\circ$	enthalpy of fusion (melting)	J mol^{-1}
$\Delta_{\text{sol}}H^\circ$	enthalpy of solution	J mol^{-1}
$\Delta_{\text{r}}H^\circ$	enthalpy of reaction	J mol^{-1}
$\Delta_{\text{vap}}H^\circ$	enthalpy of vaporization	J mol^{-1}
$\Delta_{\text{mix}}H^\circ$	enthalpy of mixing	J mol^{-1}
$\Delta_{\text{trs}}H^\circ$	enthalpy of transition	J mol^{-1}
$\Delta_{\text{f}}H^\circ$	enthalpy of formation	J mol^{-1}
$(H_T^\circ - H_{298}^\circ)$	enthalpy at temperature T relative to 298 K	J mol^{-1}
ΔG°	the Gibbs free energy	J mol^{-1}
$\Delta_{\text{f}}G^\circ$	the Gibbs energy of formation	J mol^{-1}
$\Delta_{\text{r}}G^\circ$	the Gibbs energy of reaction	J mol^{-1}

Notation specific to aluminum production

Variable	Description	Unit
w_{CaF_2}	mass fraction of CaF_2	-
w_{AlF_3}	mass fraction of AlF_3	-
$w_{\text{Al}_2\text{O}_3}$	mass fraction of Al_2O_3	-
$w_{\text{Na}_3\text{AlF}_6}$	mass fraction of Na_3AlF_6	-
j_{AlF_3}	molar flow of AlF_3	mol s^{-1}
$j_{\text{Al}_2\text{O}_3}$	molar flow of Al_2O_3	mol s^{-1}
$j_{\text{Na}_3\text{AlF}_6}$	molar flow of Na_3AlF_6	mol s^{-1}
n_{AlF_3}	amount of substance AlF_3	mol
$n_{\text{Al}_2\text{O}_3}$	amount of substance Al_2O_3	mol
$n_{\text{Na}_3\text{AlF}_6}$	amount of substance Na_3AlF_6	mol
n_{CaF_2}	amount of substance CaF_2	mol
$r_{\text{Al}_2\text{O}_3}$	molar generation/consumption of Al_2O_3	mol s^{-1}
r_{Al}	molar generation/consumption of Al	mol s^{-1}
r_{CO_2}	molar generation/consumption of CO_2	mol s^{-1}
r_{CO}	molar generation/consumption of CO	mol s^{-1}
r_{C}	molar generation/consumption of C	mol s^{-1}
R_{meas}	measured resistance over the bath	Ω
I_{meas}	measured current through the cell	A
U_{cell}	overall cell voltage	V
U_{ext}	external voltage	V
U_{bath}	ohmic bath voltage	V
P_{bath}	ohmic energy input to the bath	J s^{-1}
P_{input}	ohmic and non-ohmic energy input to the bath	J s^{-1}
P_{cell}	overall energy input to the cell	J s^{-1}
Q_{conv}	convective heat flow	J s^{-1}
Q_{cond}	conductive heat flow	J s^{-1}
Q_{rad}	heat radiation	J s^{-1}
Δj_{AlF_3}	estimated equivalent AlF_3 disturbance	mol s^{-1}
K_{AlF_3}	estimation constant for AlF_3 estimation	
ΔQ	estimated equivalent energy disturbances	J s^{-1}
K_Q	estimation constant for energy estimation	

continued on next page

Specific notation continued

Variable	Description	Unit
T_{bath}	temperature in bath	K
T_{liq}	liquidus temperature in bath	K
T_0	outer steel shell temperature	K
ΔT	superheat in bath	K
$\mathcal{E}\mathcal{C}$	energy consumption (usually in kWh (kg Al) ⁻¹)	J s ⁻¹ mol ⁻¹
$\mathcal{C}\mathcal{E}$	current efficiency	-
$\Delta\mathcal{C}\mathcal{E}$	change in current efficiency	-
x	fraction of produced Al that back reacts	-
E_{rev}	reversible cell potential	V
E°	standard potential of cell reaction	V
E^{iso}	isothermal potential of cell reaction	V
E_{bath}	decomposition voltage, including overvoltages	V
η_{cc}	cathodic concentration overvoltage	V
η_{ac}	anodic concentration overvoltage	V
η_{ar}	anodic reaction overvoltage	V
z	the number of electrons involved in a reaction	-
\mathcal{F}	Faraday constant, $\mathcal{F} = 96485$	C mol ⁻¹
$A_{\text{bath,ledge}}$	contact area between bath and side ledge	m ²
$A_{\text{metal,cathode}}$	contact area between metal and cathode	m ²
$h_{\text{bath,ledge}}$	heat transfer coefficient between bath and ledge	J K ⁻¹ s ⁻¹ m ⁻²
l_{ledge}	side ledge thickness	m
k_{ledge}	thermal conductivity of side ledge	J K ⁻¹ s ⁻¹ m ⁻¹
l_{wall}	carbon wall thickness	m
k_{wall}	thermal conductivity of carbon wall	J K ⁻¹ s ⁻¹ m ⁻¹
l_{cathode}	cathode thickness	m
k_{cathode}	thermal conductivity of cathode	J K ⁻¹ s ⁻¹ m ⁻¹

Acronyms and abbreviations

Mathematics

ODE	ordinary differential equation
DAE	differential algebraic equation
PDE	partial differential equation

Methodology

PTD	process topology diagram
TRAV	transport, reaction/generation and accumulation view
<i>TC</i>	topological components
<i>ETC</i>	elementary topological components
<i>CTC</i>	composite topological components
<i>ED</i>	elementary device
<i>ED_{mass}</i>	elementary device, mass view
<i>ED_{energy}</i>	elementary device, energy view
<i>EC</i>	elementary connection
<i>EC_{mass}</i>	elementary connection, mass view
<i>EC_{energy}</i>	elementary connection, energy view
<i>T</i>	transport set
<i>T_S</i>	chemical species transport set
<i>T_E</i>	energy transport set
<i>RG</i>	reaction/generation set
<i>R</i>	reaction set
<i>R''</i>	surface reaction set
<i>R'''</i>	volume reaction set
<i>G</i>	generation set
<i>G_E</i>	electric energy generation set
<i>G_M</i>	mechanical energy generation set
<i>A</i>	accumulation set
<i>A_S</i>	chemical species accumulation set
<i>A_E</i>	energy accumulation set
<i>S</i>	base set of species
<i>E</i>	base set of energy
<i>P_D</i>	phenomena related to devices
<i>P_{D,mass}</i>	phenomena related to devices, mass view
<i>P_{D,energy}</i>	phenomena related to devices, energy view
<i>P_C</i>	phenomena related to connections
<i>P_{C,mass}</i>	phenomena related to connections, mass view
<i>P_{C,energy}</i>	phenomena related to connections, energy view

Aluminum

ACD	anode-cathode-distance
pr	primary reaction
br	back reaction
opt	optimum
sat	saturation

Terminology

CSTR	Continuous Stirred Tank Reactor
liquidus temperature	freezing point of bath at current composition
superheat	temperature difference between bulk bath temperature and liquidus temperature
excess AlF_3	mass fraction of AlF_3 , also termed acidity
ballistic simulation	simulation without state estimation
long-term prediction	simulation of a model with a time horizon of days and weeks

Symbols used in thesis layout

◇◇◇	symbol that ends Comments
■	symbol that ends unnumbered sections
▲	symbol that ends Examples

Chapter 1

Introduction

1.1 Motivation and background

The work presented in this thesis is motivated from both the academic and industrial points of view. The academic part is concerned with the development of a modeling methodology for chemical unit processes in general, whereas the industrial part focuses on the modeling of an aluminum electrolysis cell in particular.

1.1.1 Modeling of chemical processes

In the process industries, a lot of effort is put into the development of both static and dynamic mathematical models of unit processes. Common for many modelers is the tendency to start from scratch each time a new model is to be developed. There are several reasons for this strategy. One is that existing models do not satisfy the present problem definition, and another is that the support for changing only portions of an existing model, without achieving inconsistency, is lacking. Besides, many companies in the process industries in Norway, for example, look upon the modeling process as a means for modelers to learn and get valuable insight of a process (Foss *et al.* 1997). Hence, modeling from scratch implies that modelers themselves are aware of assumptions made during the modeling phase. This is important, since documentation of model assumptions is often lacking.

There are several modeling aids or tools available today. Many of these tools are related to plant modeling where the modeling problem consists of selecting models of unit processes from a library, connecting them together and choosing parameter values. On the other hand, model *development*

of non-standard, complex *units* still remains a difficult activity (Pantelides and Britt 1994). This thesis focuses on a framework supporting the development of such units. As there is a general focus on processes where the *inner* structure and behavior is complex, a representation supporting this is needed.

For plant modeling, the geometry of process units is often given by the physical arrangement of each unit, and the pipes are readily given. However, for unit processes the geometry of the inner structure, i.e. the physical placement of each chemical phase relative to each other, is much more interconnected in that each phase depends directly on the extent of other phases. In addition, as the number of pipes connected to a plant unit is determined by the physical arrangement, the number of pipes, or actually *boundaries*, within a unit process may change from one model to another depending on the model assumptions. This implies that a modeling methodology for unit processes should aim at being flexible and at the same time, produce consistent models.

A multicomponent mixture flowing in pipes will typically be characterized by an overall *volumetric* flow rate. Moreover, if the unit is believed to be well mixed, the state of the outgoing flow will be similar to that of the unit. On the other hand, the flow of compounds between phases *within* a unit process does *not* have the characteristics of pipe flow, and hence, each compound will often have separate flow characteristics. Furthermore, even if a well mixed situation is assumed for a phase, all the species existing inside the phase do not necessarily flow in every possible direction. It is believed that these characteristics need special consideration in the development of a modeling methodology for unit processes.

In order to develop consistent mathematical models and validate the assumptions used, it is often of crucial importance for modelers to enter into a fruitful discussion with different process domain experts. A representation based on detailed equations is not necessarily the best way to obtain efficient interaction. Hence, in many cases, the best way to support this communication is to represent the model graphically in some sense.

In considering a chemical reactor as a case, one of the most interesting aspects would be the reactions occurring. This kind of information is often given in the form $A + B \rightarrow C$, which is an understandable abstraction of this knowledge. In addition, assumptions regarding stirring, input and output flows and heat loss could be incorporated. Visualizing a CSTR¹ with emphasis on the above factors could result in a sketch similar to Fig. 1.1.

¹Continuous Stirred Tank Reactor.

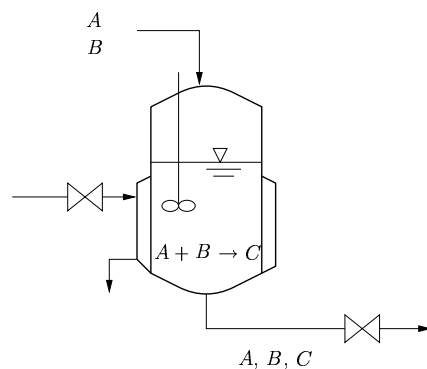


Figure 1.1: Sketch of a simple CSTR with one reaction.

The information modelers or process engineers can extract from Fig. 1.1 can be enough to generate the structure of a set of balance equations in a mathematical model description. In order to make a complete model, additional information is needed such as the activation energy for the reaction. The CSTR is an example of a relatively simple chemical process. If a unit process is given in the form of an aluminum electrolysis cell as shown in Fig. 1.2, where there are several, partially unknown complex reactions together with complex mass and heat transfer between phases, producing a consistent structure of balance equations becomes much more difficult.

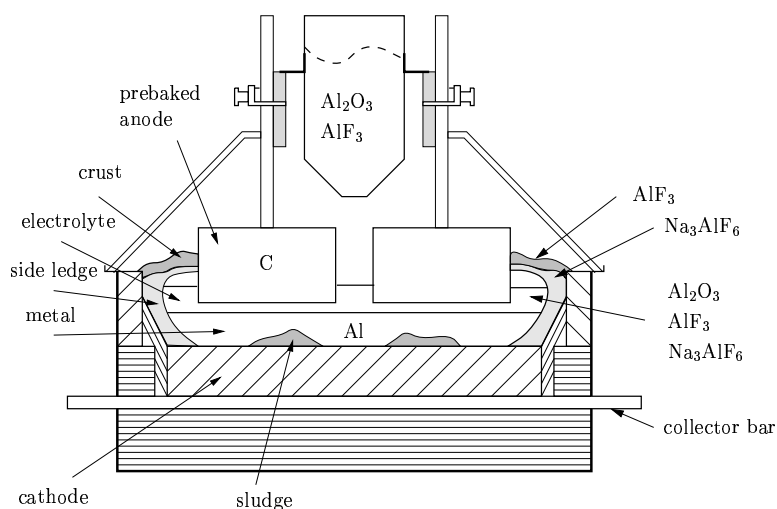


Figure 1.2: Illustration of an aluminum electrolysis cell.

1.1.2 AlF_3 and bath temperature dynamics

The aim of the aluminum industry is to achieve stable cell conditions during normal operation. This will reduce energy consumption, prolong cell life and minimize the use of expensive additions like AlF_3 and Na_2CO_3 used in present control practice. Such stable cell conditions are only partially achieved when *i*) alumina additions are used to control the alumina concentration, *ii*) anode beam movements are used to keep the measured resistance at a reference level, and *iii*) AlF_3 additions are used to control the excess AlF_3 .

From industrial cells it is experienced that bath temperature and excess AlF_3 have unpredictable behavior in that sudden changes occur, even if the preceding AlF_3 additions have been close to the average consumption. When the excess AlF_3 is low and the bath temperature is high, the corrective action is usually to add more AlF_3 . In spite of that, the expected increase in excess AlF_3 is often delayed for several days, and more AlF_3 is added. This over-compensation results in oscillations in excess AlF_3 (typically between 7 and 14 wt.%), which is detrimental from both operational and economic points of view.

The question is then whether *i*) the delayed increase in excess AlF_3 *causes* the drop in temperature (due to lowered liquidus temperature, increased superheat and increased side ledge melting), or *ii*) the delayed increase in excess AlF_3 is *caused* by the temperature drop (due to reduced superheat and increased side ledge freezing). It is a question of cause and effect within the cell. Nevertheless, the explanation of *why* there seems to be a delay is still not resolved.

Due to the lack of continuous, direct or indirect measurements of excess AlF_3 in the bath, the level is determined by time-consuming sample preparation and chemical analyses. The excess AlF_3 is not only dependent on the amount of AlF_3 dissolved in the bath, but also on the amount of *all* other compounds, especially the thermal driven freezing and melting of Na_3AlF_6 . Therefore, the control of excess AlF_3 becomes a highly multivariable control problem. This is illustrated in a schematic manner in Fig. 1.3.

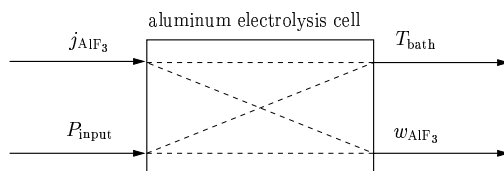


Figure 1.3: Visualization of the highly multivariable aluminum electrolysis cell.

The control inputs are AlF_3 additions, j_{AlF_3} , and energy input to the bath, P_{input} . This energy input is the energy needed to reduce Al_2O_3 and the resistive energy generated in the bath. The measurements are excess AlF_3 , w_{AlF_3} , and bath temperature, T_{bath} . Other aspects having impact on the control problem are the lack of detailed information of the fluoride and sodium content in alumina, the rate of sodium penetration into the cathode, the amount of fluoride evaporating from the bath and the amount of AlF_3 present in the side ledge and sludge. In addition, variations in heat loss from the bath, variations in current efficiency, creation and deformation of crust, anode changing, and tapping of the metal and bath also have impact on the control problem.

Due to a lack of basic understanding of the AlF_3 variations, present control algorithms are based on analyses of historical data and practical experience. Despite new and improved control strategies, the fluctuations in the excess AlF_3 are considered high in most cell lines. Hence, the motivation for focusing on AlF_3 and temperature dynamics is primarily to gain insight into the phenomena of the process, and secondly to use this knowledge to improve cell control. This again may result in increased current efficiency and reduced energy consumption.

1.2 Previous work

A considerable amount of work is published on both process modeling related subjects and on aluminum production in general. The number of publications focusing on AlF_3 and temperature control found in the *open* literature is, however, small compared to the number of contributions on other topics of aluminum production. This may be due to confidentiality restrictions imposed by the various smelter companies on this type of information.

1.2.1 Unit process modeling and representation

Most of the literature available on process modeling concerns issues of plant modeling, as described in Sec. 1.1.1. Some examples of existing modeling tools are MODEL.LA (Stephanopoulos *et al.* 1990), OMOLA (Mattson and Anderson 1992, Nilsson 1993), CADAS (Eikaas 1990), ASCEND (Piela *et al.* 1991), gPROMS (Pantelides and Barton 1993) and Dymola (Elmqvist *et al.* 1993). These tools may be classified as *i*) general modeling languages covering chemical, mechanical and electrical modeling, or *ii*) as process modeling languages intended for chemical modeling only. Most tools are

supported by object-oriented features, and several also support the modeling of hybrid systems, i.e. combined continuous time and discrete event systems. Another feature of these tools is the use of the modularization principle, i.e. the organizing of the plant model in a hierarchy of topological submodels at several levels. For a more thorough review of this literature, cf. Marquardt (1994).

Other contributions focusing on modeling aids include the thesis by Telnes (1992) which describes the modeling of dynamic processes based on elementary physics. The emphasis is on defining phenomenological characteristics of the system. Another approach is the hybrid phenomena theory (HPT) (Woods 1993) which defines a representation in which knowledge of physical interaction may be expressed.

On the subject of unit process modeling, one of the first attempts to build process modules from a set of building blocks (or primitives), is reported in Preisig *et al.* (1989). This contribution describes the modeling of physical-chemical-biological systems, and the primitives are thermodynamic systems and reaction parts. The representation is a mixture of information and physical based knowledge. Further, knowledge is divided into hard and soft knowledge, where hard knowledge is factual and soft knowledge is empirical. This work is continued in Preisig *et al.* (1990).

The contribution of Preisig (1994) discusses the species distribution in a network of system components. The modeling approach is to include all species and reactions to form the *maximum* set, and reduce this set by including more process knowledge and thereby excluding relations in the maximum set.

Dieterich and Eigenberger (1995) shows how to generate equations for one dimensional problems from first principles. The equations are generated from a data bank of general equations of change (see Bird *et al.* (1960)) on the basis of the model assumptions. This involves a symbolic manipulation using Maple, reducing the errors introduced by modelers in the manipulation phase. Other papers focusing on the task of automatic generation and representation of model equations are Perkins *et al.* (1994) and Bogusch and Marquardt (1995). As a means to improve the modeling activity, a modeling support system is described in Vázquez-Román *et al.* (1996). A graphical user interface (GUI) is developed in order to include model assumptions in the form of answering questions regarding the physical and chemical behavior of the system, and not in the form of mathematical equations. To guarantee consistency of the generated models, several modeling rules are integrated in the GUI.

A methodology for automatic generation of problem specific process models to be used in simulation related to *process design* and *operation* is presented

in Jensen and Gani (1996). The system generates the problem specific model equations from a reference model which contains all the necessary terms for modeling a chemical process. The model generation approach is based on user defined control shells and a reference model. From a description of control shells, the algorithm either neglects or expands the various terms of the reference model. Besides the balance equations, the reference model also includes constraint equations. These equations are grouped into closure, equilibrium and boundaries constraints.

A paper by Perkins *et al.* (1994) describes the automatic generation of a mathematical model from a purely physical description. This contribution discusses the problem related to high index model formulation through equilibration of phases and appearing and disappearing phases. It is stated that there is a need to provide language for the user to describe the relevant assumptions and provisions.

Another approach using a graphical user interface is the Powersim modeling tool (ModellData 1994). The user interface represents the differential and algebraic equations (including parameters) graphically, which makes it easy to use. Among more recent work in the area of unit process modeling is the thesis by Wasbø (1996). The modeling methodology presented in that thesis and the one in this thesis is based on joint work in Drengstig *et al.* (1996). While Wasbø (1996) focuses on data structures and how to fit the methodology in an object-oriented environment, the focus in this thesis is on the graphical user interface.

A common feature of most contributions is the limitation to lumped parameters system.

Lately there has been a focus on the *process of modeling*, i.e. how to structure the model development itself. It has been stated that understanding the nature of the modeling process, and developing a meta-model for that process are important future goals for process systems engineers (Ponton 1995). Some general properties of the modeling process is presented in Lohmann and Marquardt (1996), as means for further investigation into the modeling process and development of computer-aided modeling tool supporting the modeling process. An industrial approach to the process of modeling is presented in Foss *et al.* (1997). A set of experienced modelers from two different countries are interviewed with respect to industrial practice and comprehension of the modeling process.

1.2.2 AlF_3 and bath temperature control

The issue of AlF_3 and temperature control has been intensively discussed in the aluminum community for the last decade. As mentioned in Sec. 1.1.2,

the aluminum industry often experiences time delays from AlF_3 additions to the observed response in excess AlF_3 . The reason for this delay is not fully understood, and focus has been on explaining *where* the AlF_3 resides inside the cells. Several hypotheses have been presented, based on both laboratory experiments using small scale cells under ideal conditions and experience with industrial cells. From laboratory studies it has been observed that AlF_3 dissolves much faster than Al_2O_3 (Rolseth 1997). A model where sodium and fluoride containing compounds are deposited in the cathode was suggested by Entner (1992). This could in effect be the same as having a sludge phase on the cathode. The model is used in a control strategy for AlF_3 , and it is further developed in Entner (1993). However, the bath temperature fluctuations using the AlF_3 controller were not reduced significantly, and a control scheme for both excess AlF_3 and the bath temperature was developed by Entner (1995). This is further refined by Entner and Gudmundsson (1996).

Based on the observed correlation between the bath temperature and excess AlF_3 , Desclaux (1987) compared two control strategies, i.e. AlF_3 additions based on *i*) bath composition analyses and *ii*) temperature measurements. One conclusion is that both control practices are equivalent, though temperature measurements are easier, faster and more precise than the bath composition analyses. The success of this control strategy is, however, dependent on a fast equilibrium between the composition of the bath and its temperature. Wilson (1992) developed and implemented a control strategy where AlF_3 additions were based on bath temperature and cell age only. The performance is reported to be good, handling a range of operational changes.

In addition to bath composition analyses, bath temperature and cell age, other cell variables and parameters can be used in the AlF_3 control strategy. Peyneau (1988) describes a control strategy developed by Aluminium Pechiney using up to 8 different cell parameters for bath composition control, with the energy induced by anode effects being the most important additional parameter.

It is known that the energy balance, in addition to AlF_3 additions, also affects the excess AlF_3 through the interaction with the side ledge. In order to investigate the effect of the energy balance on the excess AlF_3 , Taylor (1992) performed a simple input/output calculation of AlF_3 and showed that the changes in the mass balance for AlF_3 cannot explain the observed changes in excess AlF_3 . Therefore, one conclusion is that the energy balance is more important than previously expected.

None of the contributions discussed above give explanations to the underlying cause of the cell behavior that is experienced.

Very few contributions have concentrated on the dynamic simulation of an aluminum electrolysis cell. Taylor (1991) focused on the development of static and dynamic energy balance models for aluminum cells. The approach was to divide the cell cavity into several small CSTRs representing parts of the bath. In Tabsh *et al.* (1996) a dynamic mass and energy balance model of 11 chemical species is presented. The model is simulated and verified against temperature, alumina concentration and excess AlF_3 . This model is not used for control purposes.

As mentioned in the beginning of Sec. 1.2, there are numerous contributions on other topics of aluminum electrolysis. The alumina concentration control naturally features in subjects related to cell control. Over the years, several control strategies are suggested in the literature, examples include Gran (1980), Borg *et al.* (1986), Robilliard and Rolofs (1989), and Balchen (1992).

1.3 Contributions of the thesis

- **A modeling methodology for chemical unit processes**

A modeling methodology based on a graphical process representation scheme is developed. The main application area is to lumped parameters system of complex unit processes. This work is reported in Drengstig *et al.* (1996) and Drengstig *et al.* (1997d). The inclusion of different model assumptions is emphasized. A prototype version of a modeling tool is implemented in the Matlab and Simulink environment.

- **A dynamic model of an aluminum electrolysis cell**

Using the modeling methodology, a dynamic mathematical model of an aluminum electrolysis cell with focus on excess AlF_3 and bath temperature dynamics is developed. This work is reported in a preliminary version in Drengstig and Foss (1995) and later in Drengstig *et al.* (1997c). Based on model validation, the following contributions are presented:

- *An AlF_3 control strategy*

The results demonstrate that optimal control of excess AlF_3 and bath temperature is obtained by using an almost constant AlF_3 input and energy inputs to compensate for the variations. This is reported in Drengstig *et al.* (1997b).

- *A study on the long-term prediction properties*

In order to be useful in simple dynamic models, current efficiency models are often limited to consider only bath composition and bath temperature. On the other hand, due to the

inherent *positive* feedback from the back reaction to bath temperature, satisfactory long-term *prediction* of bath temperature and excess AlF_3 is hypothesized as impossible with a current efficiency model considering only bath composition and bath temperature. This work is reported in Drengstig *et al.* (1997a).

1.4 Outline of the thesis

The structure of this thesis reflects the dual focus of the approach used in this work.

- **Part I:** This part concerns the development and implementation of the modeling methodology. It is divided into the following chapters:
 - **Chapter 2:** The development of a formal graphical based process representation is presented in this chapter. The representation is divided into a topological and a phenomenological abstraction, and this again is divided into a mass based and an energy based representation. The relation between graphical symbols and model equations is shown.
 - **Chapter 3:** Different kinds of model assumptions are discussed in this chapter. The relationship between these assumptions and the graphical representation is addressed. Further, it is stressed that some assumptions should be made prior to the modularization and others after. The modeling process using the proposed representation is highlighted through examples.
 - **Chapter 4:** This chapter describes the implementation of the methodology in Matlab (The MathWorks 1992a) and Simulink (The MathWorks 1992b), and how the representation is adapted in order to fit the implementation environment.
- **Part II:** This part concerns the development of a dynamic model of an aluminum electrolysis cell. It is divided into the following chapters:
 - **Chapter 5:** A process description is given, with basic thermodynamics for electrolytic cells.
 - **Chapter 6:** The modeling methodology is employed to develop and represent a comprehensive dynamic mathematical model of the aluminum cell. Based on model assumptions, this model is reduced to a simpler one which is used in the following chapters.
 - **Chapter 7:** In this chapter, the simple dynamic model is validated against known behavior and real data.

- **Chapter 8:** Based on the validation result, estimation of equivalent AlF_3 and energy disturbances is performed, using real data of excess AlF_3 and bath temperature.
- **Chapter 9:** A novel control strategy is suggested, and the impact of current efficiency models on the long-term prediction properties of dynamic models is discussed.
- **Conclusions and suggestions for future work:** These are presented in **Chapter 10**.

Part I

Modeling methodology

Chapter 2

A formal graphical based process representation

This chapter defines a consistent and formal graphical representation of chemical unit processes. The topological and phenomenological abstraction processes are introduced in Secs. 2.2 and 2.3, respectively. These sections are based on Drengstig *et al.* (1996), and this contribution was also the basis for the work regarding modeling methodology presented in the thesis by Wasbø (1996).

A further refinement of the methodology is given in Sec. 2.4, where a separation of the representation is proposed. This section is based on Drengstig *et al.* (1997d). A conceptual interpretation of the symbols is given in Sec. 2.5, and the relation between symbols and equations is discussed in Sec. 2.6.

For background knowledge to the topological and phenomenological abstraction processes, the system classification in App. A is referred to.

2.1 Introduction

As described in Marquardt *et al.* (1993), the structuring of systems in general and mathematical models in particular, can be oriented along two coordinates; the *structural* and *phenomenological* axes. Further, the development of mathematical process models can be achieved via two *abstraction* processes: structural and phenomenological. Hence, the abstraction processes can be oriented along two similar coordinates. These axes cannot be regarded as independent. Changing the structure (topology) of a system may influence the phenomena taking place in the system components. Changing the phenomena in a system component is, however, less likely to influence the topological structure of the system.

2.2 Topological process abstraction

The proposed formalism of Marquardt (1994) that uses devices and connections for representing the topological abstraction of chemical processes, forms the basis for the approach in this thesis. Similar concepts are found in Perkins *et al.* (1994) and Stephanopoulos *et al.* (1990). The devices represent control volumes, i.e. having accumulation properties, while a connection represents a coupling of control volumes, without accumulation, though involving some kind of flow. The process is decomposed into components represented by devices and connections at several levels.

2.2.1 Definitions

The following definitions of levels of abstraction and modeling components are advocated:

Definition 2.1

Topological process abstraction means the abstraction of a system into a network of topology components.

Definition 2.2

Elementary topology components means the parts of a system represented by connections and devices. *Composite topology components* are components containing a set of composite and/or elementary topology components, though the composite topology components are at the *lowest* level composed of elementary devices and connections. Only the elementary topology components contain a phenomenological description. *Topology components* is the term covering both elementary and composite components.

2.2.2 Topological sets

Based on the above definition of topology components, different sets of topological components are defined. The set of elementary topological components, *ETC*, consists of both elementary devices, *ED*, and connections, *EC*, i.e. $ETC = ED \cup EC$. Furthermore, the set of composite topological components, *CTC*, consists of both composite devices, *CD*, and connections, *CC*, i.e. $CTC = CD \cup CC$. The overall set of topology components, *TC*, is therefore $TC = ETC \cup CTC$.

There is no unique approach for the modularization of chemical processes. The basis may vary from chemical phase to temperature zone modularization within the same model, depending on the process at hand and the scope of the model. The approach employed in this thesis is to choose the thermodynamic phase as a basis for modularization.

Chemical processes are typically affected by control inputs influencing the overall behavior of the plant. The controllers can be viewed upon as being a special case of topology components. In Marquardt (1994) this is defined as *abstract signal transformers*. Other specializations of topological components are terminals, i.e. components that represent the sources and the sinks of the process. This might be the feed, the drain or the surroundings. The elements of ED can therefore be found; $ED = \text{phase} \cup \text{source/sink} \cup \text{controller}$. Note that the sources and sinks do not share the properties of a phase in that they are believed to be infinite in size.

Similar to phase boundaries represented as EC , there is a “boundary” between processes and controllers, i.e. the signal wires. Hence, a signal connection is defined for that purpose. The elements of EC can be found; $EC = \text{phase boundary} \cup \text{signal connection}$. In order to connect the topology components into a complete network, different links, or lines, are introduced. The component connecting line connect phases, phase boundaries and elements of CTC , whereas controllers and signal connections are connected by signal lines. Finally, the relation element relates the topological components to possible higher level composite components. The set of connecting elements are therefore $CE = \text{component connecting line} \cup \text{signal line} \cup \text{relation element}$.

Comment:

The choice of thermodynamic phase as a basis for modularization is similar to the approach found in Preisig *et al.* (1989) which also has been elaborated by Perkins *et al.* (1994). An alternative choice is found in Telnes (1992), where the basis is a homogeneous substance, implying that a fluid with evenly distributed bubbles is considered a phase. The *generalized phase* of Marquardt (1992) comprise one or more thermodynamic phases. The choice of thermodynamic state as a basis is believed to be simpler in that each phase can be characterized completely in terms of a small, standard set of quantities such as component holdups and internal energy (Pantelides and Britt 1994). Hence, the control volumes in this thesis are termed devices according to Marquardt (1994), though the meaning of them are more related to the phases in Preisig *et al.* (1989) and Perkins *et al.* (1994). Nevertheless, model assumptions affect the level of modularization, and deviations from the phase concept will exist. This is discussed in Ch. 3.




◇◇◇

2.2.3 Topological component symbols

Well designed visual information (graphical displays being one example) is normally better absorbed than information given in other ways¹. In a control room in a plant, or in discussions between experts with different disciplinary backgrounds, it is important to have a good exchange of information. For this reason, a useful idea is to define a concept for graphical visualization of information. Symbols for the topological components based on the sets in Sec. 2.2.2 are defined as follows:

The symbols for the elements of the *ED* set are given in Table 2.1.

Table 2.1: Symbols for the elements of the *ED* set.

elements:	phase	source/sink	controller
symbol:			

In order to separate elements of the *ED* set from elements of the *EC* set, the symbols for the latter elements use rounded corners as shown in Tables 2.2 and 2.3, respectively.

Table 2.2: Symbols for the elements of the *EC* set.


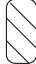

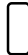
elements:	phase boundary	signal connection
symbol:		

Table 2.3: Symbols for the elements of the *CTC* set.

elements:	composite device	composite connection
symbol:		

¹That is, unless the ability to see has been significantly impaired.

The symbols for composite components in Table 2.3 are similar to the elementary component symbol, though indicated with a thicker border to be separable. A complete symbol base includes symbols for the connecting elements, *CE*. These are shown in Table 2.4.

Table 2.4: Symbols for the elements of the *CE* set.

elements:	component connecting line	signal line	relation element
symbol:	=	→	○

These symbols are to be employed in a Process Topology Diagram (PTD) for topological component representation.

2.2.4 Aggregation vs. decomposition

Aggregation, i.e. the bottom-up approach, is the *grouping* of elementary and/or composite topology components into composite components. If only parts of a model are modeled very detailed, aggregation can be a useful functionality in order to represent the entire process topology on the same level of abstraction. Consequently, aggregation is used for *representation* purposes, and does not change the underlying model equation *structure*.

The opposite of aggregation is decomposition, i.e. the top-down approach. Elementary components are *replaced* by composite components which are decomposed into elementary topology components on the next level of abstraction. The decision about when to end the decomposition is basically determined by the modeling assumptions and the accuracy of the model. Therefore, decomposition is *not* motivated from a representation point of view, but rather to refine the model equation structure.

Comment:

The choice of thermodynamic phase as a *basis* for modularization implies that the phase in this context is non-decomposable. Nevertheless, this section describes decomposition as a method to refine the model, which is contradictory to the non-decomposable phase. Consequently, the model can only be refined if the original decomposition was subjected to model assumptions which produced a coarse decomposition of the process². Furthermore, this actually implies another form of aggregation, i.e. the *replacement* of a detailed part of a model represented as *several* elementary

²This will be further discussed in Ch. 3.

components with a coarse one represented as *one* elementary component. This is not to be confused with the aggregation described above.

◇◇◇

2.2.5 Modeling rules

The rules for constructing the network of composite and elementary topology components are simple. They are divided into **connectivity**, **content**, and **aggregation** rules for *ETC* and *CTC*.

Connectivity rules for *ETC* and *CTC* elements:

RULE 1. A connection must be linked to *at least two* devices.

RULE 2. A device can stand alone, or be linked to an unrestricted number of connections.

RULE 3. All devices must be separated by connections and vice versa.

Content rules for *ETC* elements:

RULE 4. The *ED* elements describing the chemical process itself (i.e. no control systems etc.) represent a *single phase*. Multiple phases are thus described by composite topological components.

Aggregation rules for *CTC* elements:

RULE 5. *CTC* elements cannot be empty, stand-alone components. They are aggregations of *TC* elements. On the lowest *TC* level, a *CTC* element must consist of *ETC* elements only.

RULE 6. *CC* elements are aggregated in such a way that only connections form the interface towards other *TC* elements.

RULE 7. *CD* elements are aggregated in such a way that only devices form the interface towards other *TC* elements.

The implication of RULE 5 is that *CTC* elements cannot be recursive. That is, a *CTC* element cannot contain (an instance of) itself.

Example 1

To exemplify the representation, consider the simple CSTR in Fig. 1.1. This is, however, not an example process that gives the methodology credit. The usefulness of the methodology will thus be demonstrated on the aluminum cell in Ch. 6. The reasons for using the CSTR are that it is a process most chemical and control engineers understand thoroughly, and its complexity

is appropriate to demonstrate the methodology without an extensive, additional process description.

The following elementary devices can be identified from Fig. 1.1:

$$ED = \{\text{cooling}, \text{reactor_content}, \text{source_1}, \text{source_2}, \text{sink_1}, \text{sink_2}\}, \quad (2.1)$$

and the following elementary connections:

$$EC = \{\text{pipe_in}, \text{pipe_out}, \text{valve_1}, \text{valve_2}, \text{wall}\}. \quad (2.2)$$

The PTD for this unit process could be as in Fig. 2.1.

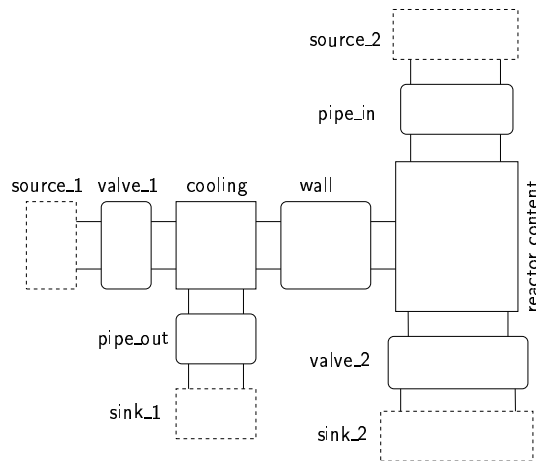


Figure 2.1: PTD of the CSTR example.

According to the choice of modularization basis, the wall should have been a device. Thus, the representation of the wall in Fig. 2.1 actually visualizes the underlying assumption that the wall dynamic is not considered important. In addition, the vapor phase of the reactor is neglected. Consequently, these examples demonstrate the level of assumptions made prior to the decomposition, and this will be discussed further in Ch. 3.

In order to further exemplify the representation, consider a composite device, CD , of the cooling, reactor_content and wall system:

$$CD = \{\text{reactor}\}. \quad (2.3)$$

This will give the PTD shown in Fig. 2.2.

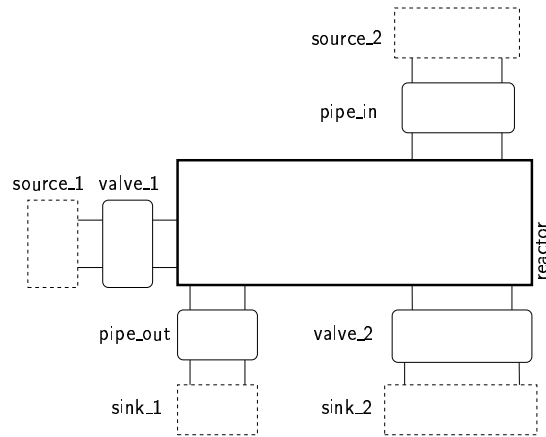


Figure 2.2: Use of composite components in the CSTR example.

The composite device reactor is given in Fig. 2.3.

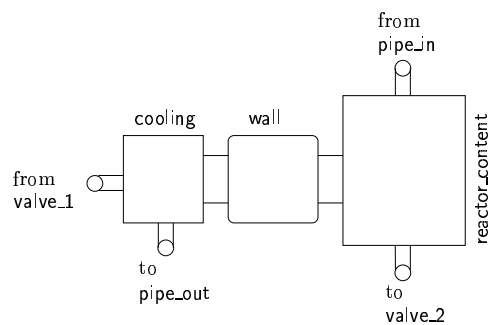


Figure 2.3: PTD of the reactor_content, wall and cooling part.

The *CE* elements indicated in Fig. 2.3 are believed to be generated automatically. ▲

2.3 Phenomenological process abstraction

The definition of phenomenological process abstraction advocated here is given in Sec. 2.3.1. This has resemblance to the definition of *Process quantities* in the behavioral description defined by Marquardt (1994) and to the one presented by Woods (1993). On this abstraction level, the focus is on the phenomena taking place.

2.3.1 Definitions

Similar to the definition of topological process abstraction and topology components, phenomenological process abstraction and phenomenological components may be defined.

Definition 2.3

Phenomenological process abstraction means the abstraction of the behavior of topological components into a network of phenomenological components representing chemical species, energy and phenomena.

Definition 2.4

Phenomenological components means components that represent the phenomena taking place within topological components.

2.3.2 Phenomenological sets

An important tool in representing and understanding a process is a rigorous description of the process characteristics. Based on the process classification in App. A, the fundamental process characteristics that are being considered can be divided into three categories:

1. TRANSPORT
2. REACTION/GENERATION
3. ACCUMULATION

These generalized characteristics are closely related and take place in a vast number of systems, i.e. all systems involving dynamics. This classification is certainly not a new encounter. Since only the lowest topological level contains a phenomenological description, the phenomenological sets are restricted to *ETC* only.

In the context of chemical processes, the TRANSPORT, REACTION/GENERATION and ACCUMULATION phenomena are related to the following *extensive* quantities:

- *mass*
- *energy*
- *momentum*

In the following, momentum is not considered. The quantity *mass* is the mass of each chemical compound or element, and it is henceforth termed *chemical species*. A base set containing all the species used in the modeling is defined, $S = \{\text{chemical species}\}$. The size of S will vary, depending on the modeling task. In addition, a base set of the energy must be included; $E = \{\text{energy}\}$. Normally, the E -set will contain only one element. These two sets, even if they describe different aspects of the process have some properties in common. Both will have the ability to accumulate in control volumes, and to flow across control volume boundaries.

The S and E sets, the topological sets defined in Sec. 2.2.2 and the three fundamental process characteristics above are now used to identify the following sets:

- The TRANSPORT phenomena are described in Sec. A.1.2. Applied to the elements of S and E , i.e. $\text{TRANSPORT}(S, E)$, the following set is identified:

$$T = \text{chemical species transfer} \cup \text{energy transfer} = T_S \cup T_E.$$

- The REACTION/GENERATION phenomena are described in Sec. A.1.3. The kind of a reaction is dependent on the type of elementary topological component (ETC) in which the reaction occurs. The following sets are identified:

$$R = \text{surface reaction} \cup \text{volumetric reaction} = R'' \cup R''' \text{ and}$$

$$G = \text{electrical energy generation} \cup \text{mechanical energy generation}$$

$= G_E \cup G_M$, where $RG = R \cup G = R'' \cup R''' \cup G_E \cup G_M$. A surface reaction is allowed to take place only on surfaces, defined in EC , while a volumetric reaction is allowed only in ED . The number of apostrophes (') indicates the spatial dimension of the space the reaction occurs in.

- By applying the ACCUMULATION to the elements of S and E , i.e. $\text{ACCUMULATION}(S, E)$, the following set is identified:

$$A = \text{chemical species accumulation} \cup \text{energy accumulation} = A_S \cup A_E.$$

Note that all the subsets of T , RG and A , respectively, are disjoint:

$$T_S \subset T, \quad T_E \subset T \quad \text{and} \quad T_S \cap T_E = \emptyset$$

$$R \subset RG, \quad G \subset RG \quad \text{and} \quad R \cap G = \emptyset$$

$$A_S \subset A, \quad A_E \subset A \quad \text{and} \quad A_S \cap A_E = \emptyset$$

In addition, the subsets of R and G are also disjoint:

$$R'' \subset R, \quad R''' \subset R \quad \text{and} \quad R'' \cap R''' = \emptyset$$

$$G_E \subset G, \quad G_M \subset G \quad \text{and} \quad G_E \cap G_M = \emptyset$$

According to the definition of *elementary topological components*, the elements of the set A are restricted to elementary devices. Similarly, the elements of T are restricted to elementary connections. The set RG was identified by employing the REACTION/GENERATION on ETC , and it is differentiated into elements related to both elementary devices and connections. Therefore, the overall set of phenomena related to elementary devices, P_D , and the overall set of phenomena related to elementary connections, P_C , are defined as follows. The P_D set can be written as

$$P_D = A \cup RG \setminus \{R''\} = A \cup R''' \cup G, \quad (2.4)$$

and P_C as

$$P_C = T \cup RG \setminus \{R''' \cup G_M\} = T \cup R'' \cup G_E. \quad (2.5)$$

The relationship between these sets and elements of ETC is depicted in Fig. 2.4.

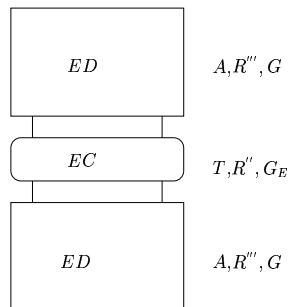







Figure 2.4: Elementary topology components related to phenomena sets.

2.3.3 Phenomenological component symbols

Similarly to the definition of symbols for the topological components in Sec. 2.2.3, symbols for the phenomenological components are defined. The symbols for the elements of the subsets of A are shown in Table 2.5

Table 2.5: Symbols for the elements of the accumulation set A .

Subset	Phenomenological components
$A_S \subset A$	gas  liquid  solid  unspecified 
$A_E \subset A$	

The general symbol for chemical species accumulation, A_S , is a square and the symbol for energy accumulation, A_E , is triangular. Besides, the aggregate state of the species is indicated on the symbol. This is redundant information since topological components are identified based on phase. However, the use of these symbols is optional, and the unspecified symbol for chemical species accumulation might be preferred.

The symbols for the elements of the subset of RG are shown in Table 2.6. The general symbol for a reaction is a circle, and for energy generation a hexagon.

Table 2.6: Symbols for the elements of the reaction/generation set RG .





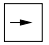




Subset	Phenomenological components
$R \subset RG$	surface  volumetric 
$G \subset RG$	electrical  mechanical 

Table 2.7: Symbols for the elements of the transport set T .



Subset	Phenomenological components
$T_S \subset T$	convection  diffusion 
$T_E \subset T$	convection  conduction  radiation 

The symbols for the elements of the subsets of T are shown in Table 2.7. Similar to the accumulation symbols in Table 2.5, squares and triangles are used for chemical species flow and energy transfer, respectively. In order to differentiate between the type of transfer, additional symbols are introduced. An arrow indicates convection, while a single inclined line indicates heat conduction or mass diffusion, and finally, a star indicates radiation.

Similar to the PTD introduced in Sec. 2.2.3, a TRANSPORT, REACTION/GENERATION AND ACCUMULATION VIEW (TRAV) is introduced for the phenomenological representation.

In order to make the TRAV more complete with respect to the knowledge it contains, there has to be some kind of relation between the different symbols. For this purpose, arrows are defined, which can be separated according to the sets they relate to, see Table 2.8.

Table 2.8: Set of arrows.

Arrows	Symbolic meaning	Related sets
	direction of mass transfer	A_S, T_S, R
	direction of energy transfer	A_E, T_E, G

The arrows are given a direction by the modeler, and this direction indicates the *positive* reference direction. Bidirectional flow is possible, though a reference direction is still needed. Therefore, bidirectional flow is indicated by a unidirectional arrow. The only case where bidirectional arrows are used is for equilibrium modeling, and this is discussed in Ch. 3.

Comment:

Note that the flow expressions cannot be observed directly from the symbols on the TRAV. Note further that the symbol for energy transfer represents *both* pure heat flow and energy flow related to mass flow.



Example 1, continued

The use of the phenomenological symbols is exemplified by continuing the CSTR example from page 20, which uses Fig. 2.1 as the basis. From the

short process description and the visualization in Fig. 1.1, the base set of species can be written as

$$S = \{A, B, C, H_2O\}, \quad (2.6)$$

and the energy set as

$$E = \{H\}. \quad (2.7)$$

Remember that the temperature dynamics of the wall is already assumed rapid compared to other dynamics. Moreover, the *heat transfer coefficient* from wall to the cooling is assumed large. This means that the model considers heat convection from the reactor_content to the wall and heat conduction through the wall.

Using the elements from (2.1) and (2.2), the following P_D elements are defined. Note the component name in the subscript.

$$\left. \begin{aligned} P_{D,cooling} &= \{H_2O, H\} \\ P_{D,reactor_content} &= \{R_1, A, B, C, H\} \\ P_{D,source_1} &= \{H_2O, H\} \\ P_{D,source_2} &= \{A, B, H\} \\ P_{D,sink_1} &= \{H_2O, H\} \\ P_{D,sink_2} &= \{A, B, C, H\} \end{aligned} \right\} \quad (2.8)$$

Similar for the P_C elements:

$$\left. \begin{aligned} P_{C,pipe_in} &= \{A, B\} \\ P_{C,pipe_out} &= \{H_2O\} \\ P_{C,valve_1} &= \{H_2O\} \\ P_{C,valve_2} &= \{A, B, C\} \\ P_{C,wall} &= \{Q_{conv}, Q_{cond}\} \end{aligned} \right\} \quad (2.9)$$

The elements of the subsets of the T , RG and A sets are:

$$\left. \begin{aligned} T_S &= \{A_{conv}, B_{conv}, C_{conv}, H_2O_{conv}\}, & T_E &= \{Q_{conv}, Q_{cond}\}, \\ R'' &= \{\}, & R''' &= \{R_1\}, & G_E &= \{\}, & G_M &= \{\}, \\ A_S &= \{A, B, C, H_2O\}, & A_E &= \{H\}. \end{aligned} \right\} \quad (2.10)$$

Employing these symbols and relations on the topological structure shown in Fig. 2.1, the following combined PTD and TRAV representation is generated. Note that the aggregate state is indicated on the phenomenological symbols.

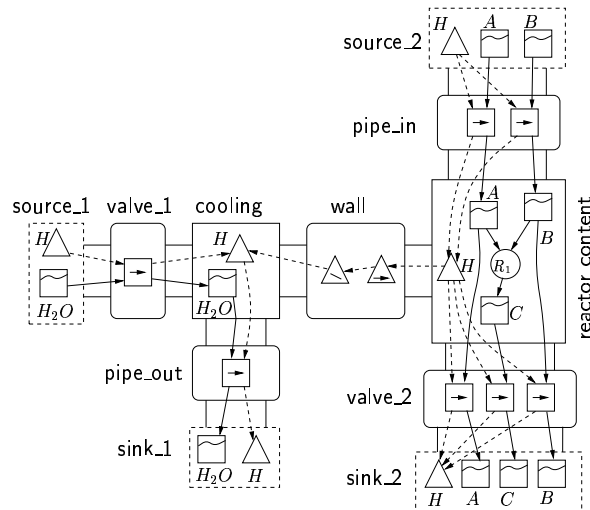


Figure 2.5: PTD and TRAV of the CSTR example.

▲

Comment:

Note also, for the sake of presentation, that the topological components are transparent in that the TRAV of each component is visible on the PTD level. This will, however, not necessarily be the property of an implementation. The functionality will typically be to click on each topological component to view its inner structure.

◇◇◇

It is experienced that when the number of symbols inside each topological component becomes large, the TRAV becomes difficult to read for the modeler. This can to some degree be verified from Fig. 2.5. As a means to improve the representation, one suggestion is separating the PTD and TRAV into a mass and energy based representation. This is an optional representation depending on the level of complexity.

Note that each symbol in the pipe_in connection, for example, carries redundant information in that wherever mass flows, energy also flows. As these flows are linearly dependent, this supports a separation of the representation where the redundant information is hidden. This implies that the arrow for energy transfer in Table 2.8 represents *pure* heat flow *only*. Since the energy accumulation symbol includes the hidden mass flow related energy, there is no conflict with respect to equations and consistency using these separate representations.

2.4 Separated mass and energy representation

This section is based on the work in Drengstig *et al.* (1997d) and presents new material compared to Drengstig *et al.* (1996). The sets defined in Sec. 2.3 are first refined according to the separated representation, and secondly, additional modeling rules are developed.

2.4.1 Refinement of sets

Due to the separated representation, the topological components are limited to which category they belong, i.e. mass or energy. Hence, these new sets are introduced; ED_{mass} , EC_{mass} , ED_{energy} and EC_{energy} . The two device sets, ED_{mass} and ED_{energy} , are not necessarily the same, nor are the connection sets. The sets are related as follows:

$$\left. \begin{aligned} ED &= ED_{\text{mass}} \cup ED_{\text{energy}} \\ EC &= EC_{\text{mass}} \cup EC_{\text{energy}} \end{aligned} \right\} \quad (2.11)$$

The overall sets of phenomena related to elementary devices and connections, P_D and P_C , will similarly be separated according to:

$$\left. \begin{aligned} P_D &= P_{D,\text{mass}} \cup P_{D,\text{energy}} \\ P_C &= P_{C,\text{mass}} \cup P_{C,\text{energy}} \end{aligned} \right\} \quad (2.12)$$

where each set can be defined more precisely as:

$$\left. \begin{aligned} P_{D,\text{mass}} &= A_S \cup R''' \\ P_{D,\text{energy}} &= A_E \cup G \\ P_{C,\text{mass}} &= T_S \cup R'' \\ P_{C,\text{energy}} &= T_E \cup G_E \end{aligned} \right\} \quad (2.13)$$

The sets from (2.11) and (2.13) are depicted in Fig. 2.6.

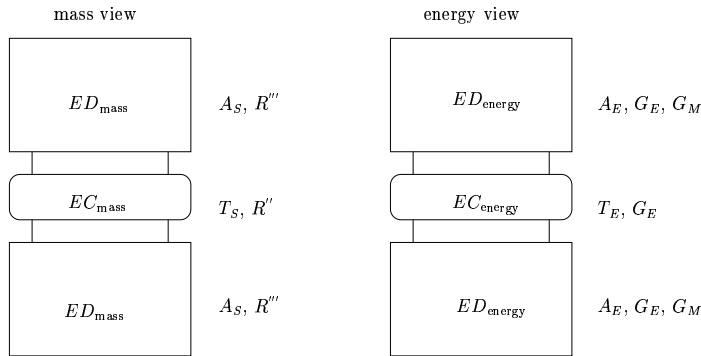


Figure 2.6: Elementary topology components related to phenomena sets.

2.4.2 Modeling rules

In this section, additional modeling rules for the phenomenological components are identified. From a chemical engineering point of view, many of these rules are trivial, and it may seem unnecessary to define them. The modeling rules from Sec. 2.2.5 are still valid.

Content rules for $P_{D,\text{mass}}$ elements:

RULE 8. A set of chemical species (from A_S) and a set of volumetric reactions (from R''') can be included.

Content rules for $P_{D,\text{energy}}$ elements:

RULE 9. *One* energy symbol (from A_E) is allowed.

RULE 10. Several electrical energy generation symbols (from G_E) and mechanical energy generation symbols (from G_M) are allowed.

Content rules for $P_{C,\text{mass}}$ elements:

RULE 11. A set of mass transfer symbols (from T_S) and a set of surface reactions (from R'') can be included.

Content rules for $P_{C,\text{energy}}$ elements:

RULE 12. A set of energy transfer symbols (from T_E) and a set of electrical energy generation symbols (from G_E) are allowed.

Note that more than one energy transfer mechanism is allowed, even if there is only one energy symbol defined in connected devices. More than one mass transfer mechanism is allowed, even for the same species.

Connectivity rules between $P_{D,\text{mass}}$ elements:

RULE 13. A_S elements can be linked to 0 or more R''' elements.

RULE 14. R''' elements must be linked to at least two A_S elements.

RULE 15. An R''' element cannot be linked to elements of other ED_{mass} than the ED_{mass} it occurs in.

RULE 16. No T_S elements allowed.

Connectivity rules between $P_{D,\text{energy}}$ elements:

RULE 17. A_E elements can be linked to G_E and G_M elements.

RULE 18. No T_E elements allowed.

Connectivity rules between $P_{C,\text{mass}}$ elements:

RULE 19. T_S elements and R'' may not be connected.

RULE 20. T_S elements belonging to *the same species* may be connected.

Connectivity rules between $P_{C,\text{energy}}$ elements:

RULE 21. T_E elements may be connected.

The two latter rules are only used when multiple mechanisms occur in serial in a connection, e.g. heat conduction in a wall and heat radiation at the wall surface.

Connectivity rules between $P_{D,\text{mass}}$ and $P_{C,\text{mass}}$ elements:

RULE 22. A_S elements may be linked to 0 or more T_S elements.

RULE 23. A_S elements may be linked to 0 or more R'' elements.

RULE 24. T_S elements may be linked to two or more A_S elements.

RULE 25. R'' elements may be linked to two or more A_S elements.

Connectivity rules between $P_{D,\text{energy}}$ and $P_{C,\text{energy}}$ elements:

RULE 26. A_E elements may be linked to 0 or more T_E elements.

RULE 27. T_E elements may be linked to two or more A_E elements.

Example 1, continued

To exemplify the use of the separated representation, consider the CSTR example starting at page 27. The base sets S and E in (2.6) and (2.7) and the subsets in (2.10) are all still valid.

First, the set of elementary devices, ED , in (2.1) is divided into the ED_{mass} and ED_{energy} elements in (2.14) and (2.15), respectively.

$$ED_{\text{mass}} = \{\text{cooling, reactor_content, source_1, source_2, sink_1, sink_2}\} \quad (2.14)$$

$$ED_{\text{energy}} = \{\text{cooling, reactor_content}\} \quad (2.15)$$

Further, the set of elementary connections, EC , in (2.2) is divided into the EC_{mass} and EC_{energy} elements in (2.16) and (2.17), respectively.

$$EC_{\text{mass}} = \{\text{pipe_in, pipe_out, valve_1, valve_2}\} \quad (2.16)$$

$$EC_{\text{energy}} = \{\text{wall}\} \quad (2.17)$$

The overall P_D elements in (2.8) would be divided into the $P_{D,\text{mass}}$ elements in (2.18) and the $P_{D,\text{energy}}$ elements in (2.19). Note that the mass and energy subscript are neglected.

$$\left. \begin{aligned}
 P_{D,cooling} &= \{H_2O\} \\
 P_{D,reactor_content} &= \{R_1, A, B, C\} \\
 P_{D,source_1} &= \{H_2O\} \\
 P_{D,source_2} &= \{A, B\} \\
 P_{D,sink_1} &= \{H_2O\} \\
 P_{D,sink_2} &= \{A, B, C\}
 \end{aligned} \right\} \quad (2.18)$$

$$\left. \begin{aligned}
 P_{D,cooling} &= \{H\} \\
 P_{D,reactor_content} &= \{H\}
 \end{aligned} \right\} \quad (2.19)$$

Further, the overall P_C elements in (2.9) would be divided into the $P_{C,mass}$ elements in (2.20) and the $P_{C,energy}$ elements in (2.21).

$$\left. \begin{aligned}
 P_{C,pipe_in} &= \{A, B\} \\
 P_{C,pipe_out} &= \{H_2O\} \\
 P_{C,valve_1} &= \{H_2O\} \\
 P_{C,valve_2} &= \{A, B, C\}
 \end{aligned} \right\} \quad (2.20)$$

$$P_{C,wall} = \{Q_{conv}, Q_{cond}\} \quad (2.21)$$

Mass view:

Based on (2.14), (2.16), (2.18) and (2.20) the mass based representation becomes as shown in Fig. 2.7.

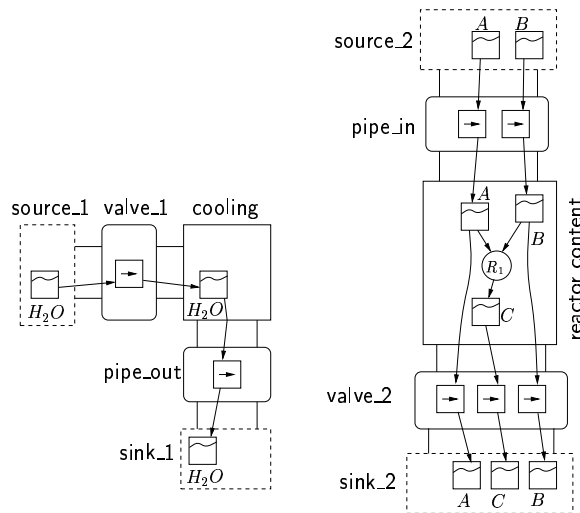


Figure 2.7: Mass based PTD and TRAV of the CSTR example.

From a mass point of view, the reactor system is divided into two completely separated parts.

Energy view:

Based on (2.15), (2.17), (2.19) and (2.21) the energy based representation becomes as shown in Fig. 2.8. Note that the energy accumulations in the sources and sinks are neglected.

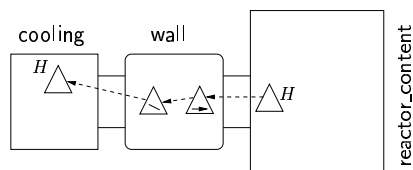


Figure 2.8: Reduced energy based PTD and TRAV of the CSTR example.

▲

Comment:

An interesting property in many cases, is that

$$ED_{\text{mass}} \cap ED_{\text{energy}} \neq \emptyset,$$

while

$$EC_{\text{mass}} \cap EC_{\text{energy}} = \emptyset.$$

The fact that the mass based and energy based representation becomes different is in general true since the focus is on completely different phenomena. This can also be seen from Example 1 above in the sets (2.14) to (2.17).

◇◇◇

2.5 Conceptual interpretation of symbols

The knowledge of the existence of chemical species is represented by a square symbol. This does not imply that the species are considered to be found in certain parts of the device. The species can be found in the entire device volume, though its existence is represented with a square symbol. Thus, the representation can be viewed as lumping the information of the *amount* of species present within a device, to a symbol in the TRAV.

By comparing the representation of chemical species with the comprehension of chemical species being something of tangible matter, the use of the symbol in the TRAV should be intuitive. When it comes to the representation of a reaction, this is not at all a tangible matter as chemical species is. On the other hand, reactions *take* place inside the devices. The representation of the chemical reaction by a circular symbol symbolically separates chemical species and reaction. This does *not* mean that the reaction only takes place within a limited part of the control volume. In addition to the phenomenological aspect, the representation also indicates the informational perspective. As an example, it can be read from the TRAV in Fig. 2.7 that “*A* and *B* reacts to *C*”.

Even though the comprehension of chemical species and reactions is different when it comes to matter, it is found convenient to represent them on the same level within the TRAV. This is because this representation facilitates model development and changes by simply adding/removing species or reactions using graphical manipulations. Another important aspect is that this kind of process visualization seems to facilitate process understanding across interdisciplinary borders.

The chemical species symbols are connected to reaction symbols using lines with an indicated direction. What these lines actually symbolize, is the material conversions from the reactants to the products inside the reactor. The lines crossing topological components represents actual input and output flow, whereas the lines connecting chemical species and reaction are artificial in that there is no actual flow inside the components. The indicated direction of the lines is not given with respect to coordinates, but rather to indicate consumption and generation of chemical species and the main process flow as mentioned in Sec. 2.3.3. Hence, vertical and horizontal lines do not contain different information.

To visualize energy flow, dashed lines are defined to separate this from the solid lines representing mass flow. Consequently, there is a strict separation of the symbols for species/energy and flow/accumulation.

2.6 Relation between symbols and equations

As discussed in Sec. 2.5, the conceptual interpretation of the accumulation symbol represents the total amount of *chemical species* and *energy* within the control volume. Thus, assigning a value to a symbol from A_S , for example, under the assumption of a lumped parameter system, implies that the value represents the total number of moles in that phase. Assigning a value to A_E represents energy U , or for condensed phases, enthalpy H

(see Sec. D.6). Consequently, the methodology is intended to use solely *extensive* quantities in contrast to *intensive* quantities. Extensive quantities are dependent on the size of the control volume, e.g. the number of moles and energy, while intensive quantities, e.g. temperature and concentration, are independent. Thus, the intensive quantities are possible to derive from the extensive quantities.

As described in Sec. A.2.3, dynamic process models of lumped systems can be given by differential and algebraic equations (DAEs). The DAEs are divided into conservation equations (differential), constitutive equations (algebraic) and rate equations (algebraic). The corresponding variables are state variables (holdups), dependent state variables (e.g. temperature) and flow variables (Moe 1995).

The PTD is a topological process representation and does *not* describe the mathematical *model* of the process. Likewise, the TRAV represents the main phenomena and does not describe a mathematical *model*. Nevertheless, there is a strong relationship between the phenomenological description and a mathematical *model structure*, and this must be a one-to-one relationship in order to be consistent. The relation between the PTD/TRAV and these equations are discussed in the following.

2.6.1 Relation to conservation equations

Consider the extensive quantity ψ , where ψ can be either mass or energy.

Mass:

For the case where ψ is the mass, or more specific, the number of moles of i , n_i , the structure of a general conservation or balance equation for ψ in an *ideally mixed system* can be written as:

$$\underbrace{\begin{bmatrix} \text{rate of} \\ \text{accumulated} \\ \psi \text{ within} \\ \text{the system} \end{bmatrix}}_{\frac{dn_i}{dt}} = \underbrace{\begin{bmatrix} \text{net rate of} \\ \text{flow of } \psi \text{ into} \\ \text{the system} \end{bmatrix}}_{j_{i,\text{in}} - j_{i,\text{out}}} + \underbrace{\begin{bmatrix} \text{net rate of} \\ \text{generation} \\ \text{of } \psi \text{ within} \\ \text{the system} \end{bmatrix}}_{r_i} \quad (2.22)$$

The net rate of the flow term comprises *all* the inlet and outlet flows and the net rate of generation comprises the appearing or disappearing of chemical species through chemical reactions. Note that $[r_i] = \text{mol s}^{-1}$. In Gerstlauer *et al.* (1993) it is shown how a generic balance equation for ideally mixed systems can be derived from a macroscopic balance equation.

Example 1, continued

Viewing the balance equation in (2.22) together with the structure of symbols and relations in the `reactor_content` of Fig. 2.7, it can be seen that the accumulation symbol \square of B has inputs, outputs and consumption flow lines attached to it. This is depicted in Fig. 2.9.

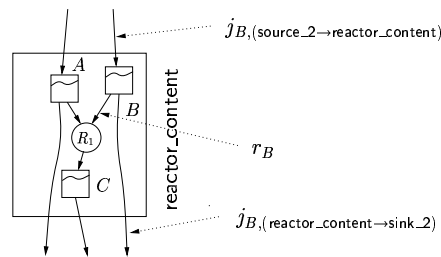


Figure 2.9: Relation between species accumulation symbols and mass balance equation structure.

The use of device names in the syntax (`source_2`→`reactor_content`) indicate the positive direction. The underlying balance or conservation equation can be interpreted from Fig. 2.9 as

$$\frac{dn_B}{dt} = j_{B,(source_2 \rightarrow reactor_content)} - j_{B,(reactor_content \rightarrow sink_2)} - r_B. \quad (2.23)$$

**Energy:**

For the case where ψ is the energy, E , the structure of a general conservation or balance equation for ψ in an *ideally mixed system* can be written:

$$\underbrace{\left[\begin{array}{c} \text{rate of} \\ \text{accumulated} \\ \psi \text{ within} \\ \text{the system} \end{array} \right]} = \underbrace{\left[\begin{array}{c} \text{net rate of} \\ \text{flow of } \psi \\ \text{into the} \\ \text{system by} \\ \text{mass flow} \end{array} \right]} + \underbrace{\left[\begin{array}{c} \text{net rate of} \\ \text{pure heat} \\ \text{flow into the} \\ \text{system from} \\ \text{the} \\ \text{surroundings} \end{array} \right]} - \underbrace{\left[\begin{array}{c} \text{net rate of} \\ \text{work done by} \\ \text{the system on} \\ \text{the} \\ \text{surroundings} \end{array} \right]} \\ \frac{dE}{dt} = \epsilon_{in} - \epsilon_{out} + Q - W \quad (2.24)$$

The net rate of pure heat flow comprises conductive, convective and radiative heat. However, the statement above is not complete in that the electrical energy generation introduced in Sec. A.1.3, is not included. Thus, this term, P , should enter the energy balance next to the work W in (2.24). In Sec. D.6, the energy balance in (2.24) is derived to

$$\frac{d}{dt} \int_V (c\tilde{H} - p) dV = - \oint_{\partial V} c\tilde{H} v^T n dA + Q - W_s. \quad (\text{D.17})$$

By including the electrical energy generation P , assuming constant pressure ($\frac{d}{dt} \int_V p dV = 0$) and using

$$- \oint_{\partial V} cv^T n dA = j_{\text{in}} - j_{\text{out}}, \quad (2.25)$$

integration of (D.17) over the entire control volume V gives:

$$\frac{dH}{dt} = j_{\text{in}} \tilde{H}_{\text{in}} - j_{\text{out}} \tilde{H} + Q - W_s + P. \quad (2.26)$$

Note that the specific enthalpy of the outgoing flow is not indicated as \tilde{H}_{out} since this is equal to the specific enthalpy *within* the system.

Example 1, continued

Viewing the balance equation in (2.26) together with the structure of symbols in the `reactor_content` in Fig. 2.8, there is not a *visual* mapping similar to Fig. 2.9. Nevertheless, there is a hidden mapping corresponding to the hidden relationship between the mass flow symbols and the energy balance described in Sec. 2.4. This is illustrated in Fig. 2.10

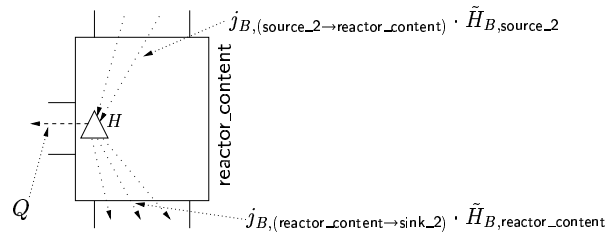


Figure 2.10: Relation between energy accumulation symbols and energy balance equation structure.

The dotted lines connected to the energy symbol represents the hidden relationship. Hence, the overall energy balance for reactor_content becomes:

$$\begin{aligned} \frac{dH_{\text{reactor_content}}}{dt} &= \sum_{i=\{A,B\}} j_{i,(\text{source_2} \rightarrow \text{reactor_content})} \cdot \tilde{H}_{i,\text{source_2}} \\ &\quad - \sum_{i=\{A,B,C\}} j_{i,(\text{reactor_content} \rightarrow \text{sink_2})} \cdot \tilde{H}_{i,\text{reactor_content}} \\ &\quad - Q \end{aligned} \quad (2.27)$$

▲

Comment:

Many chemical engineers are used to work with energy balances where the heat of reactions, $\Delta_r H^\circ$, are included. As can be seen, neither the mass or the energy based representation of the reactor_content, nor the energy balance in (2.26) include this quantity. According to the definition of $\Delta_r H^\circ$ in (D.1), this quantity can be derived from the heat of formations of the reactants and products. Consequently, a *prerequisite* for consistent model development using the methodology presented in this thesis is that the chemical species are characterized with respect to the base line of enthalpy defined in Sec. D.1.5. This means that the model formulation does not consider the heat of reaction since this quantity is found in the difference in the specific enthalpy of the compounds participating in the reactions.

◇◇◇

■

2.6.2 Relation to rate equations

The relationship between flow symbols and rate equations can be illustrated by considering the symbol for heat convection and conduction in the wall, \triangleleft and \triangle in Fig. 2.8. This is depicted in Fig. 2.11.

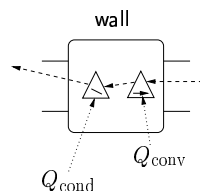


Figure 2.11: Relation between transport symbols and rate equations.

The expression for Q_{conv} and Q_{cond} is typically given as

$$Q_{\text{conv}} = hA_{\text{wall}}(T_{\text{reactor_content}} - T_{\text{wall}}), \quad (2.28)$$

$$Q_{\text{cond}} = \frac{k_{\text{wall}}A_{\text{wall}}}{l_{\text{wall}}}(T_{\text{wall}} - T_{\text{cooling}}). \quad (2.29)$$

Since these are in series, they will be equated as $Q_{\text{conv}} = Q_{\text{cond}} = Q$. The intermediate T_{wall} will then be eliminated. This is due to the neglected dynamics of a wall device, and the resulting heat loss would be:

$$Q = \frac{A_{\text{wall}}}{\frac{1}{h} + \frac{l_{\text{wall}}}{k_{\text{wall}}}}(T_{\text{reactor_content}} - T_{\text{cooling}}). \quad (2.30)$$

The TRAV representation is thus a *visualization* of the mathematical model *structure* of the process.

2.6.3 Relation to constitutive equations

The constitutive equations relate the holdups or state variables to the dependent state variables such as thermodynamic property functions and geometrical calculation. In the context of the PTD and TRAV, these constitutive equations are related to the *elementary devices*. Since the elementary devices are considered containers of species and energy represented through conservation equations, the calculation of dependent state variables is based upon the content of each device. An illustration of this relationship is given in Fig. 2.12.

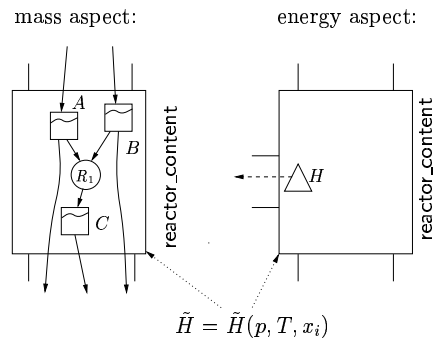


Figure 2.12: Relation between topological symbols and constitutive equations.

This implies that a set of constitutive equations is automatically related to each elementary device, and the modeler could specify which dependent state variables to calculate.

2.7 Discussion

There are both advantages and disadvantages with the proposed modeling methodology. One of the advantages is that the process is represented in a formal way, and this facilitates interdisciplinary understanding of the process and the model assumptions made. Another is that the methodology removes the possibility for erroneous coding from the modelers. Instead, the errors are introduced on the graphical user interface, which is an environment for easier recognition of modeling errors.

A limitation to the concept is the representation possibilities when it comes to high number of reactions and chemical species occurring inside the process. If this number is above a certain level, the gain of using the internal representation is diminished. In Wasbø (1996) there are some suggestions about how to overcome this by using a set of derived symbols for vectors of species, energy, reactions and transport mechanisms. Other strategies might be to color a subset of the network of species and reactions. Modeling of for instance hydrocarbons with a vast number of species often involve distribution of chain lengths. The modeling methodology in this thesis does not support chain length distribution modeling.

This chapter has shown that the balance equation *structure* of each balanced quantity can be read directly from the lines attached to each accumulation symbol on the TRAV. This facilitates a *mapping* of the TRAV structure into a set of *balance equations* of extensive variables. Further, the complete model equation *structure* including algebraic equations can be formulated directly from the combined use of the PTD and the TRAV. On the other hand, when it comes to including details in the underlying *algebraic* equations, this is still done on the basis of equations. The detailed calculation of the flow terms are not possible to resolve from the information in the TRAV, and *must* come from a more detailed, mathematical description of the particular flows. In many cases, the work related to algebraic equations is limited to parameterize a set of well known equations like Fick's law of mass diffusion or Fourier's law for heat conduction.

In OMOLA (Nilsson 1993), the topological abstraction consists of MODELS and TERMINALS, where the TERMINALS work as information gates between the MODELS. Compared to OMOLA, the approach in this thesis is more focused on phenomenological modeling of chemical systems, supporting detailed modeling of species and reactions. OMOLA is a more general tool, suited for a wide range of systems, and therefore does not have specific support for phenomenological modeling of chemical systems.

The phenomenological components here are comparable with the *species* defined by Preisig (1994). The chosen representation also has some similarities with the symbols used in ModellData (1994). The idea of dividing

the physical system into a topological model, a phenomenological model, and a mathematical description is very similar to the ideas in the hybrid phenomena theory (HPT) (Woods 1993). The representation is well suited to be organized in an object-oriented environment, as shown by Wasbø (1996). A similar object oriented approach for a modeling system from first principles is found in Telnes (1992).

Chapter 3

Model assumptions and the modeling process

In order to reuse models efficiently, assumptions made during the model development phase are important to document. This is due to the fact that assumptions impose constraints on models, decreasing the reusability through increased specialization. In addition, proper documentation will support the communication between different modelers participating in a modeling project.

Model assumptions are included at *every* stage of the modeling process. Some of the assumptions are commonly accepted, others are not so obvious, and must be validated and documented by experiments or simulations. Other documentation strategies are textual description and graphical representation. It is believed that these or similar strategies increase the model value in a life time perspective. From a practical point of view, documentation is often left to the final stage of a project due to time or economic constraints. Furthermore, it is sometimes even neglected (Foss *et al.* 1997). In order to analyze the effect of model assumptions in a formal way, Hangos and Cameron (1997) define a syntax for model assumptions.

In this chapter, the impact of assumptions on the modeling methodology is studied and a documentation strategy based on the inclusion of the assumptions on the graphical representation is suggested. This is presented in Sec. 3.1. The modeling of the PTD and TRAV is discussed in Sec. 3.2.

3.1 Model assumptions

There is a large variety of model assumptions and they can be classified along several axes. Some assumptions are motivated by *i*) knowledge about

chemistry, *ii*) computational aspects and numerical properties, *iii*) experience, *iv*) the degree of model accuracy, or *v*) purpose of the model. In the control community, models for control purposes are often very simplified versions of more complex ones.

Some typical examples of model assumptions related to the modeling of chemical processes are neglecting rapid dynamics, quasi steady state assumptions, compressibility/incompressibility of liquids and solids, specifications of flows and holdups, and reaction and phase equilibrium. These assumptions will have different impacts on the model equation set, and some of them lead to high index formulations. For a thorough introduction to index analysis, cf. Moe (1995).

As briefly discussed in Ch. 2, model assumptions are often made prior to the modularization of a process. In this context it is probably true that an experienced modeler would identify more assumptions prior to the modularization than a novice modeler. Such an assumption is the neglected dynamics of the wall in the CSTR example. As shown, these assumptions are *implicitly* documented on the PTD and TRAV. Such assumptions should also be explicitly written down. This will inform other users that the modeler was aware of the assumptions made.

Furthermore, it should also be possible to include assumptions after the modularization. For this reason, there is in this thesis a differentiation between assumptions made prior to and after the modularization, i.e. *a priori* and *a posteriori* assumptions. This will be discussed in Secs. 3.1.1 and 3.1.2, respectively. The symbols for the *a posteriori* assumptions are introduced in Sec. 3.1.3. In addition, a possible classification of model assumptions will be discussed in Sec. 3.1.4, and a procedure for consistent model generation is given in Sec. 3.1.5. Finally, several examples highlighting the representation of *a posteriori* assumptions will be given.

3.1.1 A priori assumptions

As mentioned in Ch. 2, the basis for modularization is the thermodynamic phase. The idea now is to exploit that whenever this concept is abandoned, it is due to some kind of assumptions. These assumptions are then implicitly visualized on the PTD and TRAV, and it should be further possible for modelers to textually state each assumption. By studying Fig. 2.1, the following *a priori* assumptions are found:

(A.1) the dynamics of the wall is neglected.

(A.2) the gas phase of the reactor_content is neglected.

(A.3) the heat convection from the wall to the cooling is assumed to be rapid.

The idea of allowing topological components such as the wall to deviate from the thermodynamic phase concept has at least two effects. First, the formalism related to the modularization is diminished, allowing modelers to include their experience and knowledge in order to develop simplified models. Second, it turns out to be an appropriate method to identify and document model assumptions made prior to the modularization. The former effect is important to include, because the purpose of models may vary, and hence, so must the level of topological details. The chosen PTD structure will then reflect the modeler's choices and understanding of the process. This means that the original choice of phase has the synergy effect that assumptions are easier recognized and the model representation provides more information.

Note that the implication of the comment on page 19 and RULE 4 on page 20 can be summarized as follows. A priori assumptions represented as *replacement* of a detailed part with a coarse part (as in assumption (A.1)), are subjected to the following modeling rules:

RULE 28. It is possible to replace a combination of connection₁ – device – connection₂, with a connection.

RULE 29. It is *not* possible to replace a combination of device₁ – connection – device₂, with a device, since this would be violation of RULE 4.

Note that a prerequisite for RULE 29 is that device₁ and device₂ are different phases. Thus, if the devices are of the same phase, i.e. as in the case of spatial discretization, this rule does not apply. An alternative rule for RULE 29 is RULE 30.

RULE 30. If a device is assumed unimportant, remove it (as in assumption (A.2)).

An interesting property of *some* a priori assumptions is that the PTD becomes less able to imitate the structure and phenomena of the real process. This will be illustrated in Secs. 6.2 and 6.3 where a model of the aluminum electrolysis cell is developed.

3.1.2 A posteriori assumptions

As opposed to a priori assumptions, the a posteriori assumptions consider assumptions that affect the equation structure through constraints. Therefore, in order to maintain the one-to-one relationship between the graphical

representation and the underlying equations, these a posteriori assumptions *cannot* be made prior to the modularization. Thus, they are imposed onto a developed model representation and are graphically represented. The reason for focusing on this one-to-one relationship is the consistency it introduces for different representations, i.e. two equal PTD and TRAV representations should represent *one* mathematical model structure only.

The a posteriori assumptions may generate high index models which call for some kind of *equation manipulation*. The a posteriori assumptions considered in this thesis are:

1. phase and reaction equilibrium, i.e. equilibrium constraints.
2. specifications on holdups or dependent state variables, i.e. constraints imposed through specification.

The basis for the equation manipulation is the complete set of DAEs generated according to the relation between symbols and equations described in Sec. 2.6. The generation of these equations may follow the FLD¹ algorithm presented in Wasbø and Foss (1997). As these equations are unconstrained, the a posteriori assumptions will impose constraints. A prerequisite for this model formulation is the existence of suitable software algorithms able to manipulate and analyze equation structures. Such algorithms include the index reduction algorithm described in Moe (1995) and the degree of freedom analysis. The unconstrained equation set and the constraints imposed by model assumptions would generate an overall model in the form of

$$\begin{aligned} \dot{x} &= f(x, y, u), \\ 0 &= g(x, y), \end{aligned} \tag{3.1}$$

where x is the states, y the outputs and u the inputs.

It is believed that very few modelers gain knowledge from studying and working with manipulated equations, and the intention here is to decouple modelers from the task of manipulating equations themselves. This has the synergy effect that erroneous calculations are almost removed. Furthermore, the original equation set in the form of (3.1), possibly including some sort of textual based information about the assumptions, is believed to be far more valuable. Hence, the manipulation into simulation ready code should be hidden for modelers as far as possible.

3.1.3 Symbols




The a posteriori assumptions listed in Sec. 3.1.2 should all be explicitly represented on the PTD and TRAV. For this reason, the following symbols are defined. The a priori assumptions are, as mentioned, already implicitly represented.

¹Formal language description.

Equilibrium constraints

A bidirectional arrow is introduced for both phase and reaction equilibrium, as shown in Table 3.1.

Table 3.1: Arrows for equilibrium modeling.

Arrows	Symbolic meaning	Related sets
	reaction equilibrium	A_S, T_S, R
	phase (material part) equilibrium	A_S, T_S, R
	phase (thermal part) equilibrium	A_E, T_E, G

These arrows are also separated according to the sets they relate to, similar to the arrows in Table 2.8. Note that the reaction equilibrium arrows are different from the phase equilibrium arrows. This is done in order to still visualize the reactants and products of reactions.

The rules for non-equilibrium systems apply for equilibrium systems, though the only difference is that bidirectional arrows are used where equilibrium is assumed. This introduces one additional rule:

RULE 31. The arrows connecting one element of T or RG to elements of A must all be either unidirectional or bidirectional.

This means that a reaction cannot be in equilibrium for some of the species taking part, and not for others. Note that the above rule is stated for *each* element of T and RG separately. This means that both equilibrium and non-equilibrium reactions are allowed within the same TRAV.

An example is developing an equilibrium model for a flash unit, where the modeler is forced to identify the phases before imposing the equilibrium assumption on the model². In traditional modeling, this assumption is often done simultaneously with the development of the mathematical model. The benefits of introducing the equilibrium afterwards is that the model may easily be changed to a non-equilibrium model by just changing the arrows in the TRAV, and the representation would still be valid. ■





²As stated in RULE 29.

Constraints imposed through specifications

A balance equation is in general manipulated by the flows as shown in (2.22) and (2.24). The flows are either specified or expressed by rate equations as shown in Sec. 2.6.2. However, specifications imposed on the holdups or the dependent state variables, will generate a high index model (Moe 1995). Then the flows are *forced* to satisfy certain values in order to fulfill the imposed constraint on the balanced quantity. As visualized in Fig. 23 in Moe (1995), the information flow between holdups, dependent state variables and flows is reversed.

From a representational point of view, there are *two* different views on specifications imposing constraints. That is, the representation should explicitly visualize *i*) which balanced quantity that is constrained, and *ii*) which flow that is forced to satisfy certain values. As shown in Moe (1995), the forced flow is the result of the index reduction algorithm. In addition, it is also possible that some assumptions cause both a flow and a balanced quantity to be forced to some value. Two main symbols are therefore defined, i.e. one symbol for the quantity that is constrained, and one symbol for the quantity that is forced to satisfy certain values. These are depicted in Table 3.2.

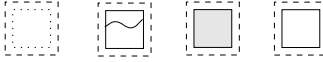

Table 3.2: Main symbols for specified (constrained) and forced quantities.

Description	Main symbols	Related sets
Specified quantity (constrained)	 	A_S, A_E
Forced quantity	 	A_S, A_E, T_S, T_E

It can be seen that the specified quantity and the forced quantity symbols are variants of the general mass/energy flow/accumulation symbols. Note, however, that elements of the transport sets T_S and T_E are *not* considered to be constrained through specifications. This is due to the fact that specifications to these elements do not call for an equation manipulation. In order to use the symbols in Table 3.2, they are combined with the related sets given in Tables 2.5 and 2.7.

The combination of specified quantity from Table 3.2 and its related sets is given in Table 3.3.

Table 3.3: Symbols of constrained phenomenological components.

A posteriori assumption	Symbols of the A set
specification to chemical species, A_S	
specification to energy, A_E	

There are several possible specifications related to each balanced quantity. For example, related to a chemical species is the specification of *i*) constant amount, *ii*) constant mol fraction or *iii*) constant concentration. This variety of specifications is neither possible nor interesting to visualize, though the involved species is indicated. This implies that the *actual* specification must be included by the modeler elsewhere. Hence, each symbol in Table 3.3 has *several* meanings, and must be further investigated to identify *what* particular specification is used.

The symbols for the combination of forced quantity from Table 3.2 and its related sets is given in Tables 3.4 and 3.5.

Table 3.4: Symbols of forced phenomenological components of balanced quantities.

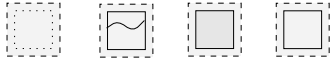



Forced quantity	Symbols of the A set
forced chemical species, A_S	
forced energy, A_E	

Table 3.5: Symbols of forced phenomenological components of flows.

Forced quantity	Symbols of the T set
forced flow of species, T_S	
forced flow of heat, T_E	

Some assumptions or constraints are related to the physical extent of process equipment. An example is constant volume. Consequently, these are related to specifications to *topological components*. On the other hand, some assumptions impose constraints on both mass and energy balances, exemplified by constant pressure of a gas device. Since the energy balance and all the mass balances are interconnected by the pressure through some equation of state, e.g.

$$pV = nRT, \quad (3.2)$$

it is evident that the assumption of constant pressure will impose constraints on these elements. Hence, since the constant pressure assumption affects the entire content of devices, a symbol on the *ED* is defined for this assumption. The choice of symbol is inspired by the actual assumption. As an example, the letter *V* is used for the constant volume assumption as shown in Table 3.6. These symbols will be employed on both the mass and energy based representation.

Table 3.6: Symbols of constrained topological components.

Specified quantity	Symbols of the <i>ED</i> and <i>CD</i> set
constant volume of a phase device	V
constant pressure of a phase device	p
constant volume of a composite device	V

The variety of symbols introduced in this section covers a vast number of assumptions and specifications commonly used in chemical engineering. ■

3.1.4 Classification of model assumptions

This section attempts to qualitatively classify the model assumptions defined in Secs. 3.1.1 and 3.1.2. This is depicted in Fig. 3.1.

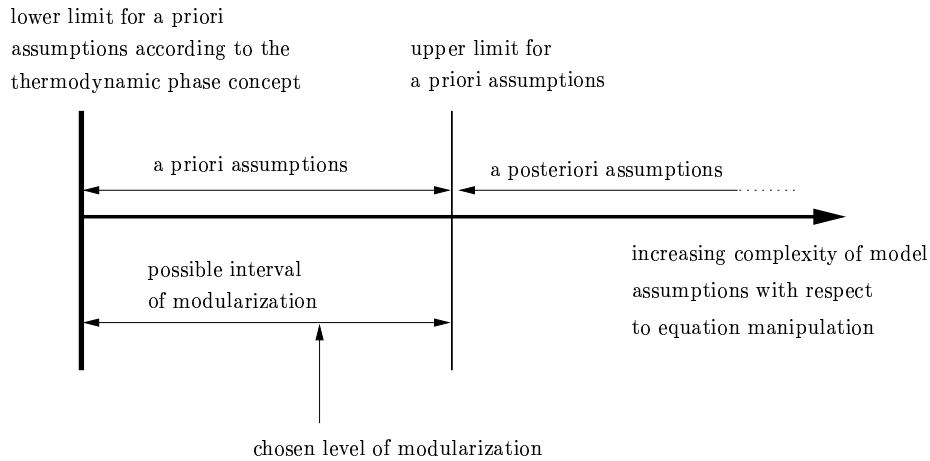


Figure 3.1: Possible classification of model assumptions.

The x -axis represents increasing complexity of model assumptions, and it is divided into regions where different assumptions are applicable. The lower limit of complexity represents the case where no a priori assumptions are imposed and the modularization of the process follows the thermodynamic phase concept. As long as the a priori assumptions are valid, is it possible to perform modularization.

The upper limit for a priori assumptions is determined by the impact of the assumptions on the equation set. The assumptions to the left of this limit do not call for equation manipulation, whereas those to the right do. An important property of these assumptions, is that the a priori assumptions are applicable after the modularization, but not vice versa.

3.1.5 Procedure for consistent process model generation

Based on the methodology in Ch. 2 and the different assumptions presented in this chapter, a possible structuring of the overall model generation is depicted in Fig. 3.2.

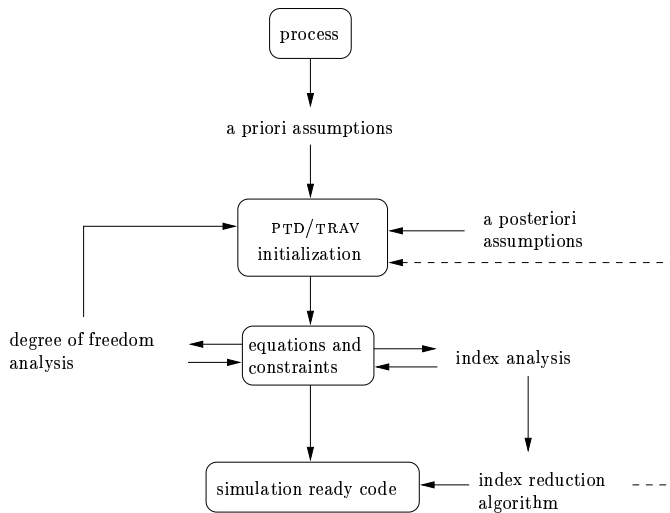


Figure 3.2: Possible structuring of the overall model generation.

The first step decompose the process with respect to the a priori assumptions. Thereafter, the modeler imposes a posteriori assumptions on the developed PTD and TRAV. This will generate a set of DAEs with constraints. Several consistency checks are performed on this set, such as the degree of freedom (DOF) analysis. If it is not consistent, the modeler must change the specifications given in the TRAV. Another consistency check is the index analysis which may call for some index reduction algorithm. The dashed line indicates the representation of the forced quantities on the PTD and TRAV as described in Sec. 3.1.3. Finally, a consistent set of simulation ready code is generated.

3.1.6 Examples

The use of the introduced symbols for different model assumptions is exemplified through several case studies which all generate high index models.

Example 1, continued

By assuming that the reaction R_1 in the reactor_content of Fig. 2.7 is in equilibrium, the TRAV for this device should be changed into Fig. 3.3.

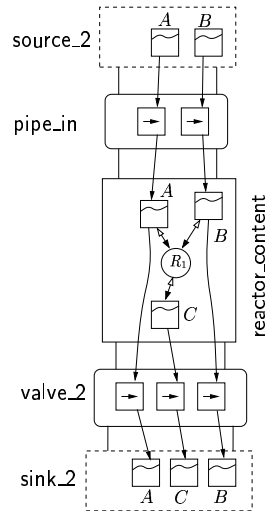


Figure 3.3: Reaction equilibrium modeling.

In order for reaction R_1 to be in equilibrium it has to be reversible. Extending the reaction to include stoichiometric parameters different from unity, gives:



The implication of reaction equilibrium requires a manipulation of the balance equations generated. Prior to the equilibrium, the balance equations are:

$$\left. \begin{aligned} \frac{dn_A}{dt} &= j_{A,\text{in}} - j_{A,\text{out}} - r_A \\ \frac{dn_B}{dt} &= j_{B,\text{in}} - j_{B,\text{out}} - r_B \\ \frac{dn_C}{dt} &= -j_{C,\text{out}} + r_C \end{aligned} \right\} \quad (3.4)$$

The reaction rates are

$$r = -\frac{1}{a}r_A = -\frac{1}{b}r_B = \frac{1}{c}r_C, \quad (3.5)$$

where r_A could be

$$r_A = k_1 x_A x_B - k_{-1} x_C, \quad (3.6)$$

or more general

$$r = f(n_A, n_B, n_C, k_1, k_{-1}). \quad (3.7)$$

The assumption that the reaction rates are fast compared to other dynamics of the system, i.e. reaction equilibrium, is now introduced. This must be treated as an a posteriori assumption. Furthermore, the net reaction rate will be 0 as the equilibrium is established. The approach of an equation manipulation algorithm is to make the equation system *reaction invariant*, i.e. independent of the reaction. This is achieved by adding combinations of n_A, n_B , and n_C from (3.4). Examples are $n_A + n_C$ and $n_B + n_C$ as shown below.

$$\left. \begin{aligned} \frac{d(c \cdot n_A + a \cdot n_C)}{dt} &= c \cdot (j_{A,\text{in}} - j_{A,\text{out}}) - a \cdot j_{C,\text{out}} \\ \frac{d(c \cdot n_B + b \cdot n_C)}{dt} &= c \cdot (j_{B,\text{in}} - j_{B,\text{out}}) - b \cdot j_{C,\text{out}} \end{aligned} \right\} \quad (3.8)$$

Together with (3.7) for $r = 0$, i.e.

$$0 = f(n_A, n_B, n_C, k_1, k_{-1}), \quad (3.9)$$

equations (3.8) and (3.9) will substitute (3.4) and (3.7). \blacktriangle

The procedure for combining reactants and products into reaction invariants in (3.8), is not as straightforward as shown above if some species are participating in several equilibrium reactions. Such an example is presented by Støle-Hansen and Dotterud (1996), and will be used in Example 2.

Example 2

The precipitation processes given by Støle-Hansen and Dotterud (1996) includes 6 reactions. The TRAV for this process is given in Fig. 3.4.

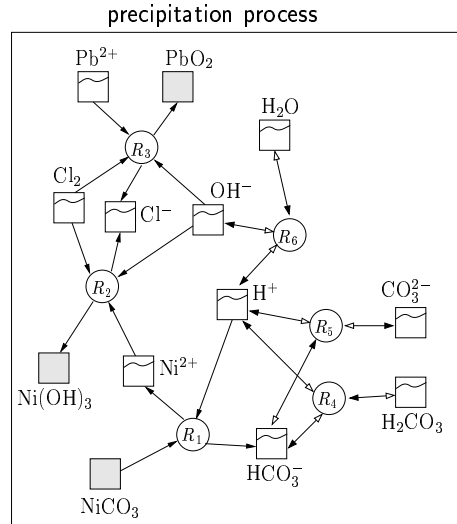


Figure 3.4: A precipitation process with several equilibrium reactions, from Støle-Hansen and Dotterud (1996).

Note that there are neither inputs nor outputs, and that reactions R_4, R_5 and R_6 are equilibrium reactions. There are 13 species present, and 7 of these are not related to equilibrium relations, i.e. $\text{PbO}_2, \text{Pb}^{2+}, \text{Cl}_2, \text{Cl}^-, \text{Ni}(\text{OH})_3, \text{Ni}^{2+}$ and NiCO_3 . This implies that 6 additional equations must be generated from an equation manipulation algorithm in order to have a complete model. Similar to Example 1 and (3.9), there is an equilibrium relation for each equilibrium reaction. These are given as

$$\frac{c_{\text{H}^+} c_{\text{HCO}_3^-}}{c_{\text{H}_2\text{CO}_3}} = K_{R_4}, \quad \frac{c_{\text{H}^+} c_{\text{CO}_3^{2-}}}{c_{\text{HCO}_3^-}} = K_{R_5}, \quad c_{\text{H}^+} c_{\text{OH}^-} = K_{R_6}. \quad (3.10)$$

The 3 remaining equations must be generated by a combination of the 6 species involved in the equilibrium reactions. There are several ways of obtaining a reaction invariant system. The results from two methods will be presented, i.e. the method used in Example 1, and the method used in Støle-Hansen and Dotterud (1996). Finally, a comparison of the resulting equation set from Støle-Hansen and Dotterud (1996) and from the approach used here is given.

The following 6 balance equations for the 6 species involved are generated prior to the assumption of reaction equilibrium.

I	$\frac{dn_{\text{H}_2\text{O}}}{dt} = -r_{R_6}$	H, O
II	$\frac{dn_{\text{OH}^-}}{dt} = r_{R_6}$	H, O
III	$\frac{dn_{\text{H}^+}}{dt} = r_{R_4} + r_{R_5} + r_{R_6}$	H
IV	$\frac{dn_{\text{CO}_3^{2-}}}{dt} = r_{R_5}$	C, O
V	$\frac{dn_{\text{HCO}_3^-}}{dt} = -r_{R_5} + r_{R_4}$	H, C, O
VI	$\frac{dn_{\text{H}_2\text{CO}_3}}{dt} = -r_{R_4}$	H, C, O

The method from Example 1 could generate the following reaction invariant combinations of I–VI for the 3 missing equations:

1. I + II
2. IV + V + VI
3. III + I + VI – IV

In order to indicate the variety, the latter could be replaced by:

3. III + I + V + 2·VI

The method used in Støle-Hansen and Dotterud (1996) is based on the conservation of *elements*. The elements constituting the compounds in the equations I–VI are indicated to the right. This generates the following combinations:

- | | |
|--------------------------------------------------------------------------------|---|
| 1. $2\cdot\text{I} + \text{II} + \text{III} + \text{V} + 2\cdot\text{VI}$ | H |
| 2. $\text{IV} + \text{V} + \text{VI}$ | C |
| 3. $\text{I} + \text{II} + 3\cdot\text{IV} + 3\cdot\text{V} + 3\cdot\text{VI}$ | O |

The resulting equation set in Støle-Hansen and Dotterud (1996) consists of 7 balance equations of reaction invariants, 3 equilibrium relations and 3 mass balances. The resulting equation set generated using the modeling methodology in this thesis consists of 7 mass balances, 3 equilibrium relations and 3 balance equations of reaction invariants. The reason for this discrepancy is that the approach in Støle-Hansen and Dotterud (1996) employs the conservation of *all* the elements in the process, not only H, O and C. There is further no relation to balance equations for unconstrained species. ▲

The next example considers a simple vaporizer with only two chemical species and assumed phase equilibrium.

Example 3

This would give the PTD and TRAV in Fig. 3.5.

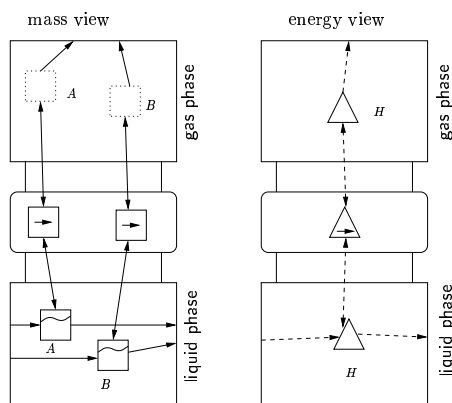


Figure 3.5: PTD and TRAV of vaporizer with assumed chemical equilibrium.

An equation manipulation algorithm for such a system is given by Ponton and Gawthrop (1991). This algorithm is used to manipulate high index models into low index ones. The approach is similar to the reaction invariants above. The aim is to eliminate the infinite rate term in the balance equations. In this case, this is achieved by adding the mass balance for each phase for each species. Instead of 6 balance equations originally, the manipulated set consists of 3 balance equations. ▲

The fourth example is a gas system similar to an example used in Moe (1995).

Example 4

A constant volume gas pipe under the assumption of constant pressure would be represented as in Fig. 3.6.

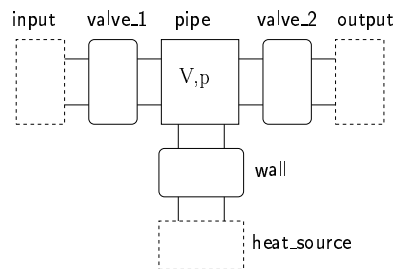


Figure 3.6: A combined mass and energy based PTD of a gas reactor with assumed constant volume and pressure.

The result of the index reduction algorithm in Moe (1995) is that the energy balance is removed and the flow out of the valve_2 is given as a function of the mass flow in valve_1 and the energy added through the wall. This implies that the phenomenological components in valve_2 is given as forced flows as shown in Table 3.5. Moreover, the energy balance is also represented as a forced balanced quantity given in Table 3.4. ▲

The fifth and last example is a tank with two species, A and B .

Example 5

If the amount of *one* of the species in the tank is assumed to be constant, there are at least two ways of representing this assumption. This is depicted in Fig. 3.7 for species B .

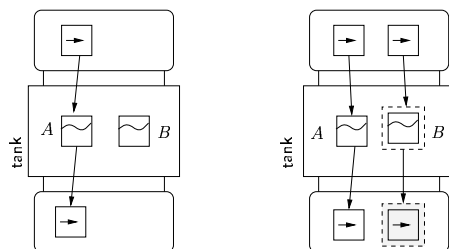


Figure 3.7: Alternative representations of mass based PTD and TRAV of constant amount of species B .

The first approach is to remove any input, output and consumption/generation lines attached to the symbol, shown on the left hand side of Fig. 3.7. This is an adequate model if the impact of B on the energy balance is negligible, or if the energy balance is not included. On the other hand, if this cannot be assumed, the right hand model must be employed. First, a constraint is imposed on the balance equation of B in the tank. The result of the index reduction algorithm shown as a dashed line in Fig. 3.2 *automatically* updates the PTD and TRAV. The outflow of B is therefore forced to a certain value, and the symbol changes as shown in Fig. 3.7. Of course, in this case the outflow will be equivalent to the input flow. ▲

3.2 The modeling process

A discussion of some aspects of the modeling of the PTD and TRAV is given in this section. In addition, some possible user interfaces for the purpose of model initialization and specification is presented.

3.2.1 Modeling the PTD

From the sketches of the CSTR and the aluminum electrolysis cell in Figs. 1.1 and 1.2, it should be possible to make a PTD of each process based on knowledge about the physical placement of each topological component. In the CSTR example used so far, the structure of the PTD in Fig. 2.1 on page 21 only *implicitly* uses the information about the physical placement of devices. That is, there is no explicit reason for representing the PTD as it is done in Fig. 2.1. The only sensible reason is that it should imitate the original CSTR sketch in Fig. 1.1, and it should correspond to the modeler's understanding of the process. Due to the lack of a formal procedure to arrange each topological component within the PTD, there are many possible combinations of PTDs for *one* process.

This is exemplified in Fig. 3.8 where the complete PTD structure for the CSTR has been changed. An important feature is that the mathematical model is *not* changed.

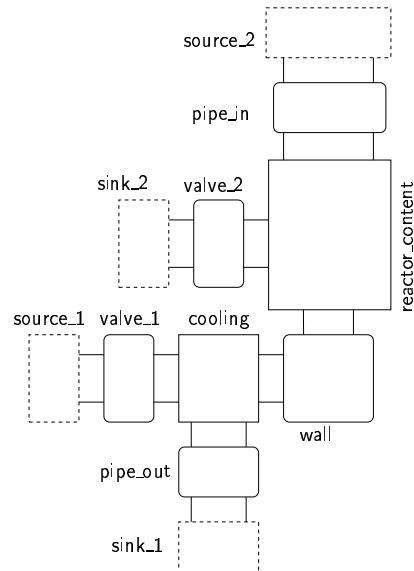


Figure 3.8: Alternative PTD representation of the CSTR.

The representation in Fig. 3.8 is not satisfactory and it neither contributes to the understanding of the process, nor to the communication with other resource personnel. It is therefore important for modelers to strive to imitate the real process when constructing the PTD. Due to the large degree of freedom in arranging the topological components, they should be arranged according to a common or joint understanding of the process among the involved personnel. Otherwise, the PTD structure is only of minor importance, and it might lead to misunderstandings.

One possible approach to improve the PTD resemblance of the process, is to carefully recognize the physical placement of each device of the real process within a network as shown in Fig. 3.9. Note that the sources and sinks are included as types of volume elements.

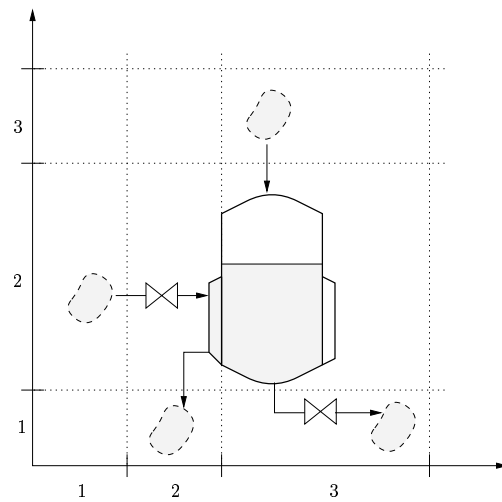


Figure 3.9: A topological network applied to the CSTR example.

This network divides the process into spatial zones forming a basis for selecting an appropriate PTD structure. This is shown in Fig. 3.10.

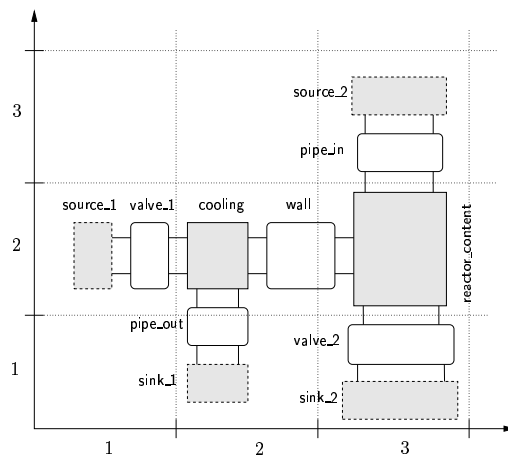


Figure 3.10: PTD structure of the CSTR applied in a network according to Fig. 3.9.

It is believed that such or similar structuring of the PTD increases the value of the representation.

3.2.2 Modeling the TRAV

An attempt to structure the PTD layout with respect to the spatial configuration of the real process parts was given in the previous section. A similar structuring of the TRAV layout is not interesting in that control volumes are assumed to be ideally mixed. Consequently, one layout is as good as another, and there are no mathematical or informational benefits in structuring the TRAV layout. There are, however, other interesting aspects about the TRAV.

The separated representation introduced in Sec. 2.4 supports consistent modeling through a method which automatically determines the elements of connections from the knowledge of the elements of the adjacent devices. This ensures that chemical species transported through a connection have to exist within the devices on each side of the connections. On the other hand, this method is only unidirectional in that devices might contain species that are not transported through a connected connection.

Consider two devices from the ED_{mass} set, `device1` and `device2`, which are connected with one element from the EC_{mass} set, `connection1`. Remember from (2.13) on page 30 that the PC_{mass} set consists of the T_S and R'' sets. By taking the intersection between `device1` and `device2`, it is possible to identify the T_S part of the $PC_{\text{mass,connection1}}$ set as

$$P_{C,\text{mass,connection1}} = P_{D,\text{mass,device1}} \cap P_{D,\text{mass,device2}}. \quad (3.11)$$

Generalizing this to consider the transport part of both PC_{mass} and PC_{energy} (T_S and T_E) and extending it to m devices connected to one connection, (3.11) can be written more generally as

$$P_C = \bigcup_{i=1}^{m-1} \bigcup_{j=i+1}^m (P_{D,i} \cap P_{D,j}). \quad (3.12)$$

This method can be incorporated into a modeling tool through a suitable algorithm, and each time the model is changed, either by adding or removing chemical species or topological components, the algorithm is rerun to guarantee consistency. Note that this method does not identify possible reactions. This could possibly be accomplished by supporting the algorithm with a knowledge base of reactions.

The use of (3.11) is exemplified on the CSTR.

Example 1, continued

The $P_{D,\text{mass}}$ elements in (2.18) on page 33 is:

$$\left. \begin{aligned}
 P_{D,\text{cooling}} &= \{H_2O\} \\
 P_{D,\text{reactor_content}} &= \{R_1, A, B, C\} \\
 P_{D,\text{source_1}} &= \{H_2O\} \\
 P_{D,\text{source_2}} &= \{A, B\} \\
 P_{D,\text{sink_1}} &= \{H_2O\} \\
 P_{D,\text{sink_2}} &= \{A, B, C\}
 \end{aligned} \right\} \quad (2.18)$$

Then, the $P_{C,\text{mass}}$ elements found in (2.20) could be identified as:

$$\left. \begin{aligned}
 P_{C,\text{pipe_in}} &= P_{D,\text{source_2}} \cap P_{D,\text{reactor_content}} = \{A, B\} \\
 P_{C,\text{pipe_out}} &= P_{D,\text{cooling}} \cap P_{D,\text{source_1}} = \{H_2O\} \\
 P_{C,\text{valve_1}} &= P_{D,\text{source_1}} \cap P_{D,\text{sink_1}} = \{H_2O\} \\
 P_{C,\text{valve_2}} &= P_{D,\text{reactor_content}} \cap P_{D,\text{sink_2}} = \{A, B, C\}
 \end{aligned} \right\} \quad (3.13)$$

In this context it is possible to foresee a user interface as shown in Fig. 3.11 for the possible set of elements in the pipe_in connection.

Connection: pipe_in

Device upstream: source_2
Species: A, B

Device downstream: reactor_content
Species: A, B, C

Possible elements: $T_S = \{A, B\}$

Specifications (user input):

Include:

Figure 3.11: A possible user interface for the pipe_in connection.

▲

The algorithm according to (3.12) will sort out the maximum set of possible flows. As indicated in Fig. 3.11, it could be the modeler who decides which species to include. Hence, for a model of a water impermeable membrane system with water in both phases, the modeler would not include water in the connection, even if the algorithm suggests doing so. The functionality of letting the modeler decide which species to include is a trade-off between the modeler's freedom and the degree of automatically generated consistency. In the next section, possible user interfaces for the purpose of model initialization and specification are proposed.

3.2.3 Initialization of elements of the set A

This section describes the initialization of the elements of the set A introduced in Sec. 2.3.2. The subsets of A are species accumulation A_S and energy accumulation A_E .

Initialization of A_S elements

By clicking on each symbol of the A_S elements on the TRAV, exemplified by species A , B and C in Fig. 3.3, modelers specify the initial value for each species. The initial value is given in mol, for example. ■

Initialization of A_E elements

The initial value of the A_E element of an elementary device with N chemical species is calculated using the following relationship:

$$H = \sum_{i=1}^N n_i \tilde{H}_i + \Delta_{\text{mix}} H, \quad (3.14)$$

where the specific enthalpy \tilde{H}_i is typically found from thermodynamic tables for each species at the present temperature T . Depending on the aggregate state of the individual species within a device, \tilde{H}_i is calculated differently for each species³. For instance, if the B species in the reactor_content is dissolved in a solvent, e.g. the A species, the dissolved B would have the following specific enthalpy at temperature $T_{\text{reactor_content}}$:

$$\tilde{H}_{B,\text{reactor_content}} = \Delta_f H_{298,B}^\circ + \int_{298}^{T_{\text{reactor_content}}} c_{p,B} dT + \Delta_{\text{sol}} H_B^\circ, \quad (3.15)$$

while the solvent A would typically have this specific enthalpy:

$$\tilde{H}_{A,\text{reactor_content}} = \Delta_f H_{298,A}^\circ + \int_{298}^{T_{\text{reactor_content}}} c_{p,A} dT + \Delta_{\text{fus}} H_A^\circ. \quad (3.16)$$

As mentioned in the comment on page 39 in Sec. 2.6.1, the enthalpy of reaction, $\Delta_r H^\circ$, is not considered in this model formulation. ■

³Thus, the specification of \tilde{H}_i is therefore strongly related to the initialization of the A_S elements described above.

3.2.4 Specification of elements of the set T

In this section, the specification of the set T is described. The subsets of T are species transport T_S and energy transport T_E .

Specification of T_S elements

For plant modeling, the specific enthalpy of the flowing medium is equal to the specific enthalpy of the upstream device. Furthermore, if the flow is bidirectional, a discontinuity in specific enthalpy is expected as the flow changes direction. On the other hand, this is not necessarily so for complex unit processes due to the strong interaction and the physical nearness of the devices. This calls for a *manual* specification of the flowing fluid, where modelers have the possibility to decide whether the flowing species has the specific enthalpy of the upstream or downstream device. A possible user interface for this purpose is given in Fig. 3.12 for the species B in the pipe_in connection.

Connection: pipe_in

Device upstream: source_2

Device downstream: reactor_content

Species: B

Specific energy:

source: $\tilde{H}_B = \Delta_f H_{298,B}^\circ + \int_{298}^{T_{\text{source}_2}} c_{p,B} dT + \Delta_{\text{sol}} H_B^\circ$

reactor_content: $\tilde{H}_B = \Delta_f H_{298,B}^\circ + \int_{298}^{T_{\text{reactor_content}}} c_{p,B} dT + \Delta_{\text{sol}} H_B^\circ$

Specifications (user input):

Type of flow: unidirectional bidirectional

Source of energy transformation, positive direction (if other than Device downstream):

- source_2 → reactor_content:

Flow expression:

Figure 3.12: A possible user interface for specification of T_S elements.

The source of energy transformation is included in order to specify which device provides the energy needed to transform the species into another

energy level. This is found to be a necessary specification for non-standard unit operations with strongly interacting phases. This will be highlighted on the aluminum cell in Ch. 6. ■

Specification of T_E elements

By clicking on each symbol for heat flow, modelers may specify the heat flow expressions modeled as convective, conductive or radiative heat flow. ■

3.2.5 Specification of elements of the set RG

In this section, the specification of the set RG is described. The subsets of RG included here are surface reaction R'' and volume reaction R''' .

Specification of R'' elements

Surface reactions typically have the reactants and the products in different devices. In addition, since there is no energy balance in a connection, the energy needed or produced from the reaction must be related to one or several of the adjacent devices. If the reaction occurs on a phase boundary between a liquid and a solid phase, it could be assumed that the liquid phase is a better conductor for heat. This means that the energy needed or supplied should be related to that device. However, this is energy which is found in the difference between the energy level of reactants and products. This will be further exemplified in Sec. 6.2.2 for the aluminum cell. ■

Specification of R''' elements

The specification of a volume reaction is simpler. All the species participating in the reaction are included in the device, and each species is specified at a certain energy level. A possible user interface is shown in Fig. 3.13.

Device: reactor_content	
Reactant:	A, B
Product:	C
Volume reaction:	R_1
Specifications (user input):	
Stoichiometric coefficients:	<input type="text" value="[a, b], [c]"/>
Parameters:	<input type="text" value="k<sub>0</sub>, R, E"/>
Equilibrium:	<input type="checkbox"/>

Figure 3.13: A possible user interface for specification of R''' elements.

■

3.3 Discussion

This chapter has introduced model assumptions on the representation from Ch. 2. It has also discussed the process of modeling the PTD and TRAV, and the impact on the mathematical model equations from the model assumptions.

The reason for focusing on the one-to-one relationship between model representation and model equations, is that it is imperative that an implementation should be unambiguously given a set of assumptions. As an example, if the system to be modeled is believed to be characterized as phase equilibrium, it is possible to imagine two approaches. First, one can assume the equilibrium a priori and lump both phases into one device. This approach is often used by chemical engineers. The other approach is to identify both phases and introduce the equilibrium a posteriori. The ambiguity here is two different representations of the same model. It is likely that less indeterminism will reduce any confusion and errors by modelers.

Another interesting topic regarding modeling support is the degree of automation. The more automation provided by the support system, the more decoupled the modeler is from the original problem formulation. One can, of course, differentiate the automation to only consider the consistency of models, and retain a certain degree of freedom in the model formulation task. It is important that such a modeling support system is not restricted to be a tool for novice users, but can also provide means of supporting advanced users. This will increase its usability.

Chapter 4

Implementation of the modeling methodology

4.1 Introduction

A suitable software environment must be chosen in order to implement the modeling methodology. The usability of a modeling tool depends on being supported by a graphical editor and the ability for graphical manipulation through mouse driven commands or similar.

A modeling tool is an environment where several separate functionalities are combined to form a complete environment for *modeling*, *analysis* and *simulation* of any class of process, e.g. chemical, mechanical or electrical. The *modeling* part includes the support for process abstraction such as graphical representation of process structure and behavior, and guidance to model development. Within the *analysis* part there is the functionality for index analysis, algebraic loops detection and degree of freedom analysis. Finally, within the *simulation* part there must be a solution engine with its functionality, e.g. support for different integration routines and the ability to solve lumped as well as distributed parameter systems. A review of recent progress in process modeling environments is given in Pantelides and Britt (1994).

In this work, the modeling methodology is implemented in the environment supported by Matlab (The MathWorks 1992*a*) and Simulink (The MathWorks 1992*b*). The methodology is also implemented in C++ as reported in Wasbø (1996). In that implementation focus is placed on the use of object-oriented features.

Some characteristics about Simulink are presented in Sec. 4.2. The symbols defined in Ch. 2 are implemented and stored in a library. These symbols are given in Sec. 4.3. Since Simulink does not offer an environment for *direct* implementation of the methodology, the necessary mapping or transformation of the formalism is described in Sec. 4.4. The specification menus for the symbols in Sec. 4.3 are given in Sec. 4.5.

4.2 About Simulink

4.2.1 General

There are several reasons for choosing Simulink as an implementation environment. First, Simulink is a tool for simulating dynamic systems and it adds many features that are specific to dynamic systems while retaining all of Matlab's general purpose functionality. Second, to facilitate model definition, Simulink adds a class of windows called *block diagram* windows, in which models are created and edited by mouse driven commands. In addition, there is support for object-orientation to a limited extent.

In Secs. 2.2.3 and 2.3.3, different symbols for different process characteristics and phenomena were introduced. The support for advanced graphics is, however, limited in Simulink. Lines can only be vertical or horizontal, and the inputs and outputs of graphical objects must be on opposite sides. On the other hand, different colors are available and if used consistently, they may actually improve the user interface. To this author's knowledge, the support for thermodynamic packages within the Matlab environment is limited. This implies that these properties have to be manually implemented.

Due to the fact that the TRAV represents the phenomenological aspect of the process, there is no explicit information about information exchange. Simulink, on the other hand, operates on the *informational exchange level* between its graphical symbols. That is, the graphical objects communicate through information exchange lines on the user interface. This requires a transformation of the methodology in order to fit the Simulink environment. This will be described in Sec. 4.4. Of course, any implementation of any methodology finally has to end with an information flow at the lowest level, although this flow might be hidden for the end user. Unfortunately this is not the case with Simulink.

Another reason for choosing Simulink is that minimal effort is required for setting up a model rapidly. Consequently, Simulink is well suited as a prototype environment. It is easy to get started, it is, however, less easy to incorporate advanced graphical functionality.

4.2.2 S-Functions and S-functions

A key component of Simulink is the S-functions, which is a powerful mechanism for augmenting and extending Simulink's capabilities.

An S-function is a programmatic description of a dynamic system (The MathWorks 1994). S-functions can be written using Matlab, C or Fortran, and can describe continuous, discrete, and hybrid systems. The S-functions are embedded into the block diagram using a special block in the predefined Simulink library called an *S-Function* block. The S-Function block's dialog box is used to specify the name of the underlying S-function (The MathWorks 1994). This is illustrated in Fig. 4.1 for the S-function termed `system`. Note that parameters may be specified as inputs to the S-function model file.

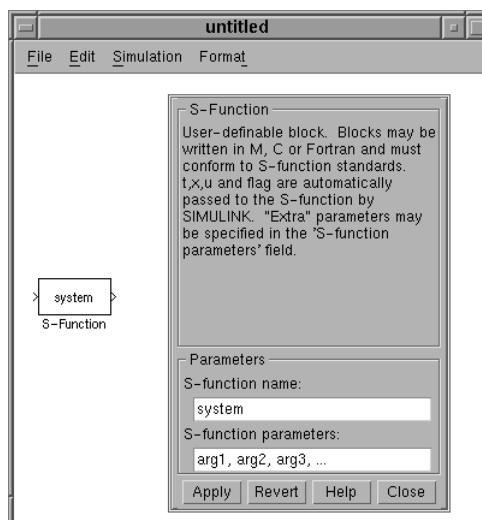


Figure 4.1: The embedding of S-functions into S-Function blocks.

The idea in this work is to use the S-Function block for each phenomenological symbol defined in Tables 2.5 to 2.7. Hence, the S-function file for species accumulation will then be included several times in a model. This is possible due to a data structure called the `SimStruct` that encapsulates all the data associated with an S-function. This data structure provides object-oriented techniques like data abstraction, modularity and reentrancy (The MathWorks 1994). On the other hand, techniques like inheritance, polymorphism or message passing features are not included. This implies that if a library of S-Function blocks are developed according to the defined phenomenological symbols, each S-Function block copied from the library into a model can be interpreted as an *instantiation* of the corresponding S-function file.

A visualization of the relation between the model file `system.mex`, the instantiations and S-Function blocks is shown in Fig. 4.2. It is also shown how multiple use of the same S-Function block is possible due to reentrant S-functions.

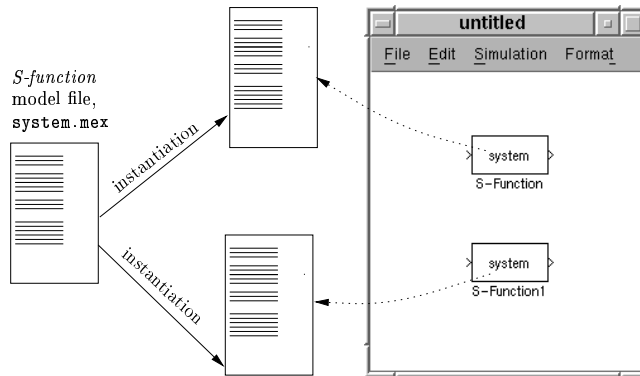


Figure 4.2: The relation between S-function model file, instantiations and S-Function blocks.

4.2.3 S-function behavior

S-functions are used to implement the relation between phenomenological symbols and equations described in Sec. 2.6. Because of the variety of equations, especially rate equations, it is not convenient to develop an S-function for each possible equation. This is mainly due to the size of the S-function files and the corresponding maintenance problem. The approach chosen here is to develop *two* main S-functions, i.e. one with accumulation properties (corresponding to differential equations) and one without accumulation properties (corresponding to algebraic equations).

To accomplish this, the S-functions need to be initialized according to the intended behavior. This initialization is performed as exemplified below, where `S` is the `SimStruct` data structure. The figure given next to the `S` is the number of each quantity.

```
{
ssSetNumContStates( S, 1); /* continuous states */
ssSetNumDiscStates( S, 0); /* discrete states */
ssSetNumInputs(    S, DYNAMICALLY_SIZED); /* inputs */
ssSetNumOutputs(   S, 2); /* outputs */
ssSetDirectFeedThrough(S, 0); /* direct feedthrough flag */
ssSetNumSampleTimes( S, 1); /* sample times */
ssSetNumInputArgs(  S, 3); /* input arguments */
ssSetNumRWork(     S, 0); /* real work vectors */
ssSetNumIWork(     S, 2); /* integer work vectors */
ssSetNumPWork(     S, 3); /* pointer work vectors */
}
```


As can be seen, modelers have a large degree of freedom in specifying the behavior of each S-function. The accumulation behavior is specified in the `ssSetNumContStates`. To obtain no-accumulation behavior, the `ssSetNumContStates` is set to 0, and the `ssSetDirectFeedThrough` is set to 1. Note that the `ssSetNumInputs` is specified as `DYNAMICALLY_SIZED`. This is an important property of S-functions, and is a prerequisite for successful modeling using the concepts developed in this thesis. The functionality of this specification is that the S-Function block is responsible for detecting the number of inputs itself. This implies that modelers can add inputs and outputs on the block diagram with no fear of inconsistency.

The two main S-functions are rather large due to extensive consistency checks and data preparation. In order to obtain the intended model behavior using specific rate and balance equations, each S-Function block is given a model behavior file name in the parameter input field of the dialog box shown in Fig. 4.1. The file with this file name is then called from the corresponding S-function, implying that each particular S-function is specified with a certain type of behavior. These model behavior files are less complex and easier to maintain. A visualization of the relation between the two S-function files, the instantiations and the additional model behavior files is given in Fig. 4.3.

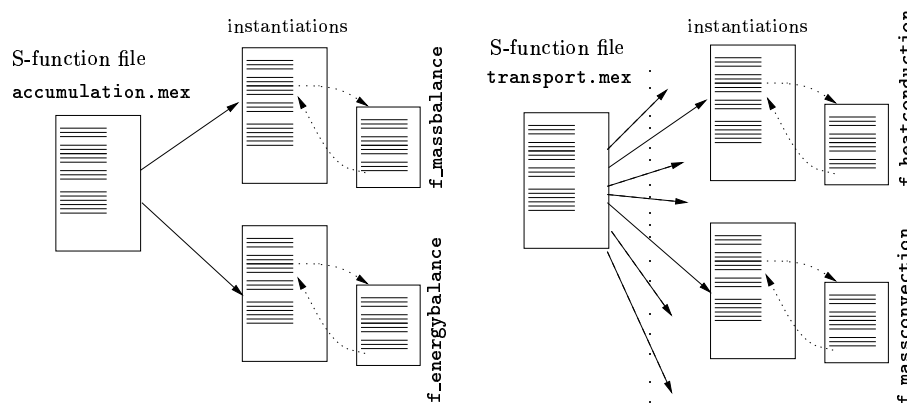


Figure 4.3: The relation between the two S-function files, the instantiations and the additional model files.

The `accumulation.mex` is the S-function describing differential equations and `transport.mex` is the S-function describing rate and constitutive equations. Note that only two model files employ the `accumulation.mex` S-function, while the `transport.mex` is extensively used. A complete description of the `accumulation.mex` S-function file and the `f_heat_convection.mex` model file are given in Secs. C.1 and C.2, respectively.

4.2.4 Masking

A powerful property of Simulink is the *masking* functionality. Several blocks can be grouped together and masked as *one* block, and new functionality can be developed by creating new blocks for a dedicated requirement. The stand-alone S-Function block in Fig. 4.1 can also be masked. In this case, there are at least two favorable properties of masking. First, the input arguments given as parameters, e.g. the `arg1`, `arg2`, `arg3` in Fig. 4.1, can be presented in a more user-friendly fashion, see Fig. 4.4. This menu appears by clicking on a masked block.

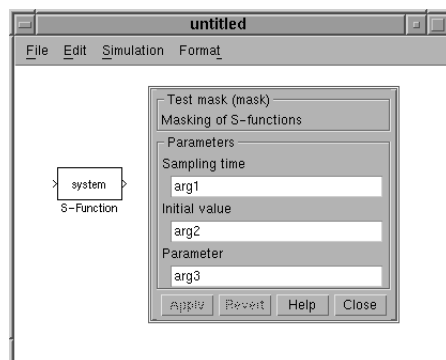


Figure 4.4: A masked S-Function block and its mask menu.

The second property is the possibility to change the layout of the block, imitating the symbols defined in Ch. 2. These are shown in Sec. 4.3.

4.2.5 Multiplexing

The network of information in Simulink models can become very complex and unstructured. For this reason, Simulink offers a functionality of multiplexing several lines into one to improve the representation. The symbols for the multiplexers and demultiplexers are given in Fig. 4.5. The use of multiplexers, however, actually diminishes the resemblance between the methodology in Ch. 2 and the implementation. Thus, this is a trade-off between functionality and the degree of adaption.

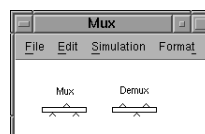


Figure 4.5: Some useful accessories.

4.3 Topological and phenomenological symbols

The masked blocks for the topological and phenomenological symbols defined in Secs. 2.2.3 and 2.3.3 is presented in this section. These blocks are saved in a library.

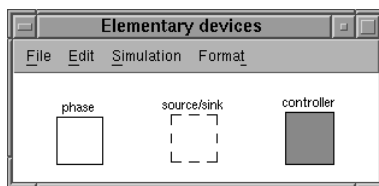


Figure 4.6: The elements of the ED set in Table 2.1.

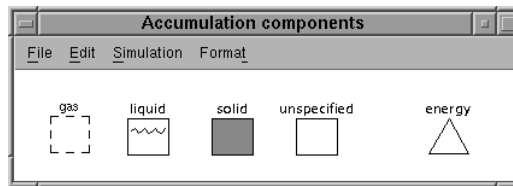


Figure 4.9: The mass and energy accumulation symbols from Table 2.5.

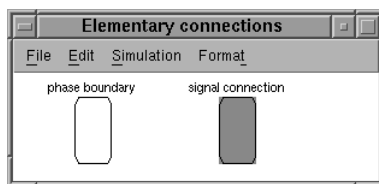


Figure 4.7: The elements of the EC set in Table 2.2.

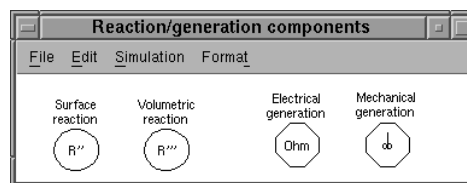


Figure 4.10: The reaction and generation symbols from Table 2.6.

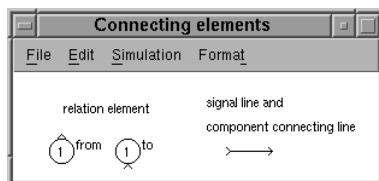


Figure 4.8: The elements of the CE set in Table 2.4.

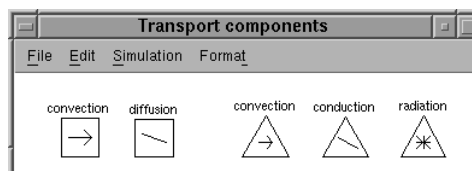


Figure 4.11: The transport symbols from Table 2.7.

Note that the composite topological symbols from Table 2.3 are similar to the symbols in Figs. 4.6 and 4.7. Note also that the relation element is different from the one defined in the methodology. In Simulink, only one component connecting line is allowed, i.e. the solid line. It is further not possible to have two graphical representations, i.e. a mass and energy based part, of the same model. This implies that the *combined* mass and energy based representation must be used, and there is no difference between lines used on the TRAV and PTD.

4.4 Transformation of the modeling methodology

It is evident that both topological and phenomenological components have to exchange information in order to represent a complete model. As an example, the material flow inside connections is derived from knowledge of state information in the connected devices. In order to describe the steps in the transformation, the CSTR in Fig. 1.1 will be used. The focus will first be on the topological structure, and then on the phenomenological one.

4.4.1 Topological modeling

To limit the example, consider only the reactor system with its mass flow inputs and outputs in Fig. 2.1. The result of the transformation (or adaptation) is shown in Fig. 4.12.

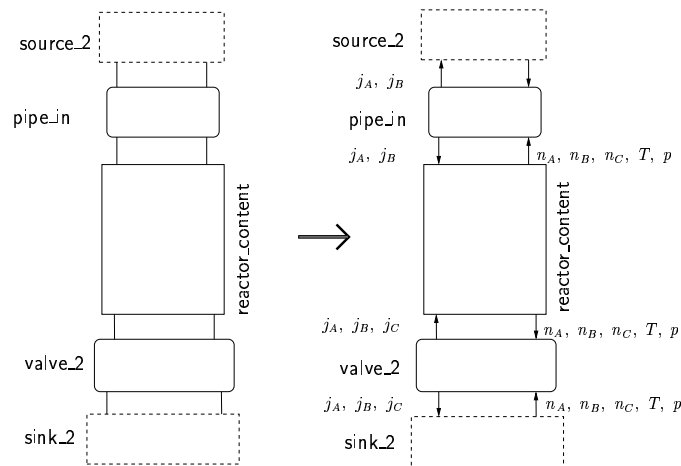


Figure 4.12: The transformation between graphical representation and implementation for topological components.

Note that the arrows in the right hand part of Fig. 4.12 must be separated from the arrows employed in the modeling methodology.

The topological components are modeled and connected together in a main block diagram. Using the blocks from the library, the implementation of the reactor part of the CSTR example in Fig. 4.12 is shown in Fig. 4.13. Note that the limitation of Simulink objects with respect to input and output lines on opposite sides, restricts the ability of the model in Fig. 4.13 to imitate Fig. 4.12. Note also that the name of the components is placed onto the symbol in Fig. 4.13.

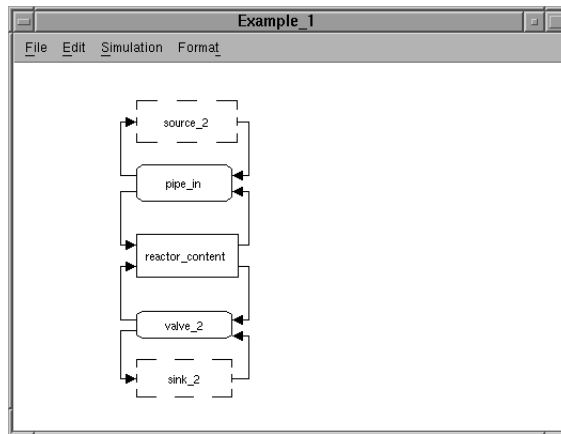


Figure 4.13: The implementation of the reactor part of the CSTR.

Each block or component in Fig. 4.13 is a subsystem. By a double-click, the view of the inner is revealed. In this case, the inner of the reactor_content is of course *empty* as shown in Fig. 4.14. This means that modelers include blocks from the library according to the TRAV structure.

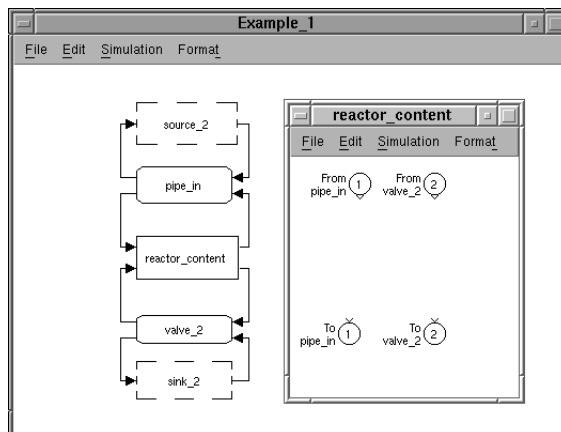


Figure 4.14: Visualization of the block diagram concept in Simulink.

Note that there is no difference in the appearance of the topological and the phenomenological representation, i.e. the TRAV is implemented in a similar block diagram as the PTD.

4.4.2 Phenomenological modeling

For the phenomenological components to communicate, there has to be a similar information flow between the components as for the topology components. This mapping is shown in Fig. 4.15 for the communication between the chemical species A , and the reaction R_1 .

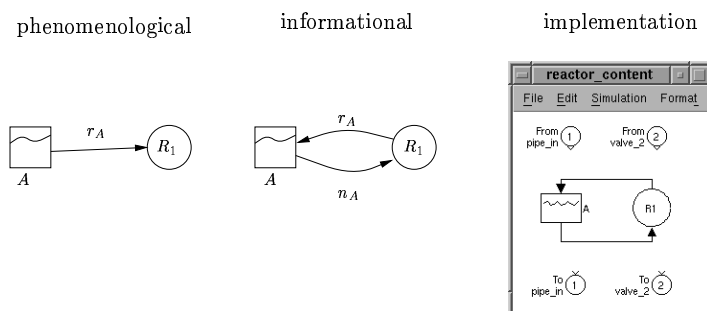


Figure 4.15: The mapping from phenomenological representation, through informational exchange perspective, to implementation.

Again, it is important to emphasize that the arrows used on the informational perspective are *neither* material nor energy flow lines. Only the reactor_content will be considered in the following. By selecting components from the library, the entire TRAV for the reactor_content in Fig. 4.16 could be as in Fig. 4.17.

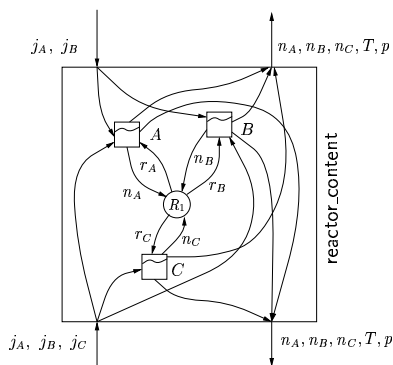


Figure 4.16: The information flow between phenomenological components of the reactor_content.

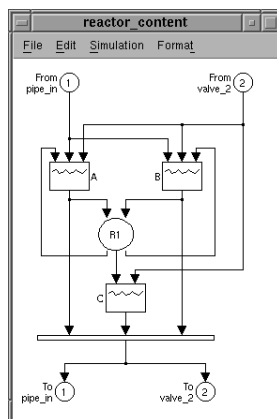


Figure 4.17: The implementation of Fig. 4.16.

Observe from Fig. 4.17 that the already mentioned multiplexer is introduced.

4.4.3 Rearranging the symbols

The symbols may be arranged to improve the user interface.

This is achieved by employing the multiplexing property more extensively as depicted in Fig. 4.18. The implication of this rearrangement is that the reaction becomes responsible for detecting and selecting the necessary information in order to calculate its output. It is not obvious anymore which components are participating in the reaction. This can be accomplished, as shown, by adding the string “ $A + B \rightarrow C$ ” to the reaction component.

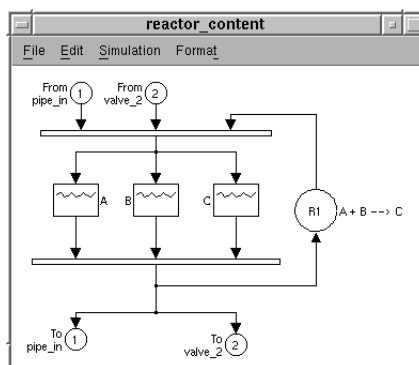


Figure 4.18: Rearranging the layout from Fig. 4.17.

Note that T and p are included in Fig. 4.16, but not in Fig. 4.17. Due to the lack of support for a thermodynamic package, modelers need to include these routines themselves.

In addition, there is no straightforward method to interpret each subsystem as a stand-alone system where the included phenomenological components are arguments to a *hidden* thermodynamic subroutine. Hence, the block for this routine must be physically placed *on* the block diagram. This block will receive information from all mass balances and the energy balance, and calculate the temperature and other possible dependent state variables. This is shown in Fig. 4.19, where the energy balance is also included. Due to the rearrangement of the symbols, it is no longer obvious how the TRAV was originally.

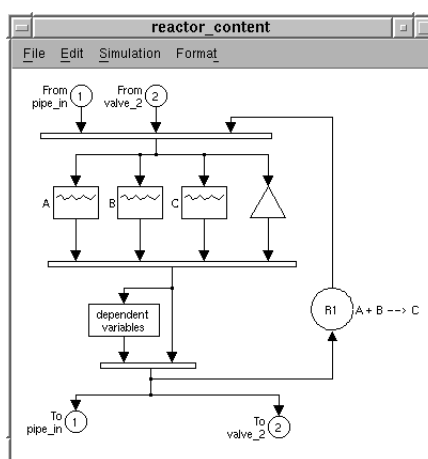


Figure 4.19: Block diagram of the reactor_content, including the energy balance and dependent state variables block.

4.4.4 Resolving the consistency

In order to achieve flexible and efficient modeling, modelers provide information to each S-function file instantiation (through the parameter input) about what sort of information each file is expected to receive from the `DYNAMICALLY_SIZED` input. To identify this information, each variable (state, dependent and flow variables) is assigned a tag with a name that is exclusive for this variable.

Note that the flow of species, j_A , j_B and j_C in Fig. 4.16 has neither any indication of positive or negative direction, nor which *ETC* they belong to. There is therefore no difference between the tag names of the flow going in opposite directions, exemplified by j_B^+ and j_B^- , where $j_B^+ + j_B^- = 0$.

To resolve this with the *same* tag name as in the approach here, the *value* is inverted according to the defined positive direction, and the tag name is kept. This will ensure consistency. The inverting mechanism described above must be included on the representation. Consequently, an *inverter* block is defined for this, see Fig. 4.20.

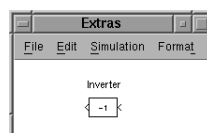


Figure 4.20: The inverter and To Workspace block.

4.5 Model initialization and specification

The information given to each instantiated S-function file is provided in the mask menu for each block. In addition to the model file and the tag names, other input arguments are the initial value and an identifier string used for debugging. Some of the mask menus for the symbols in Sec. 4.3 are presented in the following. The information given in the menus are related to the CSTR example.

4.5.1 Initialization of elements of the set A

This section has a similar structure as Sec. 3.2.3, where the initialization of accumulation elements was briefly discussed.

Initialization of A_S elements

The arguments needed to completely specify the accumulation component of B , is shown in Fig. 4.21.

This menu appears by double clicking on the graphical symbol. The tag names for the HOLDUP of B is `n_B`, the molar FLOW of B is `j_B` and the GENERATION of B in R_1 is `r_B`. Note the resemblance to the structure in (2.23). The initial value is given in moles.

As stated in footnote 3 on page 63, the specification of the specific enthalpy, \tilde{H}_i , is related to the initialization of A_S elements. This is indicated in the **Energy specification** in Fig. 4.21.

Figure 4.21: The mask menu for specifying the mass balance of B in reactor_content.

The arguments in the **Energy specification** correspond to a specific enthalpy of B similar to (3.15):

$$\tilde{H}_{B,\text{reactor_content}} = \Delta_f H_{298,B}^\circ + \int_{298}^{T_{\text{reactor_content}}} c_{p,B} dT + \Delta_{\text{sol}} H_B^\circ. \quad (3.15)$$

However, as discussed in Sec. D.3.2, approximated values for \tilde{H}_i are used, and (3.15) is therefore replaced with

$$\tilde{H}_{B,\text{reactor_content}} = \Delta_f H_{298,B}^\circ + \bar{c}_{p,B}(T_{\text{reactor_content}} - 298) + \Delta_{\text{sol}} H_B^\circ \quad (4.1)$$

in the implementation. ■

Initialization of special A_S elements

As mentioned in Sec. 2.2.2, sources and sinks are not considered to share the properties of a phase. A species symbol from Table 2.5 on page 26 modeled within a source could, hence, represent a data input file.

Thus, the mask menu for this special kind of A_S elements will therefore be considerably different than species *accumulation*. An example is the **Species input** mask menu shown in Fig. 4.22. The information given in Fig. 4.22 indicate that the data file is named `input_B`. Moreover, the specific enthalpy of B in the `source_2` device is specified as `[Hf_B, cp_B, Hsol_B]` in the **Energy specification**. This corresponds to:

$$\bar{H}_{B,source_2} = \Delta_f H_{298,B}^\circ + \bar{c}_{p,B}(T_{source_2} - 298) + \Delta_{sol} H_B^\circ. \quad (4.2)$$

Figure 4.22: The mask menu for B in `source_2`.

Initialization of A_E elements

The energy balance mask menu is given in Fig. 4.23.

The arguments given correspond to (2.27). The tag name for the HOLDUP of H is `enthalpy`, whereas the tag name for the enthalpy flow related to mass flow (the $j_i \cdot \bar{H}_i$ terms in (2.27)) is `enthalpy_flow`. Note that all 5 mass flows (2 input and 3 output indicated in Fig. 2.10) use this mutual specification for enthalpy flow related to mass flow. Further, the tag for conductive heat flow is `heat_conduction` and is given in the **PURE HEAT FLOW** field. There are also **WORK** and **POWER** specifications available.

Figure 4.23: The mask menu for specifying the energy balance in the `reactor_content` device.

Note that the menu in Fig. 4.23 does not correspond to the implementation in Fig. 4.19 since the heat loss through the wall is not included in Fig. 4.19. The initial value of the enthalpy, termed `enthalpy_reactor_0`, is calculated from:

$$H = \sum_{i=1}^N n_i \tilde{H}_i + \Delta_{\text{mix}} H, \quad \forall i = \{A, B, C\}, \quad (4.3)$$

which is an approximation of (3.14) due to the use of \tilde{H}_i . ■

4.5.2 Specification of elements of the set T

This section has a similar structure as Sec. 3.2.4, where the specification of the transport elements was briefly discussed.

Specification of T_S elements

To exemplify the specification of elements of the set T_S , consider the mask menu for the flow of B in the `pipe_in` connection, shown in Fig. 4.24.

Since mass flow also involves energy flow, the mask menus for this property consist of a **Mass part** and an **Energy part**. For the **Mass part**, the **INPUT** is `j_B` which is specified as **OUTPUT** in Fig. 4.22. Since the transport in *this* particular connection is a direct feedthrough, the **OUTPUT** is also `j_B`, and the model file name is `f_direct_feed_through`. As discussed in Sec. 3.2.4 and illustrated in Fig. 3.12, modelers have to specify the specific enthalpy of the flowing species.

There is a difference in the specific enthalpy of the adjacent devices of the `pipe_in` connection as can be seen from (4.1) and (4.2).

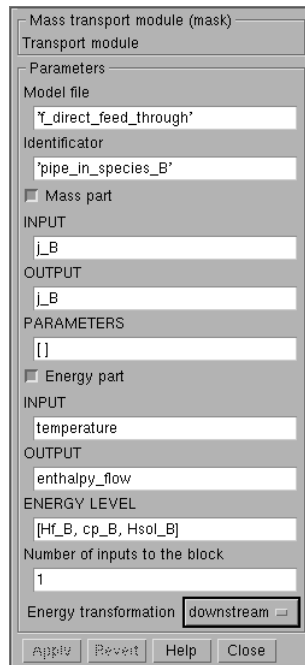


Figure 4.24: The mask menu for flow of species. Species B is dissolved.

However, as indicated in (2.27) and Fig. 2.10, the specific enthalpy of the incoming B is already assumed to be similar to the specific enthalpy of the `source_2` device, i.e. as (4.2). Consequently, it is the `reactor_content`, or the *downstream* device specified in the **Energy transformation** in Fig. 4.24, that contributes to the energy transformation. Hence, the `temperature` tag in the **INPUT** field in the **Energy part** indicates the `source_2` temperature, and the specific enthalpy of the flowing B is in the `pipe_in` connection is

$$\tilde{H}_B = \Delta_f H_{298,B}^\circ + \bar{c}_{p,B}(T_{\text{source}_2} - 298) + \Delta_{\text{sol}} H_B^\circ. \quad (4.4)$$

The `enthalpy_flow` tag in the **OUTPUT** field is the enthalpy flow related to mass flow. This is, as mentioned, included in the **FLOW** field in the energy balance mask menu in Fig. 4.23.

Assuming that B is solid in the `source_2` device, the **Energy specification** in Fig. 4.22 is changed to `[Hf_B, cp_B]` and (4.2) is similarly changed to

$$\tilde{H}_{B,\text{source}_2} = \Delta_f H_{298,B}^\circ + \bar{c}_{p,B}(T_{\text{source}_2} - 298). \quad (4.5)$$

This implies that the **ENERGY LEVEL** in Fig. 4.24 is also changed to `[Hf_B, cp_B]`. ■

Specification of T_E elements

The specification of the conductive heat flow in the wall is given in Fig. 4.25, and corresponds to (2.30). The `temperature` tag here is used for the temperature of both the `reactor_content` and cooling. As a result, the implementation uses the same tag for different measures of the same quantity. This reduces the variety of tags.

The consistency is resolved from exploiting the knowledge of the positive direction, as discussed in Sec. 4.4.4. This means that the S-function will identify 2 **INPUTs** satisfying the `temperature` tag, and these are sorted according to the order they were identified, i.e. according to the positive direction. The tag for the conductive heat flow is still `heat_conduction`, corresponding to the **PURE HEAT FLOW** in Fig. 4.23.

Note the parameters included in the **PARAMETERS** field. ■

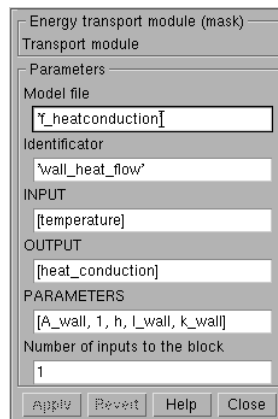


Figure 4.25: The mask menu for heat conduction.

4.5.3 Specification of elements of the set RG

To exemplify the mask menu for the reaction/generation set, consider reaction R_1 in the reactor_content.

This mask menu is given in Fig. 4.26. The tags for the reaction rates are `r_A`, `r_B`, `r_C` given in the `OUTPUT` field. The `r_B` is specified in the `GENERATION` part of Fig. 4.21. The `INPUT` consists of tags corresponding to both extensive and intensive (dependent) variables. The intensive variables are calculated from the dependent variables block shown in Fig. 4.27 below. The model file with the behavior of R_1 is termed `f_1order_reaction`.

Figure 4.26: The mask menu for volume reaction R_1 .

4.5.4 Specification of constitutive equations

The mask menu for the dependent state variables block is given in Fig. 4.27. The tags for the extensive variables of the reactor_content device are included in the `INPUT` field.

The `temperature` and `volume` tag needed as `INPUT` in Fig. 4.26, is specified as `OUTPUT`. Other possible variables are `mass_fraction`, `density` and `mol_fraction`. The argument `reactor_thermodynamic` in the `PARAMETERS` field contains the knowledge of the specific enthalpy of each species discussed in Sec. 3.2.3. Further, it contains thermodynamic knowledge of each species.

Figure 4.27: The mask menu for the dependent variables.

4.6 Discussion

This chapter has described the necessary transformation of the methodology presented in Ch. 2 into the environment supported by Simulink. Even if Simulink's ability to imitate the original representation is limited, it has proven a useful aid in the modeling process. This is due to the use of graphical manipulations and the automatic updating of the underlying equations after model changes. This also means that less time has been spent on code checking since each accumulation symbol is related to a predefined equation structure. Consequently, little effort has been required here for code generation.

Due to the limitations of Simulink discussed above, several features of the proposed methodology in Ch. 2 and Ch. 3 are not implemented. Some examples are *i*) the separation into mass and energy based representations, *ii*) graphical features, *iii*) the whole concept of introducing a posteriori assumptions and the corresponding equation manipulation. To this author's knowledge, it is not possible to include these functionalities in Simulink.

These restrictions call for an alternative modeling and simulation environment where the limitations of Simulink are resolved. Such an environment could possibly be Visual C++. This is, however, a topic for future work.

Part II

Application

Chapter 5

Process description

This chapter gives a process description of the aluminum electrolysis cell including topics of cell control. The chapter is organized as follows. After a short introduction in Sec. 5.1, the main raw materials are described in Sec. 5.2. The fundamentals of aluminum production with emphasis on AlF_3 dynamics is given in Sec. 5.3, and issues of cell control are discussed in Sec. 5.4. Finally, Sec. 5.5 gives a short review of thermodynamic aspects. The focus in this thesis is on prebaked cells.

The material presented in Secs. 5.1 to 5.3 is mainly taken from Grjotheim *et al.* (1982), Grjotheim and Welch (1988), Grjotheim and Kvande (1993) and PIL (1993).

5.1 Introduction

5.1.1 History

Aluminum is the most abundant metal in the earth's crust (7.3 wt.%). Due to aluminum's affinity to oxygen, it is not found as an element, but as aluminum oxide (Al_2O_3). This compound is also referred to as *alumina*. The fundamental concept of aluminum production is using electricity to reduce alumina to aluminum and oxygen. A prerequisite for this is that the alumina is melted or dissolved. The melting point of alumina is close to $\theta = 2030^\circ\text{C}$. This is in general too high for commercial production. In order to produce aluminum more efficiently, i.e. at a lower operating temperature, scientists in the 19th century sought to identify a chemical compound that acted as a solvent for alumina. In 1886 Paul Héroult from France and Charles Hall the USA independently patented the electrolysis of cryolite-alumina melts. This process is referred to as the Hall-Héroult process. The

operating temperature of their melts was approximately 1010°C , which is the melting point of cryolite (Na_3AlF_6). The contemporary development of the fundamentals of aluminum electrolysis is not the only parallel between Hall and Héroult. They were both born in 1863 and both died in 1914.

Despite many attempts to improve the process of aluminum reduction by using other solvents or other compounds containing aluminum (aluminum chloride), the fundamentals from Hall and Héroult is still used. In spite of this “stagnation”, drastic improvements have been made over the years, ranging from cell design, cell size, additives, to different kinds of feeding strategies.

There are two types of cells used in the smelter industry today, Søderberg and prebaked cells, with Søderberg being the oldest technology. New plants use prebaked cells exclusively. The major difference between these two cell types is the anode. Søderberg cells use one, continuous anode while prebaked cells use several stand-alone anodes. For Søderberg cells the anode bakes itself using heat from the bath, while prebaked cells use premanufactured anodes. A schematic sketch of a prebaked cell is given in Fig. 5.1.

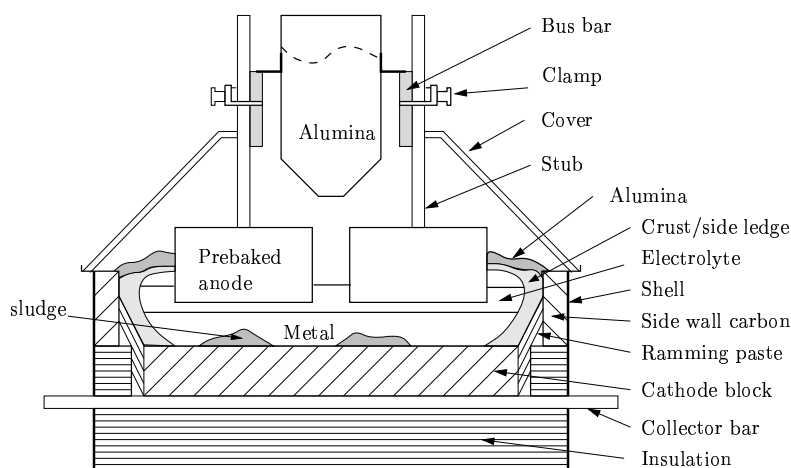


Figure 5.1: Illustration of a prebaked anode cell.

During recent decades, environmental considerations have been taken very seriously in aluminum production. Earlier, small communities experienced environmental destruction particularly from fluoride emission¹. To over-

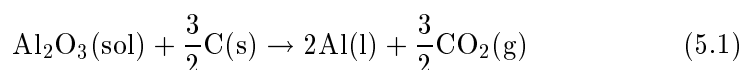
¹It is common to distinguish between *emission* and *evolution*, where emission is what escapes over roof and evolution is what recycles in the dry scrubber.

come this problem, the ability of alumina to absorb fluoride gas was included into the process. By driving cell fume (gas and particles) counter-current alumina in big dry scrubbing units, fluoride emission to the environment dropped to an acceptable level. This absorption process has also had another positive effect in that the need for fluoride in the cells has been reduced because of the recirculation of fluoride absorbed by the alumina. Almost 80-90% of the fluoride evaporating from the pot line is compensated by this recirculation (PIL 1993).

The price (with no compensation for inflation) of aluminum has been relatively stable in this century, implying that aluminum was a rather expensive metal early in the 20th century. Nevertheless, even if the fundamentals of the process are still the same, the energy consumption, \mathcal{EC} , has decreased from 28 kWh kg⁻¹ aluminum in the beginning of this century to around 13 kWh kg⁻¹ aluminum for the best smelters today². This reduction is due to increased cell size, improved cell control and bath additives (Grjotheim and Welch 1988). The challenge for the industry today is to further reduce and maintain consistently low energy consumption through cell stabilization, even though 12-13 kWh kg⁻¹ aluminum seems to be a lower limit for prebaked cells that are magnetically well balanced.

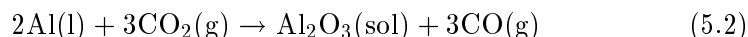
5.1.2 Performance measures

The overall primary electrochemical reaction in an electrolysis cell is:



The reaction in (5.1) is endothermic. The heat needed is supplied from the heat produced from current passing the ohmic resistive bath. The bath under the anodes, i.e. the interpolar space, is therefore somewhat warmer than the bath in the side channels. The interpolar distance is also referred to as the anode-cathode-distance (ACD), where the cathode is referred to as the metal surface.

Due to the reactivity of pure aluminum at the operating temperature, and the presence of CO₂ gas from (5.1), some dissolved aluminum in the bath will back react according to:



This reaction reduces the performance of the cell, and this is represented in the *current efficiency*, \mathcal{CE} . It is defined as the ratio of actual metal

²Theoretical minimum is 6.34 kWh kg⁻¹ aluminum, including preheating of reactants (Grjotheim and Kvande 1993).

produced to the theoretical amount given by Faraday's law. For a good smelter using prebaked cells this efficiency is in the area of 94%. For old Söderberg cells it is often as low as 88%. There are also other effects having impact on the \mathcal{CE} , though the back-reaction in (5.2) is the dominant part.

Another performance measure is the actual energy consumption, \mathcal{EC} . Generally, \mathcal{EC} has a minimum at some ACD, i.e. ACD_{opt} . This is due to the fact that reduction of the ACD below ACD_{opt} makes the CO_2 bubble layer underneath the anodes closer to the metal surface. For this reason, the back reaction in (5.2) increases accordingly, reducing the \mathcal{CE} and thereby increasing the \mathcal{EC} . Moreover, increasing of the ACD beyond ACD_{opt} reduces the back reaction, though \mathcal{EC} increases due to increased cell voltage. This results in an optimal ACD value, which is a compromise between the wish for low \mathcal{EC} and high \mathcal{CE} . Laboratory studies indicate that the ACD does not influence the \mathcal{CE} unless very low ACD (Solli *et al.* 1994). However, both the \mathcal{CE} and the \mathcal{EC} are dependent on cell size, cell control and bath additives.

5.1.3 Electric input

One of the largest expenses for an aluminum smelter plant is the cost related to energy consumption. As mentioned, the need for power to produce 1 kg aluminum is in the area of 13-14 kWh for prebaked cells and 16-17 kWh for Söderberg cells. With an annual production of almost one million tonnes of aluminum in Norway, it requires approximately 10% of the country's total annual power production (PIL 1993). It is therefore desirable to keep the energy consumption at the lowest possible level.

The incoming voltage to a plant is usually 300 kV alternating current. It is usually transformed in two steps. First to 30 kV and subsequently to a voltage depending on the number of cells and the cell size, typically 1000 V. Normally there are 200 cells in a pot line. The electrolysis process requires direct current, implying that the incoming voltage has to be rectified. The amplitude of the current is between 100-200 kA for most smelters.

The physical size of cells is usually reported in amperes (kA) and not in the actual size. This is because there is an optimal *current density*. This is usually in the area of 0.7-0.9 A cm^{-2} , meaning that the physical size and the amperage can be viewed as two different variables giving the same information. As the cell size increases, some problems of minor significance for smaller cells, are amplified. The major one is magnetically induced movement in the metal. This movement causes the metal and bath to circulate, introducing a skew metal surface and increasing control problems. To some degree this problem is handled by configuration of the risers which

will, to some degree, balance the magnetic impact. Cells that are well compensated experience in turn other problems like decreased solubility for alumina and decreased self-feeding from sludge because of the reduced bath and metal movement.

If one analyzes the total voltage (approximately 4.5 V) applied to a cell, the decomposition depicted in Fig. 5.2 is typical.

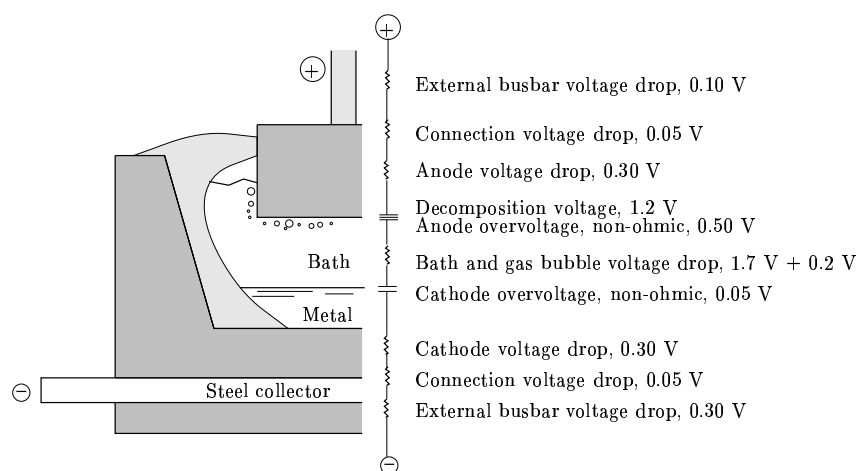


Figure 5.2: Decomposition of the voltage drop through a cell, from Grjotheim and Welch (1988).

Note that the ohmic bath resistivity is more than one third of the total resistance. The bath resistivity is linearly dependent on the ACD, and it is optimal from an energy consumption point of view to keep the ACD as small as possible. On the other hand, if the ACD is too small, the heat generation from the bath could be too low to maintain the required bath temperature and side ledge thickness. This implies that the choice of the optimal ACD discussed in Sec. 5.1.2 also depends on cell design. Under normal operating conditions the ACD is between 4 and 5 cm. The metal depth is normally between 16 and 20 cm, implying that Fig. 5.2 gives an incorrect representation with respect to both ACD and metal depth.

The energy generated in the bath is lost as heat to the surroundings. According to Grjotheim and Kvande (1993), approximately 50% of the total heat loss escapes through the top of the cell, 40% escapes through the side and 10% escapes through the bottom.

In the decomposition of the total voltage presented above, the term *over-voltage* is introduced. This can be looked upon as additional voltage re-

quirements due to physical constraints. We distinguish between two kinds of overvoltage (Grjotheim and Kvande 1993):

- charge transfer overvoltage or reaction overvoltage
- concentration overvoltage (polarization)

Charge transfer overvoltage is due to the slow rate of electron transfer, requiring an additional voltage to maintain a high production rate. Concentration overvoltage is due to limited transportation of the reacting compounds to the reacting surfaces. For a thorough introduction to voltage analysis, see Welch (1989).

5.2 Raw materials

The most important materials used to produce aluminum are discussed in this section. These raw materials, together with products and byproducts are depicted in Fig. 5.3.

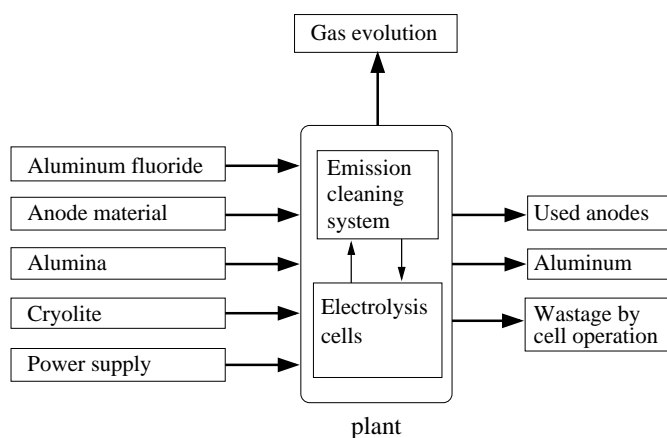


Figure 5.3: Raw material, products and byproducts of aluminum production.

To produce 1000 kg aluminum with a prebaked cell, the typical inputs are:

Table 5.1: Inputs required to produce 1000 kg aluminum in pre-baked cells.

Alumina	1930 kg
Anode material	420-550 kg
Cryolite	20 kg
Aluminum fluoride	30 kg
Power	13000-14000 kWh

In subsequent sections, these materials will be discussed in more detail. The power input was discussed in Sec. 5.1.3.

5.2.1 Aluminum oxide, Al_2O_3

Nearby the town Les Baux in France, a new ore was discovered in 1822. This ore showed large contents of aluminum oxide (Al_2O_3), and because of its origin, it got the name Bauxite. Bauxite has similar characteristics to clay, but due to ferro containing compounds, it has a distinct red appearance. The sources in Les Baux are now empty, and the main production is in tropical and sub-tropical regions. There are 3 main types of bauxite (Grjotheim and Kvande 1993):

- Gibbsite, $\text{Al}(\text{OH})_3$
- Böhmite, $\text{AlO}(\text{OH})$
- Diaspor, $\text{Al}_2\text{O}_3 \cdot \text{H}_2\text{O}$

The main difference is how aluminum is combined with oxygen and hydrogen. Bauxite as an ore cannot be melted as it is (unlike iron ore), and it has therefore to be treated chemically to extract alumina. This chemical process is called the *Bayer process*³, and is divided into the following 5 main stages (Grjotheim and Kvande 1993):

- **Extraction** of sodium aluminate from crushed bauxite mixed with soda (NaOH) under high pressure and temperature.
- **Clarification** of the mixture from the extraction process removes any impurities like iron oxide, sand and other minerals.
- **Precipitation** of aluminum hydroxide from sodium aluminate is done with seed additions.
- **Filtration** of aluminum hydroxide.
- **Calcination** at $\theta = 1200^\circ\text{C}$ to remove the chemical bounded water in the crystals, making oxides from hydroxides.

Al_2O_3 can be classified according to several different characteristics such as chemical purity, degree of calcination, surface area, grain size and density (Grjotheim and Kvande 1993). Because of these individual differences, each alumina producer has different alumina quality. When changing alumina in a plant, it is observed that the cell behavior changes accordingly. The relationship between alumina quality and cell behavior has not been determined in full detail. In addition to serve as the main raw material,

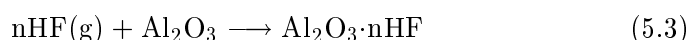
³Developed in 1888 by Karl Josef Bayer.

alumina has several other functions in production. First of all, it serves as an absorbent for fluoride in the dry scrubber, second as cover on the cells to reduce energy dissipation, and third it hinders burning (soot formation) when oxygen reacts with the hot anode surface above the bath level.

One of the major impurities in alumina is Na_2O . This reacts with AlF_3 and forms Na_3AlF_6 and Al_2O_3 . Calcium oxide, CaO , is also present, and is the main source for the content of CaF_2 in the bath. CaF_2 is built up to a concentration between 4 and 6 mass% in the bath without any other additions. This concentration is stable because the rate of addition of CaO is balanced by the rate of loss of calcium into the aluminum produced and also in the anode gases (Grjotheim and Kvande 1993).

Secondary alumina

As previously mentioned, alumina's properties are important in the fluoride absorption (chemisorption) process. The cell fume from all cells are driven counter-current with the alumina feed. The following reaction scheme is suggested



The residence time of alumina determines the degree of absorption (Grjotheim and Welch 1988). The level of fluoride (F) in the secondary alumina varies between 1 and 2 mass%⁴. As a matter of notation, the alumina from the dry scrubber is referred to as *secondary alumina*. The fundamentals of dry scrubbing can be found in Johansen (1993). ■

5.2.2 Cryolite, Na_3AlF_6

Cryolite is a double salt consisting of sodium fluoride and aluminum fluoride in the form $3(\text{NaF})\text{AlF}_3$ or Na_3AlF_6 . The largest natural occurrence of cryolite was found at Ivigtut on Greenland (PIL 1993). This source is now empty, and cryolite is nowadays produced synthetically. Cryolite's melting point is $\theta = 1010^\circ\text{C}$, but the addition of AlF_3 and CaF_2 reduces this melting point (Grjotheim and Kvande 1993). The ability of cryolite to dissolve alumina is approximately 10%, depending on temperature and other additives. Melted cryolite is extremely corrosive, and this hinders continuous measurements of the bath composition and temperature. The only component able to withstand the corrosive cryolite is *frozen* cryolite, and this is why cells need the protective layer from a side ledge as illustrated in Fig. 5.1.

⁴From an unpublished report from Hydro Aluminum a.s.

5.2.3 Aluminum fluoride, AlF_3

Aluminum fluoride is added to improve some of the bath properties. These improvements include lowered liquidus temperature⁵, reduced aluminum solubility, improved current efficiency and lowered density. On the other hand, the disadvantages of increased AlF_3 content are e.g. increased ohmic resistance, increased fluoride volatility and lowered alumina solubility.

The mass fraction (or mass%) of AlF_3 relative to Na_3AlF_6 is referred to as the *excess* AlF_3 ⁶ in the literature. This thesis, however, employs excess AlF_3 as the *mass fraction* of AlF_3 relative to *all* bath components, w_{AlF_3} . Other definitions used for this quantity are the (a) cryolite ratio, expressing the molar ratio of NaF to AlF_3 , and (b) bath ratio, expressing the mass ratio of the same components (Grjotheim and Kvande 1993).

During electrolysis there is a net consumption of fluoride through emission. Under normal operating conditions the emission is 15-30 kg tonne^{-1} aluminum. Aluminum fluoride is made synthetically, and its purity is around 90% AlF_3 with the remaining 10% being Al_2O_3 .

To compensate for high excess AlF_3 values, sodium carbonate (Na_2CO_3) is sometimes added. The addition of this compound will consume AlF_3 according to:



5.2.4 Carbon, C

For anode production (prebaked), the raw materials are tar, coke and pitch mixed together according to a recipe, and baked in special furnaces (PIL 1993). The share of each ingredient and the baking temperature and duration determines the quality of the anodes (Gundersen 1997). An optimal anode should be resistant to the corrosive bath, have low ohmic resistance, handle the thermal shock when exposed to the bath, and finally it should neither be too solid, nor too porous.

The anode consumption during the production of aluminum is a self-regulating process. If one anode is set too low in the bath, it will draw more current than the others, resulting in increased consumption from this anode. Thus, theoretically, there will not be significant differences in the ACDs. Something that influences this is sludge (frozen bath and alumina) formation on top of the cathode, disturbing the current distribution in the cell.

⁵Liquidus temperature is the freezing temperature of the bath at the current composition. It is generally 3-10 K lower than the bulk temperature of the bath.

⁶This quantity is also termed *acidity*.

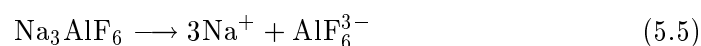
5.3 Fundamentals of the Hall-Héroult process

This section describes the Hall-Héroult process in more detail. Aspects that are important for the fluoride balance in particular, are emphasized. The most important reactions and phenomena will be presented, including the relationship between the mass and energy balances. The intention is to indicate the variety of possible reactions and compounds/ions, and provide a background for the abstraction performed in the model development in Ch. 6.

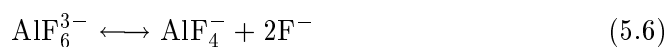
5.3.1 Bath properties

The structure of molten salts is in general described in terms of ionic species (Grjotheim and Kvande 1993). The literature on aluminum production presents numerous possible reactions and compounds/ions within the bath. The main reason for this variety is the lack of *detailed* knowledge about what phenomena are actually taking place within the cell cavity during normal and abnormal situations. This section describes *some* of the suggested reactions and ions, which is only a subset of those found in Grjotheim and Welch (1988), Grjotheim *et al.* (1982) and Grjotheim and Kvande (1993). A comprehensive overview of the main complex ions existing in the bath is given in Sterten (1980). The main raw materials are believed to dissociate/react as follows:

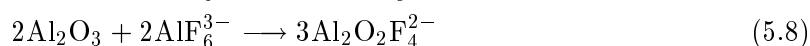
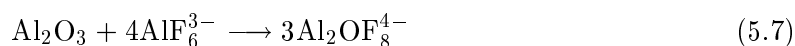
Cryolite is believed to completely dissociate into:



whereas AlF_6^{3-} only partially dissociates into:



Alumina is suggested to react according to:



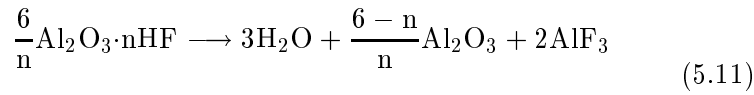
This implies that the alumina is not only dissolved in the electrolyte, but it also undergoes a reaction into ionic species. The aluminum fluoride is believed to dissolve and react as follows:



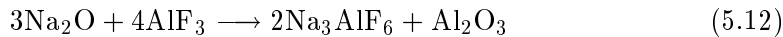
Thus, the effect of AlF_3 additions is to increase the AlF_4^- ion concentration and decrease the concentration of AlF_6^{3-} and F^- ions (Grjotheim and Kvande 1993). The impurities in the alumina listed in Sec. 5.2.1 will also undergo reactions. The CaO will form CaF_2 according to:



The fluoride (or actually HF as shown in (5.3)) in the secondary alumina will react in the bath with aluminum to form AlF_3 as:



For the work in this thesis, the most important information from (5.11) is that 6 moles of F are needed to produce 2 moles of AlF_3 . As mentioned, the amount of CaF_2 does not change substantially during operation. The content of Na_2O in the secondary alumina reacts as:

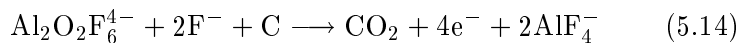
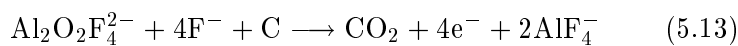


As mentioned earlier, the bath is constantly circulating, due to the magnetically induced circulation of the metal. Further, local dominating bath movement is provided by the bubbles underneath the anode escaping to the bath surface. The bubble layer underneath the anode introduces ohmic resistance, but this is often included in the total bath resistivity. The bubble voltage constitutes approximately 0.2 V as indicated in Fig. 5.2. A relationship between metal solubility, bubble layer and bath resistivity in order to minimize the energy consumption is given in Kvande *et al.* (1994).

The bath zone can be divided into the interpolar space (40% of the bath volume), the center channel (20%), the side channels (25%) and the channels between the anodes (5%) (Grjotheim and Kvande 1993). The channels serve as buffers of molten bath to dissolved alumina.

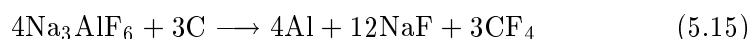
Anode reactions

At the anode surface the following reactions are suggested (Grjotheim and Kvande 1993):



where the electrons are mainly carried by Na^+ ions in the electrolyte.

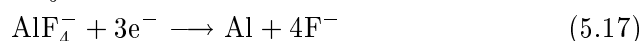
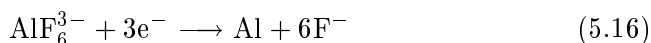
When the feeding of alumina is low, the concentration of the oxygen containing compounds from (5.7) and (5.8) used in (5.13) and (5.14) is small, resulting in electrolysis of *cryolite*. The phenomena is termed the *anode effect*. The following reaction is suggested (Nordmo and Thonstad 1984):



The CF_4 gas produced gives an insulating layer underneath the anode and this again causes the cell voltage to rise to 30-70 V. This bubble voltage is considerably higher than the CO_2 bubble voltage. Nowadays smelters try to avoid anode effects due to the instability they introduce in bath temperature and side ledge thickness. In addition, the AlF_3 emission during an anode effect is considerably higher than during normal as mentioned in Sec. 5.2.3. Previously, the anode effect was looked upon as a tool for cleaning up the cell with respect to sludge and thick side ledge, and was therefore extensively used in cell control. ■

Cathode reactions

At the metal surface, which acts as the cathode, the following reactions are suggested (Grjotheim and Kvande 1993):



For a detailed introduction to electrode reactions, see Haupin (1989). ■

Comment:

By combination of (5.8), (5.13) and (5.17), it is possible to obtain the primary reaction given in (5.1).

◇◇◇

5.3.2 Sludge formation and sodium swelling

Even if the amount of sludge has been reduced from the time of the side-breaking cells, it is believed that portions of the alumina and fluoride fed through point-breakers still fall through as sludge. The sludge introduces additional resistivity and changes the current distribution of the cell. The amount of sludge will also interfere with the ACD, by raising the metal level. Fig. 5.4 shows how the sludge is believed to be located on top of the cathode.

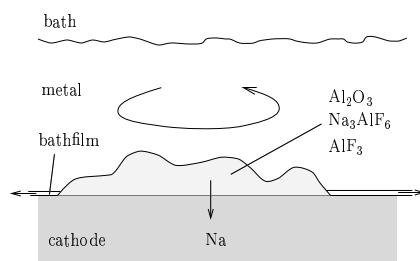


Figure 5.4: Schematic sketch of sludge.

In the early life of a cell, the cathode and cell lining absorb large quantities of sodium (Na). To compensate for this consumption, additions of sodium carbonate (Na_2CO_3) are necessary for as long as this period lasts, normally 100 days. After this period, fluoride emission dominates, and normal operating conditions are established. This is illustrated in Fig. 5.5. The sodium penetration into the cathode is, however, continuous throughout the entire lifetime of the cell.

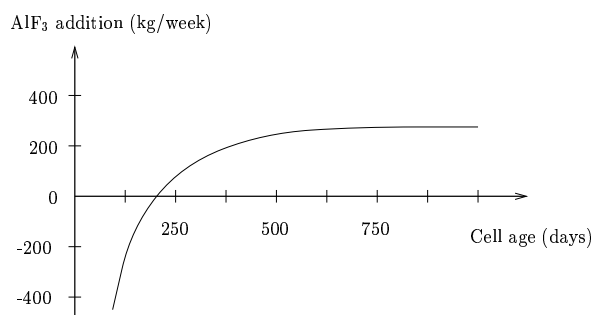


Figure 5.5: AlF_3 additions as a function of days, from Wilson (1992). Negative AlF_3 additions correspond to additions of Na_2CO_3 , see (5.4).

To prevent the buildup of sludge, it is important that the magnetic compensation of the cells is *not* too good. The circulating motion of the metal is believed to cause a bath film between the cathode and the metal, whereas this bath film transports dissolved sludge back to the bath. This phenomena is called self-feeding, and is illustrated in Fig. 5.4. Results of sludge analysis are presented in Taylor *et al.* (1990), and sludge quality and sludge resistance are discussed in Welch (1989).

5.3.3 Side ledge properties

According to the phase diagram for the NaF – AlF₃ system sketched in Fig. 5.6, the side ledge consists of pure solid cryolite if the phase change occurs during equilibrium. If the composition of the liquid is above Na₃AlF₆ and the phase change does not occur at equilibrium, the frozen material will have a composition above pure Na₃AlF₆.

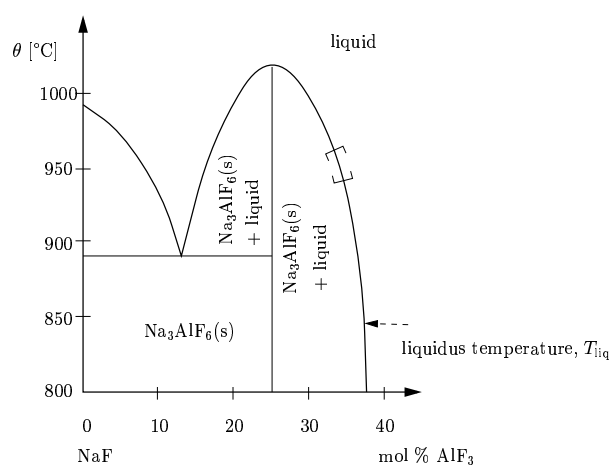


Figure 5.6: Sketch of a phase diagram of the system NaF – AlF₃. The typical operating area is indicated with brackets.

Note that this phase diagram is only a sketch. A prerequisite for equilibrium conditions are slow phase changes. This is, however, not always the situation in industrial cells, and the side ledge can therefore be expected to consist of small amounts of other bath components.

Assuming that the side ledge is in equilibrium with the bath during electrolysis, this implies that variations in the side ledge thickness are caused by differences in the heat transported from the bath to the side ledge and through the side ledge. An illustration of a side ledge profile and the self-feeding discussed in Sec. 5.3.2 is given in Fig. 5.7.

An aluminum cell holds a self-regulating property in that it regulates the side ledge thickness given the bath and liquidus temperatures together with bath and side ledge compositions. Generally, if the difference between the bath and liquidus temperature increases, the side ledge will melt. This lost insulation will eventually make the cell cool off, and the side ledge thickness will increase accordingly.

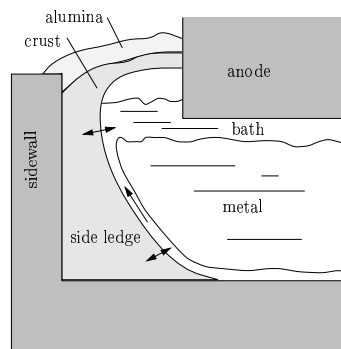


Figure 5.7: Side ledge profile and self-feeding.

Since the bath composition is different from the side ledge composition, the fluoride concentration in the bath will change as the side ledge varies. This change will thereafter produce changes in liquidus temperature according to the phase diagram. This will be further discussed in Sec. 5.4. For an introduction to liquidus point prediction in laboratory cells, cf. Taylor *et al.* (1990) and Haupin (1992).

A typical temperature profile of the bath/side ledge boundary layer is sketched in Fig. 5.8.

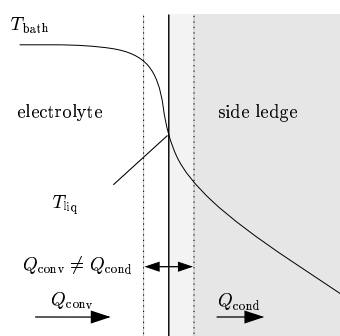
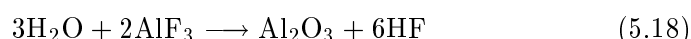


Figure 5.8: Temperature profile from bath to side ledge.

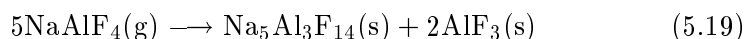
As opposed to heat transfer through a non-melting wall where $Q_{\text{conv}} = Q_{\text{cond}}$, there will typically be a discrepancy between Q_{conv} and Q_{cond} for a melting wall like the side ledge, and this property will suppress any sudden changes in Q_{conv} by melting or freezing (Taylor 1991). A method for calculation of the side ledge profile is given in Pfundt *et al.* (1989).

5.3.4 Fluoride vaporization

The main volatile fluoride containing species produced in a cell are HF(g) and NaAlF₄(g). Measurements of vapor from industrial cells indicate that there are only insignificant amounts of other compounds (Qiu *et al.* 1991). Almost all of HF leaving the cell is absorbed in the dry scrubber, and fed back to the cells. The formation of HF is primarily due to moisture in the alumina, according to the reaction (Grjotheim and Welch 1988):



NaAlF₄ condenses at $\theta = 550^\circ\text{C}$ (Qiu *et al.* 1991), and is believed to form very fine particulate material according to (Grjotheim and Welch 1988):



As NaAlF₄ leaves the bath surface, it is possible to imagine that these particulates will be retained within the crust, making the crust acidic. These phenomena are depicted in Fig. 5.9.

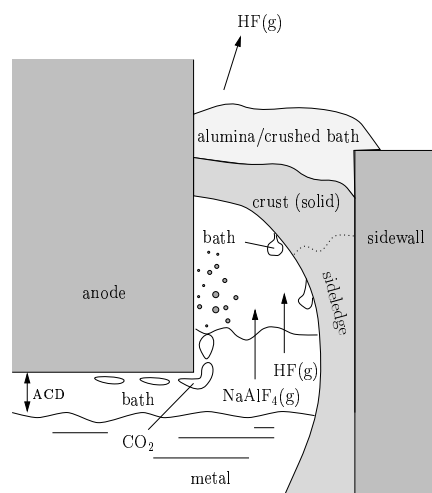


Figure 5.9: Illustration of gaseous and particulate fluoride vaporization.

In the context of AlF₃ dynamics, it could be important to determine the interaction between the bath and crust. Remember that NaAlF₄ (or NaF-AlF₃) is very acidic (50 mol% AlF₃) compared to Na₃AlF₆ (25 mol% AlF₃). Vapor pressure calculation of NaAlF₄ can be found in Haupin and Kvande (1993).

Other gases leaving the bath include the CO_2 production from (5.1). This will look like boiling bath from a bath surface point of view. As the bubbles reach the surface, they release vapor and small droplets of bath. Note that the strict separation between the crust and the alumina covering indicated in Fig. 5.9 is not as distinct at all for real industrial cells.

There have been many attempts to describe the formation of crust, including its acidity, its composition, its content of alumina and how it changes according to changes in the bath and cell operations. Laboratory studies are reported in Eggen *et al.* (1992) and Rye (1992), whereas an industrial approach is given in Liu *et al.* (1992). Note, however, that the analysis results from laboratory studies are seldom in accordance with those found from industrial cells.

At low temperature the amount of volatile species is reduced. At high excess AlF_3 content the same species becomes more volatile (Haupin and Kvande 1993). Several papers have been published concerning emission monitoring from cells during both normal operation and anode effect (Berge and Huglen 1994, Foosnæs *et al.* 1993, Roberts and Ramsey 1994).

5.4 Cell control

In controlling an aluminum cell there are three main controlled variables; alumina concentration, temperature and acidity, and three control inputs; alumina addition, AlF_3 addition and anode beam adjustments. This is a multivariable control problem since there is interaction between the different variables. The control of the alumina concentration is, however, usually considered as an isolated problem.

5.4.1 Alumina control

Before the introduction of point feeders in the late 70's, the anode effect was used to control the addition of alumina. The effect was termed *light* because a light bulb in parallel with the cell lightened up as the voltage increased. The control strategy was based on the fact that the measured resistance of the bath increases as the alumina concentration decreases below a minimum value. In Fig. 5.10 (redrawn from Grjotheim and Welch (1988)), this minima is approximately 3%.

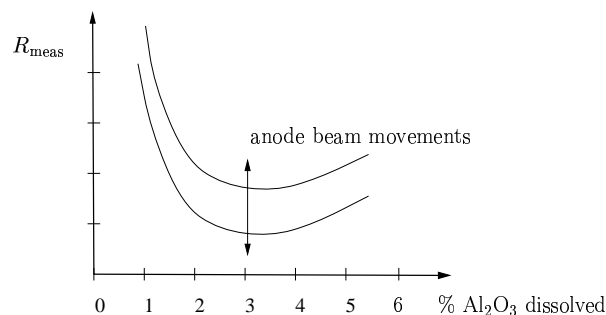


Figure 5.10: Typical measured resistance vs. alumina concentration.

The introduction of point feeders in prebaked cells made it possible to add alumina in portions of 2 kg instead of 100 kg like before. This again made it possible to achieve tighter control of the alumina concentration.

It is desirable to operate close to the minima in Fig. 5.10 in order to reduce the heat production from the bath. The operating point in industrial cells aims to be to the *left* of this minima, and the alumina concentration is therefore believed to decrease if the measured resistance increases. Bearing in mind that the ACD also have an impact on the measured resistance, it is not possible to detect the Al_2O_3 concentration from *one* resistance measure only. Consequently, the technique used to control the operating position on the resistance curve is to overfeed and underfeed alumina. This ensures that the resistivity measure will change, and at a fixed ACD, this change is mainly caused by the change in Al_2O_3 concentration.

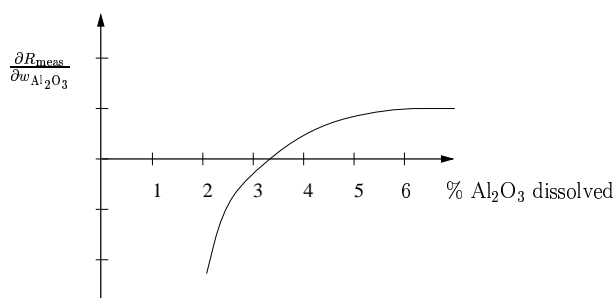


Figure 5.11: The derivative of the resistance curve in Fig. 5.10.

An alternative view of the resistance curve is shown in Fig. 5.11, where the derivative of the resistivity with respect to the mass fraction of Al_2O_3 is depicted.

From a control point of view, several incidents are considered to be disturbance components. These include: metal and bath tapping, anode effect, anode change, removal of bath and carbon lumps, degree of covering and visual inspection of the anodes.

5.4.2 Fluoride and temperature control

The multivariable nature of an aluminum smelter cell with respect to excess AlF_3 and bath temperature can be visualized as in Fig. 5.12.

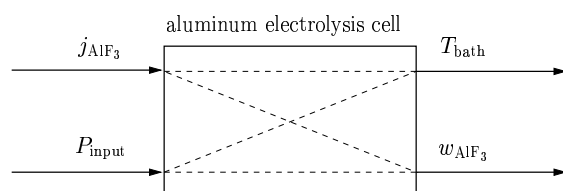


Figure 5.12: The multivariable nature of an aluminum cell.

Fluoride control is complicated by the fact that there are no available online measurements (directly or derived) for acidity. The addition or control of AlF_3 is based on the latest analysis of bath samples, bath temperature and trends in acidity and bath temperature. Motivated by the need for some sort of online control of acidity, many researchers have reported successful implementation of such controllers based on bath temperature measurements, see Wilson (1992), Salt (1990) and Desclaux (1987). The basis is the correlation existing between liquidus temperature and acidity (from phase diagram in Fig. 5.6) modified by the impact of power modulation to counteract low bath temperature, which in turn will give the observed linear correlation seen in Fig. 5.13.

A lot of information is hidden in Fig. 5.13, such as alumina concentration and *superheat*⁷. In mathematical terms one can say that the correlation is a projection from what is at least 4 dimensional space onto a 2 dimensional space. Thus, the interpretation of the correlation is limited because the hidden information is valuable. In Grjotheim and Kvande (1993) it is shown that this linear relationship between temperature and excess AlF_3 reaches $\theta = 800^\circ\text{C}$ at 27% acidity.

⁷Defined as the difference between bath and liquidus temperatures, see footnote 5 on page 95.

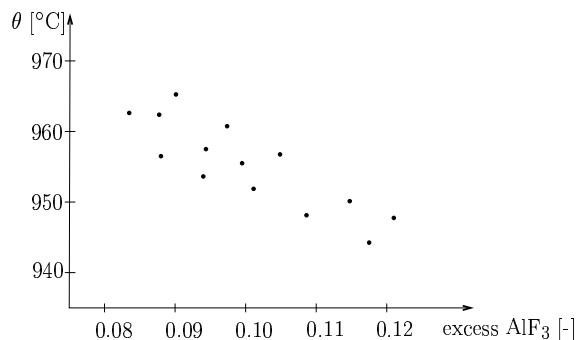


Figure 5.13: A typical relation between bath temperature and excess AlF₃ based on measurements.

As the AlF₃ content increases above the cryolite composition, the liquidus temperature curve in Fig. 5.6 becomes steeper. This implies that control of excess AlF₃ at high acidity becomes more sensitive to changes in temperature and bath composition. The freezing or melting of the side ledge is due to the bath temperature (energy balance) and the liquidus temperature (compositional balance) changing at different rates (Taylor 1991). The driving force for melting/freezing is therefore changes in the superheat. This means that it is important to understand how the energy and compositional balances interact. A complicating factor in this context is the different composition of the side ledge and the bath (according to the phase diagram). It has been stated that the observed imbalance in excess AlF₃ in reduction cells is not due to material imbalance, but rather energy imbalance (Taylor 1992).

As mentioned earlier, superheat is the driving force in heat flow dynamics. In the literature formulas are given for calculating the liquidus temperature using the alumina concentration, acidity and other parameters, see Haupin (1992), for example.

Depending on what incidents and measurements one wishes to use in the decision of fluoride addition, several strategies are possible, cf. Sec. 1.2.2.

The control algorithms described above use both mass and energy balance information. In spite of the known relationship between acidity and temperature, there is a tendency in industry to decouple the interactions (within narrow temperature and acidity limits) in that temperature is controlled by adjustments in reference resistance and acidity is controlled by additions of AlF₃.

In order to achieve good performance with respect to energy balance, satisfactory covering of the cells is important.

5.5 Electrochemical thermodynamics

Electrochemistry is the relationship between electrical phenomena and chemical changes. Electrochemical reactions involve the flow of electrons and ions through a conducting chemical system.

5.5.1 Galvanic and electrolytic cells

Electrochemical cells can be used in two ways. If the reaction is spontaneous, i.e. the process occurs at a finite rate without having to change any outside variable such as temperature or pressure, then the flow of electrons in the conductor can be used as a source of energy. This kind of cell is called a *galvanic* cell, an example is lead-acid batteries in cars. If the reaction is not spontaneous, an outside source of electrical energy must be placed on the cell circuit to drive the reaction to the desired products. Such a cell is called an *electrolytic* cell, exemplified by an aluminum cell.

The terms *cell potential* and *reaction potential* are related to electrochemical cells. As mentioned, galvanic cells run spontaneously, and the potential measured by the voltmeter indicates the extent of this spontaneity. The symbol for electrical potential is E , and the unit is V. The *standard potential*, with symbol E° , is the potential at standard state, i.e. the concentrations of all ions involved in the reaction is 1 M and the pressure of gases is 1 atm. At reversible conditions there is a cell potential of E_{MF} for galvanic cells and a cell potential of E_{rev} for electrolytic cells.

5.5.2 Reaction rates

In metallurgical processes the electric input is mainly used for *i*) preheating and melting of reactants, *ii*) replacing the energy lost as heat loss, and *iii*) electric work to force non-spontaneous processes to proceed. Depending on the substance, i.e. metallic or ionic, the current is transported differently. In metallic conductors, the current is transported by movable electrons. In ionic conductors, or electrolytes, the current is transported by movable ions. When a potential is applied to an electrolyte, positive ions (cations) and negative ions (anions) will move in opposite direction. Most electrolytes are in a liquid state. Electrolytes generally increase their ionic conductivity when the temperature is increased. This is due to the reduced viscosity, and easier movable ions. When directed current is transported between a metallic conductor and an electrolyte, a chemical reaction always occurs.

Note that the rate of production is $[r] = \text{mol s}^{-1}$, and that it is proportional to the current as

$$r = \frac{I}{z\mathcal{F}}. \quad (5.20)$$

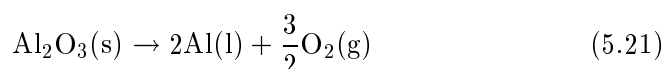
where z is the number of electrons involved in the reaction and \mathcal{F} is the Faraday constant, $\mathcal{F} = 96485 \text{ C mol}^{-1}$.

5.5.3 Standard potential of cell reactions, E°

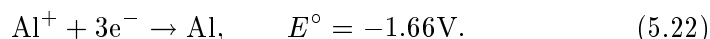
This section presents the potential needed to produce aluminum. The reduction without carbon is considered first. Then, the reduction including carbon, and finally, the back reaction is discussed.

Reduction without carbon

The reduction of Al_2O_3 can be written as:



In chemical literature, the standard potential for one of the two half reactions can be found to be



To this author's knowledge, the other half reaction is not reported, so the standard potential for reaction (5.21) must be found from the knowledge of the change in the Gibbs energy for reduction reactions. From chemical textbooks, the following relationship between E° and ΔG° is found:

$$\Delta G^\circ = -z\mathcal{F}E^\circ. \quad (5.23)$$

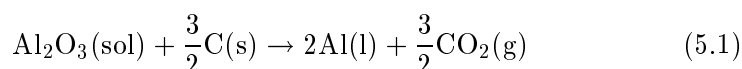
Since ΔG° is temperature dependent, a working temperature of 1250 K is chosen. In Chase *et al.* (1985), the *formation* of Al_2O_3 is found to be $\Delta_f G_{\text{Al}_2\text{O}_3, 1250}^\circ = -1278.8 \text{ kJ mol}^{-1}$, and the potential for the reduction reaction in (5.21) becomes

$$E^\circ = -\frac{1278800}{6 \cdot 96485} = -2.21\text{V}, \quad (5.24)$$

where $z = 6$ according to (5.21). A prerequisite for (5.21) is some sort of non-consumable or inert anode. The lower limit for the ACD using inert anodes is determined by the danger of short circuiting the anode and metal. Nevertheless, the limitation to this concept is the lack of an anode resistant to the corrosive bath. ■

Reduction using carbon anodes

By using consumable anodes, the voltage requirement calculated above is reduced due to the thermal energy content of anodes (Grjotheim and Kvande 1993). The standard potential of the main reaction within an aluminum electrolysis cell must therefore be discussed on the basis of the following reaction:



This is not a formation reaction, and the value of ΔG° is therefore not tabulated. The calculation of ΔG° , or more precisely, $\Delta_r G_{1250}^\circ$, follows this relationship:

$$\Delta_r G_T^\circ = \sum_{\text{products}} \nu_i (\Delta_f G_T^\circ)_i - \sum_{\text{reactants}} \nu_i (\Delta_f G_T^\circ)_i, \quad (5.25)$$

which gives $\Delta_r G_{1250}^\circ = 684.6 \text{ kJ mol}^{-1}$. The unit is here kJ per 2 mol of Al and per mol of Al_2O_3 according to (5.1). The standard potential for reaction (5.1) is then

$$E^\circ = -\frac{684600}{6.96485} = -1.1826 \text{ V}. \quad (5.26)$$

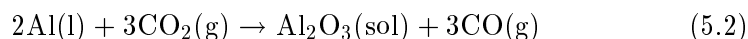
The potential requirement is reduced by over 1 V due to the use of carbon anodes. By calculating $\Delta_r G_T^\circ$ for reaction (5.1) at two different temperatures, e.g. $T = 1000 \text{ K}$ and $T = 1400 \text{ K}$, and assuming linear conditions between these temperatures, the temperature dependence of the standard potential is found, $E^\circ(T)$, as

$$E^\circ(T) = -1.8984 + 5.725 \cdot 10^{-4} T. \quad (5.27)$$

At $T = 1250 \text{ K}$, $E^\circ = -1.1827 \text{ V}$. ■

The back reaction

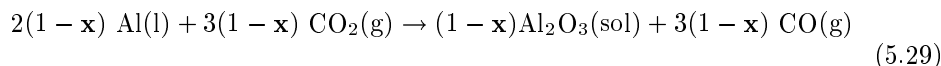
The back reaction can be written as:



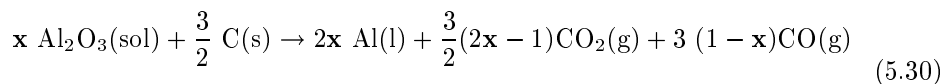
The change in the Gibbs energy for reaction (5.2) at 1250 K can be found to be $\Delta_r G_{1250}^\circ = -756.9 \text{ kJ mol}^{-1}$. Since the change in the Gibbs energy is negative, it is a spontaneous reaction. The standard potential for the reaction is

$$E^\circ = -\frac{-756900}{6.96485} = 1.31 \text{ V}. \quad (5.28)$$

The extent of the reaction is limited, i.e. between 5 and 10% back reacts according to (5.2). The current efficiency, \mathcal{CE} , is defined as the aluminum produced according to the primary reaction subtracted the fraction that back reacts, $\mathcal{CE} = (1 - \mathbf{x})$. Hence, adjusting reaction (5.2) for the fraction that back reacts, $(1 - \mathbf{x})$ produces:



Instead of considering two standard potentials, it is possible to combine reactions (5.1) and (5.29) as



and calculate the overall standard potential for this reaction. The change in the Gibbs energy at 1250 K is, $\Delta_r G_{1250}^\circ = 757\mathbf{x} - 72 \text{ kJ mol}^{-1}$, and the standard potential for is

$$E^\circ = -\frac{757\mathbf{x} + 72}{6\mathbf{x} \cdot 96485} = -1.31 + \frac{0.125}{\mathbf{x}}. \quad (5.31)$$

Inserting different values for \mathbf{x} gives the following relation between \mathcal{CE} , $\Delta_r G_{1250}^\circ$ and E° .

Table 5.2: Relation between \mathcal{CE} , $\Delta_r G_{1250}^\circ$ and E°

\mathcal{CE}	$\Delta_r G_{1250}^\circ$ [kJ mol ⁻¹]	E° [V]
1.00	685	- 1.1833
0.98	670	- 1.1807
0.95	647	- 1.1767
0.90	610	- 1.1694

5.5.4 Cell potential at reversible, non-standard condition, E_{rev}

During normal operation the standard potential, E° , is hardly at standard conditions since a condition for the use of E° is that the bath is saturated with alumina. Consequently, Nernst's equation must be considered to account for this discrepancy in fulfillment of standard conditions.

The cell potential at reversible, i.e. as $I \rightarrow 0$, and non-standard conditions, E_{rev} , is calculated using the Nernst relationship given as

$$-z\mathcal{F}E_{\text{rev}} = -z\mathcal{F}E^\circ + RT \cdot \ln Q_a, \quad (5.32)$$

where Q_a is the reaction quotient for reaction (5.1) given as

$$Q_a = \frac{p_{\text{CO}_2}^{\frac{3}{2}} a_{\text{Al}}^2}{a_{\text{Al}_2\text{O}_3} a_{\text{C}}^{\frac{3}{2}}}. \quad (5.33)$$

Employing that $p_{\text{CO}_2} = 1$, $a_{\text{Al}} = 1$ and $a_{\text{C}} = 1$ gives

$$\begin{aligned} E_{\text{rev}} &= E^\circ - \frac{RT}{z\mathcal{F}} \cdot \ln\left(\frac{1}{a_{\text{Al}_2\text{O}_3}}\right) \\ &= E^\circ + \frac{RT}{z\mathcal{F}} \cdot \ln(a_{\text{Al}_2\text{O}_3}). \end{aligned} \quad (5.34)$$

where $a_{\text{Al}_2\text{O}_3}$ is the activity of Al_2O_3 . Inserting (5.27) into (5.34) gives the following cell potential at reversible, non-standard conditions:

$$E_{\text{rev}} = -1.8984 + 5.725 \cdot 10^{-4} \cdot T + 1.44 \cdot 10^{-5} \cdot T \cdot \ln(a_{\text{Al}_2\text{O}_3}) \quad (5.35)$$

5.5.5 Overall cell voltage, U_{cell}

Since the only continuous measurements from the cell are the overall cell resistance, R_{meas} , and current, I_{meas} , the overall cell voltage is found as

$$U_{\text{cell}} = R_{\text{meas}} \cdot I_{\text{meas}}. \quad (5.36)$$

As discussed in Sec. 5.1.3 and illustrated in Fig. 5.2, the U_{cell} consists of both ohmic and non-ohmic terms as

$$U_{\text{cell}} = \sum_i U_{\text{ohmic},i} + \sum_j E_{\text{non-ohmic},j}. \quad (5.37)$$

The ohmic part may be divided into a bath potential⁸, U_{bath} , and a potential of the external cell arrangement, U_{ext} . This latter potential is typically in the area between 0.7 and 0.9 V.

The non-ohmic part potential consist of E_{rev} from (5.35) and several other non-ohmic potentials, represented as overvoltages, see Fig. 5.2. A non-ohmic cell potential, E_{bath} , may therefore be defined as

$$E_{\text{bath}} = |E_{\text{rev}}| + |\eta_{aa}| + |\eta_{ac}| + |\eta_{cc}|. \quad (5.38)$$

The overvoltages η_{aa} , η_{ac} and η_{cc} can be found in Grjotheim and Kvande (1993). During normal operation the sum of these overvoltages is approximately 0.5 V.

The overall cell voltage U_{cell} then becomes

$$U_{\text{cell}} = U_{\text{bath}} + U_{\text{ext}} + E_{\text{bath}}. \quad (5.39)$$

■

⁸Includes a potential due to the bubble layer underneath the anodes, U_{bubble} .

5.5.6 Energy consumption

Theoretical energy consumption:

In the literature, when discussing the theoretical energy requirement for the aluminum electrolysis process, this is always based on the change in enthalpy and not in the Gibbs energy. The reason for this is that one product of (5.1) is in a gaseous form, while the reactants are in a condensed phase (Grjotheim and Kvande 1993). This means that the change in entropy, ΔS° , for this reaction is positive, and the energy requirement for (5.1) is ΔH° rather than ΔG° . From

$$\Delta H^\circ = \Delta G^\circ + T\Delta S^\circ, \quad (5.40)$$

it can be seen that $\Delta H^\circ > \Delta G^\circ$. Similar to the relationship between ΔG° and E° , the following is valid

$$E^{\text{iso}} = -\frac{\Delta H^\circ}{z\mathcal{F}}, \quad (5.41)$$

where E^{iso} is termed the *isothermal* or the *thermo-neutral* potential (Sterten 1994). This quantity is related to the potential needed to obtain isothermal conditions. Thus, if the reaction was carried out with a potential according to E° (or ΔG°), insufficient energy would be available and the cell would cool unless external heat was supplied. The ΔH° can be found from

$$\Delta_r H_T^\circ = \sum_{\text{compunds}} \nu_i (\Delta_f H_T^\circ)_i - \sum_{\text{reactants}} \nu_i (\Delta_f H_T^\circ)_i. \quad (5.42)$$

The temperature dependence of $E^{\text{iso}}(T)$ for reaction (5.1) is

$$E^{\text{iso}}(T) = -1.927 + 2.476 \cdot 10^{-5} T. \quad (5.43)$$

At $T = 1250$ K, $E^{\text{iso}} = -1.8964$ V. The difference between $\Delta_r G_{1250}^\circ$ and $\Delta_r H_{1250}^\circ$ constitutes 0.7137 V, implying that this potential is needed for the reaction to be carried out electrochemically and reversibly. Disregarding other heat losses and requirements, an isothermal reaction requires an electrical energy equal to ΔH rather than ΔG .

From (5.42), the $\Delta_r H_{1250}^\circ$ of (5.1) is 548.9 kJ (mol Al)⁻¹. The theoretical need of energy to produce aluminum can be found from

$$\mathcal{EC} = \frac{\Delta_r H_{1250}^\circ}{M_{\text{Al}}} = \frac{548.9}{0.027} \cdot \frac{1\text{h}}{3600\text{s}} = 5.64 \text{ kWh (kg Al)}^{-1}.$$

In addition to this energy requirement comes the preheating of reactants, see footnote 2 on page 89, and the heat of solution of Al_2O_3 . ■

Energy consumption in industrial cells

As discussed in Sec. 5.1.3, the energy consumption in industrial prebake cells is typically 13-14 kWh (kg Al)⁻¹. This is approximately twice the theoretical need⁹, and the additional energy consumption is due to the power generated in the ohmic resistive bath, P_{bath} . Almost all this power is superfluous in that no electrochemical work is performed. The only useful work is preheating and dissolution of reactants. Hence, a prerequisite for cell operation, is that the superfluous energy is lost as heat to the surroundings. The power generated in the bath, or the *net energy input* to the bath, is calculated as

$$P_{\text{bath}} = U_{\text{bath}} \cdot I_{\text{meas}}. \quad (5.44)$$

The *required* energy input to the bath includes the energy needed to reduce alumina as

$$P_{\text{input}} = (U_{\text{bath}} + E_{\text{bath}}) I_{\text{meas}}. \quad (5.45)$$

The energy input for the overall cell can, hence, be calculated as

$$P_{\text{cell}} = (U_{\text{bath}} + E_{\text{bath}} + U_{\text{ext}}) I_{\text{meas}} = U_{\text{cell}} \cdot I_{\text{meas}}. \quad (5.46)$$

Using the reaction rate from (5.20), the current efficiency and P_{cell} , the energy consumption can, thus, be found from

$$\mathcal{EC} = \frac{P_{\text{cell}}}{r \cdot \mathcal{CE} \cdot M_{\text{Al}}} = \frac{P_{\text{cell}}}{r \cdot \mathcal{CE} \cdot M_{\text{Al}}} \cdot \frac{1\text{h}}{3600\text{s}} = \frac{(U_{\text{bath}} + E_{\text{bath}} + U_{\text{ext}}) \cdot I_{\text{meas}}}{\frac{I_{\text{meas}}}{z\mathcal{F}} \cdot \mathcal{CE} \cdot 0.027 \cdot 3600}.$$

Inserting values for the various constants, dividing by 1000 to convert from Wh to kWh, gives the following relationship

$$\mathcal{EC} = 2.978 \left(\frac{U_{\text{bath}} + E_{\text{bath}} + U_{\text{ext}}}{\mathcal{CE}} \right). \quad (5.47)$$

This means that there are two possible ways of reducing the energy consumption in practice. That is, *i*) reduction of the bath potential, U_{bath} , by reducing the ACD, for example, and *ii*) increasing the current efficiency. It is not likely that E_{bath} or U_{ext} will change with the existing technology.

Inserting into (5.47) $U_{\text{bath}} = U_{\text{ext}} = 0$, $\mathcal{CE} = 1.0$ and $E_{\text{bath}} = E^{\text{iso}}(1250) = 1.8964$ V from (5.43), the energy consumption becomes $\mathcal{EC} = 5.64$ kWh (kg Al)⁻¹. As expected, it is the value found above for the theoretical

⁹The energy efficiency, \mathcal{EE} , of aluminum electrolysis is, hence, close to 50%.

consumption. On the other hand, inserting into (5.47) values for modern prebake cells (Kvande 1991), i.e. $U_{\text{bath}} + E_{\text{bath}} + U_{\text{ext}} = U_{\text{cell}} = 4.2$ V and $\mathcal{CE} = 0.94$, the energy consumption becomes $\mathcal{EC} = 13.3$ kWh (kg Al)⁻¹. ■

Comment:

Note that (5.45) together with (5.36) and (5.39) can be written as

$$P_{\text{input}} = (R_{\text{meas}} \cdot I_{\text{meas}} - U_{\text{ext}}) I_{\text{meas}}. \quad (5.48)$$

This is an important relationship since R_{meas} and I_{meas} are the only continuous measurements available.

◇◇◇

Chapter 6

Model development

In this chapter a rather complex dynamic model of a prebaked cell is developed. The modeling methodology and the terminology defined in Ch. 2 and Ch. 3 will be used to develop and represent the model and the model assumptions. The mass and energy based representations (introduced in Sec. 2.4) for the aluminum cell are given in Secs. 6.2 and 6.3, respectively. Based on experience with the comprehensive model and model assumptions given in Sec. 6.4, a model with reduced complexity is presented in Sec. 6.5.

6.1 Introduction

As mentioned in Sec. 1.1.2, the objective of the work in this thesis is to develop a dynamic model of an aluminum electrolysis cell for AlF_3 and temperature control purposes. From the process description in Ch. 5, it is evident that such a model has to be based on some kind of abstraction and simplifications. To give examples of such simplifications, modelers have to evaluate which reactions and species to include, which phenomena can be neglected and how to simplify possible important properties. In this thesis, these choices are done in cooperation with process engineers and other resource personnel at Hydro Aluminum a.s. in Årdal.

According to the suggested modeling procedure in Fig. 3.2, the first step is to identify the *a priori* assumptions (introduced in Sec. 3.1.1). For the aluminum cell, the following *a priori* assumptions are made:

- (A.1) The existence of the various complex *ions* in Sec. 5.3.1 are not considered. Consequently, the corresponding reactions are not considered. This is partially motivated by the fact there is a large

degree of uncertainty related to these reactions, and the amount of each ion is limited. Besides, with the purpose of the model in mind, modeling of ions is not a suitable approach. Hence, the base set S (defined in Sec. 2.3.2) includes at least the following species: Na_3AlF_6 , Al_2O_3 and AlF_3 .

- (A.2) As discussed in Sec. 5.2, there are several impurities added to the bath. In the model developed here, the fluoride (F) and Na_2O from the secondary alumina is recalculated into equivalent AlF_3 input/output according to (5.11) and (5.12), respectively. This additional input is added to the registered AlF_3 input¹. In addition, 10% of the registered AlF_3 input is added to the registered Al_2O_3 input. The CaO content in alumina is not considered, since the amount of CaF_2 is approximately constant during normal operation. These assumptions imply that the reactions (5.10), (5.11) and (5.12) can be neglected. Consequently, the species CaO , F and Na_2O are neglected in the base set S . Note that CaF_2 is included since it constitutes approximately 6 mass% of the bath.
- (A.3) The energy induced by anode effects is included into the model. Reaction (5.15), however, is not included. Similar to the recalculation described in assumption (A.2), the addition of Na_2CO_3 is recomputed to negative additions of AlF_3 according to (5.4), illustrated in Fig. 5.5. These assumptions imply that NaF , Na, CF_4 and Na_2CO_3 are not considered in the base set S .
- (A.4) The HF and NaAlF_4 evaporating from the bath are recomputed to equivalent AlF_3 losses according to (5.18) and (5.19), respectively. This implies that HF, NaAlF_4 and $\text{Na}_5\text{Al}_3\text{F}_{14}$ can be neglected in the base set S .
- (A.5) Two reactions are considered, i.e. the primary reaction in (5.1) and the back reaction in (5.2). As a result, CO_2 , CO, C and Al is included in the base set S .

Other assumptions and simplifications will be included along with the model development. The base set of species, S , is given by

$$S = \{\text{Na}_3\text{AlF}_6, \text{Al}_2\text{O}_3, \text{AlF}_3, \text{CaF}_2, \text{CO}_2, \text{CO}, \text{C}, \text{Al}\}. \quad (6.1)$$

Other sets, such as A_S and T_S defined in Sec. 2.3.2, will be identified along with the mass based model development in the next section. The mass based model representation including all sets is summarized in Sec. 6.2.3.

¹This is the actual input to the cell registered by the cell computer.

Further, the base set of energy, E , is defined by

$$E = \{H\}. \quad (6.2)$$

Similarly, the other sets, e.g. A_E and T_E , will be identified during the energy based model development in Sec. 6.3. The energy based model representation including all sets is summarized in Sec. 6.3.3.

As discussed in Sec. 3.2.1, there is no unique representation of the PTD structure. In order for the PTD to imitate the real process as far as possible, an approach based on a network applied to the process was suggested (cf. Fig. 3.9). In Fig. 6.1, such a network is applied to the aluminum cell.

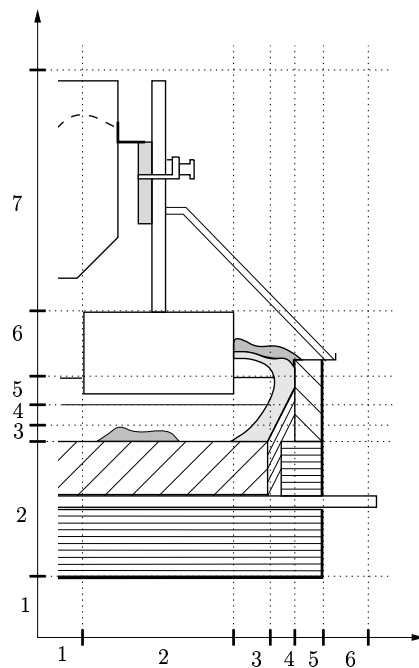


Figure 6.1: A topological network applied to the aluminum cell.

This sketch is the basis for both the mass and energy based representation given in Secs. 6.2 and 6.3. The aluminum cell is regarded to be symmetric along its center-channel, and hence, the network is applied to only one half of the process. The developed mathematical model, however, applies to the entire cell.

6.2 Mass based model development

The elementary mass based devices, ED_{mass} , and connections, EC_{mass} , were introduced in Sec. 2.4.1. The ED_{mass} and EC_{mass} sets for the aluminum cell are identified and described in detail in Secs. 6.2.1 and 6.2.2, respectively.

6.2.1 Elementary devices, ED_{mass}

As stated in Ch. 2, the basis for identifying devices is the chemical phase. From the process description in Ch. 5 and the partitioning in Fig. 6.1, the following mass based preliminary PTD layout is identified.

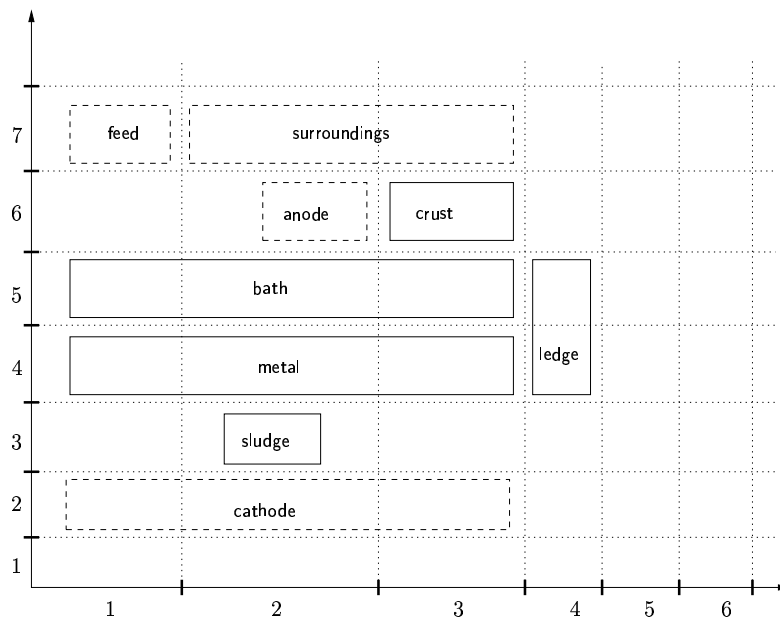


Figure 6.2: Preliminary mass based PTD of the aluminum cell.

Note that the ledge² device represents the entire ledge inside the cell. Similarly, the anode device represents all the anodes.

For the purpose of the model developed here, the following a priori assumption are added:

(A.6) The sodium swelling into the cathode is neglected.

²The names of topological components are typeset in the sans serif font.

The following ED_{mass} set is, hence, identified for the aluminum cell:

$$ED_{\text{mass}} = \{\text{feed, crust, ledge, bath,} \\ \text{sludge, anode, surroundings, metal}\}. \quad (6.3)$$

These will be described in more detail in the following. The presentation of each element of the ED_{mass} set in (6.3) contains *i*) a set of $P_{D,\text{mass}}$ elements (introduced in (2.13) on page 30) and, *ii*) a specification of the specific enthalpy, \tilde{H}_i , introduced in Sec. 3.2.3³. For reasons mentioned in Sec. D.3.2, approximated specific enthalpies, $\tilde{\tilde{H}}_i$, are used in this thesis. An example of such is given in Sec. 4.5.1, where (3.15) from Sec. 3.2.3 is replaced with (4.1).

Note that all the specific enthalpy are relative to the base line defined in Sec. D.1.5.

feed device

As shown in Table 5.1 on page 92, two of the main inputs to aluminum production are Al_2O_3 and AlF_3 . Na_3AlF_6 is also consumed, but the amount is very low and the influence on the fluoride balance is in this work believed to be negligible. Having assumptions **(A.2)** and **(A.3)** in mind, the following P_D elements for the feed device are considered:

$$P_{D,\text{feed}} = \{\text{Al}_2\text{O}_3, \text{AlF}_3\}. \quad (6.4)$$

The feed is actually a source device as indicated in Fig. 6.2. The specific enthalpies for the P_D elements in (6.4) at $T = T_{\text{feed}}$ are given as:

$$\left. \begin{aligned} \tilde{\tilde{H}}_{\text{AlF}_3} &= \Delta_f H_{298,\text{AlF}_3}^\circ + \bar{c}_{p,\text{AlF}_3}(T_{\text{feed}} - 298) \\ \tilde{\tilde{H}}_{\text{Al}_2\text{O}_3} &= \Delta_f H_{298,\text{Al}_2\text{O}_3}^\circ + \bar{c}_{p,\text{Al}_2\text{O}_3}(T_{\text{feed}} - 298) \end{aligned} \right\} \quad (6.5)$$

Both AlF_3 and Al_2O_3 are solids (powder), and the temperature of this powder is specified to be constant equal to $T_{\text{feed}} = 413$ K. ■

³See footnote 3 on page 63.

crust device

As indicated in Sec. 5.3.4 and Fig. 5.9, the crust could be composed of $\text{Na}_5\text{Al}_3\text{F}_{14}$, AlF_3 , Al_2O_3 and Na_3AlF_6 . In spite of that, the influences of Al_2O_3 and Na_3AlF_6 are in this work neglected. Moreover, based on assumption (A.4), the following P_D element is considered:

$$P_{D,\text{crust}} = \{\text{AlF}_3\}. \quad (6.6)$$

Since the crust is solid, and physically above the bath, the crust temperature is believed to be less than the bath temperature. For simplicity, the crust temperature is assumed to equal the liquidus temperature, and the specific enthalpy for this P_D element at $T = T_{\text{liq}}$ is given as

$$\bar{H}_{\text{AlF}_3} = \Delta_f H_{298,\text{AlF}_3}^\circ + \bar{c}_{p,\text{AlF}_3}(T_{\text{liq}} - 298). \quad (6.7)$$

The chosen crust temperature is of course too high, implying that the thermal effects of crust deformation are not satisfactory. On the other hand, this effect is believed to be negligible compared to other energy disturbances such as anode changing. ■

ledge device

As mentioned in Sec. 5.3.3, it is believed that the side ledge in industrial cells contains a small amount of other bath species than Na_3AlF_6 . However, in the models developed here it is assumed that the side ledge consists of Na_3AlF_6 only. Thus, the following P_D element is considered:

$$P_{D,\text{ledge}} = \{\text{Na}_3\text{AlF}_6\}. \quad (6.8)$$

In Fig. 5.8, the temperature profile through the side ledge is shown qualitatively. The temperature close to the bath/ledge boundary is the liquidus temperature, T_{liq} . The temperature decreases throughout the side ledge, and in this work the temperature *gradient* from the side ledge boundary to the outer steel shell is assumed constant. For this reason, there are no dynamic properties of the side ledge with respect to energy. This is further discussed in Secs. 6.2.2 and 6.3. The result of this discussion is that the specific enthalpy for the P_D element in (6.8) becomes:

$$\bar{H}_{\text{Na}_3\text{AlF}_6} = \Delta_f H_{298,\text{Na}_3\text{AlF}_6}^\circ + \bar{c}_{p,\text{Na}_3\text{AlF}_6}(T_{\text{liq}} - 298), \quad (6.9)$$

where the temperature at the bath/ledge boundary is $T = T_{\text{liq}}$.

Even if the side ledge is not believed to accumulate energy, it is still a device from a mass point of view. Hence, one of the dependent variables is the side ledge thickness, l_{ledge} . The calculation of l_{ledge} is straightforward:

$$l_{\text{ledge}} = \frac{n_{\text{Na}_3\text{AlF}_6} \cdot M_{\text{Na}_3\text{AlF}_6}}{\rho_{\text{Na}_3\text{AlF}_6(\text{s})}} \cdot \frac{1}{A_{\text{ledge,wall}}}. \quad (6.10)$$

The assumption used in (6.10) is that the side ledge is believed to be equally thick over the entire cell wall. This is of course wrong, and in contrast to the sketch in Fig. 5.7 and measurements of the side ledge profile. Nevertheless, for the purpose of this model, a side ledge profile corresponding to (6.10) is appropriate. ■

bath device

As mentioned in assumption **(A.1)**, many of the ions and the reactions described in Ch. 5 are excluded from the model formulation. Thus, the most important reactions are the reduction of Al_2O_3 in (5.1) and the back reaction in (5.2) as stated in assumption **(A.5)**. Due to the topological decomposition with respect to phase (see RULE 4 on page 20), the gaseous products and reactants of these two reactions are not included in the liquid bath device. Furthermore, even if Al is dissolved in the bath and is the reactant of (5.2), it is excluded from the $P_{D,\text{bath}}$ elements due to the low content and the purpose of the model. Thus, these assumptions have impact on the location of the reactions as will be discussed in Sec. 6.2.2. It is therefore believed to be sufficient to consider the following P_D elements in the bath:

$$P_{D,\text{bath}} = \{\text{Al}_2\text{O}_3, \text{AlF}_3, \text{Na}_3\text{AlF}_6, \text{CaF}_2\}. \quad (6.11)$$

The specific enthalpies for these elements at $T = T_{\text{bath}}$ are given as:

$$\left. \begin{aligned} \tilde{H}_{\text{AlF}_3} &= \Delta_f H_{298,\text{AlF}_3}^\circ + \bar{c}_{p,\text{AlF}_3}(T_{\text{bath}} - 298) + \Delta_{\text{sol}} H_{\text{AlF}_3}^\circ \\ \tilde{H}_{\text{Al}_2\text{O}_3} &= \Delta_f H_{298,\text{Al}_2\text{O}_3}^\circ + \bar{c}_{p,\text{Al}_2\text{O}_3}(T_{\text{bath}} - 298) + \Delta_{\text{sol}} H_{\text{Al}_2\text{O}_3}^\circ \\ \tilde{H}_{\text{CaF}_2} &= \Delta_f H_{298,\text{CaF}_2}^\circ + \bar{c}_{p,\text{CaF}_2}(T_{\text{bath}} - 298) \\ \tilde{H}_{\text{Na}_3\text{AlF}_6} &= \Delta_f H_{298,\text{Na}_3\text{AlF}_6}^\circ + \bar{c}_{p,\text{Na}_3\text{AlF}_6}(T_{\text{bath}} - 298) + \Delta_{\text{fus}} H_{\text{Na}_3\text{AlF}_6}^\circ \end{aligned} \right\} (6.12)$$

Remember that CaF_2 is not an additive, but rather a product of reaction (5.10). This means that there is no data of enthalpies of fusion or solution for this species in the cryolite mixture. In addition, the impact of reaction (5.10) on the energy balance is believed to be small (assumption **(A.2)**),

and the specific enthalpy of CaF_2 is therefore specified as being solid within the bath device.

There are several dependent state variables related to the bath. The most important algebraic equations included in the model are:

Liquidus temperature: The liquidus temperature equation employed here is taken from Grjotheim and Kvande (1993), though the terms comprising LiF are neglected:

$$\begin{aligned} T_{\text{liq}} = & T_{\text{liq0}} + b_1 \cdot (100 \cdot w_{\text{Al}_2\text{O}_3}) + b_2 \cdot (100 \cdot w_{\text{Al}_2\text{O}_3})^{1.2} \\ & + b_3 \cdot (100 \cdot w_{\text{AlF}_3}) + b_4 \cdot (100 \cdot w_{\text{AlF}_3})^{2.5} + b_5 \cdot (100 \cdot w_{\text{AlF}_3})^3 \\ & + b_6 \cdot (100 \cdot w_{\text{AlF}_3} \cdot 100 \cdot w_{\text{CaF}_2})^{0.7} \\ & + b_7 \cdot (100 \cdot w_{\text{CaF}_2}) + b_8 \cdot (100 \cdot w_{\text{CaF}_2})^2, \end{aligned} \quad (6.13)$$

where T_{liq0} and b_1 to b_8 are constants.

Current efficiency: The current efficiency, \mathcal{CE} , is given as⁴

$$\mathcal{CE} = f(T_{\text{bath}}, w_{\text{AlF}_3}), \quad (6.14)$$

which is a simplification of the model in Solli *et al.* (1994).

■

sludge device

As discussed in Sec. 5.3.2, some of the Al_2O_3 and AlF_3 additions are not immediately dissolved, and hence, form sludge. It is evident that bath will freeze onto the portion that is undissolved, implying that a sludge phase is composed of at least Al_2O_3 , AlF_3 and Na_3AlF_6 . Again, keeping in mind the purpose of the model, the Na_3AlF_6 in the sludge is neglected, and the following P_D elements are considered:

$$P_{D,\text{sludge}} = \{\text{Al}_2\text{O}_3, \text{AlF}_3\}. \quad (6.15)$$

As already mentioned, the aggregate state of the sludge is believed to be solid. It is further assumed that the bath preheats the sludge to the freezing-point of the bath. In the model developed here this corresponds to the liquidus temperature due to the assumption of ideally mixed bath. The specific enthalpies for the P_D elements at $T = T_{\text{liq}}$ are given as:

$$\left. \begin{aligned} \tilde{H}_{\text{AlF}_3} &= \Delta_f H_{298, \text{AlF}_3}^\circ + \bar{c}_{p, \text{AlF}_3} (T_{\text{liq}} - 298) \\ \tilde{H}_{\text{Al}_2\text{O}_3} &= \Delta_f H_{298, \text{Al}_2\text{O}_3}^\circ + \bar{c}_{p, \text{Al}_2\text{O}_3} (T_{\text{liq}} - 298) \end{aligned} \right\} \quad (6.16)$$

■

⁴From an unpublished report from Hydro Aluminium a.s.

anode device

Similar to the feed device, the anode is assumed to be a source device. The following P_D element is considered:

$$P_{D,\text{anode}} = \{\text{C}\}. \quad (6.17)$$

Approximately once a day an anode is changed and exposed to a thermal shock upon insertion into the bath. This operation is a major disturbance on the energy balance of the cell for a number of hours. For a dynamic model of *long-term* variations of excess AlF_3 , this energy loss is not modeled, although it is included in the model validation using real input data in Ch. 7. The specific enthalpy for the P_D element at $T = T_{\text{bath}}$ is therefore

$$\tilde{H}_C = \Delta_f H_{298,C}^\circ + \bar{c}_{p,C}(T_{\text{bath}} - 298). \quad (6.18)$$

■

surroundings device

The surroundings device can be interpreted as a sink device. Since mass is only added and removed from the upper side of the cell, this device corresponds to the surroundings above the cell. As mentioned in assumption (A.4) in Sec. 6.1, the evaporation of HF and NaAlF_4 is considered to be represented by equivalent evaporation of AlF_3 . Other species included are the CO_2 and CO produced from the primary and back reaction, respectively. Consequently, the following P_D elements are considered:

$$P_{D,\text{surroundings}} = \{\text{CO}_2, \text{AlF}_3, \text{CO}\}. \quad (6.19)$$

The specific enthalpies for the P_D elements at $T = T_{\text{bath}}$ are given as:

$$\left. \begin{aligned} \tilde{H}_{\text{AlF}_3} &= \Delta_f H_{298,\text{AlF}_3}^\circ + \bar{c}_{p,\text{AlF}_3}(T_{\text{bath}} - 298) + \Delta_{\text{sol}} H_{\text{AlF}_3}^\circ \\ \tilde{H}_{\text{CO}} &= \Delta_f H_{298,\text{CO}}^\circ + \bar{c}_{p,\text{CO}}(T_{\text{bath}} - 298) \\ \tilde{H}_{\text{CO}_2} &= \Delta_f H_{298,\text{CO}_2}^\circ + \bar{c}_{p,\text{CO}_2}(T_{\text{bath}} - 298) \end{aligned} \right\} \quad (6.20)$$

Note that the specific enthalpy of AlF_3 is similar to that of AlF_3 in bath. This is of course wrong, since the AlF_3 is considered gaseous. Hence, there should have been included an enthalpy of vaporization, $\Delta_{\text{vap}} H_{\text{AlF}_3}^\circ$, which should represent the evaporation of HF and NaAlF_4 . In spite of that, this effect is assumed negligible compared to other uncertainties related to the energy balance of the bath. ■

metal device

Since any polluting elements are neglected in the metal, for instance iron, the following P_D element is considered:

$$P_{D,\text{metal}} = \{\text{Al}\}. \quad (6.21)$$

The aggregate state of the aluminum produced according to (5.1) is liquid. The specific enthalpy for the P_D at $T = T_{\text{metal}}$ element is, hence, given as

$$\bar{H}_{\text{Al}} = \Delta_{\text{f}} H_{298,\text{Al}}^{\circ} + \bar{c}_{p,\text{Al}}(T_{\text{metal}} - 298) + \Delta_{\text{fus}} H_{\text{Al}}^{\circ}. \quad (6.22)$$

Note that the produced metal is believed to be at temperature T_{metal} rather than T_{bath} . ■

6.2.2 Elementary connections, EC_{mass}

Based on the ED_{mass} elements in (6.3) and their physical placement within the cell cavity (see Fig. 6.2), the following EC_{mass} elements could be identified:

$$\begin{aligned} EC_{\text{mass}} = \{ & \text{feed/bath, bath/ledge, bath/metal,} \\ & \text{bath/crust, bath/surroundings, metal/ledge} \\ & \text{anode/bath, metal/sludge, sludge/bath,} \\ & \text{anode/surroundings, crust/surroundings}\}. \end{aligned} \quad (6.23)$$

Due to assumption **(A.6)**, the connections metal/cathode and sludge/cathode are already neglected.

The convention for generating a connection name is to use the names of the adjacent devices, separated by “/”. The order of the device names indicate the recommended positive direction.

Due to a priori model assumptions, the connections in (6.23) are not applicable. As an example, the additions of Al_2O_3 will first be added to the bath where the undissolved portion falls through the metal and settles on the cathode block. A model of this behavior would include Al_2O_3 in the metal device, or a *virtual* connection, bath/sludge, which represents the “boundary” that the metal phase is for the Al_2O_3 flow. Consequently, since the Al_2O_3 addition is actually divided into dissolved and undissolved Al_2O_3 , the connections feed/bath, bath/metal and metal/sludge are lumped into the feed/bath::sludge connection. Thus, in the case of more than two adjacent devices, the connection name includes the additional device names, separated by “:”. This means that there will be several positive directions.

Thus, the following a priori assumptions are made:

- (A.7) As mentioned above, the connections feed/bath, bath/metal and metal/sludge are lumped into the virtual feed/bath::sludge connection.
- (A.8) For the purpose of the model, it is not interesting to consider mass flow from the anode to the surroundings. Neither is the connection crust/surroundings considered. The mass flow from the bath to the surroundings is therefore modeled in the bath/surroundings connection.
- (A.9) The mass transport between metal and ledge is not considered.
- (A.10) Due to the a priori assumption (A.5), another virtual connection is introduced, anode::bath/surroundings::metal. This will be discussed below (page 134).
- (A.11) Undissolved AlF_3 and Al_2O_3 is assumed to form sludge on the top of the cathode.

The following EC_{mass} elements, are hence, considered:

$$EC_{\text{mass}} = \{ \text{bath/ledge}, \text{feed/bath::sludge}, \text{sludge/bath}, \\ \text{bath/crust}, \text{bath/surroundings}, \\ \text{anode::bath/surroundings::metal} \}. \quad (6.24)$$

These will be explained in more detail in the following. The complete mass based PTD layout of the devices in (6.3) and the connections in (6.24) are shown in Fig. 6.3. Note that the structure has changed due to the assumptions made, and that the relation to the network in Fig. 6.2 is relaxed.

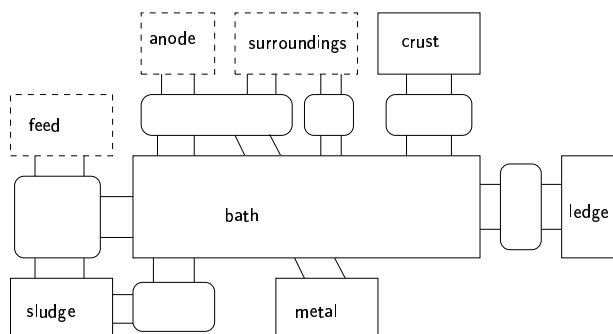


Figure 6.3: Complete mass based PTD of the elements in (6.3) and (6.24).

The presentation of each element of the EC_{mass} set in (6.24) contains *i*) a set of $P_{C,\text{mass}}$ elements identified by using (3.12) and, *ii*) a specification of \bar{H}_i of the flowing medium, i.e. whether it is similar to the upstream or downstream device as discussed in Sec. 3.2.4 and illustrated in Fig. 3.12. An example of this specification is given in (4.4) and Fig. 4.24 in Sec. 4.5.2.

bath/ledge connection

Based on (3.11) and the P_D elements of bath and ledge, the following P_C elements are found for this connection as:

$$P_{C,\text{bath/ledge}} = P_{D,\text{bath}} \cap P_{D,\text{ledge}} = \{\text{Na}_3\text{AlF}_6\}. \quad (6.25)$$

Remember from (6.9) and (6.12) that the specific enthalpies of Na_3AlF_6 are:

$$\begin{aligned} \bar{H}_{\text{Na}_3\text{AlF}_6,\text{ledge}} &= \Delta_f H_{298,\text{Na}_3\text{AlF}_6}^\circ + \bar{c}_{p,\text{Na}_3\text{AlF}_6} (T_{\text{liq}} - 298), \\ \bar{H}_{\text{Na}_3\text{AlF}_6,\text{bath}} &= \Delta_f H_{298,\text{Na}_3\text{AlF}_6}^\circ + \bar{c}_{p,\text{Na}_3\text{AlF}_6} (T_{\text{bath}} - 298) + \Delta_{\text{fus}} H_{\text{Na}_3\text{AlF}_6}^\circ. \end{aligned}$$

Thus, there is a discrepancy, and the specific enthalpy of the *flowing* Na_3AlF_6 in *both* directions must be determined. Therefore, a reexamination of the basic theory for the melting and freezing phenomena is given.

Principles of melting and freezing of side ledge: The flow of Na_3AlF_6 between the bath and side ledge is thermally controlled. The difference in *convective* heat from the bath to the side ledge boundary and the *conductive* heat through the side ledge determines the flow of Na_3AlF_6 as visualized in Fig. 6.4.

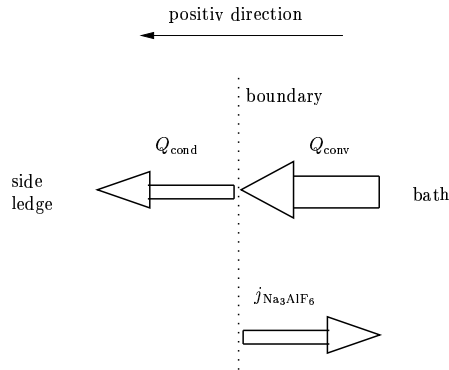


Figure 6.4: Visualization of a melting situation.

Note that the melting direction is opposite to the defined positive direction. The excess energy ($Q_{\text{conv}} - Q_{\text{cond}}$) is believed to melt the side ledge if $Q_{\text{conv}} > Q_{\text{cond}}$. The excess energy also heats up the melted Na_3AlF_6 from T_{liq} to T_{bath} . Thus,

$$Q_{\text{conv}} - Q_{\text{cond}} = -j_{\text{Na}_3\text{AlF}_6} (\Delta_{\text{fus}} H_{\text{Na}_3\text{AlF}_6}^{\circ} + \bar{c}_{p,\text{Na}_3\text{AlF}_6} (T_{\text{bath}} - T_{\text{liq}})). \quad (6.26)$$

The molar flow of Na_3AlF_6 is then

$$j_{\text{Na}_3\text{AlF}_6} = \frac{-(Q_{\text{conv}} - Q_{\text{cond}})}{\Delta_{\text{fus}} H_{\text{Na}_3\text{AlF}_6}^{\circ} + \bar{c}_{p,\text{Na}_3\text{AlF}_6} (T_{\text{bath}} - T_{\text{liq}})}. \quad (6.27)$$

Note, however, that the heating of Na_3AlF_6 from 1216 K to 1221 K, is only 1% of $\Delta_{\text{fus}} H_{\text{Na}_3\text{AlF}_6}^{\circ}$. The calculation of Q_{cond} and Q_{conv} in (6.27) is discussed in Sec. 6.2.2.

As discussed in Sec. 3.2.4, the specific enthalpy of the flowing medium is in general equal to the specific enthalpy of the upstream device. On the other hand, this is not necessarily so for complex unit processes due to the strong interaction and the physical nearness of the devices. This is also the case for the aluminum cell, where, for example, the bath is believed to be a better heat conductor than the side ledge. Consequently, the bath acts both as drain and source of energy when Na_3AlF_6 freezes or melts. In other words, the side ledge is considered unable to receive the energy released as heat when mass enters the phase, i.e. at freezing conditions. Hence, the specific enthalpy of Na_3AlF_6 flowing in *both* directions is given as:

$$\bar{H}_{\text{Na}_3\text{AlF}_6} = \Delta_{\text{f}} H_{298,\text{Na}_3\text{AlF}_6}^{\circ} + \bar{c}_{p,\text{Na}_3\text{AlF}_6} (T_{\text{liq}} - 298). \quad (6.28)$$

This corresponds to the energy level in the ledge, and hence, it is *frozen* Na_3AlF_6 that flows in both directions in the bath/ledge boundary. A possible user interface, similar to the one in Fig. 3.12, is given in Fig. 6.5 for this connection.

Connection: bath/ledge

Device upstream: bath

Device downstream: ledge

Species: Na_3AlF_6

Specific energy:

bath: $\bar{H}_{\text{Na}_3\text{AlF}_6} = \Delta_f H_{298, \text{Na}_3\text{AlF}_6}^\circ + \bar{c}_{p, \text{Na}_3\text{AlF}_6} (T_{\text{bath}} - 298) + \Delta_{\text{fus}} H_{\text{Na}_3\text{AlF}_6}^\circ$

ledge: $\bar{H}_{\text{Na}_3\text{AlF}_6} = \Delta_f H_{298, \text{Na}_3\text{AlF}_6}^\circ + \bar{c}_{p, \text{Na}_3\text{AlF}_6} (T_{\text{liq}} - 298)$

Specifications (user input):

Type of flow: unidirectional bidirectional

Source of energy transformation, positive direction (if other than Device downstream):

- bath \rightarrow ledge:

Source of energy transformation, negative direction (if other than Device upstream):

- ledge \rightarrow bath:

Flow expression:

Figure 6.5: A possible user interface for Na_3AlF_6 in bath/ledge connection.

■

feed/bath::sludge connection

Fig. 5.4 shows how it is believed that the sludge is situated on top of the cathode, and how it is believed to be fed back to the bath. This connection is, however, not considered with the self-feeding property. This connection describes a *virtual* connection between the feed, bath and sludge device as described in assumption (A.7). The reason for it being virtual, is the physical distance between these devices in the real process. Remember from (A.11) that undissolved AlF_3 and Al_2O_3 falls *through* the metal, and hence, this connection represents more than just a boundary.

From the description of the feed, bath and sludge devices, (3.12) is employed

to identify the following P_C elements:

$$\begin{aligned}
 P_{C,\text{feed/bath::sludge}} &= (P_{D,\text{feed}} \cap P_{D,\text{bath}}) \cup \\
 &\quad (P_{D,\text{feed}} \cap P_{D,\text{sludge}}) \cup \\
 &\quad (P_{D,\text{bath}} \cap P_{D,\text{sludge}}) \\
 &= \{\text{Al}_2\text{O}_3, \text{AlF}_3\}.
 \end{aligned} \tag{6.29}$$

Note that there are two positive directions, from feed to sludge and from feed to bath. The PTD and TRAV for this connection and the adjacent devices can be illustrated as in Fig. 6.6.

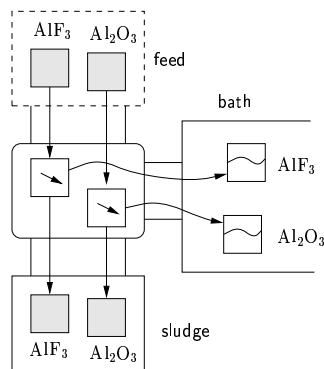


Figure 6.6: PTD and TRAV of AlF_3 and Al_2O_3 additions.

Due to different properties and characteristics of AlF_3 and Al_2O_3 , e.g. different values of $\Delta_{\text{sol}}H^\circ$, the ability to form sludge will be different.

In order to determine the specific enthalpy of each flowing species, recall from (6.5), (6.12) and (6.16) for Al_2O_3 , for example, (AlF_3 is similar), that

$$\bar{H}_{\text{Al}_2\text{O}_3,\text{feed}} = \Delta_f H_{298,\text{Al}_2\text{O}_3}^\circ + \bar{c}_{p,\text{Al}_2\text{O}_3}(T_{\text{feed}} - 298), \tag{6.5}$$

$$\bar{H}_{\text{Al}_2\text{O}_3,\text{bath}} = \Delta_f H_{298,\text{Al}_2\text{O}_3}^\circ + \bar{c}_{p,\text{Al}_2\text{O}_3}(T_{\text{bath}} - 298) + \Delta_{\text{sol}}H_{\text{Al}_2\text{O}_3}^\circ, \tag{6.12}$$

$$\bar{H}_{\text{Al}_2\text{O}_3,\text{sludge}} = \Delta_f H_{298,\text{Al}_2\text{O}_3}^\circ + \bar{c}_{p,\text{Al}_2\text{O}_3}(T_{\text{liq}} - 298). \tag{6.16}$$

Since the bath is the source for heat production, it is natural to believe that the bath provides all the energy needed within the cell cavity. As will be discussed in Sec. 6.3, there is no energy balance in the sludge device. The preheating from T_{feed} to T_{liq} of the additives forming sludge should therefore

be taken care of by the bath in order to generate consistent equations. Thus, a user interface for this purpose, similar to Figs. 3.12 and 6.5, is depicted in Fig. 6.7.

Connection: feed/bath::sludge

Device upstream: feed

Device downstream: bath, sludge

Species: Al₂O₃

Specific energy:

feed: $\tilde{H}_{\text{Al}_2\text{O}_3} = \Delta_f H_{298, \text{Al}_2\text{O}_3}^\circ + \bar{c}_{p, \text{Al}_2\text{O}_3} (T_{\text{feed}} - 298)$

bath: $\tilde{H}_{\text{Al}_2\text{O}_3} = \Delta_f H_{298, \text{Al}_2\text{O}_3}^\circ + \bar{c}_{p, \text{Al}_2\text{O}_3} (T_{\text{bath}} - 298) + \Delta_{\text{sol}} H_{\text{Al}_2\text{O}_3}^\circ$

sludge: $\tilde{H}_{\text{Al}_2\text{O}_3} = \Delta_f H_{298, \text{Al}_2\text{O}_3}^\circ + \bar{c}_{p, \text{Al}_2\text{O}_3} (T_{\text{liq}} - 298)$

Specifications (user input):

Type of flow: unidirectional bidirectional

Source of energy transformation, positive direction (if other than Device downstream):

- feed → bath:

- feed → sludge:

Flow expression:

Flow expression:

Figure 6.7: A possible user interface for the Al₂O₃ in feed/bath::sludge connection.

The input given in Fig. 6.7 will generate the following mass and energy balance equations for the bath and sludge devices (note that feed is a source). Only those terms related to this connection are included.

For the bath device:

$$\frac{dn_{\text{Al}_2\text{O}_3}}{dt} = j_{\text{Al}_2\text{O}_3, \text{feed} \rightarrow \text{bath}} \quad (6.30)$$

$$\begin{aligned} \frac{dH}{dt} = & j_{\text{Al}_2\text{O}_3, \text{feed} \rightarrow \text{bath}} \cdot \tilde{H}_{\text{Al}_2\text{O}_3, \text{feed}} + \\ & j_{\text{Al}_2\text{O}_3, \text{feed} \rightarrow \text{sludge}} \cdot \tilde{H}_{\text{Al}_2\text{O}_3, \text{feed}} - \\ & j_{\text{Al}_2\text{O}_3, \text{feed} \rightarrow \text{sludge}} \cdot \tilde{H}_{\text{Al}_2\text{O}_3, \text{sludge}} \end{aligned} \quad (6.31)$$

The two last terms in the energy balance represent the complete dissolution and freezing of $j_{\text{Al}_2\text{O}_3, \text{feed} \rightarrow \text{sludge}}$. After some calculation, the net effect of these two terms on the energy balance can be found to be:

$$j_{\text{Al}_2\text{O}_3, \text{feed} \rightarrow \text{sludge}} \cdot \bar{c}_{p, \text{Al}_2\text{O}_3} (T_{\text{feed}} - T_{\text{liq}}).$$

For the sludge device:

$$\frac{dn_{\text{Al}_2\text{O}_3}}{dt} = j_{\text{Al}_2\text{O}_3, \text{feed} \rightarrow \text{sludge}} \quad (6.32)$$

If modelers forget to name any source for energy transformation in the $\text{feed} \rightarrow \text{sludge}$ case, the underlying system should generate an error message based on the fact that there is no energy balance in the sludge device. Hence, the specification of energy transformation as in Fig. 6.7 can be used together with the possible existence of an energy balance to generate support for modelers.

Comment:

In Ch. 5 it was claimed that the amount of Na_3AlF_6 freezing onto the lumps of added AlF_3 and Al_2O_3 was negligible. In a model where this freezing is believed to be important, Fig. 6.6 would then be expanded to Fig. 6.8.

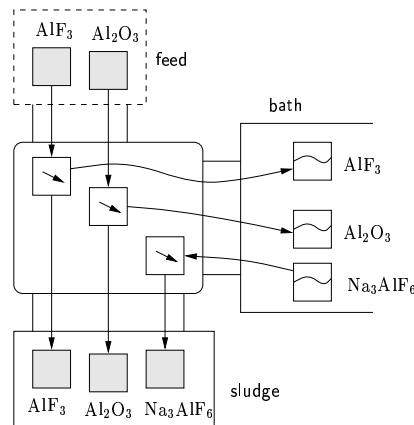


Figure 6.8: PTD and TRAV of AlF_3 and Al_2O_3 additions, including freezing of Na_3AlF_6 .

The use of (3.12) would produce the following P_C elements:

$$P_{C, \text{feed}/\text{bath}::\text{sludge}} = \{\text{Al}_2\text{O}_3, \text{AlF}_3, \text{Na}_3\text{AlF}_6\}. \quad (6.33)$$

A possible user interface for the Na_3AlF_6 species is depicted in Fig. 6.9.

Connection: feed/bath::sludge

Device upstream: **bath**

Device downstream: **sludge**

Species: Na_3AlF_6

Specific energy:

bath: $\tilde{H}_{\text{Na}_3\text{AlF}_6} = \Delta_f H_{298, \text{Na}_3\text{AlF}_6}^\circ + \bar{c}_{p, \text{Na}_3\text{AlF}_6} (T_{\text{bath}} - 298) + \Delta_{\text{fus}} H_{\text{Na}_3\text{AlF}_6}^\circ$

sludge: $\tilde{H}_{\text{Na}_3\text{AlF}_6} = \Delta_f H_{298, \text{Na}_3\text{AlF}_6}^\circ + \bar{c}_{p, \text{Na}_3\text{AlF}_6} (T_{\text{liq}} - 298)$

Specifications (user input):

Type of flow: unidirectional bidirectional

Source of energy transformation, positive direction (if other than Device downstream):

- bath → sludge:

Flow expression:

Figure 6.9: A possible user interface for Na_3AlF_6 in the feed/bath::sludge connection.

Note that the devices upstream and downstream for Na_3AlF_6 are different than those for Al_2O_3 and AlF_3 . There is also another positive direction as seen from the direction of the mass based arrows.

For the Na_3AlF_6 in the bath device:

$$\frac{dn_{\text{Na}_3\text{AlF}_6}}{dt} = -j_{\text{Na}_3\text{AlF}_6, \text{bath} \rightarrow \text{sludge}} \quad (6.34)$$

$$\frac{dH}{dt} = -j_{\text{Na}_3\text{AlF}_6, \text{bath} \rightarrow \text{sludge}} \cdot \tilde{H}_{\text{Na}_3\text{AlF}_6, \text{sludge}} \quad (6.35)$$

Even if $j_{\text{Na}_3\text{AlF}_6, \text{bath} \rightarrow \text{sludge}}$ is negative, the change in H relative to the change in $n_{\text{Na}_3\text{AlF}_6}$ gives a rise in temperature since solid Na_3AlF_6 leaves the bath. The result is that the bath actually receives energy corresponding to:

$$j_{\text{Na}_3\text{AlF}_6, \text{bath} \rightarrow \text{sludge}} \cdot \bar{c}_{p, \text{Na}_3\text{AlF}_6} (T_{\text{bath}} - T_{\text{liq}}).$$

◇◇◇

■

sludge/bath connection

This connection describes the self-feeding from sludge to bath. The following P_C elements are considered:

$$P_{C,\text{sludge/bath}} = P_{D,\text{sludge}} \cap P_{D,\text{bath}} = \{\text{Al}_2\text{O}_3, \text{AlF}_3\}. \quad (6.36)$$

This is a unidirectional flow connection, and the specific enthalpies of the flowing Al_2O_3 and AlF_3 at $T = T_{\text{liq}}$ are given as:

$$\left. \begin{aligned} \tilde{H}_{\text{Al}_2\text{O}_3} &= \Delta_f H_{298, \text{Al}_2\text{O}_3}^\circ + \bar{c}_{p, \text{Al}_2\text{O}_3}(T_{\text{liq}} - 298) \\ \tilde{H}_{\text{AlF}_3} &= \Delta_f H_{298, \text{AlF}_3}^\circ + \bar{c}_{p, \text{AlF}_3}(T_{\text{liq}} - 298) \end{aligned} \right\} \quad (6.37)$$

which corresponds to the specific enthalpy of the upstream device, i.e. sludge. ■

bath/crust connection

Based on the crust and bath devices on pages 120 and 121, respectively, the following P_C elements are considered:

$$P_{C,\text{bath/crust}} = P_{D,\text{bath}} \cap P_{D,\text{crust}} = \{\text{AlF}_3\}. \quad (6.38)$$

The specific enthalpy of AlF_3 flowing in the positive direction at $T = T_{\text{bath}}$ is given as:

$$\tilde{H}_{\text{AlF}_3} = \Delta_f H_{298, \text{AlF}_3}^\circ + \bar{c}_{p, \text{AlF}_3}(T_{\text{bath}} - 298) + \Delta_{\text{sol}} H_{\text{AlF}_3}^\circ. \quad (6.39)$$

Since lumps of crust might fall into the bath, there is also a flow in the negative direction. Consequently, the specific enthalpy for this flow at $T = T_{\text{liq}}$ is:

$$\tilde{H}_{\text{AlF}_3} = \Delta_f H_{298, \text{AlF}_3}^\circ + \bar{c}_{p, \text{AlF}_3}(T_{\text{liq}} - 298). \quad (6.40)$$

Thus, the energy related to the evaporated AlF_3 is considered lost when the fume is condensed in the crust device. ■

bath/surroundings connection

Based on the bath and surroundings devices, the following P_C element is considered:

$$P_{C,\text{bath/surroundings}} = P_{D,\text{bath}} \cap P_{D,\text{surroundings}} = \{\text{AlF}_3\}. \quad (6.41)$$

The specific enthalpy of the evaporating AlF_3 at $T = T_{\text{bath}}$ is similar to (6.39):

$$\tilde{H}_{\text{AlF}_3} = \Delta_f H_{298,\text{AlF}_3}^\circ + \bar{c}_{p,\text{AlF}_3}(T_{\text{bath}} - 298) + \Delta_{\text{sol}} H_{\text{AlF}_3}^\circ. \quad (6.42)$$

The expression for the equivalent AlF_3 evaporation is given below.

Equivalent AlF_3 evaporation: Since there are no continuous measurements of HF and NaAlF_4 evaporation, one has to use relationships where some other known quantities or state variables determine this evaporation. Such a relationship is given as⁵

$$j_{\text{AlF}_3} = f(T_{\text{bath}}, w_{\text{AlF}_3}, w_{\text{Al}_2\text{O}_3}, \mathcal{CE}). \quad (6.43)$$

This is a simplified version of Haupin's formula (Haupin and Kvande 1993), and the evaporation model comprises both particulate and gaseous fluoride containing compounds.

■

anode::bath/surroundings::metal connection

As discussed in assumptions (A.1) to (A.5), all other reactions except (5.1) and (5.2) are neglected. However, reaction (5.1) is made up of two half reactions, i.e. one reduction and one oxidation reaction as commented upon on page 98. The reduction and oxidation reactions are situated at different locations within the cell cavity, i.e. one at the anode surface and the other at the cathode surface as discussed in Sec. 5.3.1. The use of (5.1) implies that both these surface reactions have to be lumped into *one* surface reaction, though it is not evident where to place this new reaction on the TRAV. For this reason, another *virtual* connection must be defined which relates the devices where the involved species are located. The reaction (5.2) is also included in the same connection. This example shows that the level of assumption and simplification made prior to the modularization

⁵From an unpublished report from Hydro Aluminium a.s.

discussed in Sec. 3.1.1 may produce unrealistic topological components. As a result, the suggested connections bath/anode and bath/metal in (6.23) are neglected in the mass based topological decomposition. From an energy based topological decomposition, however, the bath/metal connection is included as discussed in Sec. 6.3, Fig. 6.17.

Note that the *positive* direction in this case with two upstream and two downstream devices are from anode:bath to surroundings::metal. As discussed in Sec. 3.2.2, the use of (3.12) will not identify possible reactions, and hence,

$$P_{C,\text{anode}::\text{bath}/\text{surroundings}::\text{metal}} = \emptyset. \quad (6.44)$$

On the other hand, based on the above discussion,

$$P_{C,\text{anode}::\text{bath}/\text{surroundings}::\text{metal}} = \{R''_{\text{pr}}, R''_{\text{br}}\}, \quad (6.45)$$

where subscript pr and br indicate the primary and back reactions, respectively. Both reactions are presented in Fig. 6.10. The use of the dashed line will be discussed below.

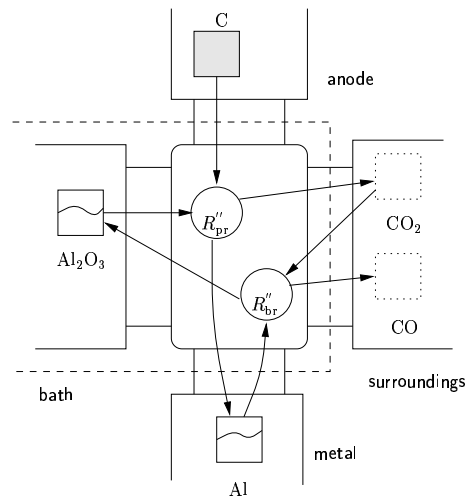


Figure 6.10: PTD and TRAV of primary and back reaction.

This connection actually relates devices that are physically separated by other devices, i.e. the liquid aluminum is located below the bath and is never exposed to the surroundings, even if Fig. 6.10 indicates this. The two reactions in (6.45) will be further discussed below.

Primary reaction: The primary reaction involves the following species:

$$R''_{pr} = \{\text{Al}_2\text{O}_3, \text{C}, \text{Al}, \text{CO}_2\}. \quad (6.46)$$

Surface reactions must be handled with care when it comes to dealing with energy balances. If all the reactants and products were existing *within* the bath device, the change in the energy balance, i.e. the heat of reaction $\Delta_r H^\circ$, would correspond to the changes in the amount of each species as discussed in Sec. 2.6.1. However, in the case illustrated in Fig. 6.10, the existence of C, CO₂ or Al is not modeled in the bath. This implies that the energy required to produce CO₂ and Al must be taken from a device. As **bath** is specified to be the source of energy, every species participating in the primary reaction will relate to the **bath** device and exploit its direction relative to the direction of the **bath** species (Al₂O₃). This is illustrated in Fig. 6.10 with a dashed line being this new boundary. A corresponding user interface is shown in Fig. 6.11.

Connection: anode::bath/surroundings::metal

Reactant: anode (C), bath (Al₂O₃)

Product: surroundings (CO₂), metal (Al)

Surface reaction: R'_{pr}

Specific energy:

anode: $\tilde{H}_C = \Delta_f H_{298,C}^\circ + \bar{c}_{p,C}(T_{\text{bath}} - 298)$

bath: $\tilde{H}_{\text{Al}_2\text{O}_3} = \Delta_f H_{298,\text{Al}_2\text{O}_3}^\circ + \bar{c}_{p,\text{Al}_2\text{O}_3}(T_{\text{bath}} - 298) + \Delta_{\text{sol}} H_{\text{Al}_2\text{O}_3}^\circ$

surroundings: $\tilde{H}_{\text{CO}_2} = \Delta_f H_{298,\text{CO}_2}^\circ + \bar{c}_{p,\text{CO}_2}(T_{\text{bath}} - 298)$

metal: $\tilde{H}_{\text{Al}} = \Delta_f H_{298,\text{Al}}^\circ + \bar{c}_{p,\text{Al}}(T_{\text{metal}} - 298) + \Delta_{\text{fus}} H_{\text{Al}}^\circ$

Specifications (user input):

Source/sink of energy:

Stoichiometric coefficients:

Equilibrium:

Figure 6.11: A possible user interface of the primary reaction in the anode::bath/surroundings::metal connection.

The specifications in Fig. 6.11 will generate the following balance equations in the **bath** and **metal** devices.

For the **bath** device:

$$\frac{dn_{\text{Al}_2\text{O}_3}}{dt} = -r_{\text{Al}_2\text{O}_3,\text{pr}} \quad (6.47)$$

$$\frac{dH}{dt} = r_{C,pr} \cdot \tilde{H}_{C,anode} - r_{CO_2,pr} \cdot \tilde{H}_{CO_2,surroundings} - r_{Al,pr} \cdot \tilde{H}_{Al,metal} \quad (6.48)$$

Note that $r_{Al_2O_3,pr}$ is not included in (6.48). For the metal device:

$$\frac{dn_{Al}}{dt} = r_{Al,pr} \quad (6.49)$$

$$\frac{dH}{dt} = r_{Al,pr} \cdot \tilde{H}_{Al,metal} \quad (6.50)$$

Since Al is considered to be produced at T_{metal} , there is a net energy input to the bath corresponding to $r_{Al,pr} \cdot \bar{c}_{p,Al}(T_{bath} - T_{metal})$.

Back reaction: The back reaction involves the following species:

$$R''_{br} = \{Al, CO_2, Al_2O_3, CO\}. \quad (6.51)$$

and a similar user interface as shown in Fig. 6.11 is shown in Fig. 6.12 for the back reaction.

Connection: anode::bath/surroundings::metal

Reactant: metal (Al), surroundings (CO₂)

Product: bath (Al₂O₃), surroundings (CO)

Surface reaction: R''_{br}

Specific energy:

metal: $\tilde{H}_{Al} = \Delta_f H_{298,Al}^\circ + \bar{c}_{p,Al}(T_{metal} - 298) + \Delta_{fus} H_{Al}^\circ$

surroundings: $\tilde{H}_{CO_2} = \Delta_f H_{298,CO_2}^\circ + \bar{c}_{p,CO_2}(T_{bath} - 298)$

bath: $\tilde{H}_{Al_2O_3} = \Delta_f H_{298,Al_2O_3}^\circ + \bar{c}_{p,Al_2O_3}(T_{bath} - 298) + \Delta_{sol} H_{Al_2O_3}^\circ$

surroundings: $\tilde{H}_{CO} = \Delta_f H_{298,CO}^\circ + \bar{c}_{p,CO}(T_{bath} - 298)$

Specifications (user input):

Source/sink of energy:

Stoichiometric coefficients:

Equilibrium:

Figure 6.12: A possible user interface of the back reaction in the anode::bath/surroundings::metal connection.

The specifications in Fig. 6.12 will generate the following balance equations in the bath device.

$$\frac{dn_{\text{Al}_2\text{O}_3}}{dt} = r_{\text{Al}_2\text{O}_3, \text{br}} \quad (6.52)$$

$$\begin{aligned} \frac{dH}{dt} = & r_{\text{Al}, \text{br}} \cdot \bar{H}_{\text{Al}, \text{metal}} + \\ & r_{\text{CO}_2, \text{br}} \cdot \bar{H}_{\text{CO}_2, \text{surroundings}} - r_{\text{CO}, \text{br}} \cdot \bar{H}_{\text{CO}, \text{surroundings}} \end{aligned} \quad (6.53)$$

■

6.2.3 Mass based representation

The mass based model development described above can be represented by the PTD and TRAV in Fig. 6.13.

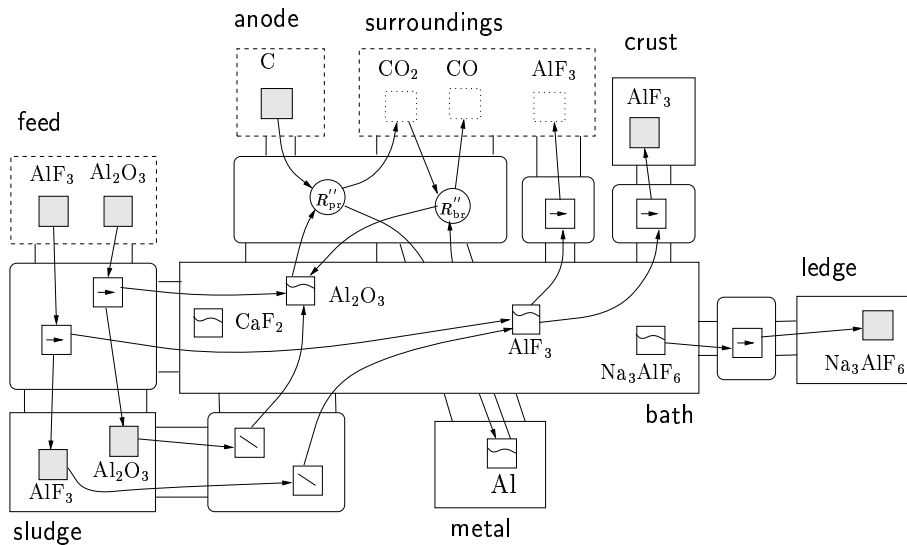


Figure 6.13: PTD and TRAV of the aluminum electrolysis cell, mass aspect. Note that arrows for mass transfer to and from the A_S element in the metal device is hidden under the bath device.

Even if this is a comprehensive model, there are several model assumptions made a priori which are implicitly represented in Fig. 6.13. To repeat, the base set of species, S , from (6.1) are

$$S = \{\text{Na}_3\text{AlF}_6, \text{Al}_2\text{O}_3, \text{AlF}_3, \text{CaF}_2, \text{CO}_2, \text{CO}, \text{C}, \text{Al}\}.$$

The T_S set becomes:

$$T_S = \{\text{Na}_3\text{AlF}_{6\text{conv}}, \text{Al}_2\text{O}_{3\text{conv}}, \text{AlF}_{3\text{conv}}, \text{Al}_2\text{O}_{3\text{diff}}, \text{AlF}_{3\text{diff}}\}, \quad (6.54)$$

and the accumulated species are:

$$A_S = \{\text{Na}_3\text{AlF}_6, \text{Al}_2\text{O}_3, \text{AlF}_3, \text{CaF}_2, \text{Al}\}. \quad (6.55)$$

Note that accumulation of CO, C and CO₂ are not considered. Further,

$$R'' = \{R''_{\text{pr}}, R''_{\text{br}}\}, \quad (6.56)$$

and

$$R''' = \{\}. \quad (6.57)$$

6.3 Energy based model development

The elementary energy based devices, ED_{energy} , and connections, EC_{energy} , were introduced in Sec. 2.4.1. In this section, the ED_{energy} and EC_{energy} sets of the aluminum are identified and described in detail in Secs. 6.3.1 and 6.3.2, respectively.

6.3.1 Elementary devices, ED_{energy}

From Sec. 5.1.3, the heat loss is divided in three directions, i.e. upwards, downwards and sideways. The process description in Ch. 5 and the partitioning in Fig. 6.1 enable the following preliminary energy based PTD layout to be identified.

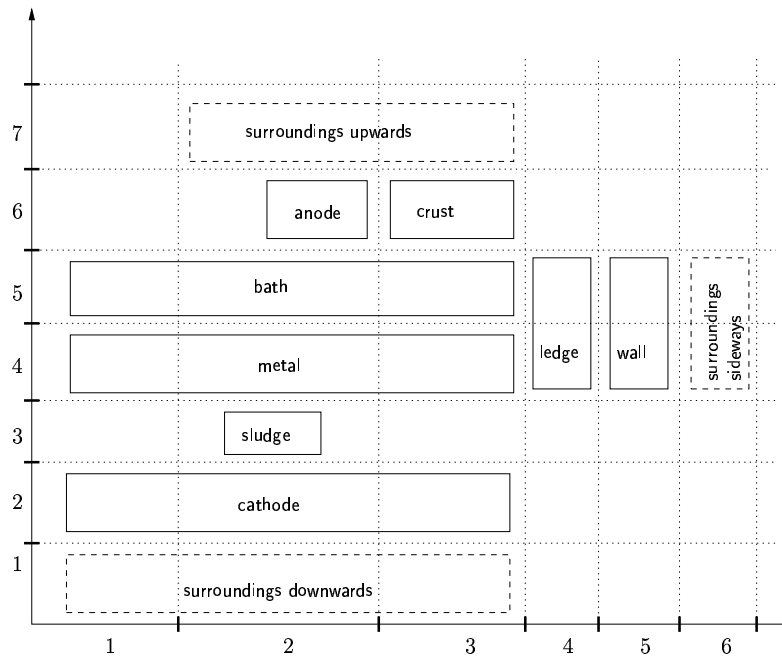


Figure 6.14: Preliminary energy based PTD of the aluminum cell.

Bearing the purpose of the model in mind, the following a priori assumptions are included:

- (A.12) The energy balances of the solid phases are neglected, i.e. the anode, the crust, the ledge, the wall, the sludge and the cathode block. This implies that these devices are replaced by connections.
- (A.13) The heat loss from the metal to the surroundings sideways is neglected.

This produces the following reduced energy based PTD.

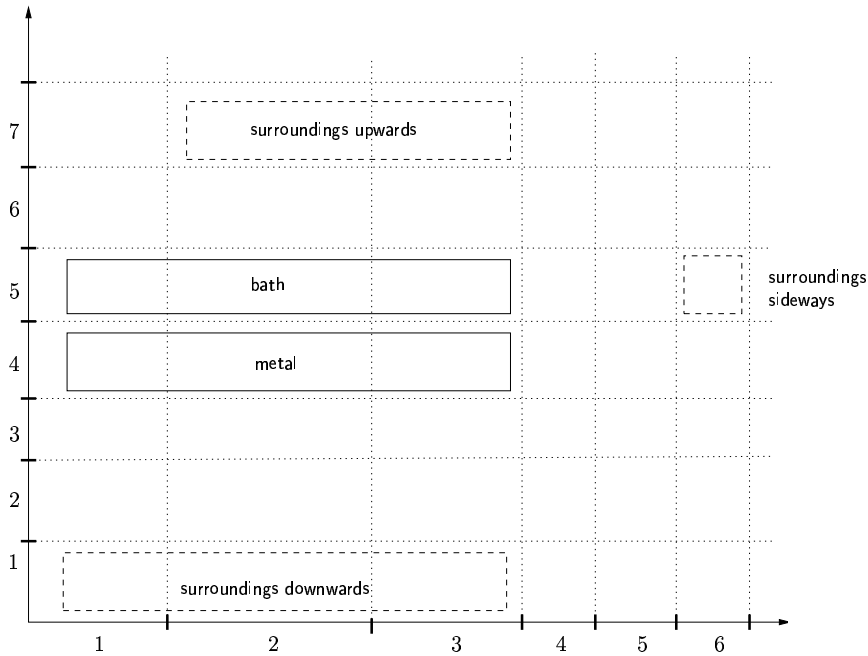


Figure 6.15: Reduced preliminary energy based PTD of the aluminum cell.

In accordance with Fig. 6.15, the following energy based elementary devices are identified:

$$ED_{\text{energy}} = \{\text{surroundings upwards, metal, bath, surroundings sideways, surroundings downwards}\}. \quad (6.58)$$

Note that the devices surroundings upwards, surroundings sideways and surroundings downwards are considered as sinks of energy. This leaves the bath and metal devices to be described.

The presentation of each device of the ED_{energy} set in Sec. 6.3.1 contains a set of $P_{D,\text{energy}}$ elements (introduced in (2.13) on page 30).

bath device:

Since the heat generation is solely assumed to exist in the bath, the following P_D elements are included:

$$P_{D,\text{bath}} = \{H, P_{\text{input}}\}. \quad (6.59)$$

Sec. 5.5 described different potentials within the aluminum cell. In the model developed here, the sum of E_{rev} from (5.35) and the different over-voltages are assumed constant, $E_{\text{bath}} = E_{\text{bath},0}$. Furthermore, U_{ext} is also assumed constant equal $U_{\text{ext},0}$. The cell potential from (5.39) then becomes:

$$U_{\text{cell}} = U_{\text{bath}} + U_{\text{ext},0} + E_{\text{bath},0}. \quad (6.60)$$

The required energy input to the cell is then from (5.48),

$$P_{\text{input}} = (R_{\text{meas}} I_{\text{meas}} - U_{\text{ext},0}) I_{\text{meas}}. \quad (6.61)$$

This means that the measured resistance and current become inputs to the model. The overall enthalpy of the bath follows (3.14), though using approximated values of \bar{H} . This gives

$$H = \sum_{i=1}^N n_i \bar{H}_i + \Delta_{\text{mix}} H. \quad (6.62)$$

The individual \bar{H} is taken from (6.12) in the bath device in Sec. 6.2. The enthalpy of mixing, $\Delta_{\text{mix}} H$, is neglected according to Sec. D.4. ■

metal device:

The following P_D element is considered:

$$P_{D,\text{metal}} = \{H\}. \quad (6.63)$$

There is virtually no heat production in the metal. The resistance is very low compared to the bath, and hence, the heat production is negligible. ■

6.3.2 Elementary connections, EC_{energy}

Based on the ED_{energy} elements in (6.58), the following connections are identified:

$$EC_{\text{energy}} = \{\text{bath/surroundings upwards, bath/surroundings sideways, bath/metal, metal/surroundings downwards}\}. \quad (6.64)$$

The complete energy based PTD layout of the devices in (6.58) and the connections in (6.64) is shown in Fig. 6.16.

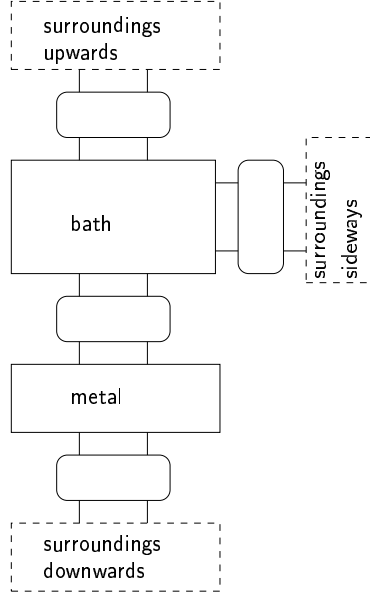


Figure 6.16: Complete energy based PTD of the elements in (6.58) and (6.64).

The presentation of each connection of the EC_{energy} set in Sec. 6.3.2 contains *i*) a set of $P_{C,\text{energy}}$ elements identified from the process description and, *ii*) a specification of these elements.

bath/surroundings upwards connection

The heat loss from bath to surroundings upwards is characterized both as convective heat flow and radiation. For this reason, the following P_C elements are included:

$$P_{C,\text{bath/surroundings upwards}} = \{Q_{\text{conv}}, Q_{\text{rad}}\}. \quad (6.65)$$

The convective heat loss is modeled as a function of temperature as:

$$Q_{\text{conv}} = Q_{\text{loss},0} + b_{Q_{\text{loss}}}(T_{\text{bath}} - T_{\text{bath},0}), \quad (6.66)$$

where $T_{\text{bath},0}$, $b_{Q_{\text{loss}}}$ and $Q_{\text{loss},0}$ are constants. However, $Q_{\text{loss},0}$ could also have been a function of the crust thickness calculated from the crust device. The radiation is given as:

$$Q_{\text{rad}} = b_{\text{rad}}(T_{\text{bath}}^4 - T_{\text{surroundings upwards}}^4), \quad (6.67)$$

where b_{rad} is a constant. ■

bath/surroundings sideways connection

The flow of Na_3AlF_6 between the ledge and bath is determined by the difference in convective heat flow from bath to side ledge and the conductive heat flow through the side ledge and the carbon wall. Recall the simplified sketch of a melting situation shown in Fig. 6.4. Since the convective heat flow is different from the conductive heat flow through the ledge and wall, i.e. $Q_{\text{conv}} \neq Q_{\text{cond}}$, the symbol for heat convection is not included in this connection in the TRAV. This implies that the expression for Q_{conv} is solely used to calculate $j_{\text{Na}_3\text{AlF}_6}$ as shown in (6.27). Q_{conv} is calculated as:

$$Q_{\text{conv}} = h_{\text{bath,ledge}} A_{\text{bath,ledge}} (T_{\text{bath}} - T_{\text{liq}}), \quad (6.68)$$

where the heat transfer coefficient between bath and side ledge, $h_{\text{bath,ledge}}$, is found to vary between 500 and 1000 $\text{J K}^{-1}\text{s}^{-1}\text{m}^{-2}$ (Grjotheim and Kvande 1993). In the model developed here, it is assumed constant.

The effect of not equalizing Q_{cond} and Q_{conv} , implies that T_{liq} is *not* eliminated as shown for T_{wall} in (2.28) to (2.30). As a result, the heat flow from the bath to surroundings sideways consists of two conductive heat flows in series, and the following P_C elements are considered:

$$P_{C,\text{bath/surroundings sideways}} = \{Q_{\text{cond,ledge}}, Q_{\text{cond,wall}}\} \quad (6.69)$$

Note that the convective heat flow from the steel shell to the surroundings sideways is not considered.

Since the two flows are equal, it is possible to derive *one* expression for the overall heat flow, following the example in (2.30). This gives for Q :

$$Q = \frac{A_{\text{bath,ledge}}}{\frac{l_{\text{ledge}}}{k_{\text{ledge}}} + \frac{l_{\text{wall}}}{k_{\text{wall}}}} (T_{\text{liq}} - T_0). \quad (6.70)$$

Note that the same area, $A_{\text{bath,ledge}}$, is used for both flows, and that this area is assumed constant. The calculation of l_{ledge} follows (6.10). ■

bath/metal connection

The heat flow from bath to metal is characterized as convective flow. The following P_C element is therefore included:

$$P_{C,\text{bath/metal}} = \{Q_{\text{conv}}\}. \quad (6.71)$$

The calculation is straightforward:

$$Q_{\text{conv}} = h_{\text{bath,metal}} A_{\text{bath,metal}} (T_{\text{bath}} - T_{\text{metal}}). \quad (6.72)$$

■

metal/surroundings downwards connection

As for the heat flow in bath/surroundings sideways, the heat flow from metal to surroundings downwards is also conductive heat flow. Consequently, the following P_C element is considered:

$$P_{C,\text{metal/surroundings downwards}} = \{Q_{\text{cond}}\}, \quad (6.73)$$

where the convective heat loss from the steel shell to the surroundings downwards is also here neglected. The calculation of Q_{cond} is straightforward:

$$Q_{\text{cond}} = \frac{A_{\text{metal,cathode}}}{\frac{l_{\text{cathode}}}{k_{\text{cathode}}}} (T_{\text{metal}} - T_0). \quad (6.74)$$

Note that the temperature on the side of and under the cell is T_0 . ■

6.3.3 Energy based representation

The energy based model development described above can be represented in a PTD and TRAV as in Fig. 6.17.

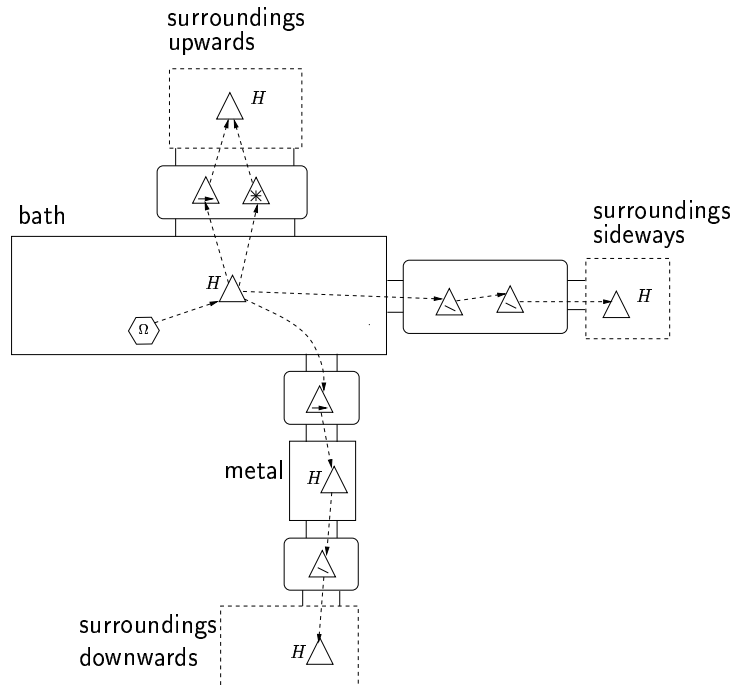


Figure 6.17: PTD and TRAV of the aluminum electrolysis cell, energy aspect.

From (6.2), the following set is found:

$$E = \{H\}.$$

Moreover, the accumulation element is:

$$A_E = \{H\}. \quad (6.75)$$

Further, these energy flows are considered

$$T_E = \{Q_{\text{conv}}, Q_{\text{cond}}, Q_{\text{rad}}\}, \quad (6.76)$$

and the heat generation in the bath as:

$$G_E = \{P_{\text{input}}\}, \quad G_M = \{\}. \quad (6.77)$$

6.4 Additional model assumptions

The total number of dynamic states are 10, i.e. 2 energy balances and 8 mass balances. Note that the amount of CaF_2 is assumed constant. The mass accumulation symbols in the feed, anode and surroundings devices in Fig. 6.13 are sinks and sources, implying that they are not dynamic states. This is also the case for the energy accumulation symbols in the surroundings upwards, surroundings sideways and surroundings downwards devices in Fig. 6.17.

The model in Figs. 6.13 and 6.17 was initially used in the investigation of the cell dynamics. The result from these studies are summarized in the following additional assumptions.

- (A.14) It is found that the existence of the liquid aluminum phase has negligible impact on the simulation results, even though the content of this phase changes significantly. The metal device is therefore considered a sink device in both representations, and the convective heat loss from (6.72) is considered constant. This is accomplished by specifying T_{metal} to be 5K lower than T_{bath} .
- (A.15) The use of sludge as a buffer for AlF_3 did not improve the simulation results. This is supported by the observation that the delay of Al_2O_3 from sludge to bath, which intuitively should be of the same order, is too small compared with the observed delay for AlF_3 . That is, if the delay is caused by the sludge phase only. Along this side of argumentation, it has been observed that AlF_3 dissolves much faster than Al_2O_3 in laboratory setups (Rolseth 1997). This

implies that it should be reasonable to assume that this condition also holds for industrial cells. This is of course a strong assumption since results obtained in laboratory setups are not always directly transferable to conditions in industrial cells. Nevertheless, AlF_3 additions are here assumed to dissolve immediately.

(A.16) For the study of AlF_3 dynamics, the Al_2O_3 additions are assumed to dissolve immediately, neglecting the sludge phase.

(A.17) Due to the lack of adequate mathematical models for the interaction between bath and crust, this phenomenon is not considered.

(A.18) The current efficiency is assumed constant due to the problem of developing a relationship handling the *positive* feedback from temperature to current efficiency in a satisfactory manner. Experience indicates that a current efficiency model should also take average anode-cathode-distance into account.

(A.19) Heat radiation from bath to surroundings upwards is neglected.⁶

(A.20) The fluoride and sodium content in the secondary alumina is assumed to be constant.

(A.21) Effects of metal and bath tapping are neglected.

As a result of these additional model assumptions, the model is simplified to consist of 5 dynamic states. These are accumulation of Na_3AlF_6 , AlF_3 , Al_2O_3 and energy in bath, and Na_3AlF_6 in the side ledge.

6.5 Simplified model representation

A simplification of the model in Figs. 6.13 and 6.17 resulting from the assumptions listed in Sec. 6.4 is represented in Figs. 6.18 and 6.19. This model is used in Ch. 7 and Ch. 8.

⁶From an internal report from Hydro Aluminium a.s.

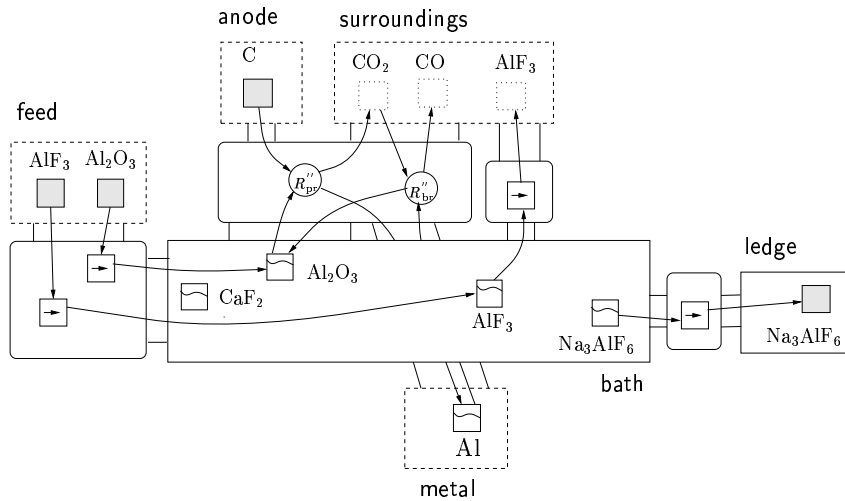


Figure 6.18: Simplified PTD and TRAV of the aluminum electrolysis cell, mass aspect.

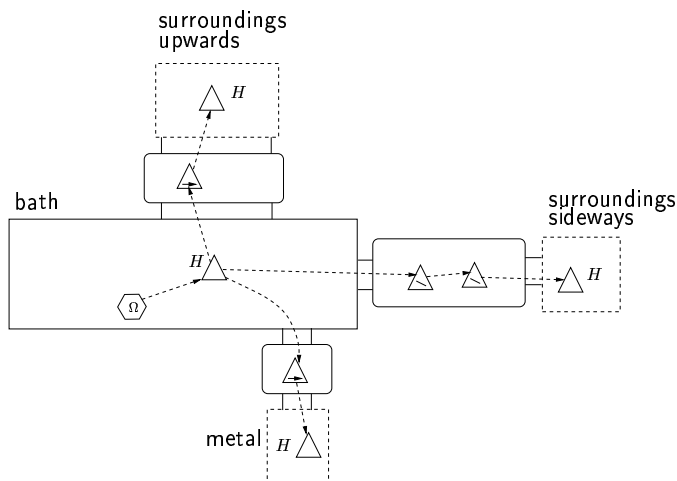


Figure 6.19: Simplified PTD and TRAV of the aluminum electrolysis cell, energy aspect.

The simplified model visualizes the efficiency and usability of the modeling methodology. By removing the neglected devices, a new representation is obtained. The underlying equation structure updates accordingly, and hence, consistency is achieved and modeling effort is reduced. The updating is performed automatically.

6.6 Discussion

This chapter has developed a comprehensive dynamic model taking into account what is believed the most important characteristics of an aluminum electrolysis cell with respect to long-term predictions of the AlF_3 dynamics. Based on experience with the model behavior, many of the detailed characteristics have been simplified in order to develop a simple model. This simplified model is used in the following chapters.

The innovative method of model presentation used in this chapter may cause some slight difficulties for some readers. There are probably several reasons for this. One of these might be that the reader is not familiar with the terminology. Another reason might be the emphasis on enthalpy specification of each species, and the absence of the heat of reactions. In this work it is argued that this approach structures the modeling problem in a favorable way. Further, experience show that coding errors are almost completely removed due to the use of the graphical language.

Chapter 7

Model validation

In order to investigate whether the model gives reasonable responses with respect to AlF_3 addition and changes in the energy balance, the model responses are validated against known behavior in Sec. 7.1 and measurements in Sec. 7.2. Thermodynamic data in the model are mainly taken from JANAF Thermochemical tables (Chase *et al.* 1985), given in App. D. The current in all simulations in this thesis is 160kA.

7.1 Validation against known behavior using step and pulse inputs

In this section, two *separate* simulations are performed using different step and pulse inputs. That is, the first simulation uses a negative step in the reference resistance corresponding to a 5.1 kJ s^{-1} drop in P_{input} , together with *constant* AlF_3 input. The second simulation uses a pulse of 112 kg AlF_3 over a period of 3 hours together with constant energy input. These inputs are shown in Figs. 7.1 and 7.2. Note that the Al_2O_3 input is held constant in both simulations in order to study the impact of the AlF_3 and energy inputs.

The selected inputs represent typical control inputs used in industry. The AlF_3 addition is rather large, but not unrealistic, compared to additions during normal operation. The amount of bath is initially 6700 kg for both simulations. The responses from both simulations are plotted together in the following.

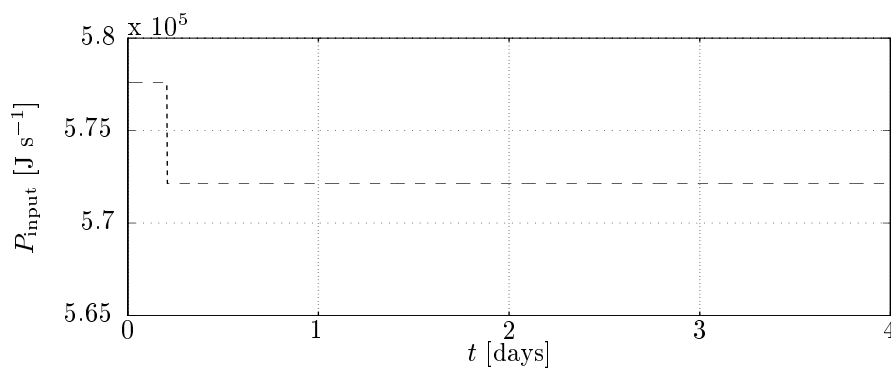


Figure 7.1: A negative step in reference resistance.

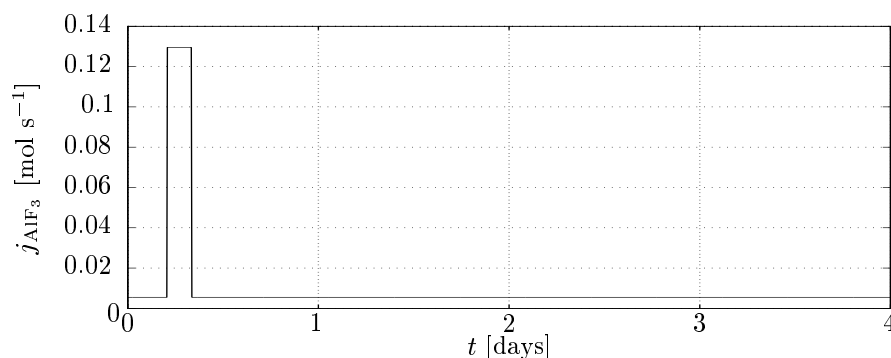


Figure 7.2: A pulse of 112 kg AlF_3 over a period of 3 hours. Note that a rate of 0.1 mol s^{-1} is equivalent to 30 kg hour^{-1} .

The expected cell behavior after the negative step in reference resistance should first of all be reduced bath temperature. In addition, some of the molten Na_3AlF_6 in the bath would freeze, suppressing the impact of the reduced energy input. This freezing of molten Na_3AlF_6 would give an increase in excess AlF_3 and an increase in side ledge thickness.

For the AlF_3 addition, an increase in excess AlF_3 is expected, but not as much as from an *isolated* bath mass balance, ($\frac{112}{6700+112} = 0.0165$). This is due to the dilution of the bath from the melting of the side ledge. As AlF_3 is added and dissolved, the liquidus temperature drops, consequently giving an increase in superheat, and thereby melting of the side ledge. The simulated responses for bath temperature, excess AlF_3 , side ledge thickness and superheat are shown in Figs. 7.3 to 7.6.

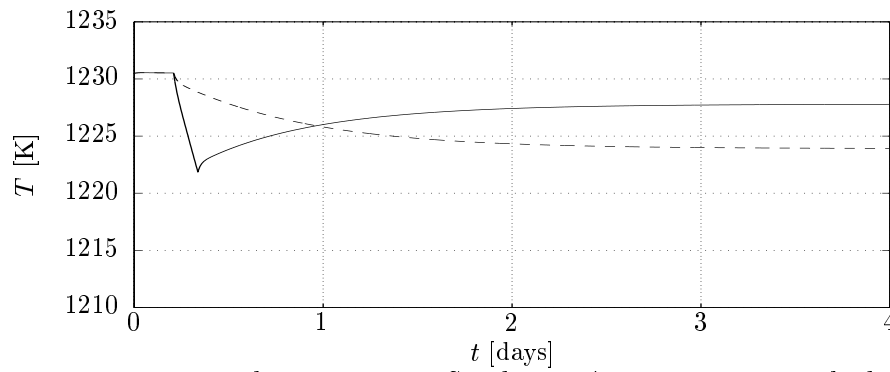


Figure 7.3: Bath temperature. Solid line: AlF_3 addition. Dashed line: Reduced reference resistance.

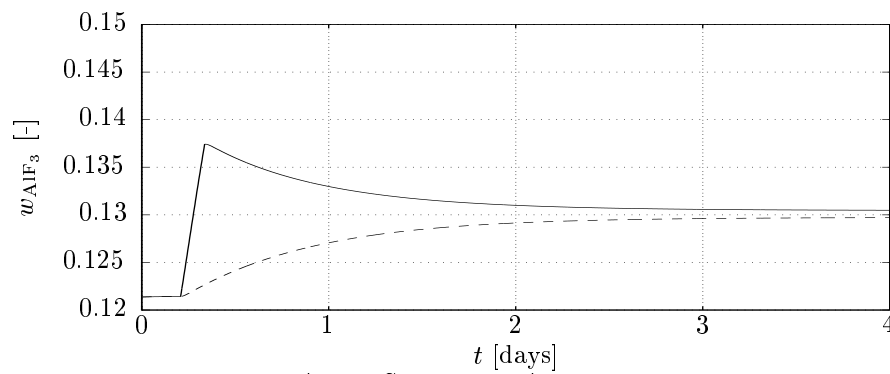


Figure 7.4: Excess AlF_3 . Solid line: AlF_3 addition. Dashed line: Reduced reference resistance.

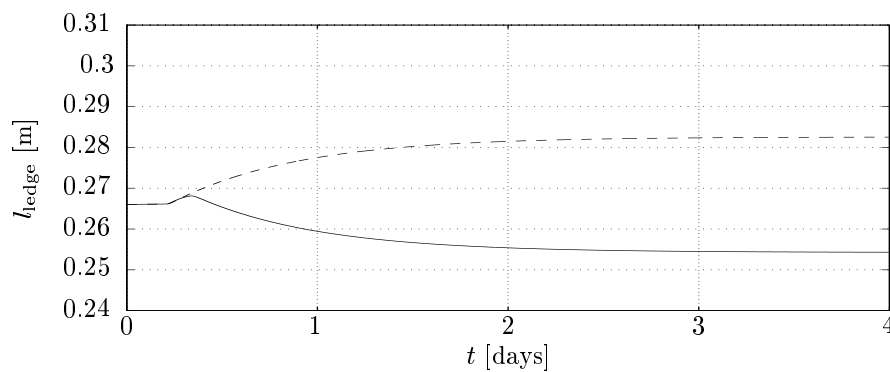


Figure 7.5: Side ledge thickness. Solid line: AlF_3 addition. Dashed line: Reduced reference resistance.

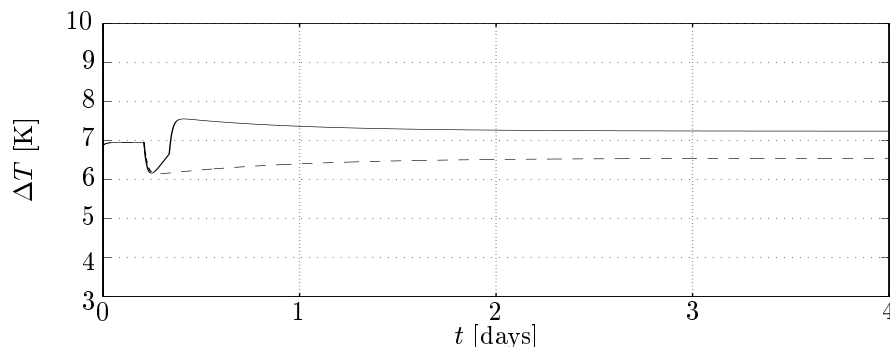


Figure 7.6: Superheat. Solid line: AlF_3 addition. Dashed line: Reduced reference resistance.

The model responses are intuitive. The resulting increase in excess AlF_3 due to AlF_3 addition is approximately half of 0.0165. On the other hand, the comparatively, rather small, negative step in energy input has a similar impact on the excess AlF_3 . Due to the assumption of a well mixed situation in the bath, additions made in the center of the cell have an immediate impact on the side ledge. One way to avoid this immediate and rather unrealistic impact is to divide the cell into two well mixed zones, one where the feeding is done and one in contact with the side ledge. The challenge is then to use reasonable convective and diffusive parameters for heat and mass flow between the zones. This approach is not addressed here.

From the model development in Sec. 6.3.2, the convective heat loss from the bath to the surroundings upwards in the bath/surroundings upwards connection is modeled as (6.66). For the two simulations in this section, the heat loss responses corresponding to (6.66) are given in Fig. 7.7.

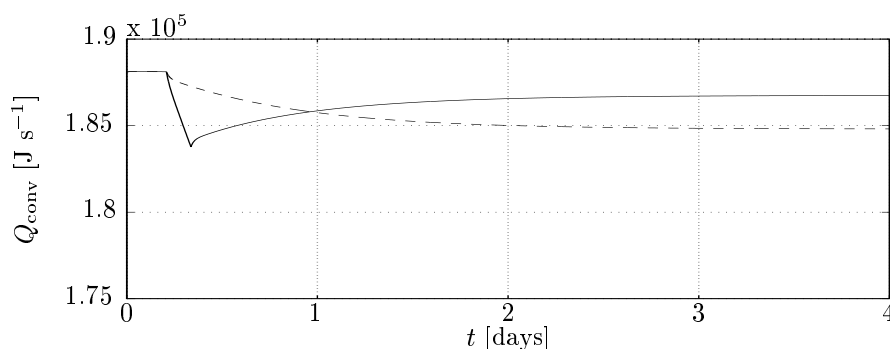


Figure 7.7: Convective heat loss from bath to surroundings upwards. Solid line: AlF_3 addition. Dashed line: Reduced reference resistance.

7.2 Validation against measurements using real input data 155

The experience with different values of the $b_{Q_{\text{loss}}}$ parameter in (6.66) is rather interesting. It has proven to have a significant influence on the time constant from the heat loss modeled in (6.66) to the bath temperature. To illustrate this, two additional simulations using the same inputs as in Figs. 7.1 and 7.2, are presented in Secs. E.1 and E.2. The influence of $b_{Q_{\text{loss}}}$ on the time constant can also be analytically determined, as shown in Sec. E.3.

An inverse response of the solid line is seen from Fig. 7.5. This is due to the addition of cold and solid AlF_3 and the immediate need for energy for heating and dissolution. The result is the freezing of Na_3AlF_6 , and a temporary increase in side ledge thickness.

In industrial cell lines it is often found conditions where increased excess AlF_3 corresponds to increased side ledge thickness. From Figs. 7.4 and 7.5 it can be concluded that these variations are caused by variations in the energy balance, which is a rather interesting result.

7.2 Validation against measurements using real input data

The simulation results shown in this section use the input data of AlF_3 addition shown in Fig. 7.8 and the energy input shown in Fig. 7.9. This latter input is calculated from (6.61).

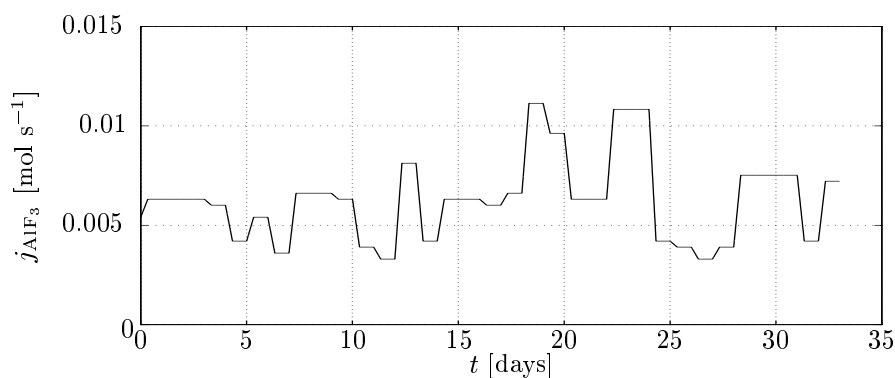


Figure 7.8: Registered AlF_3 input. Note that a rate of 0.005 mol s^{-1} is equivalent to 36 kg day^{-1} .

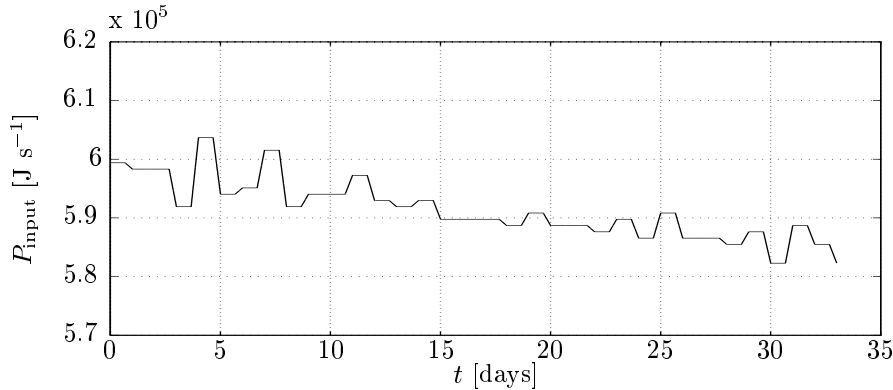


Figure 7.9: Calculated energy input to bath.

Both input variables are based on the average input every 8 hours and adjusted according to assumptions **(A.2)** and **(A.3)** in Sec. 6.1. The initial amount of bath in these simulations is 4400 kg. The registered Al_2O_3 additions are also used as model input (not shown).

As indicated in the previous section and in App. E, different heat loss models in the bath/surroundings upwards connection have a substantial impact on model behavior. In general, however, there are several other phenomena affecting the energy balance, e.g. the heat losses from bath to surroundings sideways and from bath to metal, as can be seen in Fig. 6.19. Nevertheless, from an intuitive comparison of the different heat losses, it is the convective heat flow in the bath/surroundings upwards connection represented as (6.66) that most likely represents the largest and fastest changes, and also is related to most uncertainty. The heat loss at anode changes discussed on page 123 is an example of such convective heat loss. As a result, the model validation in this section considers two different models for the heat loss from bath to surroundings upwards.

The validation is termed **Case 1** and consist of **Case 1a** where (6.66) with a value of $b_{Q_{\text{loss}}}$ as in Sec. 7.1, and **Case 1b** where a constant heat loss of 172 kJ s^{-1} is used. That is, $b_{Q_{\text{loss}}} = 0$, as in Sec. E.1. The resulting excess AlF_3 and bath temperature responses are shown in Figs. 7.10 and 7.11.

These simulations are typical candidates for the variety of results obtained from ballistic simulations¹ of the model. It should be noted that the number of moles of AlF_3 in the bath is the same for both simulations. The corresponding heat loss for the two cases is given in Fig. 7.12.

¹Here, ballistic simulation means simulation in open loop mode without state estimation.

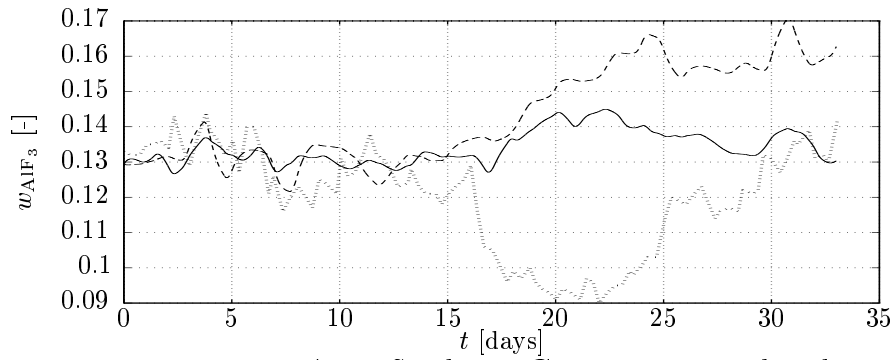


Figure 7.10: Excess AlF_3 . Solid line: **Case 1a**, varying heat loss. Dashed line: **Case 1b**, constant heat loss. Dotted line: Analyzed value.

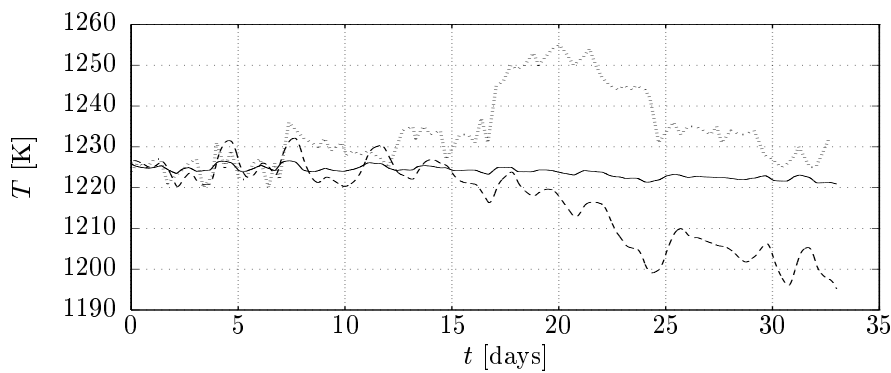


Figure 7.11: Bath temperature. Solid line: **Case 1a**, varying heat loss. Dashed line: **Case 1b**, constant heat loss. Dotted line: Measured value.

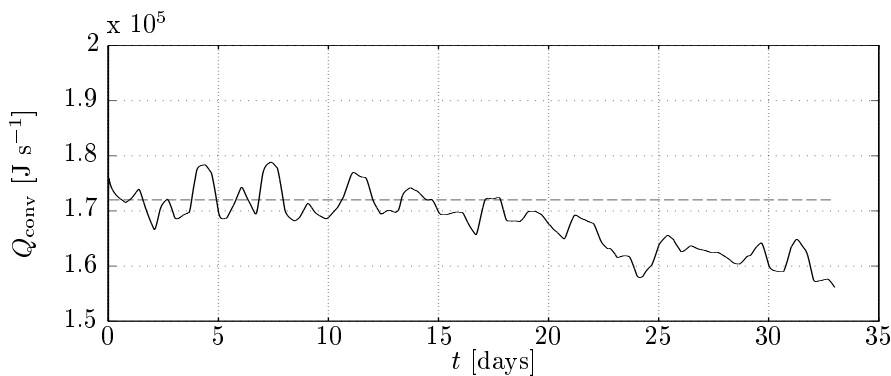


Figure 7.12: Heat loss from bath to surroundings upwards. Solid line: **Case 1a**, varying heat loss. Dashed line: **Case 1b**, constant heat loss.

The relationship for the heat loss used in **Case 1a**, i.e. $b_{Q_{\text{loss}}} \neq 0$, leads to a stabilizing effect in bath temperature, see Fig. 7.11. This can be verified by comparing the energy input, P_{input} , in Fig. 7.9 with the heat loss, Q_{conv} , in Fig. 7.12. The variations and trends in P_{input} are compensated by similar variations and trends in Q_{conv} , and hence, the net changes to the energy balance are small.

These simulations show that for the constant heat loss case, the temperature and excess AlF_3 show good conformity for the first 8 days. However, in the interval from 16 to 33 days it is revealed that there are dynamics that the model structure does not capture. One reason could be that the model structure shown in Figs. 6.18 and 6.19 is too simple. However, based on experience from more complex models, it is here believed that the chosen structure is well suited. Bearing in mind assumptions **(A.18)** and **(A.20)** from Sec. 6.4, the lack of conformity is most probably due to disturbances in the AlF_3 balance and/or disturbances in the energy balance. Hence, the next chapter focuses on explaining the lack of conformity in both excess AlF_3 and bath temperature by estimating *i*) possible AlF_3 disturbances and *ii*) possible energy disturbances.

Comment:

If the registered AlF_3 addition in Fig. 7.8 and the analyzed excess AlF_3 shown in Fig. 7.10 are isolated and studied, it supports the *impression* of a time delay as discussed in Sec. 1.1.2. There seems to be a 7 day delay from the first large addition of AlF_3 on day 18 to the analyzed response on day 25.

◇◇◇

Chapter 8

Estimation of equivalent AlF₃ and energy disturbances

Based on experience from the model validation in the previous chapter, the analyzed excess AlF₃ data shown in Fig. 7.10 are used to estimate possible AlF₃ disturbances through two different case studies. The result is presented in Sec. 8.1. The measured bath temperature data shown in Fig. 7.11 is used in Sec. 8.2 to estimate possible energy disturbances. Since the AlF₃ and the energy balance are exposed to several different disturbances, the estimated disturbances are the *equivalent* disturbances, i.e. the sources are not addressed, but rather the level of the disturbances. The estimations are performed over a period of 33 days. Sec. 8.3 discusses and compares the results from Secs. 8.1 and 8.2. Finally, the impact of current efficiency is studied in Sec. 8.4.

8.1 Estimating equivalent AlF₃ disturbance

The estimation presented in this section is termed **Case 2**, and is divided into **Case 2a** and **Case 2b**. **Case 2a** considers a temperature dependent heat loss from bath to surroundings upwards, i.e. $b_{Q_{\text{loss}}} \neq 0$ in (6.66), similar to **Case 1a**. In **Case 2b** this heat loss is kept constant at 172 kJ s⁻¹ ($b_{Q_{\text{loss}}} = 0$) similar to **Case 1b**. The estimated equivalent AlF₃ is based on the following relationship:

$$\Delta j_{\text{AlF}_3} = K_{\text{AlF}_3} (w_{\text{AlF}_3, \text{analyzed}} - w_{\text{AlF}_3, \text{simulated}}). \quad (8.1)$$

This is depicted in Fig. 8.1. Note that the disturbance is not placed on the input to the cell, but rather as an unknown disturbance. This implies that it might come from wrong scoop size in the input, from crust deformation or actually from the internal movements of AlF_3 between the sludge and the bath.

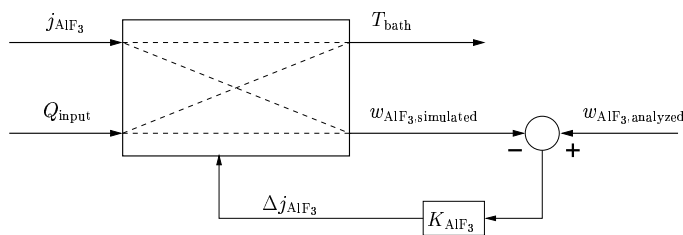


Figure 8.1: Illustration of the equivalent AlF_3 disturbance estimation.

The estimated equivalent AlF_3 disturbance is shown in Fig. 8.2. The curve has been low-pass filtered to emphasize the main variations. The registered AlF_3 input from Fig. 7.8 is included into the same figure. The AlF_3 evaporation described in the bath/surroundings connection on page 134, is held constant at an average rate corresponding to the average input rate of AlF_3 in Fig. 7.8. Note that the $w_{\text{AlF}_3,\text{simulated}}$ indicated in Fig. 8.1 will of course show very good conformity with the analyzed values for both **Case 2a** and **2b**. This is not shown here.

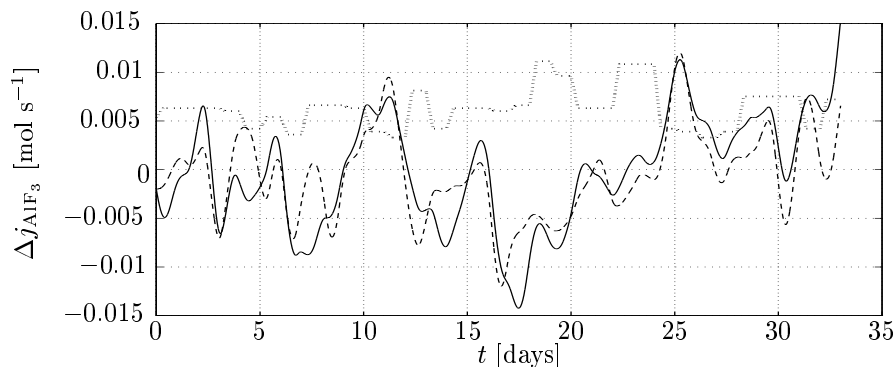


Figure 8.2: Estimated equivalent AlF_3 disturbance. Solid line: **Case 2a**, varying heat loss. Dashed line: **Case 2b**, constant heat loss. Dotted line: The registered input in Fig. 7.8.

The corresponding bath temperature responses are shown in Fig. 8.3. Note that the use of constant heat loss from bath to surroundings upwards, gives

a relatively good correspondence with measured temperature. In these estimations, positive values of Δj_{AlF_3} are regarded as solid AlF_3 additions, while negative values are regarded as AlF_3 evaporating from the bath.

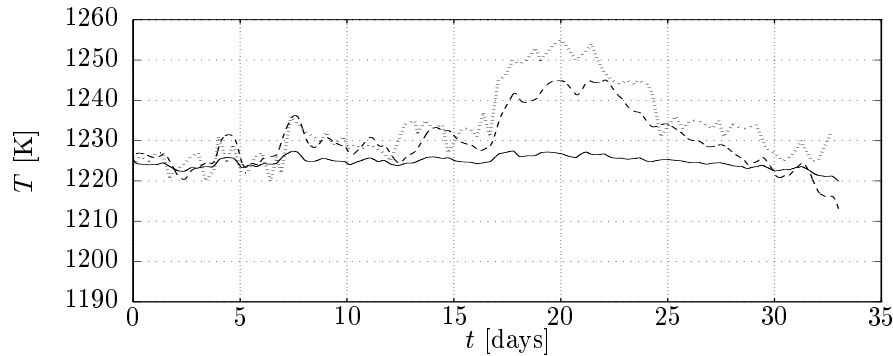


Figure 8.3: Bath temperature. Solid line: **Case 2a**, varying heat loss. Dashed line: **Case 2b**, constant heat loss. Dotted line: Measured value.

It is interesting to note that even if the estimated equivalent AlF_3 for **Case 2a** and **2b** shows similar variations, the bath temperature responses are very different. This is mainly due to the different models for the heat loss from bath to surroundings upwards used in these simulations. These convective heat losses are given in Fig. 8.4.

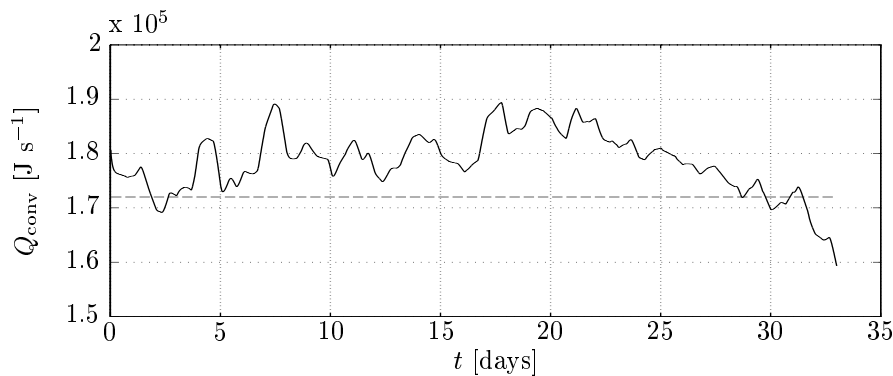


Figure 8.4: Heat loss from bath to surroundings upwards. Solid line: **Case 2a**, varying heat loss. Dashed line: **Case 2b**, constant heat loss.

In addition to the above simulation results, there are other variables of interest that reveal information about the cell state not shown in the bath

temperature and excess AlF_3 responses. Such variables are the number of moles of AlF_3 in the bath, superheat, side ledge thickness and mass fraction of CaF_2 . These are presented in Figs. 8.5 to 8.8.

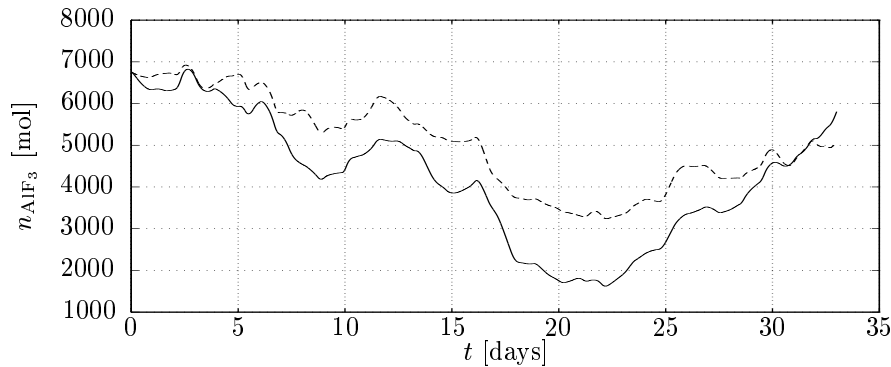


Figure 8.5: Number of moles of AlF_3 . Solid line: **Case 2a**, varying heat loss. Dashed line: **Case 2b**, constant heat loss.

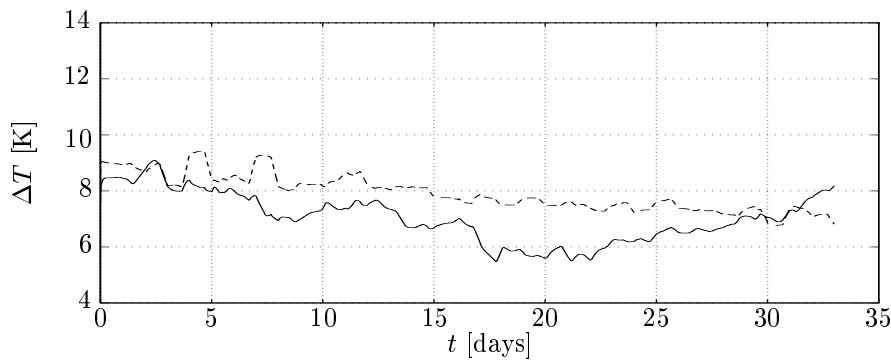


Figure 8.6: Calculated superheat. Solid line: **Case 2a**, varying heat loss. Dashed line: **Case 2b**, constant heat loss.

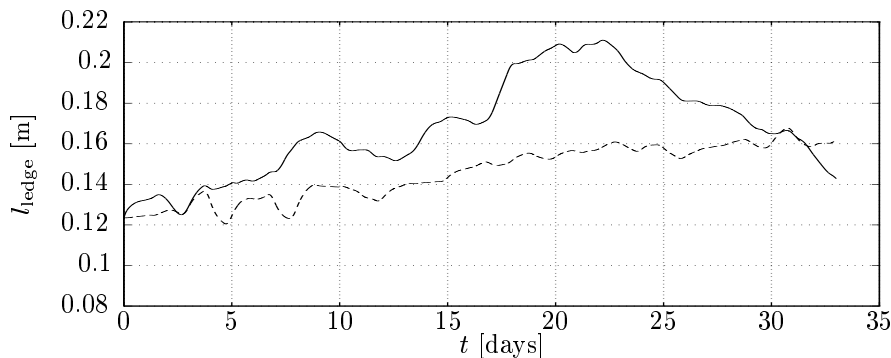


Figure 8.7: Side ledge thickness. Solid line: **Case 2a**, varying heat loss. Dashed line: **Case 2b**, constant heat loss.

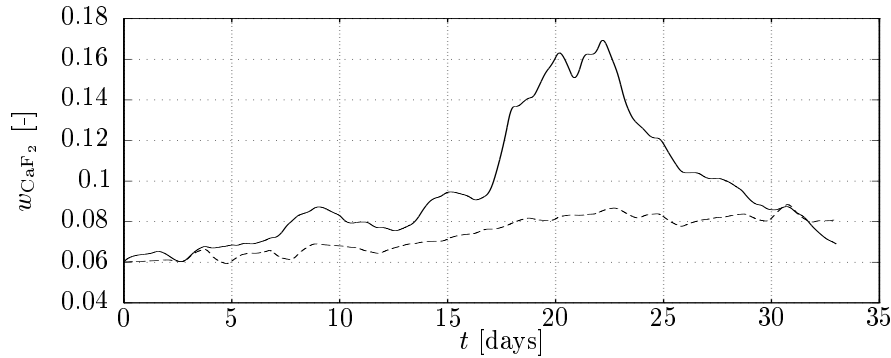


Figure 8.8: Mass fraction of CaF_2 . Solid line: **Case 2a**, varying heat loss. Dashed line: **Case 2b**, constant heat loss.

The superheat is calculated from bath temperature measurement and the calculated liquidus temperature from (6.13).

8.2 Estimating equivalent energy disturbance

The estimation presented here is termed **Case 3**. Since an estimation is made of energy disturbances, the heat flow from bath to surroundings upwards is held constant at 172 kJ s^{-1} similar to **Case 1b** and **Case 2b**. The estimated equivalent energy disturbance is based on the following relationship:

$$\Delta Q = K_Q (T_{\text{bath,measured}} - T_{\text{bath,simulated}}). \quad (8.2)$$

This is depicted in Fig. 8.9.

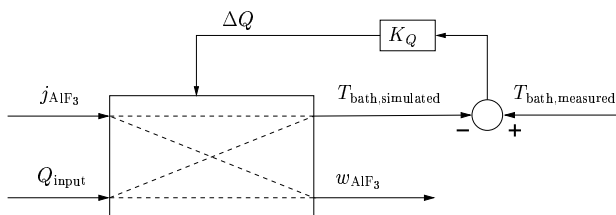


Figure 8.9: Illustration of equivalent energy disturbance estimation.

The estimated equivalent energy disturbance is shown in Fig. 8.10. The curve has been low-pass filtered to emphasize the main variations. If the

variations in Fig. 8.10 are assumed to be caused by variations in the heat loss from bath to surroundings upwards only, the magnitude of the variation is less than $\pm 10\%$ of the mean value. The bath temperature (not shown) shows very good conformity with measured values.

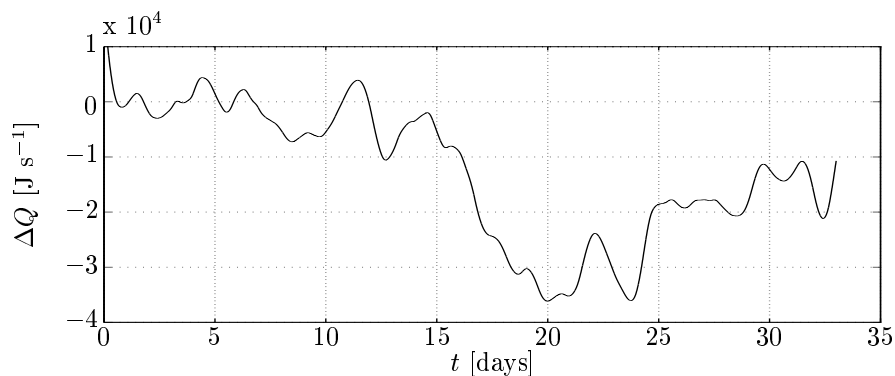


Figure 8.10: Estimated equivalent energy disturbance, **Case 3**.

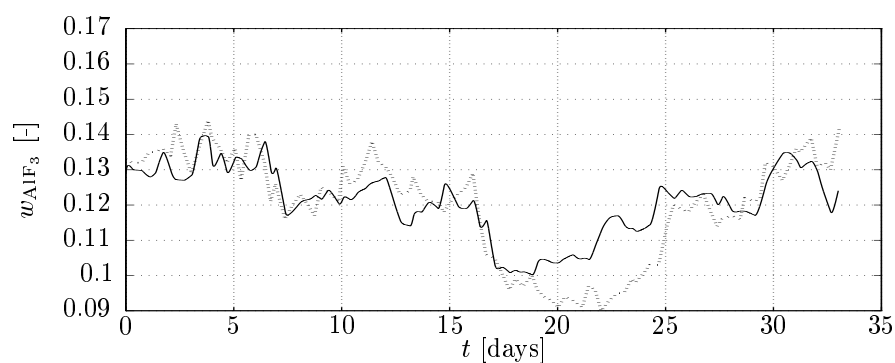


Figure 8.11: Excess AlF_3 . Solid line: **Case 3**. Dotted line: Analyzed value.

The corresponding excess AlF_3 response is given in Fig. 8.11, and it shows good conformity with the analyzed value. It should be noted, however, that the simulation result depends strongly on the initial amount of bath. More bath will diminish the excess AlF_3 variations caused by freezing and melting of Na_3AlF_6 and additions of AlF_3 will have less impact due to increased dilution.

The equivalent evaporation of AlF_3 is held constant equal to the average input rate as for **Case 2**. This is, however, not necessarily the best model, and it is believed that the fluoride evaporation is higher at high tempera-

tures. This would have improved the simulation result in Fig. 8.11 for the period between 17 and 25 days.

The number of moles of AlF_3 in the bath, the superheat, the side ledge thickness and the mass fraction of CaF_2 are shown in Figs. 8.12 to 8.15.

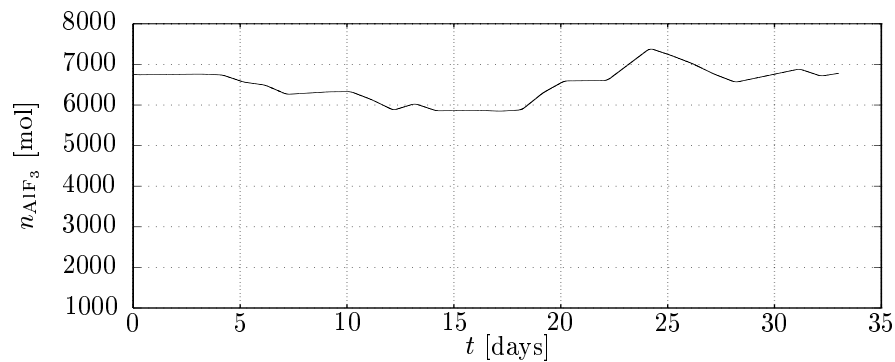


Figure 8.12: Number of moles of AlF_3 , **Case 3**.

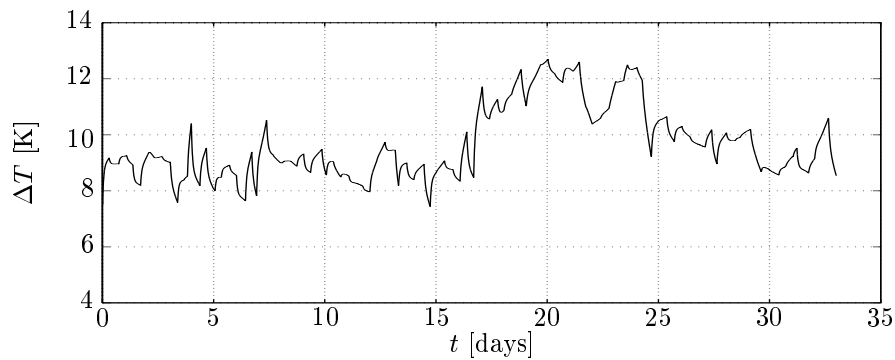


Figure 8.13: Calculated superheat, **Case 3**.

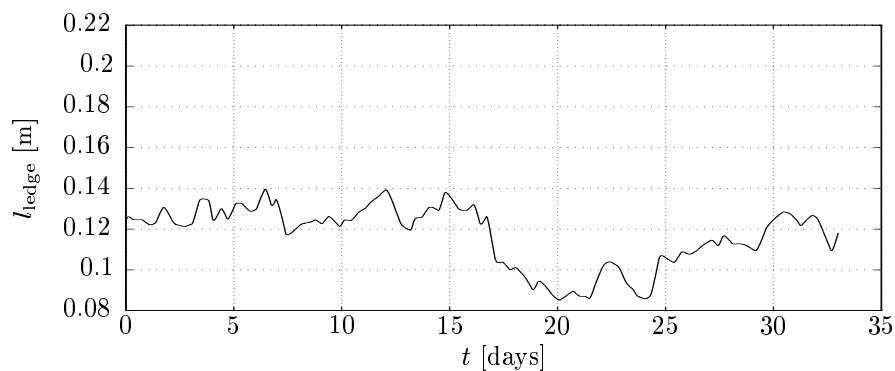


Figure 8.14: Side ledge thickness, **Case 3**.

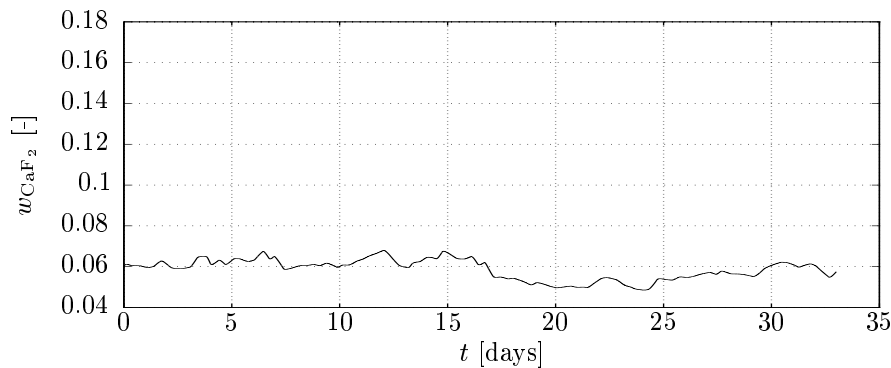


Figure 8.15: Mass fraction of CaF_2 , **Case 3**.

8.3 Discussion of estimation results

In discussing the results presented above, it is important to be aware of the assumptions made during the model development phase, and have these in mind when comparing and interpreting the results.

Due to the rather good conformity of both bath temperature and excess AlF_3 in **Case 2b** and in **Case 3**, respectively, the other cell variables have to be used in order to determine which estimated disturbance that is most likely to explain the observed cell behavior. These cell variables are verified against knowledge about how the cell behaves. For this data set, the period between day 17 and day 25 should be applicable to use as verification due to large variations in temperature and excess AlF_3 .

Generally, the mass fraction of CaF_2 is expected to vary by a fraction of ± 0.005 or less. In addition, the side ledge is believed to melt at increased temperatures, and hence, result in reduced side ledge thickness. This is due to increased superheat. By comparing the results from **Case 2** and **Case 3** with the expected behavior of these three variables (w_{CaF_2} , l_{ledge} and ΔT), **Case 3** seems to give more reasonable results than **Case 2b**. Consequently, the results obtained from **Case 2a** can be discarded.

If the actual estimated disturbances in Figs. 8.2 and 8.10 are used as means to compare the case studies, **Case 2b** shows that the model reacts with a very high loss of AlF_3 to explain the increased temperature at 17 days. Possible explanations of the large variations in estimated equivalent AlF_3 disturbance are the varying content of fluoride and sodium in the secondary alumina from the dry scrubbing process, wrong scoop size used in the model, AlF_3 rich crust falling into the bath, or variations in the rate of

sodium penetration into the cathode. Due to the size of the variations, it is, however, not likely that these factors can explain the overall disturbances alone. On the other hand, if a sludge phase of AlF_3 is believed to have a large impact on the cell behavior, parts of the estimated disturbances could indirectly visualize the internal flow of AlF_3 between the bath and the sludge. Another phenomenon that possibly has a significant influence on the excess AlF_3 is the interaction between the acidic crust and the bath. It is, however, difficult to find suitable relationships for this interaction that is applicable in dynamic models of the kind developed in this thesis.

For **Case 3**, the corresponding explanation in Fig. 8.10 to the increased temperature at 17 days, is a drop in the energy disturbance of approximately 30 kJ s^{-1} . The variation in the estimated energy disturbance is $\pm 20 \text{ kJ s}^{-1}$. Possible explanations are varying crust thickness, varying current efficiency and cell operations. Assuming that the variations are caused by changes in current efficiency only, the variation would be $\Delta\mathcal{E} = \pm 8 \%$ for a 160 kA cell. This is, of course, too large variation for one specific cell. Nevertheless, in the period between days 15 and 25, the conditions are poor for high current efficiencies, and this could explain a significant part of the variations found in Fig. 8.10. This is further investigated in Sec. 8.4.

Note that for **Case 2b** the amount of AlF_3 in the bath is reduced to half of the initial amount during the simulation. **Case 3** and Fig. 8.12, on the other hand, show that even if the amount of AlF_3 has small variations, the simulated excess AlF_3 shows good conformity in Fig. 8.11. This is mostly due to freezing and melting of side ledge as shown in Fig. 8.14.

To summarize this section, energy disturbance seems the most likely explanation to the behavior that is experienced. In order to investigate this further, the next section focuses on the impact of current efficiency variations.

8.4 The impact of current efficiency

Based on the discussion above, this section considers how to explain the estimated energy disturbance in Fig. 8.10 with special attention given to current efficiency variations. In the literature, various current efficiency models are presented (Stevens *et al.* 1992), (Solli 1993), (Grjotheim and Kvande 1993), (Solli *et al.* 1994). The models are often related to bath composition, bath temperature, current density, anode-cathode-distance, solubility of aluminum in bath, viscosity, velocity of bath and metal and other physical properties. On the other hand, several of these models are obtained from laboratory cell experiments, and are thus, not believed to

be directly applicable for industrial cells. This is because laboratory cell experiments are performed during approximate ideal conditions whereas the conditions in industrial cells are always changing and are affected by cell operation and disturbances.

It is found that increased bath temperature increases the solubility of liquid aluminum in the bath, and hence, increasing the back reaction (Grjotheim and Kvande 1993). Similarly, it is found that a low level of excess AlF_3 has a negative impact on the current efficiency. This implies that in the period between days 15 and 25, the conditions are poor for high current efficiencies. Since the only measurements are the cell resistance, excess AlF_3 and bath temperature, these measurements are used to gain some insight into the current efficiency for the period of data. For this purpose, consider the relationship in (6.14) from page 122:

$$\mathcal{CE} = f(T_{\text{bath}}, w_{\text{AlF}_3}). \quad (6.14)$$

This equation will give an a posteriori estimate of the current efficiency. Since the estimated energy disturbance in Fig. 8.10 is assumed to represent changes in current efficiency, $\Delta\mathcal{CE}$, it is possible to transform ΔQ into $\Delta\mathcal{CE}$ using the following relationship:

$$\Delta\mathcal{CE} = \frac{\Delta Q}{a_{\mathcal{CE}}}. \quad (8.3)$$

Here $a_{\mathcal{CE}}$ represents the energy gained by the bath for a fraction of 0.01 loss in current efficiency. The \mathcal{CE} from (6.14) and the $\Delta\mathcal{CE}$ from (8.3) are shown Fig. 8.16.

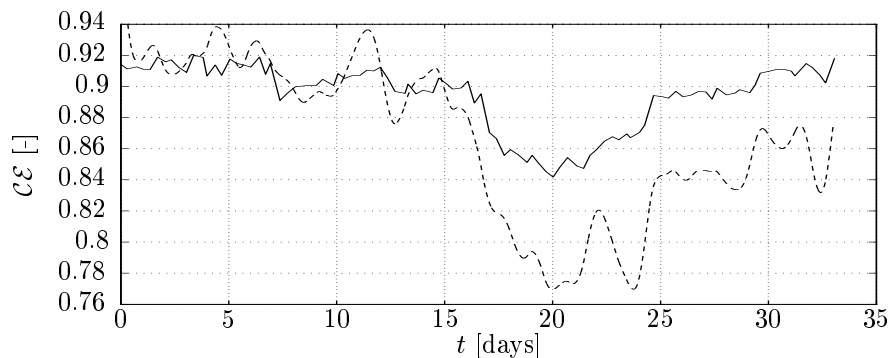


Figure 8.16: Solid line: A posteriori calculation of current efficiency using (6.14). Dashed line: Current efficiency corresponding to (8.3), adjusted 0.92, i.e. $\Delta\mathcal{CE} + 0.92$.

Note that $\Delta C\mathcal{E}$ is adjusted with an offset of 0.92 in order to fit the curves in the same scale area. It can be seen that there is good correspondence up to 17 days, where the current efficiency corresponding to the energy disturbance drops more than the current efficiency based on measurements.

These two current efficiencies are employed in two different ballistic simulations. The excess AlF_3 and bath temperature responses are shown in Figs. 8.17 and 8.18, respectively. It should be emphasized that the heat loss from bath to surroundings upwards is constant during these simulations.

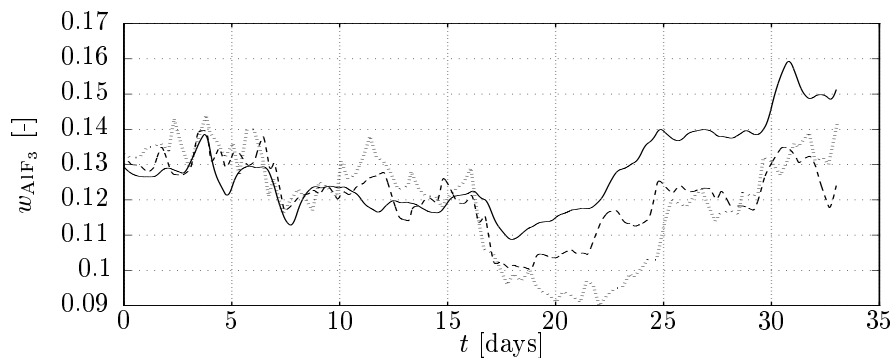


Figure 8.17: Excess AlF_3 . Solid line: Simulation using current efficiency based on (6.14). Dashed line: Simulation using current efficiency based on (8.3), adjusted 0.92. Dotted line: Analyzed value.

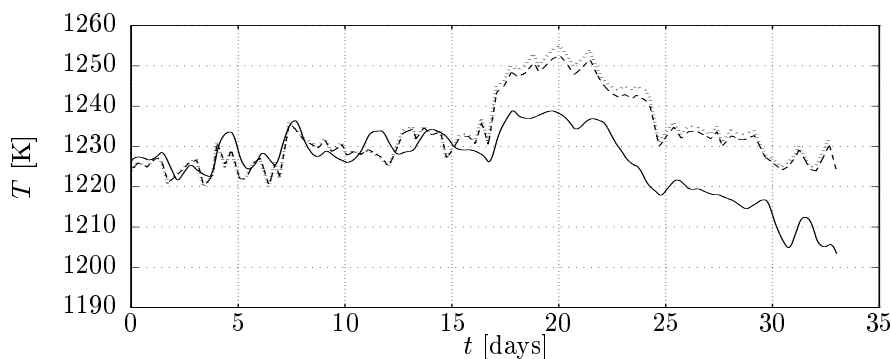


Figure 8.18: Bath temperature. Solid line: Simulation using current efficiency based on (6.14). Dashed line: Simulation using current efficiency based on (8.3), adjusted 0.92. Dotted line: Measured value.

8.5 Discussion and concluding remarks

The result with respect to bath temperature when using $\Delta\mathcal{CE}+0.92$ (dashed line) is of course good. This is due to the fact that $\Delta\mathcal{CE}$ was calculated from ΔQ in (8.3) which again was estimated from (8.2). Furthermore, the simulation based on (6.14) (solid line) shows that even if there are offsets, the trends show similarities. Consequently, if it is assumed that (6.14) is a well suited model for a posteriori estimation of current efficiency based on *measurements*, the results shown in Figs. 8.17 and 8.18 suggest that the current efficiency might be a dominating energy disturbance.

An interesting aspect of the current efficiency is the natural positive feedback from the back reaction to the temperature. The higher bath temperature, the more the aluminum back reacts, resulting in further temperature increase. This implies that if the expression in (6.14) is used in a ballistic simulation, the simulation result will be very sensitive to model inaccuracies and disturbances in the energy and AlF_3 balances. This is verified through several simulation studies, and was the main reason for assumption **(A.18)**. Due to this inherent unstable mechanism, this supports the hypothesis here that it is probably impossible to develop a model that accurately predicts the long-term bath temperature and excess AlF_3 variations when the current efficiency model is only based on bath composition and temperature. It is believed that a current efficiency model must comprise some physical quantities such as the anode-cathode-distance or the size of the side channels. However, even if such models exist in the literature, the positive feedback is not resolved, and these models are still subjected to various disturbances. Hence, the usefulness of these expressions in a long-term prediction model may be limited.

To conclude, there are at least three results to emphasize from this chapter. First, it is hypothesized that energy disturbances dominate over AlF_3 disturbances. Second, variations in current efficiency seems to be the dominating energy disturbance. These results are used to suggest a control strategy in Ch. 9. Third, due to the inherent positive feedback between current efficiency and bath temperature, it is hypothesized that long-term prediction of excess AlF_3 and bath temperature is probably impossible with a current efficiency model using only bath composition and temperature.

Chapter 9

A novel control strategy

The results summarized and discussed in the previous chapters are of vital importance to the control of excess AlF_3 and bath temperature of an electrolysis cell. To this author's knowledge, all control strategies implemented in industry use AlF_3 addition as the main control variable to keep the excess AlF_3 and temperature close to target values (see for instance Entner (1992) and Wilson (1992)). Adjustments of the energy input, or the reference resistance, are mainly used to manipulate the energy balance such that the bath temperature on average is within acceptable values when the average excess AlF_3 is close to a predefined value.

This common control strategy seems intuitively appealing since AlF_3 additions are used to increase the excess AlF_3 and frequent adjustments of the anode beam are avoided. Large and frequent anode beam adjustments result in crust deformation, and consequently disturbances in both mass and energy balances, and are traditionally considered to result in poor cell performance. On the other hand, these disturbances are small compared to the estimated AlF_3 and energy disturbances shown in Figs. 8.2 and 8.10.

9.1 Possible explanations of the observed cell behavior

From Fig. 8.2 it can be concluded that large AlF_3 additions should be avoided even when the excess AlF_3 is low. The reason is that the total amount of AlF_3 in the cell does not change substantially from one day to the next. This means that a lack of AlF_3 is not the main reason why the excess AlF_3 in some cases suddenly decreases. If large amounts of AlF_3 are added to compensate for this sudden decrease, the excess AlF_3 will attain

very high values when the underlying cause of the excess AlF_3 reduction is resolved.

Results presented in this thesis demonstrate that disturbances in the energy balance are the main reason for variations in excess AlF_3 and bath temperature. Using this as the basic hypothesis, the following discussion illustrates why there seems to be a time-lag between AlF_3 additions and corresponding responses in the excess AlF_3 , and why extensive use of AlF_3 additions to reduce the variations will reinforce long-term variations. The time constants of the dominating variations are in the order of days. When the excess AlF_3 decreases due to a disturbance in the energy balance, increased AlF_3 additions will initially just compensate for the negative trend and will not result in increased excess AlF_3 . Very large amounts of AlF_3 will, however, result in higher excess AlF_3 values. But the full effect of the additions will become apparent when the energy disturbance is resolved. Then the excess AlF_3 will become too high, and actions are needed to reduce it. Due to variations in the side ledge thickness and continuous disturbances in the energy balance, it is not straightforward to obtain the desired excess AlF_3 and at the same time make sure that the AlF_3 additions on average equal the mean AlF_3 consumption, i.e. evaporation and sodium penetration in the cathode. Consequently oscillations will occur.

A result of the work presented in this thesis is that the multivariable nature of the aluminum cell illustrated in Fig. 5.12 could be slightly changed into Fig. 9.1.

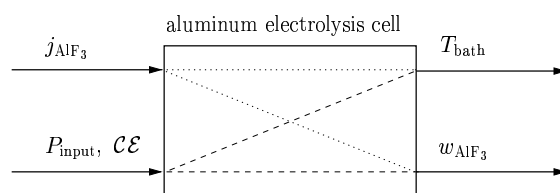


Figure 9.1: The multivariable nature of an aluminum cell, revisited.

Note that this is only a *qualitative* approach, where dotted lines imply less influence than dashed lines.

9.2 Brief description of the proposed control strategy

The obtained results demonstrate that optimal control of the excess AlF_3 and the bath temperature is obtained by an almost constant AlF_3 input

9.3 Possible consequences of the proposed control strategy 173

and energy input manipulations to compensate for the variations. Optimal control means that this is the control strategy that minimizes bath temperature and excess AlF_3 variations. Some adjustments of the AlF_3 input based on integral action, is of course needed to compensate for the cell aging, evaporation and changes in the alumina quality. The AlF_3 input adjustments should be based on a simple mass balance to make sure that the average addition is close to the average consumption and thereby avoids the long-term variations. In addition, AlF_3 may be used to treat non-conformities such as *very* high bath temperatures. Then, *operational consistency* is of vital importance to reduce the variations that usually will result when the non-conformity is resolved. Operational consistency is important because of the large time constants and the number of people involved.

In many cell lines the energy input is squeezed to a minimum. A further reduction of the reference resistance, or the anode-cathode distance, may result in reduced current efficiency. As a result, the net energy input to the energy balance will increase. Consequently, only elevation of the reference resistance is used in present control schemes. On the other hand, active use of both positive and negative changes in the reference resistance requires that the reference resistance can be decreased without resulting in an increased energy input on average. It is therefore suggested that the reference resistance is increased, if needed, to allow for temporary reductions in the energy input to compensate for high bath temperature and low excess AlF_3 . This approach introduces an additional degree of freedom that is not used in present controllers. An additional or alternative approach for manipulating the energy balance directly is to use the crust thickness as a control variable. By careful covering, monitoring and maintenance of the crust, the long-term variations can be controlled. However, this is not as powerful and immediate as anode beam movements.

To summarize, AlF_3 additions should be used when the temperature is within the normal range and the excess AlF_3 is low. Moreover, positive and negative energy manipulations should be used when *both* temperature and excess AlF_3 are outside target values.

9.3 Possible consequences of the proposed control strategy

The proposed control strategy has an impact on both energy and mass consumption. Even if the mean reference resistance is suggested to be kept above the minimum in order to introduce an additional degree of freedom

in the controller, it is important to note that energy savings can still be obtained. Many smelters operate with positive and negative effect pulses as part of the control strategy. Hence, the *average* energy input in these control schemes is larger than the lowest set point. Keeping the reference resistance suggested in this thesis lower than this *average* value will reduce the energy consumption.

If stable cell conditions can be achieved, it is advantageous for the current efficiency. The effects of improved current efficiency are increased economic turnover, reduced energy consumption and hence, less energy is available to lose as heat. This latter effect, which is necessary to maintain the energy balance of the cell, could be compensated by increased current through the cell or increased anode-cathode distance. This again improves the proposed control strategy.

Other profitable side effects of stable cell conditions are prolonging the cell life and the reduced need for expensive AlF_3 and Na_2CO_3 additions used to reach target values for excess AlF_3 .

9.4 Superheat as a parameter for control

Laboratory experiments indicate that superheat has a large impact on Al_2O_3 dissolution (Kobbeltvedt 1997). Assuming that superheat also affects the dissolution of AlF_3 , it is interesting to investigate how the superheat changes during normal operation, i.e. at irregular overfeeding and underfeeding of Al_2O_3 . For the Al_2O_3 input shown in Fig. 9.2, the period for the overfeeding and underfeeding is 3 hours. 3 hours is of course an extreme value, but it is used to illustrate the dynamics.

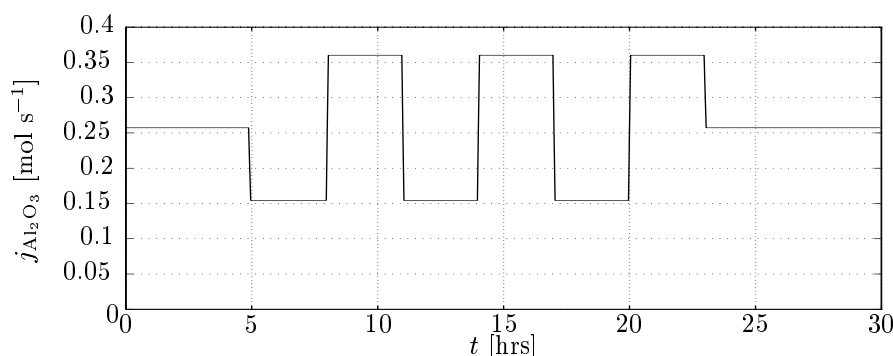


Figure 9.2: Al_2O_3 addition during normal operation. Note that a rate of 0.1 mol s^{-1} is equivalent to 880 kg day^{-1} .

The results obtained here are, similar to the result in Ch. 7, dependent on the heat loss from the bath to the surroundings upwards given in (6.66). To illustrate this, two simulations are performed, using *i*) $b_{Q_{\text{loss}}} = 0$ and *ii*) $b_{Q_{\text{loss}}} \neq 0$, as in Secs. E.1 and E.2. The response in superheat is presented in Fig. 9.3. Note that these simulations do not include a sludge phase for Al_2O_3 . The actual heat loss from bath to the surroundings upwards is shown in Fig. 9.4.

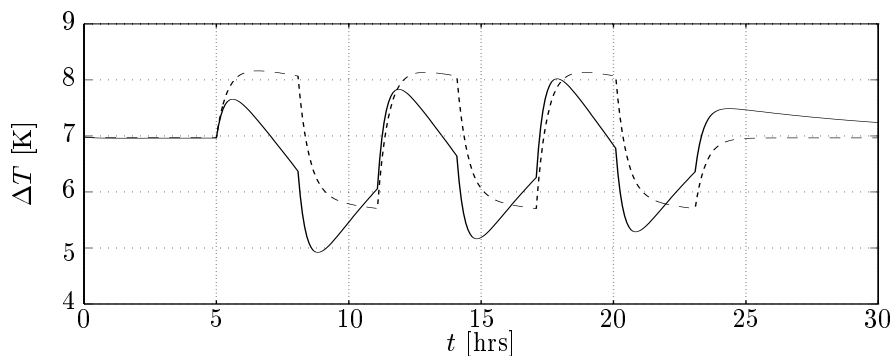


Figure 9.3: Superheat during normal operation. Solid line: Temperature dependent heat loss, $b_{Q_{\text{loss}}} \neq 0$. Dashed line: Constant heat loss, $b_{Q_{\text{loss}}} = 0$.

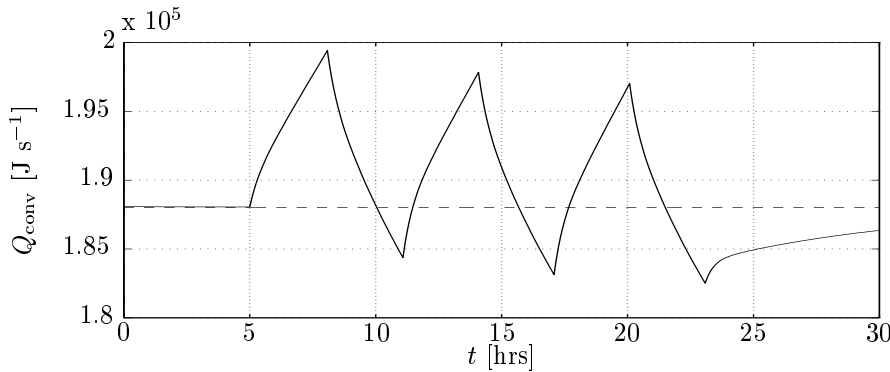


Figure 9.4: Heat loss from bath to surroundings upwards during normal operation. Solid line: Temperature dependent heat loss, $b_{Q_{\text{loss}}} \neq 0$. Dashed line: Constant heat loss, $b_{Q_{\text{loss}}} = 0$.

It can be seen that the superheat has a maximum early in the underfeeding period in both simulations. This is important to take into account if the AlF_3 feeding strategy should consider the alumina feeding which is always changing. The cause of the behavior when $b_{Q_{\text{loss}}} \neq 0$, is that the liquidus

temperature increases faster than the bath temperature during the underfeeding periods. This is also verified from the industrial data plotted in Figs. 9.5 and 9.6. The superheat in Fig. 9.6 is calculated from filtered bath temperature measurement and the calculated liquidus temperature from (6.13).

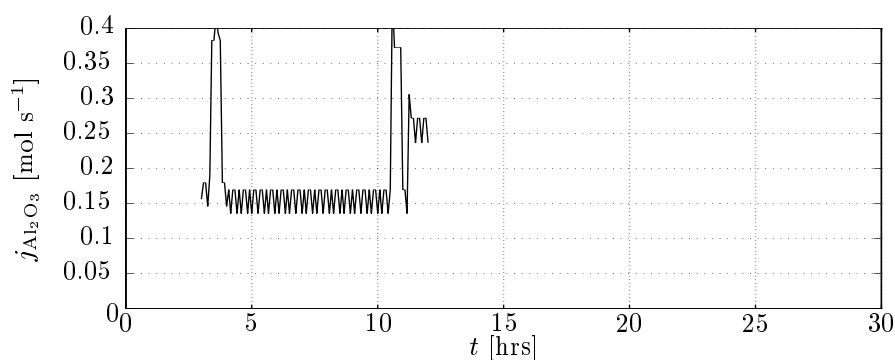


Figure 9.5: Registered Al_2O_3 addition.

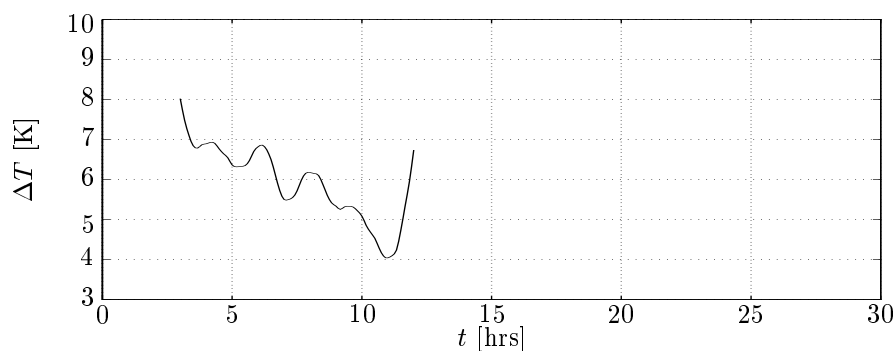


Figure 9.6: Superheat based on bath temperature measurement and liquidus temperature calculation.

It can be seen that during an underfeeding period of 6 hours, the superheat has a drop of 3 K. The energy input, P_{input} , was relatively stable in this period.

To conclude, the results presented in this section imply that if superheat is believed to be important for industrial cells when it comes to AlF_3 additions, these additions should be made at the beginning of, or at least, during an underfeeding period.

Chapter 10

Conclusions and suggestions for future work

10.1 Conclusions

10.1.1 Modeling methodology

This thesis has defined a graphical representation scheme focusing on physical phenomena of chemical unit processes. A prototype implementation is developed in Simulink, and is used for model development. Due to the modularization principle on which the representation is based, the methodology has proven to be efficient for model building and enhancement. This is a valuable property in validating different model hypotheses. Model assumptions are included both prior to and after the modularization. The a priori assumptions are implicitly represented, whereas the a posteriori assumptions are explicitly represented onto the process representation.

The primary application area is model development of complex, non-standard unit operations. Hence, it is not a tool for plant modeling using predefined model parts of more or less well understood unit operations. Models developed using the concepts presented in this thesis could, however, be incorporated into a plant modeling library at a later stage.

10.1.2 AlF_3 and bath temperature dynamics

Data analyses and dynamic simulations have shown that unknown dynamics or disturbances in the energy balance are the main sources of the rather large variations in excess AlF_3 and bath temperature which are present in

most cell lines in industry. In addition, it is found that the energy disturbances to a large extent can be explained by changes in current efficiency. It is hypothesized here that the use of a current efficiency model considering only bath composition and temperature is not sufficient for long-term prediction of bath temperature and excess AlF_3 . This is due to the inherent positive feedback from the back reaction to the bath temperature.

The obtained results demonstrate that optimal control of the excess AlF_3 and the bath temperature is obtained by almost constant AlF_3 input and energy input manipulations to compensate for the variations. The AlF_3 input adjustments needed to obtain excess AlF_3 close to the target value on average should be based on a simple mass balance to make sure that the average addition is close to the average consumption without introducing long-term variations in the excess AlF_3 .

The presented results are based on a rather simple dynamic model and a limited number of data sets from industrial cells. Nevertheless, the simulations summarize results and experience obtained through extensive simulations of various models based on different model assumptions.

10.2 Suggestions for future work

10.2.1 Implementation of the modeling methodology

The limitations of Simulink calls for an alternative implementation platform. A possible environment is Visual C++, since the method is well suited to fit into an object-oriented environment. In order to be useful as a general modeling tool for complex unit processes, the modeling methodology must include support for handling different model assumptions, model equation manipulation and documentation.

10.2.2 Decision support system

One of the major obstacles for stable control in the metal processing industries is the lack of knowledge regarding the *state* of cells and furnaces. Here, the phrase *state* means an overall evaluation of the cell state. Sudden changes are experienced, resulting in unstable conditions and reducing the turnover. For this reason, there is a large economic potential in improving existing technology with respect to cell control. However, one reason why this is difficult to achieve is that operators are an important and necessary part of the feedback loop. The knowledge operators possess is difficult to formalize, and operators may react differently to the same incidents. This

is partially due to differences in experience, education and more human related subjects. Hence, there is certainly a need for a support system which can assist operators in performing more uniform corrective action for various incidents. Such a support system could be based on an extension of the ideas presented in this thesis, through the use of modular models where new knowledge is easily incorporated.

References

- Balchen, J. G. (1992). A method for the control of alumina concentration in aluminium reduction cells. *Modelling, Identification and Control* **13**(1), 41–49.
- Berge, I. and R. Huglen (1994). Measurement and characterisation of fluorocarbon emissions from alumina reduction cells. *Light Metals 1994*, pp. 389–392.
- Bird, R. B., W. E. Stewart and E. N. Lightfoot (1960). *Transport phenomena*. John Wiley & Sons. Singapore.
- Bogusch, R. and W. Marquardt (1995). A formal representation of process model equations. *Comput. chem. Engng.* **19**, Suppl., S211–S216.
- Borg, P., T. Moen and J. Aalbu (1986). Adaptive control of alumina reduction cells with point feeders. *Modelling, Identification and Control* **7**(1), 45–56.
- Brandes, E. A. (Ed.) (1983). *Smithells Metals Reference Book*. 6 ed. Butterworths & Co.
- Chase, M. W., C. A. Davies, J. R. Downey, D. J. Frurip, R. A. McDonald and A. N. Syverud (1985). *JANAF Thermochemical Tables*. 3 ed. The American Chemical Society and the American Institute of Physics for the National Bureau of Standards.
- Cox, J. D. (1982). Notation for states and processes, significance of the word *standard* in chemical thermodynamics, and remarks on commonly tabulated forms of thermodynamic functions. *Pure & Appl. Chem.* **54**(6), 1239–1250. App. IV. to Manual of symbols and terminology for physicochemical quantities and units.
- Desclaux, P. (1987). AlF₃ additions based on bath temperature measurements. *Light Metals 1987*, pp. 309–313.
- Dieterich, E. E. and G. Eigenberger (1995). Bimap - a tool for computer aided modeling in chemical reaction engineering. *Comput. chem. Engng.* **19**, Suppl., S773–S778.

- Drengstig, T. and B. A. Foss (1995). Modularization applied to an aluminum electrolysis cell. In: *Literature for the 6th Nordic Process Control Workshop*. Mariehamn, Åland. pp. 13–19.
- Drengstig, T., D. Ljungquist and B. A. Foss (1997a). Long-term prediction of the AlF_3 and temperature dynamics of an aluminum electrolysis cell. In: *Proc. of The Ninth International Symposium on Light Metals Production*. Tromsø – Trondheim, Norway. pp. 103–117.
- Drengstig, T., D. Ljungquist and B. A. Foss (1997b). On the AlF_3 and temperature control of an aluminum electrolysis cell. *Submitted to IEEE Trans. on Control Systems Technology*.
- Drengstig, T., D. Ljungquist and B. A. Foss (1997c). A study on the AlF_3 and temperature dynamics of an aluminum electrolysis cell. In: *Literature for the 7th Nordic Process Control Workshop*. Wadahl, Norway. pp. 276–284.
- Drengstig, T., S. O. Wasbø and B. A. Foss (1996). A formal graphical based process modeling methodology. Technical Report 96-41-W. Department of Engineering Cybernetics, Norwegian University of Science and Technology (NTNU). Trondheim, Norway.
- Drengstig, T., S. O. Wasbø and B. A. Foss (1997d). A formal graphical based process modeling methodology. *Comput. chem. Engng.* **21**, Suppl., S835–S840. Based on Technical Report # 96-41-W.
- Eggen, T., S. Rolseth, K. Å. Rye and J. Thonstad (1992). Alumina crusting in cryolitic melts. Part I: Penetration of molten electrolyte into alumina. *Light Metals 1992*, pp. 495–502.
- Eikaas, T. I. (1990). Cadas - a system for computer aided design, analysis and synthesis of industrial processes. In: *Nordic CACE Symposium*. Lyngby, Denmark.
- Elmqvist, H., F. E. Cellier and M. Otter (1993). Object-oriented modeling of hybrid systems. In: *ESS'93, European Simulation Symposium*. Delft, The Netherlands.
- Entner, P. M. (1992). Control of AlF_3 concentration. *Light Metals 1992*, pp. 369–374.
- Entner, P. M. (1993). Further development of the AlF_3 -model. *Light Metals 1993*, pp. 265–268.
- Entner, P. M. (1995). Control of bath temperature. *Light Metals 1995*, pp. 227–230.
- Entner, P. M. and G. A. Gudmundsson (1996). Further development of the temperature model. *Light Metals 1996*, pp. 445–449.

- Felder, R. M. and R. W. Rousseau (1986). *Elementary principles of chemical processes*. 2 ed. John Wiley & Sons. Singapore.
- Foosnæs, T., V. Hjelle and M. Karlsen (1993). Continuous monitoring of gaseous fluoride emission. *Light Metals 1993*, pp. 407–411.
- Foss, B. A., B. Lohmann and W. Marquardt (1997). A field study of the industrial modeling process. In: *Preprints of IFAC Symp. on Advanced Control of Chemical Processes (ADCHEM'97)*. Banff, Canada. pp. 571–586.
- Gerstlauer, A., M. Hierlemann and W. Marquardt (1993). On the representation of balance equations in a knowledge-based process modeling tool. In: *CHISA'93*. Prague, Czech Republic. pp. 1–14.
- Gran, E. (1980). Multivariable control in aluminium reduction cells. *Modelling, Identification and Control* **1**(4), 247–258.
- Grjotheim, K. and B. J. Welch (1988). *Aluminium Smelter Technology – A Pure and Applied Approach*. 2 ed. Aluminium-Verlag. Düsseldorf, Germany.
- Grjotheim, K. and Kvande, H. (Eds.) (1993). *Introduction to aluminium electrolysis – Understanding the Hall-Héroult Process*. 2 ed. Aluminium-Verlag. Düsseldorf, Germany.
- Grjotheim, K., C. Krohn, M. Malinovský, K. Matiašovský and J. Thonstad (1982). *Aluminium Electrolysis*. 2 ed. Aluminium-Verlag. Düsseldorf, Germany.
- Gundersen, Ø. (1997). Topics in Carbon Modelling with Application to Carbon Anode Baking. Dr. ing. thesis. Department of Engineering Cybernetics, Norwegian University of Science and Technology (NTNU). Trondheim, Norway.
- Hangos, K. M. and I. T. Cameron (1997). The formal representation of process system modelling assumptions and their implications. *Comput. chem. Engng.* **21**, Suppl., S823–S828.
- Haupin, W. (1992). The liquidus enigma. *Light Metals 1992*, pp. 477–480.
- Haupin, W. and H. Kvande (1993). Mathematical model of fluoride evolution from Hall-Héroult cells. *Light Metals 1993*, pp. 257–263.
- Haupin, W. E. (1989). Electrode reactions in Hall-Héroult cells. In: *8th International Course on the Process Metallurgy of Aluminium*. Department of Inorganic Chemistry, Norwegian Institute of Technology (NTH). Trondheim, Norway. pp. 4.16–4.38.

- Holm, J. L. (1971). Thermodynamic properties of molten cryolite and other fluoride mixtures. Dr. ing. thesis. Department of Inorganic Chemistry, Norwegian Institute of Technology (NTH). Trondheim, Norway.
- Jensen, A. K. and R. Gani (1996). A computer aided system for generation of problem specific process models. *Comput. chem. Engng.* **20**, Suppl., S145–S150.
- Johansen, F. (1993). Kvalitetskontroll av fluorinnhold i oksidmating til aluminium elektrolysen. En systemteknisk analyse. Technical report. Department of Thermal Energy, Norwegian Institute of Technology (NTH). Trondheim, Norway. In Norwegian.
- Kobbeltvedt, Ove (1997). Dissolution kinetics for alumina in cryolite melts. Distribution of alumina in the electrolyte of industrial aluminium cells. Dr. ing. thesis. Department of Electrochemistry, Norwegian University of Science and Technology (NTNU). Trondheim, Norway.
- Kvande, H. (1991). Energy consumption in alumina reduction cells. *Light Metals 1991*, pp. 421–426.
- Kvande, H., J. Chen and W. E. Haupin (1994). Minimising energy consumption through optimizing alumina concentration in the bath of Hall-Hèroult cells. *Light Metals 1994*, pp. 429–440.
- Leitch, R. (1992). Knowledge based control: Selecting the right tool for the job. In: *Proc. of IFAC/IFMP/IMACS International Symposium on Artificial Intelligence in Real-Time Control*. pp. 25–33.
- Liu, X., M. P. Taylor and S. F. George (1992). Crust formation and deterioration in industrial cells. *Light Metals 1992*, pp. 489–494.
- Lohmann, B. and W. Marquardt (1996). On the systematization of the process of model development. *Comput. chem. Engng.* **20**, Suppl., S213–S218.
- Marquardt, W. (1992). An object-oriented representation of structured process models. *Comput. chem. Engng.* **17**, Suppl., S329–S336.
- Marquardt, W. (1994). Trends in computer-aided process modeling. In: *Proc. of PSE'94*. Kyongju, Korea. pp. 1–24.
- Marquardt, W., A. Gerstlauer and E. D. Gilles (1993). Modeling and representation of complex objects: A chemical engineering perspective. In: *Proc. of 6th Int. Conf. on IEA/AIE*. Edinburgh, Scotland. pp. 219–228.
- Mattson, S. E. and M. Anderson (1992). The ideas behind omola. In: *Proc. of the 1992 IEEE Symposium on Computer Aided Control Systems Design*. Napa, California. pp. 23–29.

- ModellData (1994). *Powersim 2.0, User's Guide and Reference*. Modell-Data.
- Moe, H. I. (1995). Dynamic Process Simulation. Studies on Modeling and Index Reduction. Dr. ing. thesis. Department of Chemical Engineering, Norwegian Institute of Technology (NTH). Trondheim, Norway.
- Nilsson, B. (1993). Object-Oriented Modeling of Chemical Processes. PhD thesis. Department of Automatic Control, Lund Institute of Technology. Sweden.
- Nordmo, F. and J. Thonstad (1984). On the anode effect in cryolite-alumina melts—III. Current-voltage behaviour during anode effect. *Electrochimica Acta* **29**(9), 1257–1262.
- Pantelides, C. C. and H. I. Britt (1994). Multipurpose process modelling environments. In: *Proc. of FOCAPD'94* (L. T. Biegler and M. F. Doherty, Eds.). Snowmass, Colorado. pp. 128–141.
- Pantelides, C. C. and P. I. Barton (1993). Equation-oriented dynamic simulation: Current status and future perspectives. *Comput. chem. Engng.* **17**, Suppl., S263–S285.
- Parsons, R. (1974). Electrochemical Nomenclature. *Pure & Appl. Chem.* **37**, 503–516. App. III. to Manual of Symbols and Terminology for Physicochemical Quantities and Units.
- Perkins, J. D., R. W. H. Sargent and R. Vázquez-Román (1994). Computer generation of process models. In: *Proc. of PSE'94*. Kyongju, Korea. pp. 123–125.
- Peyneau, J. M. (1988). The automated control of bath composition on high amperage cell. In: *Proc. of International Symposium on Reduction and Casting of Aluminum*. Montreal, Canada. pp. 189–195.
- Pfundt, H., D. Vogelsang and U. Gerling (1989). Calculation of the crust profile in aluminium reduction cells by thermal computer modelling. *Light Metals 1989*, pp. 371–377.
- Piela, P. C., T. G. Epperly, K. M. Westerberg and A. W. Westerberg (1991). ASCEND : An object-oriented computer environment for modeling and analysis:the modeling language. *Comput. chem. Engng.* **15**(1), 53–72.
- PIL (1993). Framstilling av aluminium. Federation of Norwegian Process and Manufacturing Industries. In Norwegian.
- Ponton, J. (1995). Process systems engineering: Halfway through the first century. *Comput. chem. Engng.* **50**(24), 4045–4059.

- Ponton, J. W. and P. J. Gawthrop (1991). Systematic construction of dynamic models for phase equilibrium processes. *Comput. chem. Engng.* **15**(12), 803–808.
- Preisig, H. A. (1994). Computer-aided modelling: Species topology. In: *Proc. of ADCHEM'94*. Kyoto, Japan. pp. 143–148.
- Preisig, H. A., T. Y. Lee and F. Little (1990). A prototype computer-aided modelling tool for life-support system models. In: *20th Intersociety Conference on Environmental Systems*. SAE Technical Paper Series # 901269. Williamsburg, Virginia.
- Preisig, H. A., T. Y. Lee, F. Little and B. Wright (1989). On the representation of life-support system models. In: *19th Intersociety Conference on Environmental Systems*. SAE Technical Paper Series # 891479. San Diego, California.
- Qiu, Z., J. Zhang, K. Grjotheim and H. Kvande (1991). Phase equilibrium studies on the cryolite-aluminium fluoride system. *Light Metals 1991*, pp. 315–320.
- Roberts, R. A. and P. J. Ramsey (1994). Evaluation of fluorocarbon emissions from the aluminum smelting process. *Light Metals 1994*, pp. 381–388.
- Robie, R. A., B. S. Hemingway and J. R. Fisher (1979). *Thermodynamic Properties of Minerals and Related Substances at 298.15 K and 1 Bar Pressure and at Higher Temperatures*. Geological Survey Bulletin; 1452.
- Robilliard, K. R. and B. Rolofs (1989). A demand feed strategy for aluminium electrolysis cells. *Light Metals 1989*, pp. 269–273.
- Rolseth, S. (1997). Personal communication.
- Rye, K. Å. (1992). Alumina crusting in cryolitic melts. Part II : Bulk properties of crust. *Light Metals 1992*, pp. 503–509.
- Salt, D. J. (1990). Bath chemistry control system. *Light Metals 1990*, pp. 299–304.
- Solli, P. A. (1993). Current Efficiency in Aluminium Electrolysis Cells. Dr. ing. thesis. Department of Industrial Electrochemistry, Norwegian Institute of Technology (NTH). Trondheim, Norway.
- Solli, P., T. Haarberg, T. Eggen, E. Skybakmoen and Å. Sterten (1994). A laboratory study of current efficiency in cryolitic melts. *Light Metals 1994*, pp. 195–203.

- Stephanopoulos, G., G. Henning and H. Leone (1990). MODEL.LA. A modeling language for process engineering-I. The formal network. *Comput. chem. Engng.* **14**(8), 813–846.
- Sterten, Å. (1980). Structural entities in NaF-AlF₃ melts containing alumina. *Electrochimica Acta* **25**, 1673–1677.
- Sterten, Å. (1994). *Elektrokjemi, grunnkurs*. Department of Industrial Electrochemistry, Norwegian Institute of Technology (NTH). Trondheim, Norway. In Norwegian.
- Stevens, F. J., W. Zhang, M. P. Taylor and J. J. J. Chen (1992). The interaction between current efficiency and energy balance in aluminium reduction cells. *Light Metals 1992*, pp. 541–547.
- Støle-Hansen, K. and O. M. Dotterud (1996). Dynamic modelling of pH controlled precipitation and dissolution in an aqueous solution. *Comput. chem. Engng.* **20**, Suppl., S629–S634.
- Svinsås, E. (1995). Oppløselighet av aluminiumfluorid i kryolittsmelte. Technical report. Department of Inorganic Chemistry, Norwegian Institute of Technology (NTH). Trondheim, Norway. In Norwegian.
- Tabsh, I., M. Dupuis and A. Gomes (1996). Process simulation of aluminum reduction cells. *Light Metals 1996*, pp. 451–457.
- Taylor, M. P. (1991). Static & dynamic energy balance in reduction cells. In: *10th International Course on the Process Metallurgy of Aluminium*. Department of Inorganic Chemistry, Norwegian Institute of Technology (NTH). Trondheim, Norway. pp. 14.1–14.60.
- Taylor, M. P. (1992). Fluoride material balance. In: *Fourth Australian Aluminium Smelter Technology Workshop*. Sydney, Australia. pp. 720–732.
- Taylor, M. P., X. Liu, K. J. Fraser and B. J. Welch (1990). The dynamics and performance of reduction cell electrolytes. *Light Metals 1990*, pp. 259–266.
- Telnes, K. (1992). Computer Aided Modeling of Dynamic Processes based on Elementary Physics. Dr. ing. thesis. Department of Engineering Cybernetics, Norwegian Institute of Technology (NTH). Trondheim, Norway.
- The MathWorks, Inc. (1992a). Matlab, user's and reference guide.
- The MathWorks, Inc. (1992b). Simulink, user's and reference guide.
- The MathWorks, Inc. (1994). Simulink, release notes. Ver. 1.3.

- Vázquez-Román, R., J. M. P. King and R. Bañares-Alcántara (1996). *KBMoSS*: A process engineering modelling support system. *Comput. chem. Engng.* **20**, Suppl., S309–S314.
- Wasbø, S. O. (1996). Ferromanganese Furnace Modeling using Object Oriented Principles. Dr. ing. thesis. Department of Engineering Cybernetics, Norwegian University of Science and Technology (NTNU). Trondheim, Norway.
- Wasbø, S. O. and B. A. Foss (1997). Modeling unit processes using formal language description and object-orientation. *Mathematical Modeling of Systems*. In press.
- Welch, B. J. (1989). Strategy for dynamic cell control. In: *8th International Course on the Process Metallurgy of Aluminium*. Department of Inorganic Chemistry, Norwegian Institute of Technology (NTH). Trondheim, Norway. pp. Chapter 13, 1–14.
- Whiffen, D. H. (Ed.) (1979). *Manual of symbols and terminology for physicochemical quantities and units*. 1979 ed. Pergamon Press. Oxford.
- Wilson, M. J. (1992). Practical considerations used in the development of a method for calculating aluminium fluoride additions based on cell temperatures. *Light Metals 1992*, pp. 375–378.
- Woods, E. A. (1993). The Hybrid Phenomena Theory. Dr. ing. thesis. Department of Engineering Cybernetics, Norwegian Institute of Technology (NTH). Trondheim, Norway.

Appendices

Appendix A

System classification

Systems in general and chemical processes in particular can be classified in different ways. Chemical processes may be classified according to their content and behavior. This appendix gives a review of possible classifications of chemical processes and mathematical models. This review provides background knowledge for Ch. 2.

A.1 Process classification

Process classification is a term which includes a large number of different aspects. Thus, all aspects of this cannot be covered in this thesis. However, classifications will be discussed that cover the aspects that can be regarded as important in relation to chemical unit processes.

A.1.1 Thermodynamic classification

One classification is based on thermodynamic principles, and here systems can be classified into (Felder and Rousseau 1986):

1. *Isolated systems*: These systems neither exchange energy nor matter with their surroundings.
2. *Closed systems*: These systems exchange energy with their surroundings through their boundaries, but do not exchange matter.
3. *Open systems*: These systems exchange both energy and matter with their surroundings.

A.1.2 Fundamental transport processes

Another classification is based on fundamental transport processes (Bird *et al.* 1960):

1. *Mass transfer*: Mass is being transferred within a phase or from one phase to another distinct phase. The basic mechanism is the same whether the phases are gas, solid, or liquid. Two variants of mass transfer are:
 - Diffusion
 - Convection
2. *Heat transfer*: This transport process is concerned with the transfer of heat from one place to another. Three variants of heat transfer are:
 - Conduction
 - Convection
 - Radiation
3. *Momentum transfer*: This is concerned with the transfer of momentum.

Note that heat convection is strongly dependent of mass transfer, given by mass diffusion, mass convection or both.

A.1.3 Classification of reactions and generation

Reactions may be viewed upon as a special kind of generation. Thus, in this context, the mass part of generation can be separated into reactions, leaving the generation part to energy. Hence, reactions may be classified into two main groups (Bird *et al.* 1960):

1. *Homogeneous reaction*: The reaction occurs in the entire control volume.
2. *Heterogeneous reaction*: The reaction occurs in restricted regions of the system, such as the surface reactions.

The generation of energy can be classified as:

1. *Ohmic generation*: This is energy generated according to Ohm's law.
2. *Mechanical generation*: This is energy induced by stirring or other factors

A.1.4 Classification based on chemical phase

The three fundamental aggregate states for chemical substances are:

1. Solid
2. Liquid
3. Gas

More subtle descriptions of states include liquid crystal, amorphous, polymeric and solutions. However, many processes contain several *phases* of the very same *aggregate state*, like oil and water in a separator. Hence, a classification that is relevant to chemical engineering, is the number of phases involved within the boundaries of the system.

1. *Single phase systems*: These systems involve *one* phase within their boundaries (also termed homogeneous systems).
2. *Multiple phase systems*: These systems involve more than one phase within their boundaries (also termed heterogeneous systems).

A.2 Model classification

There are many different kinds of models. A model may be given as an experimental setup in a laboratory or as an abstract set of symbols on a piece of paper. This section presents some possible model classifications for the latter.

A.2.1 Knowledge classification

There are several possible classifications of knowledge (Leitch 1992):

1. *Micro/macro level*:
Process knowledge may be represented at a high (meta) level or a more detailed level. For example, the change of particle size of a solid material in a process may be described by detailed non-linear differential equations at a micro level, while the description at a macro level is given by a time varying parameter.
2. *Theoretical/empirical model*:
The knowledge may be based on a theoretical description or a fundamental law (e.g. conservation laws), or an empirical law found from data analysis.

3. *Explicit/implicit knowledge:*

The knowledge may be expressed explicitly or implicitly. Explicit knowledge of a process may for instance be given by a mathematical model of the process. If, for instance, only a description of the *control system* for the process is available, it is possible to say something about how the system behaves, but the knowledge of the process is implicit.

A.2.2 Model representations

The models may be represented in a number of different ways. Three possible general representational axes are (Leitch 1992):

1. *Formal/informal model description:*

A model may be expressed informally by for instance a *textual* formulation of the process, or by a rigid formal description. Examples of formal descriptions are *mathematical* models and formal language or logic descriptions. Another possible model representation is a *graphical* diagram. The degree of formality depends on the rules defined for the symbols allowed in the diagram. It should also be noted that models may be formal and precise in describing one aspect of a process, but at the same time be informal and blurry regarding other aspects.

2. *Qualitative/quantitative model:*

Mathematical models are the classical example of quantitative models, where the exact size and number of process variables are calculated. A typical example of qualitative models are expert system descriptions or fuzzy logic where a model typically states the direction of movement of variables, and the approximate accumulation in terms of “high” and “low”.

3. *Procedural/declarative model description:*

A model may be given as a set of procedural steps to follow in order to obtain a solution. A declarative model description does not give any information on how the model should be handled to obtain the solution. The advantage of the latter is, however, that if the procedural description does not fit with the desires of the end-user, the model must be changed, whereas the declarative model still may be applied.

A.2.3 Mathematical classification

Systems can also be classified from a mathematical point of view. There are a large number of possible mathematical classification axes for systems. Some are listed below.

1. *Linear/nonlinear systems:*

The nonlinear systems are by far the most dominant systems in the real world. Since linear systems have pleasant mathematical properties, they are often preferred in process analysis and control design. Nonlinear systems also include bilinear systems, and systems that may be linear in some aspects, for instance linear in the input variables, which facilitates control design.

2. *Dynamic/static systems:*

Dynamic variables means dynamic in time. In process analysis, static analysis is often preferred because it is easier and faster to evaluate. Dynamic systems are more difficult to handle, but their use is increasing. Static systems are described by algebraic equations (AEs) or partial differential equations (PDEs) where the time derivative term has been neglected. Dynamic systems are, however, typically described by ordinary differential equations (ODEs) combined with AEs to form differential and algebraic equations (DAEs). A dynamic system can also be described by PDEs (including time derivatives).

3. *Lumped/distributed systems:*

Lumped systems are systems where the state variables describing the system are lumped in space (invariant in all spatial dimensions). The system is described by ODEs or DAEs. Distributed systems are systems where the state variables vary in one or more directions of the spatial coordinates. The system is described by PDEs, or even more generally by integro partial differential algebraic equations (IPDAEs).

4. *Certain/uncertain systems:*

All systems will have some degree of uncertainty connected to them. Often a system is described by for instance a set of differential equations. If the uncertainty is large, a statistical model could be used to quantify how well the model behaves.

Appendix B

Symbol notation

This appendix contains the topological and phenomenological symbols defined in Ch. 2 and Ch. 3.

B.1 Topological symbols

Table 2.1: Symbols for the elements of the ED set.

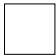

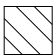
elements:	phase	source/sink	controller
symbol:			

Table 2.2: Symbols for the elements of the EC set.


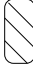
elements:	phase boundary	signal connection
symbol:		

Table 2.3: Symbols for the elements of the CTC set.

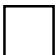
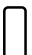


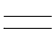
elements:	composite device	composite connection
symbol:		

Table 2.4: Symbols for the elements of the CE set.

elements:	relation element	signal line	component connecting line
symbol:			

B.2 Phenomenological symbols

Table 2.5: Symbols for the elements of the accumulation set A .






Subset	Phenomenological components
$A_S \subset A$	gas  liquid  solid  unspecified 
$A_E \subset A$	

Table 2.6: Symbols for the elements of the reaction/generation set RG .





Subset	Phenomenological components
$R \subset RG$	surface  volumetric 
$G \subset RG$	electrical  mechanical 

Table 2.7: Symbols for the elements of the transport set T .

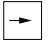






Subset	Phenomenological components
$T_S \subset T$	convection  diffusion 
$T_E \subset T$	convection  conduction  radiation 

Table 2.8: Set of arrows.

Arrows	Symbolic meaning	Related sets
	direction of mass transfer	A_S, T_S, R
	direction of energy transfer	A_E, T_E, G

B.3 Model assumption symbols

Table 3.1: Arrows for equilibrium modeling.




Arrows	Symbolic meaning	Related sets
	reaction equilibrium	A_S, T_S, R
	phase (material part) equilibrium	A_S, T_S, R
	phase (thermal part) equilibrium	A_E, T_E, G

Table 3.2: Main symbols for specified (constrained) and forced quantities.





Description	Main symbols	Related sets
Specified quantity (constrained)	 	A_S, A_E
Forced quantity	 	A_S, A_E, T_S, T_E

Table 3.3: Symbols of constrained phenomenological components.

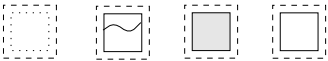

A posteriori assumption	Symbols of the A set
specification to chemical species, A_S	
specification to energy, A_E	

Table 3.4: Symbols of forced phenomenological components of balanced quantities.



Forced quantity	Symbols of the A set
forced chemical species, A_S	
forced energy, A_E	

Table 3.5: Symbols of forced phenomenological components of flows.




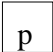

Forced quantity	Symbols of the T set
forced flow of species, T_S	
forced flow of heat, T_E	

Table 3.6: Symbols of constrained topological components.

Specified quantity	Symbols of the ED and CD set
constant volume of a phase device	
constant pressure of a phase device	
constant volume of a composite device	

Appendix C

Model files

This appendix contains the listing of two files. That is, the S-function for accumulation, `accumulation.tex`, and the model file for `f_heat_convection`.

C.1 Accumulation S-function file

```
/*
 * File name:   accumulation.c
 *
 * Explanation: Accumulation S-function for mass and energy balances
 *
 * Author:      Tormod Drengstig
 *
 * Date:        March 21, 1996
 *
 */

#define S_FUNCTION_NAME accumulation

#include <stdio.h>          /* needed for declaration of sprintf */
#ifdef MATLAB_MEX_FILE
#include "mex.h"           /* needed for declaration of mexErrMsgTxt */
#endif

#include <stdlib.h>
#include <string.h>
/*
 * need to include simstruc.h for the definition of the SimStruct and
 * its associated macro definitions.
 */

#include "simstruc.h"
#include <math.h>
#include <stdio.h>
```

```

#define FILE_NAME          ssGetArg(S,0)      /* what file to call for
 * calculation of state variable */
#define IDENTIFICATOR     ssGetArg(S,1)      /* defines who operates on the
 * S-simstruct. Used for block
 * identification purposes*/
#define HOLDUP             ssGetArg(S,2)      /* what variable is sent out */
#define TRANSPORT          ssGetArg(S,3)      /* what variable is expected in */
#define SOURCE             ssGetArg(S,4)      /* rate of production used in
 * any called equation */
#define INIT_VALUE        ssGetArg(S,5)      /* define the initial value */

#define NUM_ARGS          6                  /* Total number of input arguments */

#define MAX_NUM_IN_TRANSPORT 20             /* Max number of incoming TRANSPORT
 * to each block*/
#define MAX_NUM_IN_SOURCE  4                /* Max number of incoming source.
 * rates to each block*/
#define MAX_NUM_TOTAL      MAX_NUM_IN_TRANSPORT + MAX_NUM_IN_SOURCE

#define MAX_NUM_LETTERS_FILE 18             /* Max number of letters in filename */
#define MAX_NUM_LETTERS    40              /* Max size of identification input */

static void mdlInitializeSizes(SimStruct *S)
{
    double stateIdentifier = mxGetPr(HOLDUP)[0];

    char whoAmI[MAX_NUM_LETTERS];
    mxGetString(IDENTIFICATOR,whoAmI,MAX_NUM_LETTERS+1);

    if (ssGetNumArgs(S) != NUM_ARGS) {
        char err_msg[256];
        sprintf(err_msg, "Wrong number of input arguments
            passed to accumulator %s%d input arguments were passed in when
            expecting %d input arguments.", whoAmI, ssGetNumArgs(S), NUM_ARGS);
        mexErrMsgTxt(err_msg);
    }

    if (mxGetN(FILE_NAME) > MAX_NUM_LETTERS_FILE){
        char err_msg[256];
        sprintf(err_msg, "Wrong number of filename letters
            passed to accumulator %s%d letters were passed in when expecting
            %d letters.", whoAmI, mxGetN(FILE_NAME), MAX_NUM_LETTERS_FILE);
        mexErrMsgTxt(err_msg);
    }

    if (mxGetN(IDENTIFICATOR) > MAX_NUM_LETTERS){
        char err_msg[256];
        sprintf(err_msg, "Wrong number of letters in accumulator identifier
            passed to accumulator %s%d letters were passed in when expecting
            %d letters.", whoAmI, mxGetN(IDENTIFICATOR), MAX_NUM_LETTERS);
        mexErrMsgTxt(err_msg);
    }

    ssSetNumContStates( S, 1);              /* number of continuous states */
    ssSetNumDiscStates( S, 0);              /* number of discrete states */
    ssSetNumInputs(     S, DYNAMICALLY_SIZED); /* number of inputs */
    ssSetNumOutputs(    S, 2);              /* number of outputs */
    ssSetDirectFeedThrough(S, 0);          /* direct feedthrough flag */

```

```

    ssSetNumSampleTimes( S, 1);          /* number of sample times */
    ssSetNumInputArgs(  S, NUM_ARGS);   /* number of input arguments */
    ssSetNumRWork(      S, 0);          /* number of real work vectors */
    ssSetNumIWork(      S, 2 + MAX_NUM_TOTAL); /* number int work vectors */
    ssSetNumPWork(      S, MAX_NUM_TOTAL ); /* number of pointer work vectors */
}

static void mdlInitializeSampleTimes(SimStruct *S)
{
    ssSetSampleTimeEvent (S, 0, 0.0);
    ssSetOffsetTimeEvent (S, 0, 0.0);
}

static void mdlInitializeConditions(double *x0, SimStruct *S)
{
    int i;
    double one = 1.0;
    int *foundTag = ssGetIWork(S);
    void **pInputAdr = ssGetPWork(S);

    double initValue = mxGetPr(INIT_VALUE)[0];

    for (i=0; i<ssGetNumIWork(S); i++)
        foundTag[i] = 0;

    for (i=0; i<ssGetNumPWork(S); i++) /* initialize all pointers to &one */
        pInputAdr[i] = &one;

    x0[0] = initValue;
}

static void mdlOutputs(double *y, double *x, double *u,
                      SimStruct *S, int tid)
{
    double stateOutput;
    double stateIdentifier = mxGetPr(HOLDUP)[0];

    stateOutput = x[0];

    y[0] = stateOutput;
    y[1] = stateIdentifier;
}

static void mdlDerivatives(double *dx, double *x, double *u,
                          SimStruct *S, int tid)
{
    int *foundTag = ssGetIWork(S);
    void **pInputAdr = ssGetPWork(S);

    int numIWork = ssGetNumIWork(S);
    int numTransportInTags = mxGetN (TRANSPORT);
    double *pTransportInTag = mxGetPr(TRANSPORT);
    int numSourceInTags = mxGetN (SOURCE);
    double *pSourceInTag = mxGetPr(SOURCE);
    int numInputs = ssGetNumInputs(S);
    int nConnectedTransport = ssGetIWorkValue(S,numIWork-1);
    int nConnectedSource = ssGetIWorkValue(S,numIWork-2);
    int totNumConnected;

```

```

double t                = ssGetT(S);

double  Transport[MAX_NUM_IN_TRANSPORT];
double *pTransport[MAX_NUM_IN_TRANSPORT];
double   Source[MAX_NUM_IN_SOURCE];
double  *pSource[MAX_NUM_IN_SOURCE];
double  thisState;

double one              = 1.0;
double null            = 0.0;
int  InputType,i,j,count;

double *pArgument;
double functionOutput;
Matrix *lhs[1], *argument;
int  numOtherParameters, numRightHandSide;

char  whoAmI[MAX_NUM_LETTERS];
char  filename[MAX_NUM_LETTERS_FILE];

mxGetString(IDENTIFICATOR,whoAmI,MAX_NUM_LETTERS+1);
mxGetString(FILE_NAME,filename,MAX_NUM_LETTERS_FILE+1);

/*****
 *
 * PART 1: Identify tags and variables
 *
 *****/

if (t< 1.0) {
    nConnectedTransport = 0;
    nConnectedSource   = 0;

    for (i=0; i<MAX_NUM_IN_TRANSPORT ; i++) {
        pTransport[i] = &one;
        Transport[i]  = null;
    }
    for (i=0; i<MAX_NUM_IN_SOURCE ; i++) {
        pSource[i] = &one;
        Source[i]  = null;
    }

/*****
 * Identify the TRANSPORT
 *****/

    for (j=0; j<numTransportInTags; j++) {
        for (i=0; i<numInputs; i=i+2) {
            InputType=u[1+i];
            if (InputType==(int)pTransportInTag[j]) {
                ssSetPWorkValue(S,nConnectedTransport,&u[i]);
                ssSetIWorkValue(S,nConnectedTransport,InputType);
                nConnectedTransport++;
                if (nConnectedTransport > MAX_NUM_IN_TRANSPORT) {
                    char err_msg[256];
                    sprintf(err_msg, "Too many transport arguments passed
                        to %s. %d transport arguments were passed in
                        when expecting at most %d transport arguments.",

```

```

        whoAmI, nConnectedTransport,
        (int)MAX_NUM_IN_TRANSPORT), mexErrMsgTxt(err_msg);
    }
    ssSetIWorkValue(S,numIWork-1,nConnectedTransport);
}
}
}

/*****
* Identify the SOURCE
*****/

for (j=0; j<numSourceInTags; j++) {
    for (i=0; i<numInputs; i=i+2) {
        InputType=u[1+i];
        if (InputType==(int)pSourceInTag[j]) {
            ssSetPWorkValue(S,nConnectedTransport+nConnectedSource,&u[i]);
            ssSetIWorkValue(S,nConnectedTransport+nConnectedSource,InputType);
            nConnectedSource++;
            if (nConnectedSource > MAX_NUM_IN_SOURCE) {
                char err_msg[256];
                sprintf(err_msg, "Too many production rate arguments passed
                    to %s. %d source. rate arguments were
                    passed in when expecting at most %d source rate
                    arguments.", whoAmI, nConnectedSource,
                    (int)MAX_NUM_IN_SOURCE);
                mexErrMsgTxt(err_msg);
            }
            ssSetIWorkValue(S,numIWork-2,nConnectedSource);
        }
    }
}

/*****
* Consistency check
*****/

if ( (numTransportInTags>0 & nConnectedTransport<1) ||
    (numSourceInTags>0 & nConnectedSource<1) )
    if (ssGetRWorkValue(S,0) < 1.0){
        printf("There were unconnected informasjon in %s
            numTransportInTags %d nConnectedTransport %d
            numSourceInTags %d nConnectedSource %d ", whoAmI,
            numTransportInTags, nConnectedTransport, numSourceInTags,
            nConnectedSource);
        ssSetRWorkValue(S,0,1.0);
    }
}

/*****
*
* PART 2: Recall stored knowledge
*
*****/

thisState = x[0];

numOtherParameters = 3;

```

```

totNumConnected = nConnectedTransport + nConnectedSource;

argument = mxCreateFull(totNumConnected+numOtherParameters,1,REAL);

pArgument = mxGetPr(argument);
pArgument[0] = thisState;
pArgument[1] = nConnectedTransport;
pArgument[2] = nConnectedSource;

for (i=0; i<nConnectedTransport; i++) {
    pTransport[i] = ssGetPWorkValue(S,i);
    Transport[i] = *pTransport[i];
    pArgument[i+numOtherParameters] = Transport[i];
}

count = 0;
for (i=nConnectedTransport; i<nConnectedTransport + nConnectedSource; i++) {
    pSource[count] = ssGetPWorkValue(S,i);
    Source[count] = *pSource[count];
    pArgument[i+numOtherParameters] = Source[count];
    count++;
}

numRightHandSide = numOtherParameters + totNumConnected;

/*****
 *
 * PART 3: Call other MATLAB file
 *
 *****/

mexCallMATLAB(1,lhs,1,&argument,filename);
functionOutput = mxGetPr(lhs[0])[0];

if (functionOutput== -999.0){
    char err_msg[256];
    sprintf(err_msg, "Wrong number of input arguments
        passed to file in %s", whoAmI);
    mexErrMsgTxt(err_msg);
}

dx[0] = functionOutput;

mxFreeMatrix(lhs[0]);
mxFreeMatrix(argument);
}

static void mdlTerminate(SimStruct *S)
{
    int i;
    int *foundTag = ssGetIWork(S);
    void **pInputAdr = ssGetPWork(S);

    for (i=0; i<ssGetNumIWork(S); i++)
        foundTag[i] = NULL;

    for (i=0; i<ssGetNumPWork(S); i++)

```



```
pInputAdr[i] = NULL;

/* printf("You may plot simulation "); */

}

#include "simulink.c" /* MEX-file interface mechanism */
```

C.2 Model behavior file

```
/*
 * File name: f_heat_convection.c
 *
 * Explanation: Heat convection is described by this equation.
 *
 * heat_convection = param1 param2 (state1 - state2)
 *
 * input = [state1, state2]
 * parameters = [param1, param2]
 * output = [heat_convection]
 *
 * or combinations like below
 *
 * input = [state1, state2, param2]
 * parameters = [param1, calculated]
 * output = [heat_convection]
 *
 * Author: Tormod Drengstig
 *
 * Date: March 19, 1996
 *
 */
```

```
#include <mex.h>
#include <math.h>

void CalcFluxFunc(int length, double x[], double flux[])
{
int i, paramIndex, calcIndex;
int inputindex;

int errorLocated = 0;
int nConnectedStates = x[0];
int numParameters = x[1];
int numOutputs = x[2];
int numOtherConnected = 3;

double state1 = x[3];
double state2 = x[4];

char calculated[] = "calculated";
```

```

double parameter[numParameters];
double parameterValue;

paramIndex = numOtherConnected + nConnectedStates;
calcIndex = numOtherConnected + 2;
inputIndex = numOtherConnected + nConnectedStates;

for (i=0; i<numParameters; i++){
    if (x[i+inputIndex] == mxGetPr(mxGetMatrix(calculated))[0]) {
        parameter[i] = x[calcIndex];
        calcIndex++;
        paramIndex++;
    }
    else {
        parameter[i] = x[paramIndex];
        paramIndex++;
    }
}

parameterValue = 1;
for (i=0; i<numParameters; i++){
    parameterValue = parameterValue*parameter[i];
}

flux[0] = parameterValue*(state1 - state2);

for (i=0; i<length; i++){
    if (fabs(x[i])>pow(10,18)){
        for (i=0; i<length; i++)
            printf(" x[%d] = %f ",i,x[i]);
        flux[0]=-999;
    }
}

if (fabs(flux[0])>pow(10,18)){
    for (i=0; i<length; i++)
        printf(" x[%d] = %f",i,x[i]);
    printf(" flux = %f",flux[0]);
    flux[0]=-999;
}

if (flux[0] - flux[0] != 0){
    for (i=0; i<length; i++){
        printf("The output is NaN");
        printf(" x[%d] = %f",i,x[i]);
    }
    flux[0] = -999.0;
}

}

void ErrorFunc(double flux[])
{
flux[0] = -999.0;
}

#define X          prhs[0]
#define FLUX_OUT  plhs[0]
#define MAX(A, B)  ((A) > (B) ? (A) : (B)) /* compute the max of 2 numbers */

```

```

void mexFunction(
    int    nlhs,
    Matrix *plhs[],
    int    nrhs,
    Matrix *prhs[]
)
{
int i, checkSum, count;
int errorLocated = 0;
int m = MAX(mxGetM(X),mxGetN(X));
int numElements      = 0;
int numberOfStates   = 2;

char calculated[]     = "calculated";

numElements = (int)mxGetPr(X)[2];
FLUX_OUT = mxCreateFull(numElements,1,REAL);

count = 0;
for (i=0; i<m; i++){
    if (mxGetPr(X)[i] == mxGetPr(mexGetMatrix(calculated))[0]) {
        count++;
    }
}

checkSum = numberOfStates      +
            (int)mxGetPr(X)[1] +
            (int)mxGetPr(X)[2] +
            count + 3;

if (checkSum != m){
    printf("File: f_heat_convection Wrong number of input arguments
were passed in.
Number of states:           %d
Number of constants        %d
Number of properties       %d
numOtherConnected         %d
number of calculated parameters %d
-----
Size incoming vector       %d",
        numberOfStates, (int)mxGetPr(X)[1], (int)mxGetPr(X)[2],
        3, count, m);

    for (i=0; i<m; i++)
        printf(" x[%d] = %f", i, (double)mxGetPr(X)[i]);

    ErrorFunc(mxGetPr(FLUX_OUT));
}
else{
    for (i=0; i<m; i++){
        if ((mxGetPr(X)[i] - mxGetPr(X)[i])!=0){
            printf(" x[%d] = %f", i, (double)mxGetPr(X)[i]);
            errorLocated = 1;
        }
    }
}

if (errorLocated == 1){
    ErrorFunc(mxGetPr(FLUX_OUT));
}
}

```

```
    for (i=0; i<m; i++)
        printf(" x[%d] = %f",i,(double)mxGetPr(X)[i]);
    }
    else
        CalcFluxFunc(m,mxGetPr(X), mxGetPr(FLUX_OUT));
    }
}
```

Appendix D

Thermodynamic data

This appendix describes the general thermodynamic notation and the approximation of tabulated thermodynamic data used in the simulations in this thesis.

D.1 General introduction to notation

This section introduces the thermodynamic notation, and it is mostly taken from Cox (1982).

D.1.1 Process in thermodynamics

The word *process* in thermodynamics implies the occurrence of a change in a system, e.g. a change in the state of aggregation, or a change in the chemical species present. Thermodynamic changes are signified with the symbol Δ .

D.1.2 Standard state

As the absolute value of any thermodynamic quantity is unknown, only changes in values caused by parameters such as temperature and pressure can be determined. It is therefore important to define a base line for substances which provides a reference to such variations. The *standard state* is such a base line. The symbol for *standard* condition is usually $^\circ$.

The standard state applies to substances in a well defined state of aggregation¹ and at a well defined but arbitrarily chosen pressure. The chosen pressure is in most tabulated work either 1 atm. or 1 bar. For condensed phases this difference is insignificant. However, this may not be the case for gaseous phases.

The above definition of standard state makes no reference to temperature. Hence, it is possible to have an infinite number of standard states of a substance. The most employed reference temperatures (in Kelvin) are 0, 273.15, 293.15 and 298.15, with 298.15 K being the most favored.

D.1.3 Standard thermodynamic quantities

Some thermodynamic quantities are enthalpy, entropy and heat capacity. Using the symbol $^\circ$ together with symbols for thermodynamic quantities or for the *change* in thermodynamic quantities indicates standard conditions. Various subscripts are used to indicate changes in thermodynamic quantities. These subscripts usually annotate the Δ symbol, e.g. Δ_f for formation process, Δ_{mix} for mixing process and Δ_{fus} for melting process.

As an example, the symbol for the change in standard enthalpy due to formation of a compound from its elements is denoted $\Delta_f H^\circ$. The use of $^\circ$ here implicates that both the compound and its constituent elements are in standard states and that the elements are in their *reference states*.

D.1.4 Reference state

The reference state is related to elements only. For any temperature the reference state of the elements will normally be those that are stable at the chosen standard state pressure and at that temperature.

D.1.5 Chosen standard state

In accordance with Chase *et al.* (1985), the following convention is used in this thesis:

The reference temperature is 298.15 K. The base line for calculation of enthalpy changes is that the enthalpy of formation, $\Delta_f H^\circ$, of an element in its standard state is zero at all temperatures.

¹The three fundamental aggregation states are *solid*, *liquid* and *gas*, while more subtle descriptions of states include liquid crystal, amorphous, polymeric and solutions.

D.2 Enthalpy of reaction and formation, and heat capacity

The *heat of reaction*, $\Delta_r H^\circ$, is the difference in formation enthalpy between the products and the reactants participating in a reaction. In general, the enthalpy change involved with reactions, $\Delta_r H^\circ$, can be written as

$$\Delta_r H^\circ = \sum_{\text{compounds}} \nu_i (\Delta_f H^\circ)_i - \sum_{\text{reactants}} \nu_i (\Delta_f H^\circ)_i, \quad (\text{D.1})$$

where ν_i are the stoichiometric coefficients of the reaction. A formation reaction of a compound is the reaction in which the compound is formed from its constituent elements as they normally occur in nature, e.g. O_2 rather than O . The standard heat of such a reaction, $\Delta_r H^\circ$, is the actual standard heat of formation, $\Delta_f H^\circ$, of the compound. The reason for this is that the reactants on the left hand side in (D.1) are *elements*, and from the definition of the base line in Sec. D.1.5, the $\Delta_f H^\circ$ for the elements are zero. In addition, there is only *one* compound, and hence

$$\Delta_r H^\circ = \Delta_f H^\circ \quad (\text{D.2})$$

for a formation reaction. A more general version of (D.1) taking temperature other than 298 K into consideration is

$$\Delta_r H_T^\circ = \sum_{\text{compounds}} \nu_i (\Delta_f H_T^\circ)_i - \sum_{\text{reactants}} \nu_i (\Delta_f H_T^\circ)_i. \quad (5.42)$$

To calculate the enthalpy of formation at arbitrary temperatures, $\Delta_f H_T^\circ$, the following relationship is used:

$$\Delta_f H_T^\circ = \Delta_f H_{298}^\circ + (H_T^\circ - H_{298}^\circ)_{\text{compound}} - \sum_{\text{elements}} \nu_i (H_T^\circ - H_{298}^\circ)_i. \quad (\text{D.3})$$

A resulting feature of tabulations of $\Delta_f H^\circ$ for *compounds* is that discontinuities are sometimes to be seen. These correspond to changes in the stable reference states of the *elements* at various phase transition temperatures. This could be visualized for Al_2O_3 as in Fig. D.1. The discontinuity for Al_2O_3 at $T = 933.45$ K is due to aluminum phase transition from solid to liquid at this temperature.

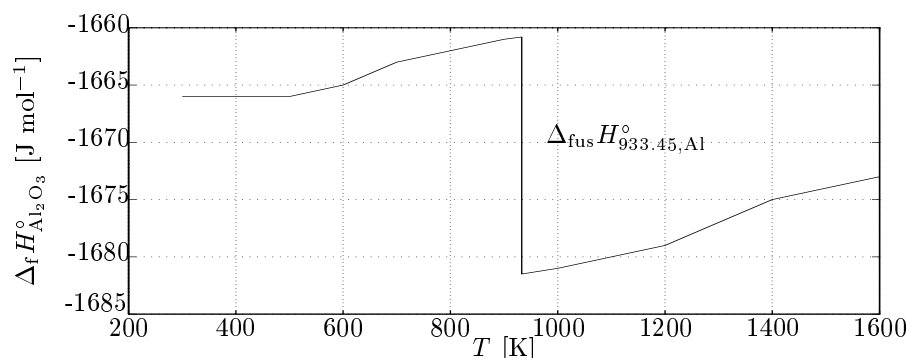


Figure D.1: The discontinuity in $\Delta_f H_{\text{Al}_2\text{O}_3}^\circ$ as a function of temperature, from Chase et al. (1985).

In thermodynamic tables, values of $(H_T^\circ - H_{298}^\circ)$ for various compounds are tabulated, and the values incorporate the following:

$$\begin{aligned}
 (H_T^\circ - H_{298}^\circ) = & \int_{298}^{T_1} c_{p,1}^\circ(T) dT + \Delta_{\text{trs}} H_{T_1}^\circ + \\
 & \int_{T_1}^{T_2} c_{p,2}^\circ(T) dT + \Delta_{\text{trs}} H_{T_2}^\circ + \\
 & \int_{T_2}^{T_3} c_{p,3}^\circ(T) dT + \Delta_{\text{fus}} H_{T_3}^\circ + \dots \quad (\text{D.4})
 \end{aligned}$$

where $T > T_3 > T_2 > T_1$ and $c_{p,1} \neq c_{p,2} \neq c_{p,3}$. Hence, it can be seen from (D.3) that the formation enthalpy at temperature T of a compound takes into account the preheating and transition of both the elements and the compound. For this reason, a similar discontinuity as for $\Delta_f H_{\text{Al}_2\text{O}_3}^\circ$ in Fig. D.1 can be found for $(H_T^\circ - H_{298}^\circ)$. This is schematically depicted in Fig. D.2.

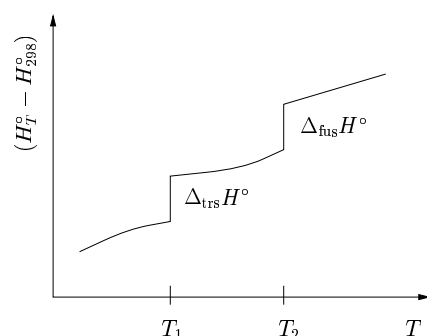


Figure D.2: Visualization of discontinuities in $(H_T^\circ - H_{298}^\circ)$.

D.3 Tabulated values

D.3.1 How to use the tables

The thermodynamic data in this thesis are mostly taken from Chase *et al.* (1985). There are three types of tables included in Chase *et al.* (1985); *i*) reference state, *ii*) single-phase and *iii*) multi-phase tables.

The reference state tables are for the *elements* only, and their purpose is to serve as a reference for all other forms of that element or any compound involving that element. The reference state tables contain data for all the possible phases of the element as a function of temperature. The discontinuities depicted in Fig. D.2 are therefore typical for these tables.

The single-phase tables and the multi-phase tables are both for elements and pure substances. A single-phase table represents only one phase. The thermodynamic values are extrapolated into temperature regions where the compound is not stable in that phase. For pure substances, neither of the discontinuities shown in Figs. D.1 and D.2 are present.

A multi-phase table contains data for two or more phases of a substance or element. In this context, it is data for pure substances that are of interest. For these tables, the discontinuities shown in Fig. D.1 and *not* those in Fig. D.2 exist at the transition temperatures of the elements constituting the substance.

D.3.2 Approximated thermodynamic data

Since Matlab has no support for thermodynamic packages, a subroutine must be included in the present model to calculate the physical properties. This subroutine is based on some approximations introduced below.

The different heat capacities in (D.4) are assumed constant over the temperature range *within* each phase as

$$c_{p,2}^{\circ} \int_{T_1}^{T_2} dT \approx \bar{c}_{p,2}(T_2 - T_1). \quad (\text{D.5})$$

Moreover, assuming that \bar{c}_p is an average of $c_{p,1}$, $c_{p,2}$ and $c_{p,3}$, the expression in (D.4) becomes

$$(H_T^{\circ} - H_{298}^{\circ}) = \bar{c}_p(T - 298) + \Delta_{\text{trs}}H_{T_1}^{\circ} + \Delta_{\text{trs}}H_{T_2}^{\circ} + \Delta_{\text{fus}}H_{T_3}^{\circ} + \dots \quad (\text{D.6})$$

Further, the different transition enthalpies are neglected. This is due to the fact that they are often small compared to the enthalpy of fusion. Using Fig. D.2, this can be visualized as in Fig. D.3.

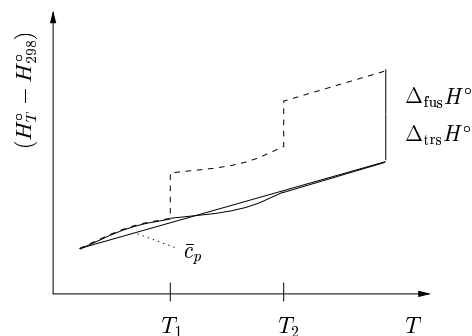


Figure D.3: Visualization of the approximation of c_p .

The functionality of the subroutine is to calculate the specific enthalpy, H_T^o or actually \tilde{H}_T , of a compound at a given temperature. Exploiting that H_{298}^o in (D.6) is the enthalpy of formation $\Delta_f H_{298}^o$, the following approximated relationship can be formulated:

$$\tilde{H}_T = \Delta_f H_{298}^o + \bar{c}_p(T - 298) + \Delta_{\text{fus}} H^o. \quad (\text{D.7})$$

In order to verify this approximation, the approximated values are compared with the values found from Chase *et al.* (1985) in the following tables. Since \tilde{H}_T is *usually* not reported in thermodynamic tables, the following relationship is used to find the comparative values:

$$\tilde{H}_T = \Delta_f H_{298}^o + (H_T^o - H_{298}^o). \quad (\text{D.8})$$

Other enthalpies, such as dissolution and mixing enthalpies will be discussed in Sec. D.4. The values of \bar{c}_p are calculated as the mean value over the temperature range from 298 K to 1300 K. However, the value is adjusted such that the value of (D.7) should be as close as possible to (D.8) around the working temperature 1200-1250 K. Note that Al uses the reference state tables and the other compounds are based on the multi-phase tables.

Table D.1: Approximated thermodynamic data of Al.

Tabulated values. Reference state table						
species	T	c_p	$(H_T^\circ - H_{298}^\circ)$	$\Delta_f H_{298}^\circ$	\tilde{H}_T (D.8)	
Al(s)	298	24.2	0	0	0	
Al(s)	933	32.9	17982	0	17982	
Al(l)	933	31.7	28693	0	28693	
Al(l)	1200	31.7	37156	0	37156	
Al(l)	1250	31.7	38744	0	38744	
Approximate values.						
	T	\bar{c}_p	$\bar{c}_p(T - 298)$	$\Delta_f H_{298}^\circ$	$\Delta_{\text{fus}} H^\circ$	$\tilde{\tilde{H}}_T$ (D.7)
Al	1200	29.3	26428	0	10711	37139
Al	1250	29.3	27893	0	10711	38604

Table D.2: Approximated thermodynamic data of AlF₃.

Tabulated values. Multi-phase table						
species	T	c_p	$(H_T^\circ - H_{298}^\circ)$	$\Delta_f H_{298}^\circ$	\tilde{H}_T (D.8)	
$\alpha - \text{AlF}_3(\text{s})$	298	75.1	0	-1510424	-1510424	
$\beta - \text{AlF}_3(\text{s})$	1200	102.9	87727	-1510424	-1422697	
$\beta - \text{AlF}_3(\text{s})$	1250	103.4	92898	-1510424	-1417526	
Approximate values.						
	T	\bar{c}_p	$\bar{c}_p(T - 298)$	$\Delta_f H_{298}^\circ$	$\Delta_{\text{fus}} H^\circ$	$\tilde{\tilde{H}}_T$ (D.7)
AlF ₃	1200	97.3	87764	-1510424	0	-1422660
AlF ₃	1250	97.3	92692	-1510424	0	-1417732

As indicated in Table D.2, there are both α and β solids of AlF₃. As mentioned above, the transition enthalpies are neglected. The $\alpha - \beta$ transition enthalpy of AlF₃ is only $\Delta_{\text{trs}} H^\circ = 0.56 \text{ kJ mol}^{-1}$.

Table D.3: Approximated thermodynamic data of Na_3AlF_6 .

Tabulated values. <i>Multi-phase table</i>						
species	T	c_p	$(H_T^\circ - H_{298}^\circ)$	$\Delta_f H_{298}^\circ$	\tilde{H}_T (D.8)	
$\text{Na}_3\text{AlF}_6(\text{s})$	298	215.7	0	-3316908	-3316908	
$\text{Na}_3\text{AlF}_6(\text{s})$	1285	332.4	281513	-3316908	-3035395	
$\text{Na}_3\text{AlF}_6(\text{l})$	1285	395.5	391552	-3316908	-2925356	
$\text{Na}_3\text{AlF}_6(\text{l})$	1300	395.5	397485	-3316908	-2919423	
Approximate values.						
	T	\bar{c}_p	$\bar{c}_p(T - 298)$	$\Delta_f H_{298}^\circ$	$\Delta_{\text{fus}} H^\circ$	\tilde{H}_T (D.7)
Na_3AlF_6	1285	277.1	273497	-3316908	119495	-2923915
Na_3AlF_6	1300	277.1	277654	-3316908	119495	-2919759

The α to β transition of Na_3AlF_6 at 836 K requires $\Delta_{\text{trs}} H^\circ = 9.456$ kJ mol^{-1} , which is approximately 10% of $\Delta_{\text{fus}} H^\circ$. Hence, for this special case, the $\Delta_{\text{trs}} H^\circ$ is added to the tabulated $\Delta_{\text{fus}} H^\circ$ of 110039 kJ mol^{-1} . This gives $\Delta_{\text{fus}} H^\circ = 119495 \text{kJ mol}^{-1}$ as shown in Table D.3.

The data table of Na_3AlF_6 indicates that the melting temperature is 1285 K, and that Na_3AlF_6 is solid below this temperature. However, as described in Ch. 5, AlF_3 and CaF_2 additions decrease the melting point. It is therefore assumed that (D.7) is valid below 1285 K for Na_3AlF_6 . The value of $\Delta_{\text{fus}} H_{\text{Na}_3\text{AlF}_6}^\circ$ is confirmed by Holm (1971).

Table D.4: Approximated thermodynamic data of Al_2O_3 .

Tabulated values. <i>Multi-phase table</i>						
species	T	c_p	$(H_T^\circ - H_{298}^\circ)$	$\Delta_f H_{298}^\circ$	\tilde{H}_T (D.8)	
$\alpha - \text{Al}_2\text{O}_3(\text{s})$	298	79.0	0	-1675692	-1675692	
$\alpha - \text{Al}_2\text{O}_3(\text{s})$	1200	128.2	103280	-1675692	-1572412	
$\alpha - \text{Al}_2\text{O}_3(\text{s})$	1250	129.1	109730	-1675692	-1565962	
Approximate values.						
	T	\bar{c}_p	$\bar{c}_p(T - 298)$	$\Delta_f H_{298}^\circ$	$\Delta_{\text{fus}} H^\circ$	\tilde{H}_T (D.7)
Al_2O_3	1200	114.7	103459	-1675692	0	-1572233
Al_2O_3	1250	114.7	109194	-1675692	0	-1566498

From the data table, four solid structures are found for Al_2O_3 : α , δ , γ and κ Al_2O_3 . In Table D.4, data from multi-phase α -solid/liquid are used.

Table D.5: Approximated thermodynamic data of CaF₂.

Tabulated values. <i>Multi-phase table</i>						
species	T	c_p	$(H_T^\circ - H_{298}^\circ)$	$\Delta_f H_{298}^\circ$	\tilde{H}_T (D.8)	
$\alpha - \text{CaF}_2(\text{s})$	298	68.5	0	-1225912	-1225912	
$\alpha - \text{CaF}_2(\text{s})$	1200	96.7	74862	-1225912	-1151050	
$\alpha - \text{CaF}_2(\text{s})$	1250	98.5	79786	-1225912	-1146126	
Approximate values.						
	T	\bar{c}_p	$\bar{c}_p(T - 298)$	$\Delta_f H_{298}^\circ$	$\Delta_{\text{fus}} H^\circ$	\tilde{H}_T (D.7)
CaF ₂	1200	83.0	74866	-1225912	0	-1151046
CaF ₂	1250	83.0	79016	-1225912	0	-1146896

Since CaF₂ is never added to the bath, but rather is the product of a reaction where CaO is the reactant, there is no value for $\Delta_{\text{fus}} H_{\text{CaF}_2}^\circ$ included in Table D.5.

D.4 Enthalpy of mixing, solution and vaporization

The enthalpy of mixing, $\Delta_{\text{mix}} H^\circ$, of NaF and Na₃AlF₆ is reported in Holm (1971) to be approximately -5000 J mol^{-1} for the composition in question, i.e. mol fraction of NaF of 0.75. On the other hand, it is difficult to find values in the literature for the composition in question, and hence, the $\Delta_{\text{mix}} H^\circ$ is neglected.

Since Na₃AlF₆ is viewed to be the solvent, there will not be a $\Delta_{\text{sol}} H^\circ$ for Na₃AlF₆. However, the additions Al₂O₃ and AlF₃ require energy to dissolve. The dissolution of AlF₃ is an endothermic process. In Svinsås (1995) this quantity is calculated to be

$$\Delta_{\text{sol}} H_{\text{AlF}_3}^\circ = 67000. \quad (\text{D.9})$$

In Taylor *et al.* (1990) it is reported that the endothermic dissolution process of alumina including preheating to working temperature requires approximately 2000 kJ/kg. This corresponds to $\Delta_{\text{sol}} H_{\text{Al}_2\text{O}_3}^\circ = 155000 \text{ J mol}^{-1}$. In Holm (1971), $\Delta_{\text{sol}} H_{\text{Al}_2\text{O}_3}^\circ$ is found to be 257000 J mol⁻¹ at low Al₂O₃ content, and it is decreased to approximate 201000 J mol⁻¹ at 7 wt.%. The following value is chosen:

$$\Delta_{\text{sol}} H_{\text{Al}_2\text{O}_3}^\circ = 220000. \quad (\text{D.10})$$

Since CaF_2 is *produced* according to (5.10) and not actually dissolved, $\Delta_{\text{sol}}H_{\text{CaF}_2}^\circ$ is neglected.

$$\Delta_{\text{sol}}H_{\text{CaF}_2}^\circ = 0. \quad (\text{D.11})$$

Similar argumentation is used to neglect the $\Delta_{\text{vap}}H^\circ$ for AlF_3 .

D.5 Summary of values

The following table contains the thermodynamic data used in this thesis. They are mainly taken from Chase *et al.* (1985), Brandes (1983), Robie *et al.* (1979) and Holm (1971).

Table D.6: Thermodynamic data of species related to aluminum production.

symbol	description	value	unit
$M_{\text{Al}_2\text{O}_3}$	molar weight of Al_2O_3	0.102	kg mol^{-1}
M_{AlF_3}	molar weight of AlF_3	0.084	kg mol^{-1}
M_{Al}	molar weight of Al	0.027	kg mol^{-1}
$M_{\text{Na}_3\text{AlF}_6}$	molar weight of Na_3AlF_6	0.210	kg mol^{-1}
M_{CaF_2}	molar weight of CaF_2	0.078	kg mol^{-1}
M_{C}	molar weight of C	0.012	kg mol^{-1}
M_{CO}	molar weight of CO	0.028	kg mol^{-1}
M_{CO_2}	molar weight of CO_2	0.044	kg mol^{-1}
$\bar{c}_{p,\text{Al}_2\text{O}_3}$	heat capacity of Al_2O_3	114.7	$\text{J K}^{-1} \text{mol}^{-1}$
\bar{c}_{p,AlF_3}	heat capacity of AlF_3	97.3	$\text{J K}^{-1} \text{mol}^{-1}$
$\bar{c}_{p,\text{Al}}$	heat capacity of Al	29.3	$\text{J K}^{-1} \text{mol}^{-1}$
$\bar{c}_{p,\text{Na}_3\text{AlF}_6}$	heat capacity of Na_3AlF_6	277.1	$\text{J K}^{-1} \text{mol}^{-1}$
\bar{c}_{p,CaF_2}	heat capacity of CaF_2	83.0	$\text{J K}^{-1} \text{mol}^{-1}$
$\bar{c}_{p,\text{C}}$	heat capacity of C	18.5	$\text{J K}^{-1} \text{mol}^{-1}$
$\bar{c}_{p,\text{CO}}$	heat capacity of CO	31.8	$\text{J K}^{-1} \text{mol}^{-1}$
\bar{c}_{p,CO_2}	heat capacity of CO_2	50.1	$\text{J K}^{-1} \text{mol}^{-1}$
$\rho_{\text{Na}_3\text{AlF}_6(\text{s})}$	mass concentration of Na_3AlF_6	2900	kg m^{-3}
$\Delta_{\text{f}}H_{298,\text{Al}_2\text{O}_3}^\circ$	heat of formation of Al_2O_3	-1675692	J mol^{-1}
$\Delta_{\text{f}}H_{298,\text{AlF}_3}^\circ$	heat of formation of AlF_3	-1510424	J mol^{-1}
$\Delta_{\text{f}}H_{298,\text{Al}}^\circ$	heat of formation of Al	0	J mol^{-1}
$\Delta_{\text{f}}H_{298,\text{Na}_3\text{AlF}_6}^\circ$	heat of formation of Na_3AlF_6	-3316908	J mol^{-1}
$\Delta_{\text{f}}H_{298,\text{CaF}_2}^\circ$	heat of formation of CaF_2	-1225912	J mol^{-1}

continued on next page

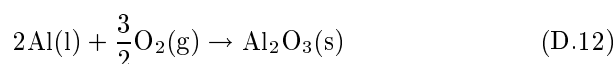
<i>continued from previous page</i>			
symbol	description	value	unit
$\Delta_f H_{298,C}^\circ$	heat of formation of C	0	J mol ⁻¹
$\Delta_f H_{298,CO}^\circ$	heat of formation of CO	-110527	J mol ⁻¹
$\Delta_f H_{298,CO_2}^\circ$	heat of formation of CO ₂	-393522	J mol ⁻¹
$\Delta_{\text{fus}} H_{Al_2O_3}^\circ$	heat of fusion of Al ₂ O ₃	0	J mol ⁻¹
$\Delta_{\text{fus}} H_{AlF_3}^\circ$	heat of fusion of AlF ₃	0	J mol ⁻¹
$\Delta_{\text{fus}} H_{933,Al}^\circ$	heat of fusion of Al	10711	J mol ⁻¹
$\Delta_{\text{fus}} H_{1285,Na_3AlF_6}^\circ$	heat of fusion of Na ₃ AlF ₆	119495	J mol ⁻¹
$\Delta_{\text{fus}} H_{1691,CaF_2}^\circ$	heat of fusion of CaF ₂	0	J mol ⁻¹
$\Delta_{\text{sol}} H_{Al_2O_3}^\circ$	heat of solution of Al ₂ O ₃	220000	J mol ⁻¹
$\Delta_{\text{sol}} H_{AlF_3}^\circ$	heat of solution of AlF ₃	67000	J mol ⁻¹
$\Delta_{\text{sol}} H_{Al}^\circ$	heat of solution of Al	0	J mol ⁻¹
$\Delta_{\text{sol}} H_{Na_3AlF_6}^\circ$	heat of solution of Na ₃ AlF ₆	0	J mol ⁻¹
$\Delta_{\text{sol}} H_{CaF_2}^\circ$	heat of solution of CaF ₂	0	J mol ⁻¹

D.5.1 Examples

In this section, the use of the thermodynamic tables will be exemplified.

Example C.1

Consider the task of calculating the value of $\Delta_f H_{1200,Al_2O_3}^\circ$ from the formation reaction of Al₂O₃ from its elements shown in (D.12)



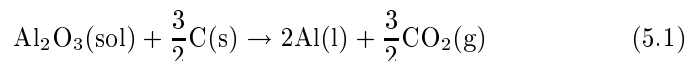
For this purpose, (D.3) is used to calculate the enthalpy change for the elements and the compound due to the temperature change. The elements and compound are indicated as subscript.

$$\begin{aligned} \Delta_f H_{1200,Al_2O_3}^\circ &= \Delta_f H_{298,Al_2O_3}^\circ + (H_{1200}^\circ - H_{298}^\circ)_{Al_2O_3} \\ &\quad - \left(2 \cdot (H_{1200}^\circ - H_{298}^\circ)_{Al} + \frac{3}{2} \cdot (H_{1200}^\circ - H_{298}^\circ)_{O_2} \right) \\ &= -1656.864 + 108.134 - \left(2 \cdot 37.156 + \frac{3}{2} \cdot 29.761 \right) \\ &= -1667.679 \text{ kJ mol}^{-1} \end{aligned}$$

This value can be verified by table lookup in Chase *et al.* (1985) where the tabulated value value of $\Delta_f H_{1200,Al_2O_3}^\circ$ is $-1667.684 \text{ kJ mol}^{-1}$. This means that this example is within the limits of accuracy. The values of $\Delta_f H_{298,Al_2O_3}^\circ$ and $(H_{1200}^\circ - H_{298}^\circ)_{Al_2O_3}$ are taken from the γ -Al₂O₃ table.

▲

Example C.2 Consider the following reaction occurring at 1200 K:



The reaction enthalpy $\Delta_r H^\circ$ can be found from (5.42) as

$$\begin{aligned} \Delta_r H_{1200}^\circ &= 2 \cdot \Delta_f H_{1200, \text{Al}}^\circ + \frac{3}{2} \cdot \Delta_f H_{1200, \text{CO}_2}^\circ \\ &\quad - \left(\Delta_f H_{1200, \text{Al}_2\text{O}_3}^\circ + \frac{3}{2} \cdot \Delta_f H_{1200, \text{C}}^\circ \right) \\ &= 2 \cdot 0 + \frac{3}{2} \cdot (-395.050) - \left(-1667.684 + \frac{3}{2} \cdot 0 \right) \\ &= 1075.109 \quad \text{kJ mol}^{-1}. \end{aligned}$$

▲

Example C.3

Consider the task of calculating the specific enthalpy of Na_3AlF_6 at 1300 K. As discussed in Sec. D.1, there are both reference state, single-phase and multi-phase tables. Each of the different tables will be used to calculate $\tilde{H}_{1300, \text{Na}_3\text{AlF}_6}$.

The purpose of this example is to show that the result is the same, though care must be taken in dealing with different tables. Note that the values calculated here are usually not tabulated. Na_3AlF_6 have α and β crystals.

Method 1, single-phase tables (separate solid α , β and liquid)

Single-phase tables (α and β solids, and liquid) gives:

- solid α table: $\Delta_f H_{298, \text{Na}_3\text{AlF}_6}^\circ = -3316.908 \text{ kJ mol}^{-1}$
- solid α table: $(H_{836}^\circ - H_{298}^\circ)_{\text{Na}_3\text{AlF}_6} = 138.797 \text{ kJ mol}^{-1}$
- $\alpha \rightarrow \beta$: $\Delta_{\text{trs}} H_{836, \text{Na}_3\text{AlF}_6}^\circ = 9.456 \text{ kJ mol}^{-1}$
- solid β table: $(H_{1285}^\circ - H_{836}^\circ)_{\text{Na}_3\text{AlF}_6} = 253.387 - 121.370 = 132.017 \text{ kJ mol}^{-1}$
- solid $\beta \rightarrow$ liquid: $\Delta_{\text{fus}} H_{1285, \text{Na}_3\text{AlF}_6}^\circ = 110.039 \text{ kJ mol}^{-1}$
- liquid table: $(H_{1300}^\circ - H_{1285}^\circ)_{\text{Na}_3\text{AlF}_6} = 327.049 - 321.116 = 5.933 \text{ kJ mol}^{-1}$

By summation, this gives for the molar specific enthalpy of Na_3AlF_6 at 1300 K, $\tilde{H}_{1300, \text{Na}_3\text{AlF}_6}$:

$$\begin{aligned} \tilde{H}_{1300, \text{Na}_3\text{AlF}_6} &= \Delta_f H_{298, \text{Na}_3\text{AlF}_6}^\circ + (H_{836}^\circ - H_{298}^\circ)_{\text{Na}_3\text{AlF}_6} \\ &\quad + \Delta_{\text{trs}} H_{836, \text{Na}_3\text{AlF}_6}^\circ + (H_{1285}^\circ - H_{836}^\circ)_{\text{Na}_3\text{AlF}_6} \\ &\quad + \Delta_{\text{fus}} H_{1285, \text{Na}_3\text{AlF}_6}^\circ + (H_{1300}^\circ - H_{1285}^\circ)_{\text{Na}_3\text{AlF}_6} \\ &= -3316.908 + 138.797 + 9.456 + 132.017 + 110.039 + 5.933 \\ &= \underline{\underline{-2920.302}} \quad \text{kJ mol}^{-1}. \end{aligned}$$

Method 2, single-phase table (extrapolated liquid)

- liquid table: $\Delta_f H_{298, \text{Na}_3\text{AlF}_6}^\circ = -3246.472 \text{ kJ mol}^{-1}$
- liquid table: $(H_{1300}^\circ - H_{298}^\circ)_{\text{Na}_3\text{AlF}_6} = 327.049 \text{ kJ mol}^{-1}$

$$\begin{aligned}\tilde{H}_{1300, \text{Na}_3\text{AlF}_6} &= \Delta_f H_{298, \text{Na}_3\text{AlF}_6}^\circ + (H_{1300}^\circ - H_{298}^\circ)_{\text{Na}_3\text{AlF}_6} \\ &= -3246.472 + 327.049 \\ &= \underline{-2919.423} \text{ kJ mol}^{-1}\end{aligned}$$

Method 3, multi-phase table (solid α , β and liquid)

- solid/liquid table: $\Delta_f H_{298, \text{Na}_3\text{AlF}_6}^\circ = -3316.908 \text{ kJ mol}^{-1}$
- solid/liquid table: $(H_{1300}^\circ - H_{298}^\circ)_{\text{Na}_3\text{AlF}_6} = 397.485 \text{ kJ mol}^{-1}$

$$\begin{aligned}\tilde{H}_{1300, \text{Na}_3\text{AlF}_6} &= \Delta_f H_{298, \text{Na}_3\text{AlF}_6}^\circ + (H_{1300}^\circ - H_{298}^\circ)_{\text{Na}_3\text{AlF}_6} \\ &= -3316.908 + 397.485 \\ &= \underline{-2919.423} \text{ kJ mol}^{-1}\end{aligned}$$

The result in method 1 is within the limits of accuracy because $\Delta_{\text{trs}} H_{836, \text{Na}_3\text{AlF}_6}^\circ = 9.456 \pm 1.7 \text{ kJ mol}^{-1}$. ▲

D.6 The energy and enthalpy balances

The term *enthalpy balance* is often found in the literature. In this section, a general energy balance is used to derive the enthalpy balance and the underlying assumptions on which it is based is emphasized. A general energy balance is written as

$$\frac{dE}{dt} = \epsilon_{\text{in}} - \epsilon_{\text{out}} + Q - W, \quad (2.24)$$

where E is the sum of internal, kinetic and potential energy as

$$E = U + E_K + E_P. \quad (\text{D.13})$$

Using molar specific notation, these elements can be written as:

$$\begin{aligned}E &= \int_V c \tilde{E} dV \\ E_K &= \int_V c \tilde{E}_K dV \\ E_P &= \int_V c \tilde{E}_P dV \\ \epsilon_{\text{in}} - \epsilon_{\text{out}} &= - \oint_{\partial V} c \tilde{E} v^T n dA \\ Q &= \oint_{\partial V} q dA \\ W &= W_s + \oint_{\partial V} p v^T n dA\end{aligned}$$

where W_s is shaft-work, v is the velocity, n the normal vector out of the control volume, c the concentration and A the area. The energy balance is then

$$\begin{aligned} \frac{d}{dt} \int_V c \tilde{E} dV &= - \oint_{\partial V} c \tilde{E} v^T n dA + Q - W \\ &= - \oint_{\partial V} c \tilde{U} v^T n dA - \oint_{\partial V} c \tilde{E}_p v^T n dA - \oint_{\partial V} c \tilde{E}_K v^T n dA \\ &\quad + Q - W_s - \oint_{\partial V} p v^T n dA. \end{aligned} \quad (\text{D.14})$$

Exploiting that

$$U = H - pV \Rightarrow c \tilde{U} = c \tilde{H} - p, \quad (\text{D.15})$$

the terms comprising the net flow of inner energy and pressure work in (D.14) can be written

$$\oint_{\partial V} c \tilde{U} v^T n dA + \oint_{\partial V} p v^T n dA = \oint_{\partial V} c \tilde{H} v^T n dA. \quad (\text{D.16})$$

As a result, the energy balance can be written

$$\frac{d}{dt} \int_V (c(\tilde{H} + \tilde{E}_K + \tilde{E}_P) - p) dV = - \oint_{\partial V} c(\tilde{H} + \tilde{E}_P + \tilde{E}_K) v^T n dA + Q - W_s.$$

In modeling of chemical processes, it is usual to eliminate the kinetic and potential energy. Hence, $E \approx U$, and this gives the following energy balance:

$$\boxed{\frac{d}{dt} \int_V (c \tilde{H} - p) dV = - \oint_{\partial V} c \tilde{H} v^T n dA + Q - W_s} \quad (\text{D.17})$$

or in the form of internal energy U :

$$\boxed{\frac{d}{dt} \int_V c \tilde{U} dV = - \oint_{\partial V} c \tilde{H} v^T n dA + Q - W_s} \quad (\text{D.17}')$$

The steady state of (D.17), is

$$0 = - \oint_{\partial V} c \tilde{H} v^T n dA + Q - W_s.$$

Based on this equation, it is often usual to talk about the dynamic *enthalpy balance* as

$$\frac{d}{dt} \int_V c \tilde{H} dV = - \oint_{\partial V} c \tilde{H} v^T n dA + Q - W_s,$$

which, of course is wrong, due to the elimination of the term $\frac{d}{dt} \int_V p dV$ in (D.17). This may have severe consequences for a gaseous system, but for condensed phases it may serve as an appropriate approximation.

Appendix E

Model simulation

This appendix presents two simulations using the inputs shown in Figs. 7.1 and 7.2 in Sec. 7.1, together with different value on the $b_{Q_{\text{loss}}}$ parameter in (6.66). The result in Sec. E.1 uses the $b_{Q_{\text{loss}}} = 0$, i.e. the heat loss to the surroundings upwards is constant. The result in Sec. E.2 uses a $b_{Q_{\text{loss}}}$ twice the value used in Sec. 7.1.

Note that due to the different time constants, the time scale of the simulations are different.

E.1 Constant heat loss, $b_{Q_{\text{loss}}} = 0$

In this section, the heat loss from bath to surroundings upwards is held constant at 188 kJ s^{-1} .

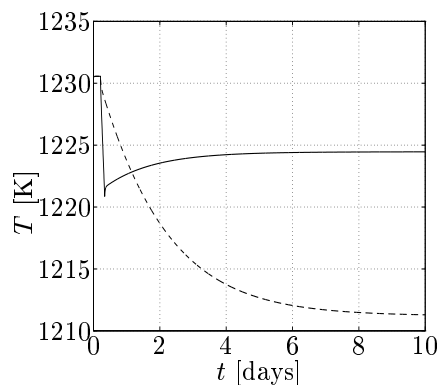


Figure E.1: Bath temperature. Solid line: AlF_3 addition. Dashed line: Reduced reference resistance.

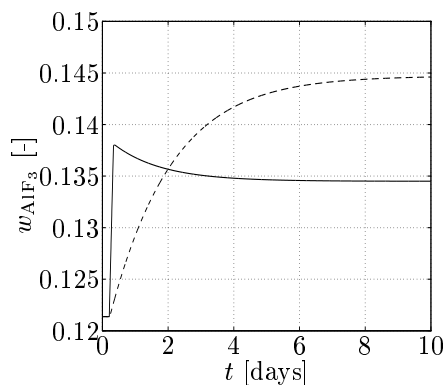


Figure E.2: Excess AlF_3 . Solid line: AlF_3 addition. Dashed line: Reduced reference resistance.

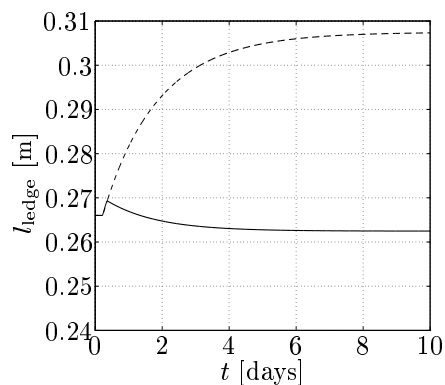


Figure E.3: Side ledge thickness. Solid line: AlF_3 addition. Dashed line: Reduced reference resistance.

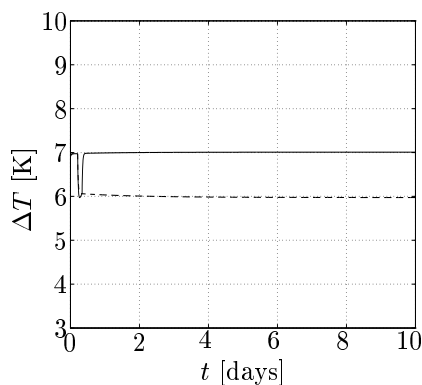


Figure E.4: Superheat. Solid line: AlF_3 addition. Dashed line: Reduced reference resistance.

E.2 Temperature dependent heat loss

In this section, $b_{Q_{\text{loss}}}$ is twice the value in Sec. 7.1. This implies that there is a stronger dependence between the bath temperature and heat loss from bath to surroundings upwards than in Sec. 7.1.

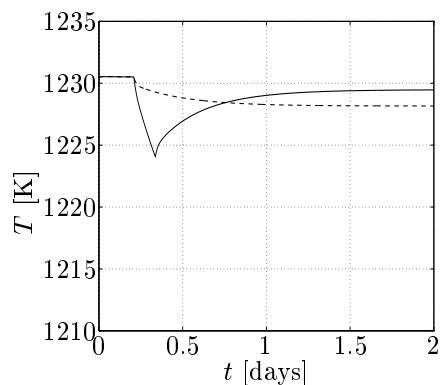


Figure E.5: Bath temperature. Solid line: AlF_3 addition. Dashed line: Reduced reference resistance.

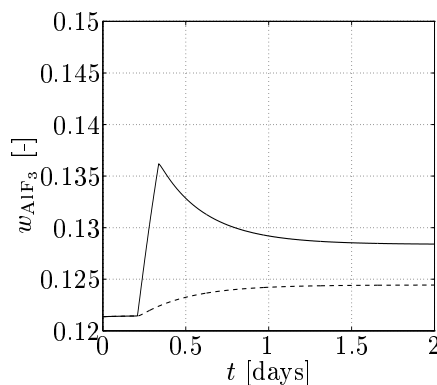


Figure E.6: Excess AlF_3 . Solid line: AlF_3 addition. Dashed line: Reduced reference resistance.

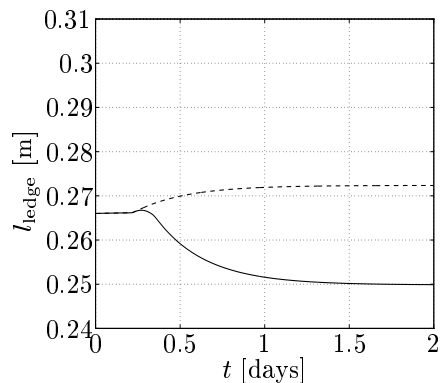


Figure E.7: Side ledge thickness. Solid line: AlF_3 addition. Dashed line: Reduced reference resistance.

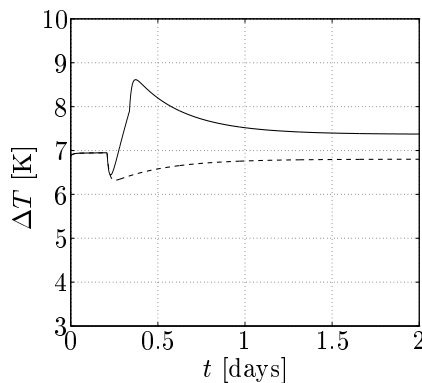


Figure E.8: Superheat. Solid line: AlF_3 addition. Dashed line: Reduced reference resistance.

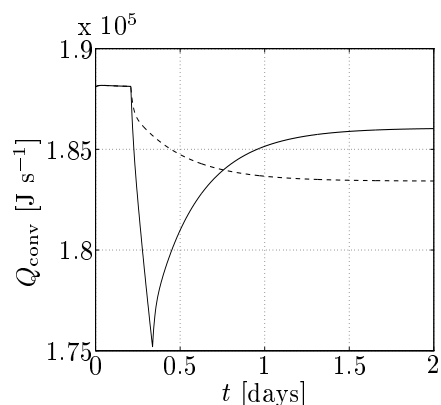


Figure E.9: Convective heat loss from bath to surroundings upwards. Solid line: AlF_3 addition. Dashed line: Reduced reference resistance.

E.3 Analytical determination of the time constant

The experienced behavior of the model with varying $b_{Q_{\text{loss}}}$ can be analytically determined from the model equations. The general balance equation for the enthalpy in the bath is given as:

$$\frac{dH_{\text{bath}}}{dt} = \sum j_i \tilde{H}_i + \sum j_o \tilde{H}_o + P_{\text{input}} - Q_{\text{conv}} + \dots \quad (\text{E.1})$$

where Q_{conv} is found from

$$Q_{\text{conv}} = Q_{\text{loss},0} + b_{Q_{\text{loss}}}(T_{\text{bath}} - T_{\text{bath},0}). \quad (6.66)$$

Assuming that everything but Q_{conv} is constant, and also that $dH_{\text{bath}} = c_{p,\text{bath}}dT_{\text{bath}}$, this gives:

$$\begin{aligned} c_{p,\text{bath}} \frac{dT_{\text{bath}}}{dt} &= \dots - Q_{\text{conv}} + \dots \\ &= \dots - (Q_{\text{loss},0} + b_{Q_{\text{loss}}}(T_{\text{bath}} - T_{\text{bath},0})) + \dots \end{aligned} \quad (E.2)$$

Simplifying this provides:

$$\frac{dT_{\text{bath}}}{dt} = -\frac{b_{Q_{\text{loss}}}}{c_{p,\text{bath}}}T_{\text{bath}} - \frac{1}{c_{p,\text{bath}}}Q_{\text{loss},0} + \frac{b_{Q_{\text{loss}}}}{c_{p,\text{bath}}}T_{\text{bath},0} + \dots \quad (E.3)$$

Inserting $b_{Q_{\text{loss}}} = 0$ in (E.3) as in Sec. E.1, implies that the responses in Figs. E.1-E.4 are driven by quantities not included in (E.3). Hence, it can be concluded that the time constant, t_c , is:

$$t_c \propto \frac{c_{p,\text{bath}}}{b_{Q_{\text{loss}}}}. \quad (E.4)$$

Consequently, increasing $b_{Q_{\text{loss}}}$ reduces t_c , as can be seen from Figs. E.5-E.9.